University of Nottingham
UK | CHINA | MALAYSIA

Insights Regarding Drug Permeation into Skin

Mohammed Hussain AL-Mayahy, MSc.

Thesis submitted to the University of Nottingham
for the degree of Doctor of Philosophy

School of Pharmacy

September 2017

Abstract

In order to develop safe and effective topical and transdermal formulations to treat either local skin disorders or for systemic drug delivery, it is first imperative to assess skin permeation using a reliable and comprehensive analysis method. The assessment of drug permeation into/across the skin is traditionally accomplished using Franz diffusion cells with subsequent analysis by conventional chromatographic methods such as HPLC and more recently using advanced imaging techniques. In this context, time of flight-secondary ion mass spectrometry (ToF-SIMS) offers distinctive advantages in mapping drugs within skin with high sensitivity and chemical specificity without the need for fluorescent tags or radiolabels. The work in this thesis uses the combination of conventional and advanced methods to evaluate drug permeation into the skin. This approach provides complementary and detailed information regarding the permeated mass, the permeation depth and the spatial distribution and localisation of drugs within skin.

As ToF-SIMS does not produce quantitative results, due to the matrix effects, a novel high throughput method was successfully developed to quantify ToF-SIMS data. This method involved the homogenisation of skin tissue followed by microarray printing of this skin homogenate with known concentrations of active pharmaceutical ingredients, specifically imiquimod and chlorhexidine. The subsequent analysis by ToF-SIMS of the resulting array allowed the generation of a calibration curve that can be used in the quantification of the unknown drug concentration in the tape strips. This work has demonstrated the potential of a method to quantify ToF-SIMS data of drugs within skin.

Imiquimod is an immune modulator drug approved by the FDA for the treatment of superficial basal cell carcinoma (BCC) but not the nodular lesions. An assessment of imiquimod permeation from commercially available Aldara™ cream into *ex vivo* porcine skin was carried out using the complementary approach of HPLC and ToF-SIMS analysis. This work represents the most detailed assessment to date of the true extent of permeation of imiquimod from Aldara™ cream as previous studies analysed the permeation of Aldara™ cream showed a limitation in the analytical methodology employed (i.e. analysis by

HPLC only). The results showed that imiquimod does permeate into the *stratum corneum* but is very limited in the deeper skin cell layers. In addition, the ToF-SIMS ion images of Aldara™ cream tape strips illustrated a non-uniform distribution of imiquimod within skin which may result in a decreased efficacy of the cream to uniformly treat whole BCC lesions giving rise to the likelihood of tumour recurrence. This offers previously unobserved insights about the spatial distribution of imiquimod delivered from Aldara™ cream.

As other studies have reported that Aldara™ cream has some limitations in the treatment of nodular BCC lesions due to the cream's inability to deliver imiquimod into the deeper more invasive nodular lesions, an enhancement of imiquimod permeation is thought to be useful to overcome these limitations. Therefore, an attempt to improve delivery of imiquimod into the deeper skin layers using microemulsions and microneedles was investigated. Imiquimod microemulsions were formulated, characterised and then tested for skin permeation enhancement. However, the assessment of imiquimod permeation from the formulated microemulsions alone and with microneedle pre-treatment using HPLC and ToF-SIMS demonstrated a limited ability of the microemulsions to improve delivery of imiquimod over Aldara™ cream. In contrast, Aldara™ cream with microneedle pre-treatment using a derma stamp electric pen showed improved delivery of imiquimod into the skin. This work is believed to be the first attempt to enhance imiquimod delivery using microemulsions and microneedles.

Utilising the high sensitivity offered by the ToF-SIMS instrument in the analysis of individual tape strips, an *in vivo* and *ex vivo* comparison of chlorhexidine permeation into the *stratum corneum* was performed using commercial products currently used in hospitals within the UK for skin antisepsis. A comparison was carried out using the tape stripping technique with subsequent analysis of an individual tape strip by ToF-SIMS. The results showed that HiBiSCRUB® 4% produces a higher concentration of chlorhexidine in the upper *stratum corneum* layers than other products. This work demonstrated the first known application of ToF-SIMS to compare the *in vivo* skin permeation of commercially available chlorhexidine products and

provides the foundation for the potential application of ToF-SIMS in assessing bioequivalence of topical products.

Acknowledgements

PhD study has been a long journey associated with many challenges and difficulties. This experience improved my thinking and taught me how to become stronger, more patient and not give up when facing obstacles. However, it would have not been possible to achieve without the support that I obtained from many people throughout this study.

Firstly, I would like to record my sincere gratitude to my first supervisor Dr David Scurr for his assistance, guidance, advice and patience throughout the PhD work and thesis writing.

I would like also to express my deep thank to my second supervisor Dr Maria Marlow for her supervision and advice throughout this project. I am extremely grateful for the support and guidance that I received from my both supervisors.

I would like to thank my internal assessor Prof Martyn Davies for his helpful suggestions and advice.

I would like also to extend my thank to Dr Andrew Hook for his help in microarray printing experiments and Prof Phil Williams for his helpful advice and discussion. To Dr Catrin Rutland and Mrs Aziza at the School of Veterinary Medicine and Science for their help and guidance regarding skin cross-sectioning.

The assistance and training received from the technical staff of Boots Science Building is greatly appreciated. I would like to thank my friends and colleagues for their support and encouragement.

A huge thank to my parents, brothers and sisters for their unconditional love and continuous encouragement. To my wonderful wife, Dina, for her affection, support, patience and unwavering belief in me. To my lovely sons, Mustaffa and Hamzah, for spreading their positive energy and enjoyment at home, they are really my prime inspiration.

Finally, I would like to thank my sponsor AL-Mustansiriyah University and the Ministry of Higher Education and Scientific Research in Iraq for funding my PhD study.

Table of Contents

List of Abbreviations

$[M+H]^+$	Molecular ion
°C	Degree centigrade
µg	Microgram
µL	Microlitre
AUC	Area under the curve
BCC	Basal cell carcinoma
CFU	Colony-forming unit
CHG	Chlorhexidine gluconate
CLSM	Confocal laser scanning microscopy
cm^2	Square centimetre
CP	ChloraPrep
D	Dermis
Da	Dalton
DESI	Desorption electrospray surface ionisation
DLS	Dynamic light scattering
DMD	Dermal microdialysis
DMSO	Dimethylsulfoxide
DNA	Deoxyribonucleic acid
DPPC	Dipalmitoylphosphatidylcholine
EPIC	The Evidence-Based Practice in Infection Control
eV	Electron volt
FDA	Food and Drug Administration
H & E	Haematoxylin and eosin
HCl	Hydrochloric acid
HLB	Hydrophilic-lipophilic balance
HM	Higher magnification
HPLC	High performance liquid chromatography
hr	hour
HS	HiBiSCRUB
Hz	Hertz
IPA	Isopropyl alcohol
IPM	Isopropyl myristate
IVIV	*In vitro in vivo*
J	Flux
keV	Killoelectron volt
KΩ	Kiloohm
LMIG	Liquid metal ion gun
LoD	Limit of detection
Log *P*	Logarithm of partition coefficient
LoQ	Limit of quantification
m/z	Mass to charge ratio
m^2	Square metre
MALDI	Matrix assisted laser desorption ionisation
mAU	Milliabsorption unit
MBC	Mimimum bactericidal concentration

MEC	Minimum effective concentration
MeOH	Methanol
mg	Milligram
mL	Millilitre
mm	Millimetre
mM	Millimolar
mN/m	Millinewton/meter
MW	Molecular weight
n	Number of samples
N	Normal concentration
NaCl	Sodium chloride
ng	Nanogram
NMF	Natural moisturising factor
o/w	Oil in water
OCT gel	Optimum cutting temperature
OCT instrument	Optical coherence tomography
OECD	The Organisation for Economic Co-operation Development
p	Significance level
PBS	Phosphate buffer saline
PD	Papillary dermis
PDI	Polydispersity index
PG	Propylene glycol
RNA	Ribonucleic acid
RSD	Relative standard deviation
S/Co-S	Surfactant/Co-surfactant
SB	*Stratum basale*
SC	*Stratum corneum*
SCCS	The Scientific Committee on Consumer Safty
SD	Standard deviation
SG	*Stratum granulosum*
SIMS	Secondary ion mass spectrometry
SP	*Stratum spinosum*
SSIs	Surgical site infections
TEA	Triethylamine
TEER	Transepithelial electric resistance
TEM	Transmission electron microscopy
TEWL	Transepidermal water loss
TLR	Toll-like receptors
ToF-SIMS	Time of flight-secondary ion mass spectrometry
t_R	Retention time
TS	Tape strip
UV	Ultraviolet
v/v	Volume by volume
VE	Viable epidermis
w/o	Water in oil
w/v	Weight by volume
w/w	Weight by weight
λ_{max}	Maximum wavelength of absorption

1 Chapter One: General Introduction

1.1 Skin structure and function

Human skin is a highly complex multi-layered structure and it represents the largest organ of the body, comprising around 10% of the body mass, it covers an average area of 1.8 m^2 in a typical adult [1]. The main function of the skin is to act as a barrier between the body and the outside environment. This barrier prevents the entry of chemicals, microorganisms, UV radiation and the loss of water and body fluids. In addition, the skin plays a role in the regulation of body temperature and it also acts as a sensory organ [2, 3]. Human skin can be divided into three layers (epidermis, dermis and subcutaneous fatty layer) [4] as shown in Figure 1.1.

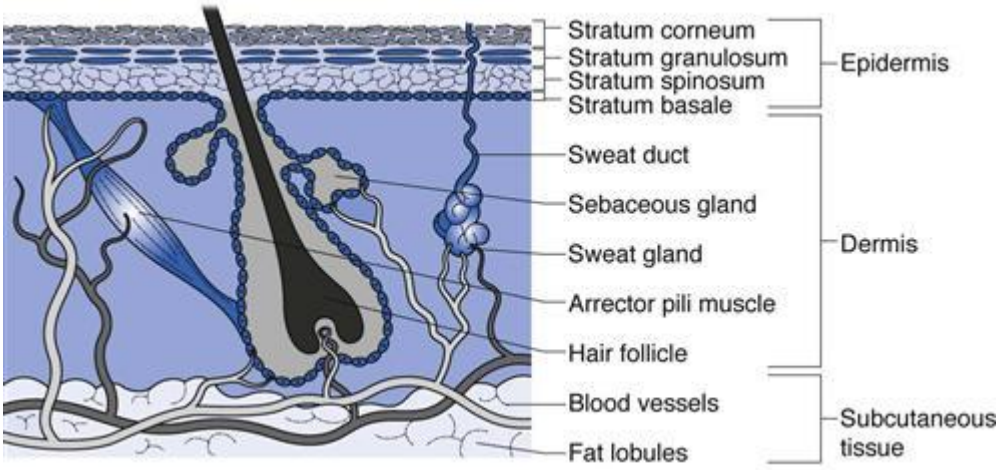

Figure 1.1: *An illustration of cross-section through human skin. Adapted from Williams C.A* [1].

1.1.1 Epidermis

The epidermis is the outer avascular layer of the skin. It is a multi-layered region that varies in thickness from 0.8 mm on the palms of the hands and soles of the feet to 0.06 mm on the eyelids [3]. It is primarily composed of keratinocytes and it is divided into multiple layers which are formed by cellular division and differentiation of the keratinocytes from the basal layer (*stratum basale*) and towards the surface. The basal layer contains columnar shaped

metabolically active keratinocytes anchored to the basement membrane by proteinaceous structures called hemidesmosomes [5]. The basal cells undergo division (via mitosis) and differentiate as they migrate outwards, forming the *stratum spinosum* or squamous cells, the *stratum granulosum* and eventually the *stratum corneum*, which is the outermost layer of the skin [1, 6-8] as shown in Figure 1.1.

Owing to the absence of the blood vessels in the epidermis, the supply of nutrients and waste removal occurs by diffusion across the epidermal-dermal barrier towards the cutaneous circulation in the dermis. The viability of the cells decreases with increasing distance from the basal layer. The term 'viable epidermis' is often used to describe the epidermal layer below the *stratum corneum* which are the *stratum granulosum, stratum spinosum* and *stratum basale* layers [3] because they contain nucleated cells responsible for the regeneration and renewal of epidermal tissue [9]. Water distribution within the epidermal layers is not homogeneous but is a gradient [10]. The results obtained from *in vivo* confocal Raman microscopy of human skin demonstrate a gradual increase in water content of the *stratum corneum* from 15% to 40% at the border of *stratum corneum-stratum granulosum* with an increase up to 70% in the deeper layers of the epidermis [11, 12].

The *stratum corneum* (or 'horny' layer) is predominantly responsible for the barrier properties of human skin which limits the permeation of chemical substances and microorganisms from the skin surface [13, 14]. The *stratum corneum* comprises only 10-15 cells in depth and is around 10-20 μm thick when dry (although it can swell to several times this when wet) [4, 14]. It is composed of anucleated flattened corneocytes packed with keratin filaments and surrounded by a lipid bilayer which is comprised largely of 25% cholesterol, 10% triglycerides, 15% fatty acids and 50% ceramides, with the absence of phospholipids [15, 16]. The resulting structure has been described as a brick wall-like structure containing corneocytes as "bricks'' embedded in a matrix or "mortar'' of intercellular lipids with desmosomes serving as rivets

between the corneocytes [1, 4, 17] as shown in Figure 1.2. The desmosomes are enzymatically digested before the desquamation process [5].

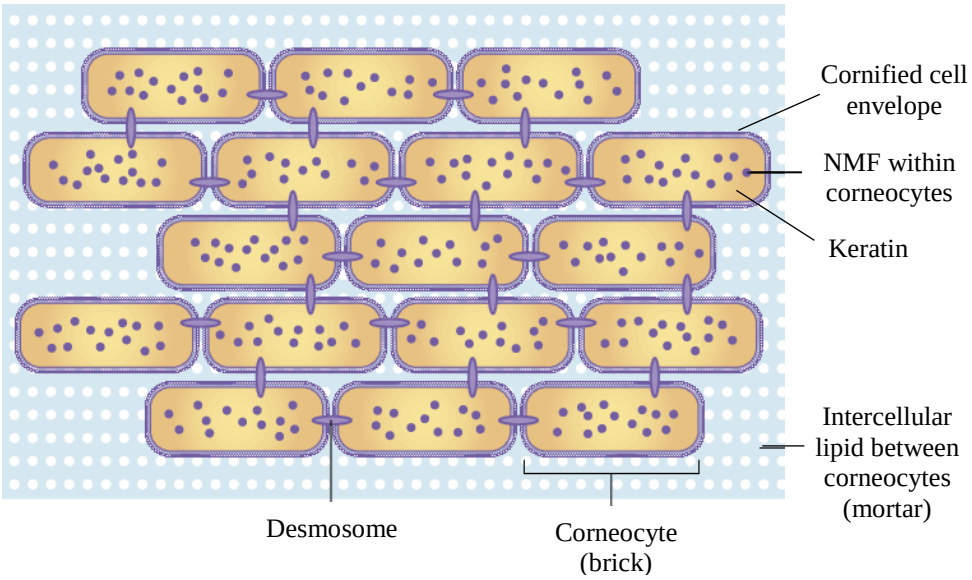

Figure 1.2: *A representation of the 'brick and mortar' model of human stratum corneum. Adapted from Beeckman et al.* [18].

The *stratum corneum* is composed of approximately 80% protein and 20% lipid [19]. The protein present within the corneocytes is mainly alpha-keratin with small amounts of beta-keratin and a proteinaceous cell envelope [4, 16]. Corneocytes also contain the natural moisturising factor (NMF) which is a mixture of free amino acids and amino acid derivatives, lactic acid, urea, citrate and sugars and it is exclusively present in the *stratum corneum* [20]. NMF is a hygroscopic material and as such it acts as a humectant by absorbing atmospheric water, thus maintaining *stratum corneum* hydration [20]. In normal skin the keratinocytes in the basal layer take approximately 21 days to migrate and differentiate into a *stratum corneum* cell [6], and these cells in turn require a further two weeks before they are shed from the *stratum corneum* [1, 21]. In addition to the keratinocytes, the epidermis and particularly the basal layer contains other specialised cell types, these are melanocytes, Langerhans cells and Merkel cells [3]. The main function of melanocytes is melanin production that provides the pigmentation of the skin and to absorb the harmful

UV radiation, thus decreasing free-radicals liberation in the *stratum basale* [22]. Langerhans cells are the antigen presenting cells in the skin localised in the superbasal layer of the epidermis. The binding of an antigen to the cell surface causes activation and migration of the Langerhans cells from the basal layer to the dermis and then on to the regional lymph nodes where they activate T cells to elicit an immune response [23]. Merkel cells are found in largest numbers around the touch sensitive sites of the body, such as the fingertips and lips and are associated with the nerve endings, their main function is cutaneous sensation [24].

1.1.2 Dermis

The dermis is the second layer below the epidermis and it is about 3-5 mm thick and composed of a network of connective tissue, mainly of collagen and elastin embedded in a mucopolysaccharide gel. This provides an aqueous environment similar to a hydrogel. Nerves, blood vessels and lymphatics traverse the matrix and skin appendages such as hair follicles, sebaceous glands, and sweat glands penetrate through it [1]. The dermis possesses a rich blood supply for temperature regulation, wound healing, oxygen and nutrients delivery to the tissues and also to remove waste materials [4, 5].

1.1.3 Subcutaneous fatty layer

The thickness of this inner layer of the skin is several millimetres and it is composed mainly from adipose tissue which insulates the body, acts as thermal barrier and provides mechanical protection against physical shock [1, 3].

1.1.4 Skin appendages

The skin appendages include sweat glands, hair follicles and the associated sebaceous glands. The sweat glands secrete sweat when stimulated either by heat or by emotional stress and sebaceous glands secrete sebum which consists of triglycerides, waxes and fatty acids to lubricate the skin surface and help to keep the pH of the skin surface at around 5. Typically the skin has hair follicles

from 50 to 100 per cm^2 but they are absent at the load bearing areas such as the soles of feet and palms of hands [3, 4].

1.2 Drug transport and permeation through the skin

For drug delivery the skin represents a formidable barrier and a difficult challenge to pharmaceutical scientists [1]. The drug molecules, in order to be transported through the skin, first must be presented to the skin surface in a dissolved form. Therefore, if the formulation contains a solid drug then dissolution within the formulation is the initial step in drug delivery. Following this, the active ingredient will partition into the outermost layer of the *stratum corneum* and diffuses through the *stratum corneum*. At the junction between *stratum corneum*-viable epidermis, there is another partitioning step and diffusion through the viable epidermis to reach the epidermis-dermis junction. Again, there is further partitioning and diffusion through the dermis to the blood vessels before removal in the systemic circulation [4] as illustrated schematically in Figure 1.3. In addition to these multiple partitioning and diffusion steps, there are other potential fates for drug molecules passing through human skin. The molecules may bind with the structural elements of the skin such as the binding of drug with the keratin present within the corneocytes at the *stratum corneum*, for example the binding of doxycycline to keratin present within the corneocytes [25] or the drug may undergo metabolism within the skin [4]. For most drug molecules the *stratum corneum* is the rate-limiting barrier for drug delivery. However, for some highly lipophilic drugs, the aqueous viable epidermis represents the main barrier to permeation [26]. A hydrophilic permeant has difficulty to penetrate the skin because it cannot easily enter the hydrophobic *stratum corneum* layer, while a lipophilic permeant can easily enter the *stratum corneum* but it may remain stored within it since the next layer (viable epidermis) has a higher water content [27]. The drug molecules have three routes to traverse the intact *stratum corneum* depending on their physicochemical properties, these being intracellular, intercellular and appendageal [28] as illustrated in Figure 1.3.

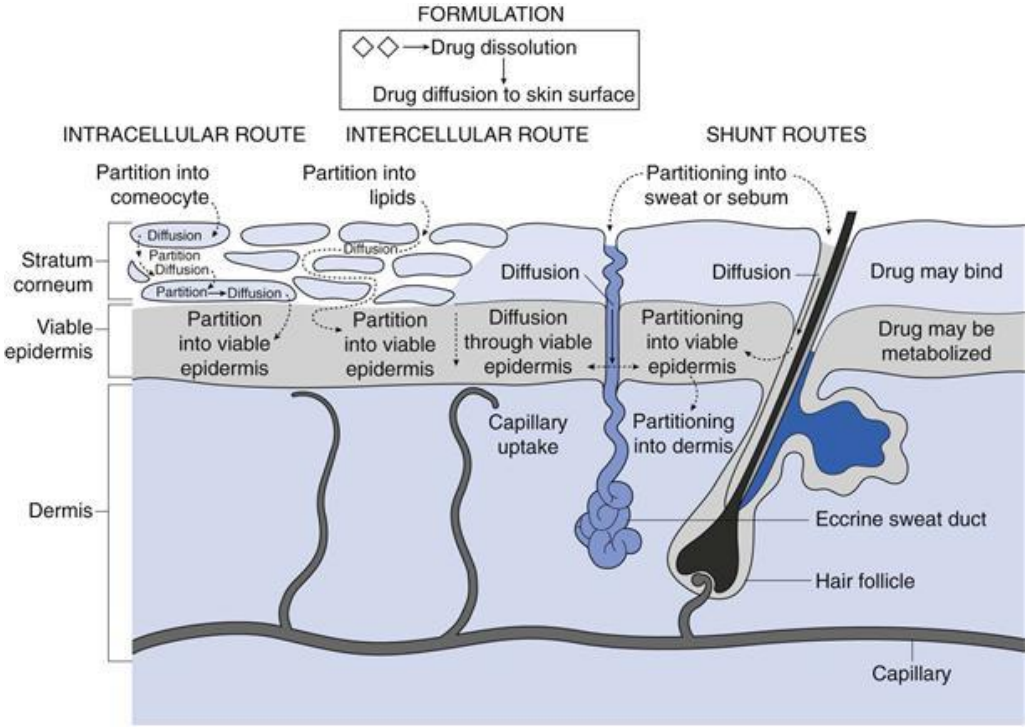

Figure 1.3: *A representation of the principle mechanisms and pathways operating during transdermal and topical drug delivery. Adapted from Williams C.A* [1].

1.2.1 Intracellular drug transport (across corneocytes)

The intracellular pathway provides a polar route for the diffusion of hydrophilic molecules. However, the corneocytes are bound to a lipid envelope that connects to the lipid bilayers. Therefore, molecules that traverse the intact *stratum corneum* via this route undergo multiple partitioning and diffusion steps between hydrophilic and hydrophobic domains which is an unfavourable process for most drugs [3, 4].

Partition: is the molecular redistribution from one domain to another, such as from an aqueous domain to a lipid domain.

Diffusion: is the movement of molecules through a domain from high concentration to low concentration.

Initially the drug molecules partition into a keratin-filled corneocyte, which is an aqueous environment and then diffuse through the corneocyte before partitioning into an intercellular lipid matrix. For intracellular transport to continue, the drug molecules must then diffuse through the lipid domain before they can again partitioning into and diffuse through the corneocytes and then lipoidal region [1, 4]. In the case of highly hydrophilic molecules, the rate-limiting barrier for permeability is the multiple lipids bilayers that the molecule must cross between the corneocytes [4].

1.2.2 Intercellular drug transport (across lipids)

This route provides the only continuous phase within the *stratum corneum* for drug transport. In this case, the drug molecules partition into the lipids between the corneocytes and then diffusion through a tortuous route within the lipid domain, 'following the mortar in the brick wall' [3, 4] (Fig. 1.3). It is now generally accepted that the intercellular route represents the major pathway for drug molecules to cross the *stratum corneum* [28, 29]. Within the intercellular lipid domains, the transport can happen via both (lipid core and polar head group) pathways. Thus, for a polar permeant the diffusion is via the polar head group pathway which is independent of the permeant's partition coefficient, while for a non-polar permeant the diffusion occurs via the lipid core pathway and increases with the increase in the permeant's partition coefficient [3]. The lipid bilayers provide the principle limiting barrier to drug permeation, since the intercellular transport occurs through the lipid domains and also the intracellular transport needs the lipid bilayers between the corneocytes to be crossed [4].

1.2.3 Appendageal (via skin appendages)

The appendages (hair follicles, sebaceous and sweat glands ducts) provide pores that overcome the *stratum corneum* barrier. This route represents a shunt route or short cut through which the drug molecules can move across the *stratum corneum* [1] such as in the case of caffeine [30] , minoxidil [31] and finasteride [32] permeation. The appendageal route is considered as a minor

route for drug transport. This is due to the fact that the appendages constitute only 0.1% of the total skin surface area [19] and the ducts of the sweat or sebaceous glands are seldom empty, containing sweat or sebum flowing out inhibiting drug delivery [4]. However, the appendages form a significant route for the transport of large polar molecules and ions that would traverse poorly across the *stratum corneum* [33]. In addition, they play a role in electrical enhancement of transdermal drug delivery (iontophoresis) [34] and also in the early stage of passive diffusion through the *stratum corneum* where the diffusion has yet to reach steady state [4]. Hair follicles can serve as a reservoir for drug molecules over a period of several days [35].

In terms of transdermal drug delivery, molecules that have been transported through the *stratum corneum* and then diffused through the lower epidermal layers (viable epidermis) will be cleared by the blood capillaries at the epidermal-dermal junction for systemic absorption. Therefore, the dermal concentration of transdermal drugs is kept low due to this rich blood flow, which provides a concentration gradient from the outside into the skin and this permits drug delivery through the skin [1].

1.3 Physicochemical properties of drugs affecting permeation

It is clear that for any permeant there are three available routes for transport across the skin but the proportion of molecules which cross by each route will vary depending on the physicochemical properties of the permeant [1].

1.3.1 Partition coefficient

The partitioning of the drug molecules into the *stratum corneum* is the rate limiting step in the permeation process and the partition coefficient of the permeant is usually the determining factor in selecting which pathway it will follow through the skin. Thus, it can be expected that a lipophilic molecule will preferentially partition into the lipid bilayers (intercellular route), whereas a hydrophilic molecule will prefer to partition into the hydrated keratin-filled

keratinocytes (intracellular route) rather than into the lipoidal domains [26]. However, this situation is not largely true for a hydrophilic permeant because the intercellular route contains desmosomes, proteins and a thin layer of water between the polar head groups in the lipoidal domains. Therefore, a hydrophilic permeant may partition into these polar regions within the lipid bilayers and cross the *stratum corneum* via the intercellular route. Consequently most drugs largely permeate through the continuous intercellular lipid bilayers by using both the lipid and polar regions of the bilayers depending on the partition coefficient of the permeant [36]. For a permeant with an intermediate partition coefficient (log *P* 1-3) the intercellular route probably predominates. For a highly lipophilic permeant (log *P* >3) the intercellular route will be the principle pathway to cross the *stratum corneum*. However, this permeant will have difficulty to partitioning out of the *stratum corneum* into the more aqueous viable epidermis. For more hydrophilic permeants (log *P* <1) the intracellular route increasingly predominates, yet there are lipid bilayers to cross between the corneocytes. The transport of a highly hydrophilic and charged permeant is predominantly through the appendageal route [4]. Lipophilic molecules are better candidates for transdermal drug delivery than hydrophilic molecules because they tend to permeate through the skin faster than the hydrophilic molecules but high lipophilicity also causes problems for clearance of the drug by the blood vessels at the epidermal-dermal boundary [1, 4]. Therefore, it is preferred that drug molecules have a balance between lipophilicity and aqueous solubility in order to cross the lipid bilayer of the *stratum corneum* and also pass through the more aqueous environment of the viable epidermis to ultimately enter the blood capillaries at the epidermal-dermal boundary [3].

1.3.2 Molecular size

The permeant's molecular weight and structure also affects its transport across the skin particularly for the large molecules. There is an inverse relationship between the transdermal flux and the molecular weight of the permeant. Thus, small molecules cross human skin faster than large molecules [37] and the skin

may prevent the passage of large molecules, such as insulin (MW 3000-7000 Da) [38] and low molecular weight heparin (MW 3000-9000 Da) [39].

1.3.3 Solubility / Melting point

There is a clear relationship between the permeant's melting point and its aqueous solubility. Most organic substances with high melting points possess relatively low aqueous solubilities [4]. The ideal permeant's melting point limit for transdermal delivery is below 200 °C [40]. The permeant should exhibit some aqueous solubility required to cross the aqueous medium of the viable epidermis and also because that most of the topical medications are generally applied from an aqueous formulation [3].

1.3.4 Hydrogen bonding

There is a possibility for a permeant having hydroxyl or carboxyl functional group in its structure to form hydrogen bonds with skin components. The permeation through the *stratum corneum* can be significantly reduced by increasing the number of hydrogen bonding groups on the permeant [41, 42], for example the diffusion coefficient and permeability of phenols is inversely related to the number of hydrogen bonding groups [43].

1.3.5 Drug dose

The drug's effective dose must be relatively low to allow the application of suitable sized patches or formulations and it must be readily released from the formulation, where poor drug release from the formulation can limit drug transport across the skin [1]. This limits the range of drugs that can be administered transdermally to obtain the required therapeutic level. There are certain parameters that can be used to predict the feasibility of an active drug ingredient for transdermal administration. These include [28, 40]:

1. Log *P*, ideally the log partition coefficient of the drug should be in the range of 1-3.
2. Molecular weight (MW), ideally the molecular weight of the drug should be less than 500 Dalton.
3. Aqueous solubility, ideally the aqueous solubility of the drug should be equal or greater than 1 mg/mL.
4. Melting point of the permeant should be less than 200 °C.
5. The effective daily dose of the drug should be in the range of 10-40 mg/day.

1.4 Pathological disorders of the skin

In general, skin disorders can be classified into [4]:

- Eruptions such as eczema, psoriasis and lichenoid eruptions.
- Infections which can be bacterial, viral or fungal.
- Ichthyoses conditions are disorders related to the keratinisation and epidermal differentiation.
- Tumours which can be either benign such as actinic keratosis or malignant such as basal cell carcinoma, squamous cell carcinoma or melanoma.

Topical formulations used in the treatment of basal cell carcinoma (BCC) and in the antisepsis of the skin against bacterial infections will be discussed here in more detail, since the work in this thesis aims to investigate the skin permeation of these formulations.

1.4.1 Basal cell carcinoma (BCC)

Basal cell carcinoma (BCC) is the most common type of skin cancer among white populations (Caucasian populations) constituting about 75%-80% of skin cancer cases [44, 45]. It has high prevalence in Europe, Australia and the U.S.A. Approximately 3-4 million cases per year of BCC occur in the United

States [46] and the incidence rate is rising by 10% annually worldwide [47]. It is an increasing health problem which puts a considerable burden on the resources of health care systems. The Medicare programme in the United States spends approximately 562 million dollars per year to treat non-melanoma skin cancer [48]. BCC is not fatal, it is a slow growing tumour with very rare opportunity for metastasis but it can cause local invasive tissue destruction on the face, neck and head affecting facial sensory organs such as the nose, ear, lips and eyelids. [46, 49]. The most relevant aetiological factors for BCC are genetic predisposition and exposure to solar radiation (UV light). In addition, increasing age, fair skin with freckles, blond or red hair, blue eyes and male sex represent other risk factors [49].

1.4.1.1 Classification of BCC

BCC can be classified morphologically into four major types [50]:

1. Superficial (15%) without penetration into the dermis.
2. Nodular including micronodular (50%) with dermis involvement.
3. Infiltrative (10%-20%) with dermis involvement.
4. Mixed (10%-15%) a combination of the above growth patterns.

Most of the truncal lesions are superficial BCC, while facial lesions are mainly nodular [51].

1.4.1.2 Treatment of BCC

The aims of BCC treatment are complete eradication of the tumour with maximum restoration of normal function and acceptable cosmetic outcome. Treatment approaches can be either surgical or non-surgical. Surgical treatments include [52]:

- Surgical excision.
- Mohs micrographic surgery.
- Curettage and electrodessication.

- Cryosurgery.

Non-surgical approaches include:

- Radiotherapy.
- Photodynamic therapy.
- Topical treatment with anticancer drugs such as imiquimod or 5-Fluorouracil.

The selection of the treatment type depends on several factors, including [47, 49]:

- The histological nature, size, depth, and location of the lesion.
- Patient general health condition.
- Patient and specialist preference.
- Cost of treatment.
- Local availability of specialised staff and services.

Surgical excision and in particular Mohs micrographic surgery represents the ‘gold standard’ treatment for BCC especially for high risk lesions because of its higher cure rate and lower recurrence rate. However, this treatment option may be unsuitable for some patients because of the invasive nature of the treatment, poor cosmetic outcome with scar formation, cost implications, need for specialist staff, equipment and long waiting list [49, 53]. Conversely, topical treatment with an anticancer drug such as imiquimod provides a non-invasive, self-administered treatment with excellent cosmetic outcome and lower cost. Therefore, it can be used as an alternative to surgery in the following cases [54]:

- Patients with multiple lesions.
- Patients with non-aggressive histological lesions.

- Patients with lesions difficult to excise either because of their location or size.
- Poor surgical candidates' patients because of underlying systemic diseases such as cardiovascular disease, pulmonary insufficiency, or with wound healing problems.
- Patients with surgical phobia.

The principle challenge for the topical treatment with anticancer drugs is to increase drug permeation at an adequate therapeutic level to eradicate tumour cells. In BCC the *stratum corneum* becomes thicker because of the hyperkeratinisation associated with the tumour lesions, this factor hinders drug permeation into the deeper skin layers. Therefore, a well-designed topical formulation for an anticancer drug is required to improve drug permeation through the thicker *stratum corneum* to reach the deeper skin layers, where the tumour cells are located [45].

1.4.1.3 Imiquimod

Imiquimod is an immune response modifier drug with antiviral and antitumor activity. Its action is indirect through stimulation of the immune system to kill viruses and tumour cells. It was initially approved by the FDA in 1997 for genital and perianal warts treatment and marketed as Aldara™ cream (5% w/w imiquimod) by 3M Pharmaceuticals, USA. In 2004, the FDA approved the use of imiquimod for the treatment of actinic keratosis and superficial BCC. [45].

1.4.1.3.1 Mechanism of action

Imiquimod stimulates both innate and acquired immunity. It activates the immune system by binding to toll-like receptor 7 (TLR-7) which causes production of cytokines such as interferon, interleukin and tumour necrosis factor. In addition, it activates Langerhans cells, the major antigen-presenting cells within the epidermis causing them to migrate from the site of treatment to

the regional lymph nodes for the activation of T lymphocytes. In addition, recent studies have shown that imiquimod can induce apoptosis to the tumour cells by direct stimulation and production of pro-apoptotic signalling via death receptors such as Fas Receptor [55].

1.4.1.3.2 Therapeutic efficacy

Imiquimod was approved by the FDA for the treatment of small, primary, superficial BCC but not nodular BCC [45]. In addition, several clinical studies have demonstrated the efficacy of imiquimod in the treatment of superficial BCC with cure rates range from 75% to 88% when used (once daily/ 5 days per week) for 6 weeks, while the cure rates in nodular BCC range from 42% to 76% for the treatment course of 12 weeks (once daily/ 5 days per week) [52, 53, 55, 56]. This difference in the clearance rate is attributed to the fact that the lesions in nodular BCC show deeper invasion within the dermis with the inability of imiquimod to reach the tumour's full depth [45]. In addition, the topical treatment of the superficial BCC lesions with Aldara™ cream has shown higher recurrence rate in comparison to surgery [56] particularly tumours with a thickness > 0.4 mm [48]. One study compared the topical imiquimod with 5-fluorouracil and photodynamic therapy and concluded that imiquimod is more effective in the treatment of superficial BCC and can be used as the first choice treatment [57].

According to Aldara™ cream leaflet, Aldara™ cream should be rubbed on the affected area and 1 cm around the affected area and it should be left for approximately 8 hours. During this time, the patient should not shower or bathe. For the treatment of superficial BCC lesions, Aldara™ cream should be applied daily for 5 consecutive days each week for 6 weeks. (e.g. Monday to Friday with no application on Saturday and Sunday). The patient should avoid sun light as much as possible during the treatment period and wear protective clothing and wide brimmed hat when outdoors. Many of the undesirable effects of Aldara™ cream are due to its local action on the skin. Local skin reactions can be a sign that imiquimod is working as intended. The treatment with

topical imiquimod is associated with local and to lesser extent systemic side effects. Local skin reactions include irritation, burning, erythema, oedema, pruritus, erosion and crusting. Whereas, systemic side effects such as headache, flu-like syndrome, fatigue, malaise, nausea and diarrhoea have been reported with some patients [55, 58].

As Aldara™ cream causes these local skin side effects and if it is applied for considerably long period of time of 6 weeks, it can compromise the barrier properties of the *stratum corneum*, allowing easier and greater permeation of imiquimod into the skin. However, in BCC the *stratum corneum* becomes thicker because of the hyperkeratinisation associated with the tumour lesions, this factor hinders drug permeation into the basal layer of the skin. Therefore, the clinical studies have demonstrated the limited efficacy of Aldara™ cream to treat deep nodular BCC lesions.

1.4.1.3.3 Physicochemical properties

Imiquimod ($C_{14}H_{16}N_4$) is a synthetic imidazoquinoline amine compound (Fig. 1.4) with a molecular weight of 240.3 g/mol and basic properties (pKa value of 7.3). It has a relatively high melting point of 297-299 °C with a very poor water solubility of less than 1 μg/mL. In addition, it is a sparingly soluble in organic solvents [59]. The lipid solubility (log *P*) of imiquimod is 2.7 [60].

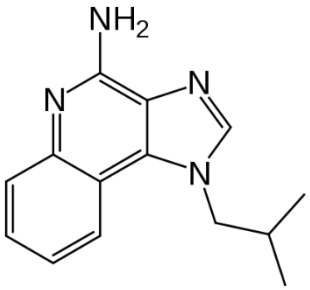

Figure 1.4: *Chemical structure of imiquimod.*

The current system of Aldara™ cream used as topical treatment of BCC lesions has shown success and gained approval for the treatment of superficial lesions. However, there are some limitations associated with this treatment such as the high recurrence rate of the superficial lesions as well as the inability of the cream to reach the deeper more invasive nodular lesions. To date, there is a gap in the available information regarding the exact depth of permeation and the spatial distribution of imiquimod when delivered from Aldara™ cream. Previous studies conducted by Stein *et al.* [61] and Rehman *et al.* [62] assessed the permeation of imiquimod into the skin from Aldara™ cream showing limitations in the analytical methodology employed. They used an inappropriate skin membrane i.e. 'rat skin' and HPLC as the analysis method. HPLC has a limited sensitivity level and does not have any imaging capability and therefore it cannot identify the spatial distribution of imiquimod within skin. Visualising the localisation of imiquimod within skin could help to understand the mechanism of permeation and provide an opportunity to develop more efficacious formulations of imiquimod in the future.

1.4.2 Bacterial infections

Intact skin is a highly efficient barrier against the ingress of microorganisms. However, the skin also carries commensal microbiota (microbial flora) which are not only found on the skin surface but rather distributed throughout the lower layers of the skin and located in numerous aggregates around hair follicles, sweat glands and sebaceous glands [63, 64]. Grice *et al.* investigated the influence of the sampling methods on the number of bacteria collected from the skin layers. They found that the number of bacteria increase with increasing depth of the skin layers sampled. They demonstrated that the number of bacteria collected from skin surface swabs is approximately 10,000 bacteria/cm^2, *stratum corneum* scrapes approximately 50,000 bacteria/cm^2 and for punch biopsies of the whole skin depth is approximately 1,000,000 bacteria/cm^2 [65]. The types of bacteria that are commonly found in skin include staphylococcal species, micrococci, corynebacteria and propionibacteria [4]. These microorganisms can cause infections at the incision site when the skin barrier integrity is breached during surgery or catheter

insertion. (i.e. the resident microbial flora exists in the patient's skin may become pathogenic and infects the incision site, in response to an impaired skin barrier) [65, 66]. For example, *Staphylococcus epidermidis* is well-known as a common skin commensal but simultaneously it is considered the most frequent cause of the hospital-acquired infections during catheters insertion procedures [63, 67]. Although, the surgical site infections (SSIs) can be caused by exogenous ingress of microorganisms into the incision site during surgery such as from the operation room environment, medical staff or surgical tools, the majority of SSIs are developed by microorganisms already present in patients' skin [68-70]. The risk for developing SSIs is dependent on many factors such as the type of wound, the virulence of the microorganism and the general health and immunity of the patient [71].

Surgical site infections are common postoperative complication with 5% of patients undergoing surgery developing them [72, 73]. SSIs can cause significant morbidity and mortality among patients following surgical operations [74]. It was reported that SSIs result in 20,000 deaths per year in the USA [75]. In addition, they can increase the length of stay and the cost of hospitalisation by 2-5 times [74]. In the UK, the treatment cost for each patient developing SSIs is increasing by as much as to £10,523 [76]. Therefore, it is necessary to reduce the microbial count in patient's skin to a minimum level prior to surgical incision using an efficient antiseptic agent. Furthermore, the applied antiseptic is required to permeate in a quick and efficient manner across the *stratum corneum* into the deeper skin layers to eradicate the microorganisms which exist there [77]. The most widely used antiseptic agent for skin antisepsis in clinical setting is chlorhexidine [78-80].

1.4.3 Chlorhexidine

Chlorhexidine is a cationic bisbiguanide compound possessing a broad spectrum antimicrobial activity with a low level of toxicity to mammalian cells. It shows activity against both gram positive and gram negative bacteria in addition to some viruses and fungi [81]. The mechanism of action of

chlorhexidine is by causing a disruption of the bacterial cell wall. At bacteriostatic concentrations, chlorhexidine binds to the bacteria cell wall phospholipids and induces structural modifications that lead to the leakage of low molecular weight intracellular components such as potassium ions. At higher bactericidal concentrations, chlorhexidine causes greater structural damage to the bacterial cell wall leading to cytoplasmic leakage and cell death [82]. Chlorhexidine is generally used as gluconate salts because of their higher water solubility. Chlorhexidine digluconate (Fig. 1.5) has a molecular weight of 897.8 g/mol. In addition, it is an ionised and water soluble compound with a partition coefficient log *P* (octanol/water) of 0.0133 [83]. The sub-optimal physicochemical properties of chlorhexidine contribute to its poor permeation into the skin which may allow potential pathogenic bacteria to remain viable at deeper skin layers. It is desirable for the topical antiseptic agents to show a rapid and efficient permeation into the lower layers of the skin and hair follicles to eradicate the bacteria present there and thus prevent the development of SSIs. However, the greater permeation of an antiseptic agent for example chlorhexidine can lead to an increase in its concentration in the systemic circulation which may result in toxic levels of chlorhexidine in blood. Therefore, it is thought that a compromise is required between the extent of permeation of chlorhexidine and the systemic absorption. This may be achieved using a formulation such as liposomes or nanocapsules that can target chlorhexidine into the deeper skin layers at a concentration just slightly above the minimum bactericidal concentration to avoid the excessive absorption of chlorhexidine into blood at the dermis layer. Several researchers have shown the limited permeability of chlorhexidine into and across the skin when they studied its permeation by Franz cell experiments using *ex vivo* rat [84], human [77, 85] or porcine skin [83, 86].

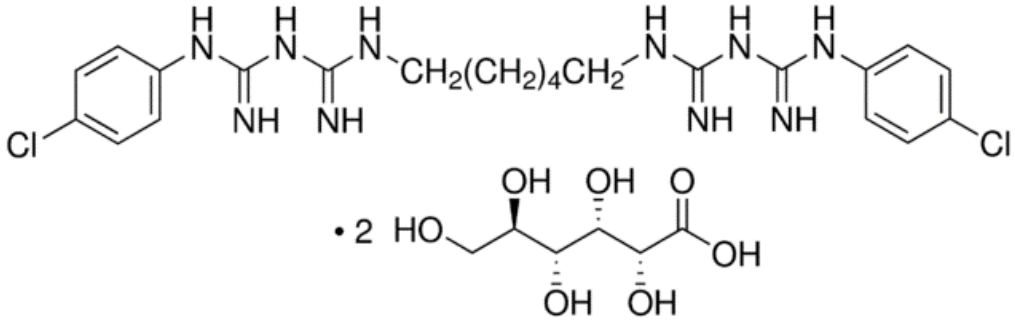

Figure 1.5: *Chemical structure of chlorhexidine digluconate.*

Lafforgue *et al.* compared the percutaneous diffusion of Hibitane® solution (chlorhexidine digluconate 5% w/v) through rat skin with and without *stratum corneum* and they found that following 48 hours exposure time, a lower quantity of chlorhexidine is diffused into the whole rat skin compared to the stripped skin without *stratum corneum* (approximately100 times less than the stripped skin) and this is related to the physicochemical properties of chlorhexidine [84]. Karpanen *et al.* demonstrated that chlorhexidine poorly permeates into the deeper skin layer following 2 and 30 minutes contact time when they studied the percutaneous permeation of chlorhexidine through *ex vivo* full-thickness human skin from aqueous solutions at a concentration of 2% w/v. The concentration of chlorhexidine as determined by HPLC in the upper 100 μm of skin is effective to eradicate microorganisms (0.157 and 0.077 μg/mg tissue for the 2 and 30 minutes respectively) but the concentration below 300 μm depth is less than 0.002 μg/mg tissue which may not be sufficient to kill bacteria present there [77]. In a following study, Karpanen *et al.* compared the skin permeation of chlorhexidine from both aqueous and alcoholic solutions at a concentration of 2% w/v. They found that the permeation of chlorhexidine following 2 and 30 minutes contact time from both solutions is limited. The detected concentration of chlorhexidine at a skin depth of 300 μm is negligible (less than 0.0008 μg/mg tissue) [85]. Recently, Judd *et al*. analysed permeation of chlorhexidine form 2% w/v aqueous solution into *ex vivo* porcine skin using ToF-SIMS. They concluded from the visualised tape strips and cross-sectioned skin samples, that the permeation of chlorhexidine is limited to the *stratum corneum* layer and penetration

enhancers are required to improve permeation of chlorhexidine and reduce the skin's microflora below the *stratum corneum* [83, 86].

A wide range of commercial products incorporating chlorhexidine are available varying in the type of vehicle (aqueous or alcoholic) and concentration (0.5-5% w/v) used. These products can be used for hand washing, body washing, skin preparation prior surgery, vaginal antisepsis and gingivitis treatment [87]. The Evidence-Based Practice in Infection Control (EPIC) guidelines recommends the use of chlorhexidine gluconate 2% in 70% isopropyl alcohol for skin antisepsis [78]. Mild adverse effects are associated with the use of topical chlorhexidine products including contact dermatitis [88]. However, in rare cases an anaphylactic shock was recorded following parenteral or mucosal administration of chlorhexidine [89].

Although, several researchers have studied the permeation of CHG into *ex vivo* rat, porcine or human skin from aqueous or alcoholic solutions of CHG, there is presently no published *in vivo* data investigating CHG permeation on human volunteers using commercial products of CHG. This investigation would provide more relevant information to the clinical setting since commercial products of CHG already used in hospitals will be tested on human subjects.

1.5 Experimental methods for assessing drug permeation into the skin

1.5.1 *In vivo* method

1.5.1.1 Clinical trials

In experimental design with the goal to evaluate the topical and transdermal permeation for *in vivo* use, the 'gold standard' would be the use of human volunteer 'clinical trials' to assess drug permeation into and through the skin but practically this is quite difficult to achieve and associated with ethical and legal constraints [4]. In addition, the comparative clinical trials are costly and

time consuming experiments recruiting large number of volunteers with clinical endpoints showing high variability [90]. Therefore, to address this situation alternative methods such as tape stripping, microdialysis, vasoconstrictor assay and *in vitro* experiments are used to assess the permeation of drugs into the skin.

1.5.1.2 *In vivo* tape stripping

In vivo tape stripping of the skin is a simple and minimally invasive technique used to estimate the quantity of a permeant in the *stratum corneum* (assess local bioavailability) for drugs whose target is the *stratum corneum*, such as UV filters [91-95], antifungals [96-98], antiseptics [83, 99] and keratolytics [100-102]. It involves a sequential application and removal of an adhesive tape onto the skin surface to collect microscopic layers composed of approximately 1 μm of *stratum corneum* [103]. Thus, it can provide information about the amount of permeated drug as a function of the *stratum corneum* depth [104]. The tape stripping process is relatively painless since it involves the removal of dead cells embedded in lipid matrix of the *stratum corneum* layer [103]. In this technique a drug is applied to a defined skin area, left for a period of time and followed by a sequential removal of the *stratum corneum* from the same treated skin area using adhesive tapes (Fig. 1.6). Thereafter, the drug content in each tape is usually determined by the conventional chromatographic methods such as HPLC following an appropriate extraction procedure. The removed tape strips contain amounts of both the applied drug and *stratum corneum*, a larger coverage of the *stratum corneum* is removed in the first few strips and reducing with subsequent tape strips removed [105]. The amount of the permeant drug also decreases with increasing depth into the *stratum corneum* [106]. In the tape stripping procedure, a roller is often used to press the tape strips by moving 10 times over them to stretch the skin surface. This will assist to avoid the effects of furrows and wrinkles during the tape stripping procedure which can cause removing parts of the *stratum corneum* from different depths with a single tape strip [107].

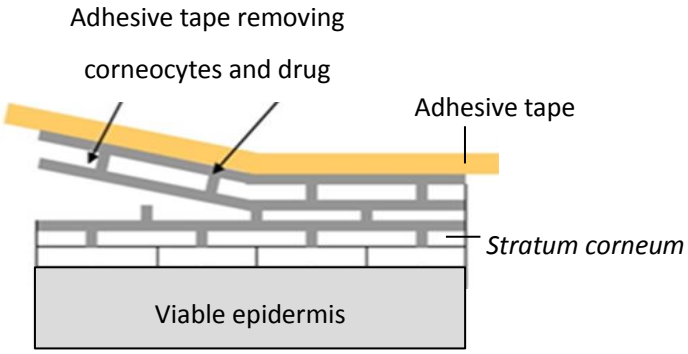

Figure 1.6: *A schematic representation of the tape stripping process.*

Although, the tape stripping technique is relatively simple, it has been shown that there are different external and internal factors that influence the amount of the *stratum corneum* removed [107]. The external factors are the type of adhesive tape used [108], vehicle composition [109], the duration of pressure [110] and the velocity of removal of the tape strips [111], while the internal factors include the anatomical site [112], age [113], skin hydration [114] and depth of skin [115]. Due to these external and internal factors, different amounts of the *stratum corneum* can be removed by a single tape strip even within the same subject and therefore, a standardised protocol for the tape stripping procedure is required to reduce the variability in the amount of the *stratum corneum* removed and obtain consistent results. In addition, it is necessary to correlate the amounts of topically applied drug in each tape strip to their location within the *stratum corneum* by determining the amount of the *stratum corneum* removed by each tape strip (i.e. normalisation of a drug concentration to the *stratum corneum* amount) [116].

Furthermore, to account for the inter-individual variation in the amounts of the *stratum corneum* removed which occur due to the inter-individual variability in the *stratum corneum* thickness (7-19 μm), the fraction of the *stratum corneum* removed (x/L) is required to be determined; where, the thickness removed (x) is divided by the total thickness of the *stratum corneum* (L). Consequently the (x/L) represents the relative depth within the *stratum corneum*. It was found that the use of this approach (fraction of the *stratum corneum* removed) has

advantages over the methods of tape strip number or the measured thickness of the *stratum corneum* removed by individual tape strip in reducing data variability and obtaining reasonably reproducible results [103].

A noteworthy point is that the *in vivo* tape stripping has certain legal and organisational constraints related to the use of the human volunteers in experimental studies including the requirement for the application of ethical approval prior to starting the experiments. Furthermore, not all drugs can be tested *in vivo* on the skin of human volunteers (i.e. only over the counter products are allowable) [104]. Therefore, *in vitro* tape stripping for the skin used in Franz cell experiments can provide a suitable model for the *in vivo* skin stripping to determine the concentration profile and total amount of the permeant within the *stratum corneum* [106]. Although, there are some limitations of the tape stripping process of being a laborious and time-consuming technique associated with some difficulties in standardising the method, it remains widely used because of its simplicity and it can be carried out at any laboratory [117].

The complete removal of the *stratum corneum* by tape stripping can be assessed visually. The skin will appear shiny by eye with a moderate exudation which indicates the total removal of the *stratum corneum* [118]. In addition, confirmation of complete removal of the *stratum corneum* can be achieved by checking cross-sections of biopsied skin samples under the microscope prior to and following tape stripping. Prior to stripping, the *stratum corneum* layer is clearly recognisable, whereas absent following the stripping process [119]. Another approach is to measure the TEWL prior to stripping and then every five strips. The stripping process can be continued until the TEWL value reaches eightfold its initial value which represents the complete removal of the *stratum corneum* [103]. TEWL refers to the total amount of water loss through the skin. It is often used as a non-invasive method for elucidation of skin barrier function. TEWL increases when there is a damage to the skin barrier [120].

1.5.1.3 Microdialysis

Dermal microdialysis (DMD) is a more invasive technique than tape stripping because it involves placing a probe (semipermeable hollow fiber structure) at the dermis level which is continuously perfused with a sterile physiological buffer at a very low flow rate using a microdialysis pump. This technique allows direct determination of unbound drug and can provide *in vivo* real-time information about permeation of drugs in addition to study the permeation from the test and reference formulations simultaneously [121, 122]. Several studies have used DMD to assess the permeation of drugs in healthy and damaged skin [123, 124] as well as to evaluate the bioequivalence of topical formulations [125, 126]. However, this technique is still more invasive and the exact positioning of the device is difficult to achieve. In addition, a special training for the laboratory personnel is required [122].

1.5.1.4 Vasoconstrictor assay (pharmacodynamic response)

A non-invasive procedure for the determination of drug content in skin for topical corticosteroids is the vasoconstrictor assay. In this assay, the ability of steroids to produce vasoconstriction of the skin blood vessels leading to blanching (whitening) at the application site is measured [103]. The blanching intensity is correlated with the formulation potency and the degree of drug delivery into the skin [127]. In contrast to clinical trials, the vasoconstrictor assay is relatively simpler to perform and requires smaller numbers of volunteers [103]. However, this assay is associated with high inter-individual variability [122].

1.5.2 *In vitro* method

Due to the difficulties associated with the *in vivo* experiments, most of the topical and transdermal drug permeation studies use *in vitro* experiments as an alternative method. *In vitro* permeation experiments can provide a platform for the initial evaluation of the permeation of topical and transdermal formulations in addition to their application in risk assessment experiments for many drugs

and chemicals. This method has the advantages of a quick and simple application with the ability to perform multiple repeats without the need to enrol large numbers of subjects. *In vitro* permeation experiments are usually performed using static diffusion cells (Franz cell) with subsequent analysis by HPLC. A typical static Franz cell is illustrated schematically in Figure 1.7, it is made of glass and consists of two-chambers (donor and receptor chambers) separated by a membrane (skin). A drug formulation is applied in the donor chamber and then samples are collected from the receptor chamber at specified time intervals. Following this, the drug concentration is measured and a permeation profile is constructed [4].

Careful selection of an appropriate membrane/skin sample is essential and it depends on the aim of the experiment. For example, if the aim of the experiment is the comparison between the release profiles from a series of formulations, then a simple polymeric membrane can be used [1]. On the other hand, if the aim is to evaluate permeability of a drug through human skin, then epidermal membrane (from *stratum corneum* to *stratum basale*) is used, since the drug is cleared by blood capillaries from the epidermal-dermal boundary *in vivo* [1]. The Scientific Committee on Consumer Safety (SCCS) recommends the use of a split-thickness skin for the *in vitro* permeation experiments utilizing human skin

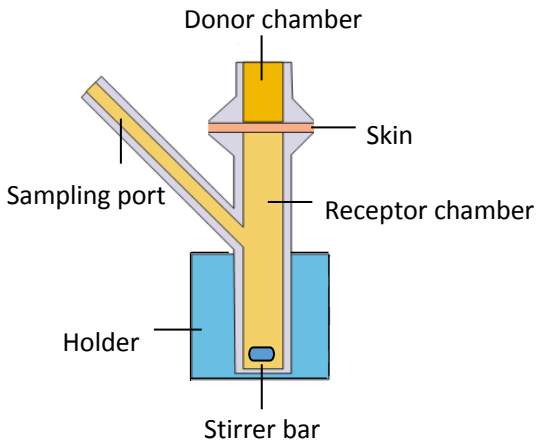

Figure 1.7: *A schematic of static Franz cell.*

as a membrane but for porcine skin a full thickness skin can be used due to the technical difficulties in obtaining intact split-thickness skin [128]. Generally, a skin integrity test is carried out prior to permeation experiments by either measuring the transepithelial electric resistance (TEER) or the transepidermal water loss (TEWL) of the membrane in order to verify the integrity of the membranes used for the *in vitro* permeation studies [4].

The *ex vivo* human skin is considered the most reliable model for *in vivo* studies [129]. However, animal skin can be used as a substitute for human skin because of the legal constraints, unavailability of human skin and variability among samples due to age, gender, race and anatomical site differences [130]. It is observed that diffusion experiments through some animals' skin, particularly small animals such as mice and rats show higher permeability results than experiments carried out by using human skin, since their skin is thinner than human skin [131]. The best natural membrane for diffusion studies is the pig skin, in particular pig ear skin which has a similar thickness, histology and permeability properties as human skin [132, 133]. Although many compounds have shown a similar permeability in both *in vivo* human skin and *ex vivo* porcine skin with an appropriate *in vivo in vitro* (IVIV) correlation, it is observed that some compounds show differences in permeability with poor IVIV correlation. The degree of similarity varies with the compound chemical properties [134]. Two critical factors are required to be considered in order to achieve a suitable IVIV correlation, these are the skin used in both *in vivo* and *ex vivo* experiments (should be from identical body site) and the vehicle (should be of identical composition and dose) [135].

The receptor solution should be a suitable solvent for the drug and sink conditions should be maintained during the experiment to allow permeation to continue as it would normally under *in-vivo* conditions with the presence of blood vessels (The concentration of the permeating molecules should not exceed 10% of its solubility in the receptor fluid) [1]. For hydrophilic and moderately lipophilic drugs (log P = 2) aqueous receptor solution such as

buffered isotonic saline pH 7.4 is mostly used. However, for more lipophilic drugs or where the aqueous solubility of the drug is low, the receptor fluid in this case needs some modifications either by the addition of solubilising agents or more commonly the addition of organic solvents like ethanol to the aqueous receptor fluid. Typically 25% ethanol/water co-solvent is usually used to provide sink conditions for lipophilic drugs. In addition, the effects of the receptor fluid on membrane integrity should be considered. The addition of a solubilising agent may damage the barrier nature of the biological membrane. Using a high concentration of ethanol in the receptor fluid may influence membrane integrity or could result in backwards flow from the receptor fluid into the donor fluid. This may change the partitioning of the drug across the membrane [4, 129]. The receptor fluid should be stirred continuously by using a magnetic stirrer bar to ensure appropriate mixing during the experiment and also to remove the molecules from directly beneath the membrane. The temperature of the skin membrane should be maintained near 32 °C to mimic the *in vivo* situation and to achieve this, the diffusion cell is submerged in a water bath at around 37 °C or water is circulated in a jacket around the cell [129]. The exposure time in the Franz cell experiments is usually maintained for 24 hours according to the recommendation of the Organisation for Economic Co-operation and Development (OECD) guidelines for skin permeation studies [136].

1.6 Techniques used to analyse drug permeation into the skin

1.6.1 Conventional chromatographic techniques

The most widely used techniques for the determination of drug concentration permeated into or across the skin are the conventional chromatographic methods (usually HPLC) [137-140]. HPLC can be used to determine the concentration of a permeant which can be analysed from the different Franz cell elements such as donor chamber wash, skin wash, pooled tape strips, remaining skin and receptor fluid. Although, HPLC represents a relatively quick, quantitative and versatile method for analysis which can be adopted for most permeants by appropriate selection of columns, mobile phase and

detectors, it suffers from issues in the detection and quantification of a permeant if it presents at low concentrations (low sensitivity) [4]. Additionally, in liquid chromatography the sample should be in a solution and therefore an efficient extraction step with solvents is required prior to injection into the HPLC system. This increases the complexity of the method and the time needed for the analysis. Furthermore, as the HPLC does not have any imaging capability, it is unable to identify the exact depth of permeation or provide information about the spatial distribution of a permeant within skin for the topically applied formulations.

1.6.2 Advanced imaging techniques

Imaging techniques with relatively high spatial resolution have been successfully used either to analyse native skin or to map the permeation and visualise the spatial distribution of a permeant within skin. Confocal laser scanning microscopy (CLSM) [141-143] can produce *in vivo* high resolution and high contrast images with the ability to capture 3D images but this is applicable only for an inherent fluorophore compound (auto-fluorescent) otherwise fluorescent tagging will be required to follow the permeation within the skin. This fluorescent tagging changes the molecular structure of the drug and influences the permeation behaviour and can yield information about the distribution and localisation which is not truly related to the native compound. This limits the number of drugs that can be analysed by CLSM [117, 144].

Vibrational spectroscopy techniques such as infrared [145-147] and Raman spectroscopy [148-150] have the advantages of label-free imaging of the skin. Nevertheless, infrared spectroscopy offers analysis of a limited spatial resolution. Raman spectroscopy and more specifically confocal Raman spectroscopy and stimulated Raman scattering microscopy provide non-invasive, *in vivo,* real-time and label-free skin imaging techniques which can produce 3D images with high sensitivity [151, 152] and depth resolution of 2 μm [117]. They have been used to map the permeation of both an active ingredient such as retinol and an excipient propylene glycol into the skin [153]

and also to monitor skin permeation of DMSO [154]. In addition, they have been utilised to profiling the distribution of ibuprofen and ketoprofen within skin [152] and studying the effect of different penetration enhancers on flufenamic acid permeation in *ex vivo* human skin [150]. However, these vibrational spectroscopy techniques have less chemical specificity than mass spectrometry methods. In addition, since the Raman signal is generally a weak signal, a prerequisite for the analysis of a compound by Raman spectroscopy is to produce a Raman signal with sufficient intensity for detection [117].

Mass spectrometry techniques such as matrix assisted laser desorption ionisation (MALDI) [155-158] have been used in the analysis of biological samples due to its molecular identification capability of high mass range materials such as lipids, peptides and proteins. It has been successfully applied to determine the existence of pharmaceutical compounds within skin but with a limited spatial resolution. Additionally, the samples cannot be analysed directly as they need further processing prior to the analysis by the application of a thin layer of matrix material onto the surface of the sample [159]. This adds additional complexity to the experimental procedure. Recently, there have been some improvements made to MALDI instrumentation to achieve a spatial resolution of 20 μm when used for assessing protein distribution in rat testis [158]. Another mass spectrometry technique is desorption electrospray surface ionisation (DESI) [160] in which the analysis of biological samples can be carried out at ambient conditions but again it offers a lower spatial resolution of approximately 100 μm which minimises the usefulness of this technique and limits its application.

Time of flight-secondary ion mass spectrometry (ToF-SIMS) offers numerous advantages that can be exploited for the analysis of biological samples (Section 1.7.7). However, to date there are only a small number of studies that utilise ToF-SIMS to explore drug permeation into the skin [83, 161].

1.7 Time of flight-secondary ion mass spectrometry (ToF-SIMS)

ToF-SIMS is a highly sensitive surface analysis technique that is used to characterise the surface chemistry of a sample including illustrating the spatial distribution. It involves the use of a primary ion beam to bombard the surface of a sample under ultra-high vacuum conditions to sputter secondary ions which are detected and separated according to their mass. When a high energy beam of ions in the order of 25 keV bombards a surface, the particle energy is transferred to the atoms of the solid by billiard-ball-type collisional process called 'collision cascade'. In this cascade of collisions that occurs between the atoms in the solid, some collisions return to the surface and result in the emission of secondary ions (Fig. 1.8). These secondary ions consist of either whole ionised molecules or fragment ions. [162].

In addition to the mass spectra obtained from ToF-SIMS analysis, the ToF-SIMS has the capability to produce ToF-SIMS ion images that illustrate the spatial distribution of different ions present in a sample by rastering (scanning) the primary ion beam onto the sample surface. ToF-SIMS instrument has the ability to map each detected ion as a function of its mass in addition to its x, y coordinates. Thus, each pixel of the image represents a full spectrum at that point. A spatial resolution of 400 μm to 1 μm can be achieved with ToF-SIMS depending on the primary ion mode [163]. ToF-SIMS ion images represent chemical maps which not only show the distribution and localisation of an exogenous compound within a tissue but also they highlight the co-localisation of the native components of that tissue and therefore permit the depth of permeation to be estimated [83].

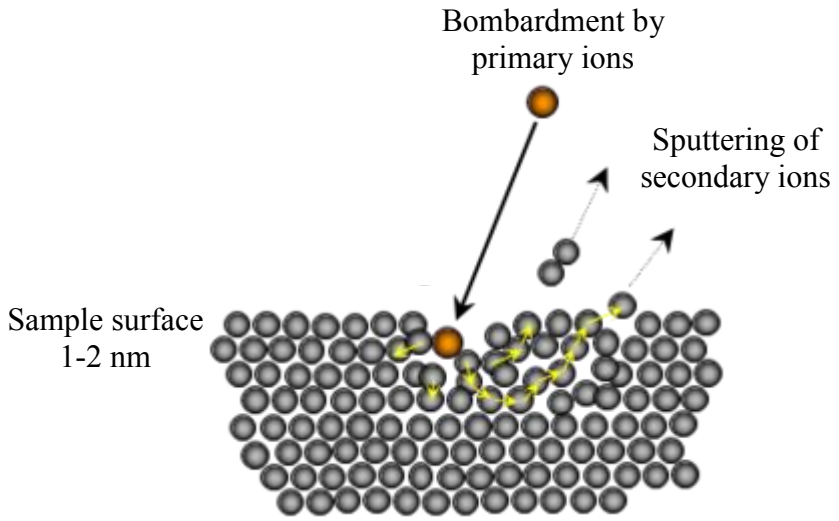

Figure 1.8: *A schematic showing the collision cascade (yellow arrows) that occurs by bombardment of a sample surface by a primary ion beam which leads to sputtering of secondary ions during SIMS analysis. Adapted from the National Institute of Standard and Technology (NIST).*

SIMS analysis that uses a low primary ion dose of $\leq 10^{13}$ ions per cm^2 is termed 'static' SIMS. This value is estimated through an approximation that one primary ion impacts an area of 10 nm^2. Therefore, to impact 1 cm^2 area, it would require 10^{13} ions to achieve the static limit [162]. Thus, to ensure the minimum damage to a sample, the primary ion dose should be kept below the static limit of 10^{13}. A ToF-SIMS instrument is mainly composed of an air-lock system, main analysis chamber, primary ion gun, time of flight mass analyser and electron flood gun as illustrated in Figure 1.9. The analysis of the samples by ToF-SIMS under ultra-high vacuum conditions (pressure $<10^{-8}$ Torr) allows the ion beam to operate in a consistent way, avoids the collision of the emitted ions with the gas phase molecules and decreases the chance for the sample surface chemistry to change or be contaminated during SIMS analysis [162].

1.7.1 Primary ion beam sources

Four types of the primary ion beam sources (surface ionisation, plasma, electron bombardment and field ionisation sources) are available and can be differentiated by the way that they produce the primary ion [162]. Only field

ionisation source is discussed here because it has been used in the ToF-SIMS instrument utilized for the analysis work in this thesis. In the field ionisation source, a very high electronic field is used to remove electrons from the atoms of a liquid metal such as bismuth which flows over a tungsten tip with a radius < 1 μm in the proximity of an extraction field ranging from 10 to 40 KeV. This causes a Taylor cone to be formed from which the primary ions are stripped [162]. Field ionisation sources are usually referred to as a liquid metal ion gun (LMIG) and they produce high current densities and a focusable ion beam and therefore they are preferred for static SIMS analysis because they offer much higher spatial resolution for imaging [164].

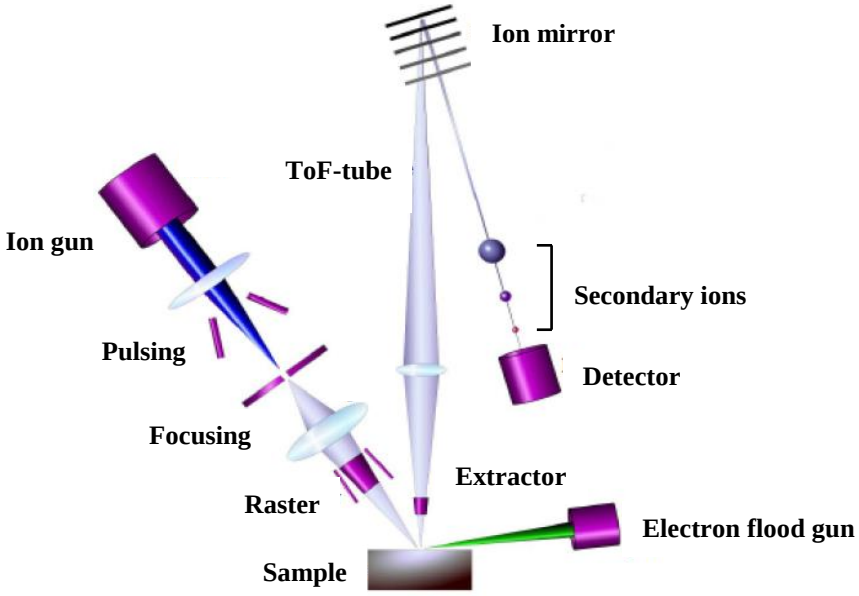

Figure 1.9: *A schematic showing the components of a ToF-SIMS instrument. Adapted from (©IONTOF GmbH).*

1.7.2 Cluster ion sources

Cluster ion or polyatomic ion sources such as Bi_n^+ or C_{60}^+ offer several advantages over monoatomic sources and have become widely used as primary ion sources. Monoatomic sources such as Ga^+ or Cs^+ possess a small size and high energy and can cause deep disruption to the sample on impact, subsequently less material is removed from the sample surface [165]. The use of cluster ion sources produce greater desorption of ions from the surface with

less penetration into the sample 'softer impact' since the energy is distributed between all the atoms in the cluster (i.e. less energy per atom) and remains closer to the surface of the sample. This produces a higher secondary ion yield with reducing damage to the sample [165-167]. It was reported that for certain organic materials, the C_{60}^{+} ion source produces a 30-100 fold increase in the secondary ion yield compared to a Ga^{+} source at the same energy [168]. This significant increase in ion yield by the use of cluster ion sources is especially useful for SIMS analysis of organic and biological materials which do not ionise as readily as inorganic materials. Additionally, it has been shown that the use of cluster ion sources results in a significant yield increase of the intact molecular species or the higher molecular weight fragment ions from the biological materials such as lipids and peptides associated with less damage to the sample surface [169, 170]. This improves the spatial resolution to the submicron level and opens new possibilities for the analysis of biological materials [170].

1.7.3 Mass analysers

The time-of-flight (ToF) analyser is considered the most popular analyser used for static SIMS analysis. It works by accelerating the secondary ions sputtered from the sample surface by the primary ion pulses to a given potential to produce ions having the same kinetic energy. The time required for the ions to travel through the ToF-tube, which has a known path length to impact on the detector, can be measured [162]. Therefore, ions with a higher mass will move slower to reach the detector compared to lower mass ions possessing the same kinetic energy. The detection of secondary ions by ToF analyser offer several advantages over other analyser types such as quadrupole analyser regarding the higher sensitivity level in addition to the detection of ions from a greater mass range with higher resolution [162, 171].

1.7.4 Charge compensation

Since most biomaterials are electrical insulators, the bombardment of a sample surface by positively charged primary ions increases the surface potential and

leads to charge accumulation on the surface and a net positive charge. This surface charge build-up can decrease or eliminate the signal of the emitted secondary ions [170]. Therefore, to counteract this effect, an electron flood gun is widely used to irradiate the sample surface with pulses of low energy electrons between the primary ion pulses which are attached to the high positively charged regions to neutralise them [162]. However, the electrons dose should be kept below 6.3×10^{18} electrons/m^2 to avoid the degradation of the sample surface [172, 173] as well as to reduce the electron-stimulated ion emission [170].

1.7.5 Ionisation and matrix effects

The ionisation and sputtering of the secondary ions from a sample surface is strongly affected by the electronic state at the material surface (molecular environment) which is commonly termed the matrix effects [162, 174]. These matrix effects prevent the ToF-SIMS instrument from being regarded as a quantitative technique. Generally, the quantification of ToF-SIMS data is challenging because the chemical environment from which a molecule is sputtered will affect the ionisation of that molecule either causing suppression or enhancement of ionisation [175, 176] which means that the secondary ion intensities (ion yields) are not directly proportional to the original concentration of molecules [177] and they can be changed according to the different chemical bonding to the matrix leading to a difficulty in the determination of absolute surface concentration [178].

Jones *et al.* investigated the effect of brain homogenate on the ionisation and detection of similar drug molecules differing only by the side chain addition, atropine (neutral molecule) and ipratropium bromide (positively charged salt). They concluded that the brain homogenate and more specifically the two main lipids, cholesterol and dipalmitoylphosphatidylcholine (DPPC), had significant different matrix effects on the ionisation and detection of the molecular ions of interest [179]. As illustrated in Figure 1.10, SIMS analysis of atropine and ipratropium bromide as pure materials on silicon shows a secondary ion yield

of atropine which is 2-3 times less than ipratropium bromide (Fig. 1.10a and b) but when mixed with brain homogenate, the secondary ion yield of atropine is 50 times less than ipratropium bromide (Fig. 1.10c and d). This suppression of ionisation can be due to the unfavourable environment for the formation of the molecular ion of atropine [179].

In another study Jones *et al.* demonstrated that in biological samples (multi-domain samples), the ability to detect the same analyte may be achieved with varying degree of success due to the matrix effects. The suppression of ionisation of an analyte in a mixture can happen due to the existence of other molecules and this depends on the chemical properties of the compounds within the mixture. The tendency of a molecule to form positively or negatively charged molecular ions depends on the relative acid/base properties of the molecules present which govern proton transfer. Additionally, Jones *et al.* concluded that care should be taken when looking at images from complex samples because the ion intensity of a molecule may be different from one area to another as a consequence of the difference in the chemical environment of these areas [180].

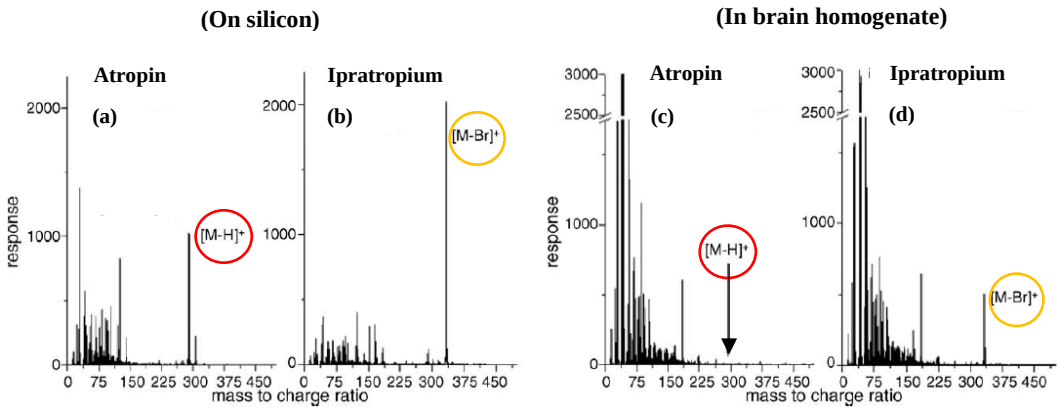

Figure 1.10: *SIMS analysis of (a) atropine on silicon, (b) ipratropium on silicon, (c) atropine in brain homogenate, (d) ipratropium in brain homogenate. Adapted from Jones et al.* [179].

1.7.6 ToF-SIMS analysis of biological tissues

ToF-SIMS provides a high mass resolution and chemical specificity for materials analysis which is important to discriminate between the complex structures in biological tissues. In addition, it produces high spatial resolution images of 1 μm for the complex multi-layered structures with sensitivity at ng/mL levels [170, 181, 182]. Furthermore, the preparation of samples for ToF-SIMS analysis is simple and does not require any extraction process often used in chromatographic methods or the addition of fluorescent tags or radio-labels [83, 163, 183] except the removal of the excess moisture from the samples prior the analysis [184]. The successful application of ToF-SIMS to analyse biological materials such as proteins [185, 186] and lipids [187-192] from either healthy [193-195] or diseased tissues [196-198] have been demonstrated in several studies. There is presently a limited number of studies that investigate the application of ToF-SIMS to map drug permeation into the skin [83, 161]. Judd *et al.* used ToF-SIMS to analyse permeation of CHG from 2% w/v aqueous solution into porcine skin [83]. The images of cross-sectioned skin samples are illustrated in Figure 1.11.

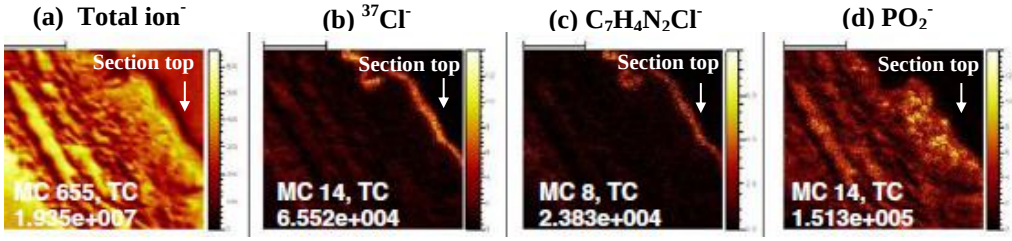

Figure 1.11: *ToF-SIMS ion images of cross-sectioned skin samples of CHG dosed porcine skin showing (a) total ion⁻, (b) $^{37}Cl^-$ ion, (c) CHG marker ion ($C_7H_4N_2Cl^-$) and (d) PO_2^- ion, where the scale bar represents 100 μm. Adapted from Judd et al.* [83].

Similarly, Sjövall *et al.* utilised ToF-SIMS to image the distribution of the active pharmaceutical ingredient (API) 'roflumilast' in mouse skin [161]. Figure 1.12 illustrates the ToF-SIMS ion images of the cross-sectioned skin samples treated with roflumilast solution.

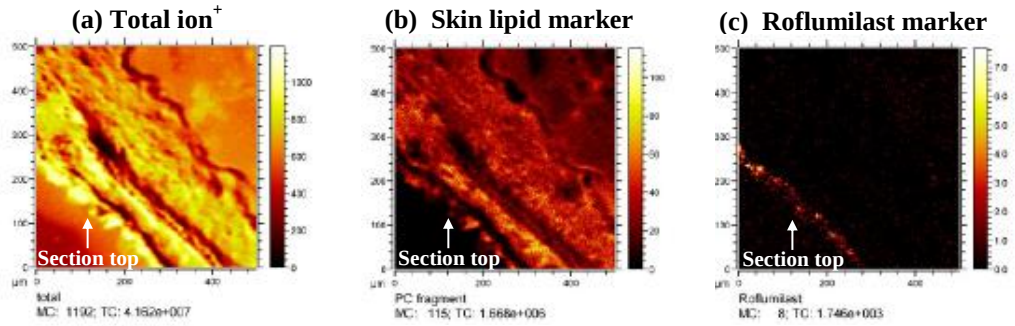

Figure 1.12: *ToF-SIMS ion images of cross-sectioned skin samples of roflumilast treated rat skin showing (a) the total ion$^+$, (b) skin lipid marker ion, and (c) roflumilast marker ion. Adapted from Sjövall et al.* [161].

1.7.7 Limitations of ToF-SIMS

The major limitation of ToF-SIMS analysis is its inability to produce quantitative results due to the matrix effects (Section 1.7.5) [170]. In addition, samples analysis by ToF-SIMS needs to be performed under ultra-high vacuum condition which is inappropriate for the *in vivo* real-time measurement (i.e. in-vacuum ToF-SIMS analysis minimises the application field to biopsies only). Furthermore, the ToF-SIMS instrument is an expensive instrument that limits its wide availability for analysis [163].

1.8 Enhancement of topical and transdermal drug delivery

The permeation of drugs into and across the skin is limited due to the effective barrier provided by the skin, particularly the *stratum corneum*. The following equation summarizes the factors affecting permeant flux into the skin:

$$\text{Flux} = \frac{\text{diffusion coefficient} \times \text{partition coefficient} \times \text{concentration}}{\text{membrane thickness}} \quad \text{(Equation 1.1)}$$

According to equation 1.1, the flux of permeant can be increased by changing the skin barrier properties (increasing diffusivity), the permeant nature (to increase partitioning) or to increase the concentration of the permeant in its

formulation (increase thermodynamic activity) [1]. Manipulation of the skin thickness is difficult, although thinner application sites can be chosen. For example, the scrotum and postauricular (behind ear) have been used for transdermal delivery of testosterone scopolamine respectively [199, 200]. In addition, some physical techniques such as microneedles can be used to overcome the *stratum corneum* barrier [201]. Figure 1.13 illustrates the general strategies for skin permeation enhancement to improve delivery of drugs into and through the skin [202, 203]. The work in this thesis (Chapter 4) involves the use of microemulsions and microneedles as enhancement methods. Therefore, they are discussed here in more details.

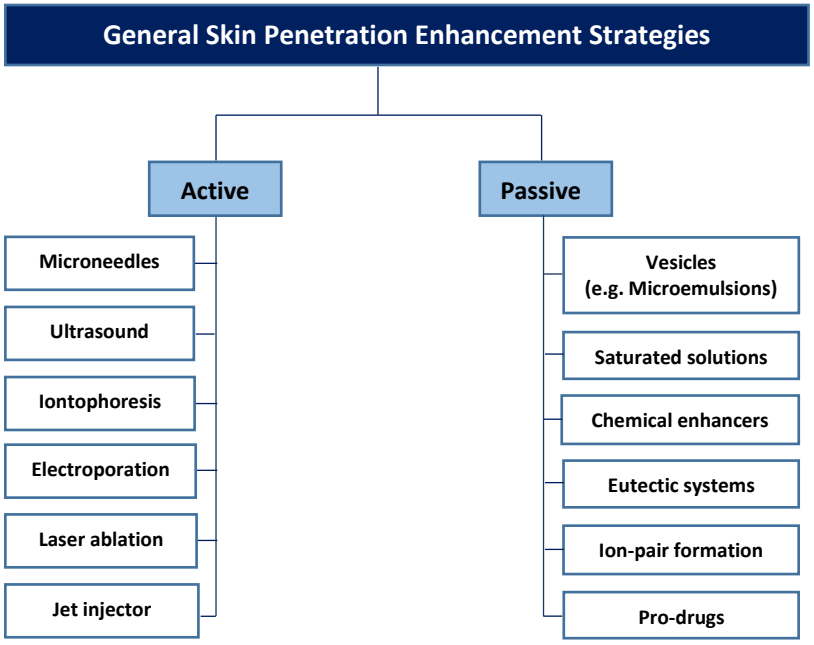

Figure 1.13: *General strategies for skin permeation enhancement. Adapted from Alkilani et al.* [202] *and Hadgraft. J, Lane E.M* [203].

1.8.1 Microemulsions

Microemulsions are transparent, thermodynamically stable, isotropic mixtures of an oil and aqueous phase with a surfactant and co-surfactant [204-207]. Microemulsions have received considerable attention as vehicles for drug delivery because of their high solubilisation capacity, thermodynamic stability, ease of formation and optical transparency [204, 205]. They have an ability to

improve the solubilisation of both lipophilic and hydrophilic drugs, which results in a high concentration gradient (thermodynamic activity) towards the skin. In addition, the microemulsion components such as the oil phase, surfactants and co-surfactants may serve as penetration enhancers to increase drug permeation [208]. Several studies have been shown the ability of microemulsions to increase transdermal drug delivery of both hydrophilic and lipophilic drugs in comparison to conventional vehicles [209-218]. For example, Sintov demonstrated that a w/o microemulsion of curcumin has shown significantly higher skin permeation compared to a micellar system, surfactant-oil mixture and a plain solution of curcumin [219] as illustrated in Figure 1.14.

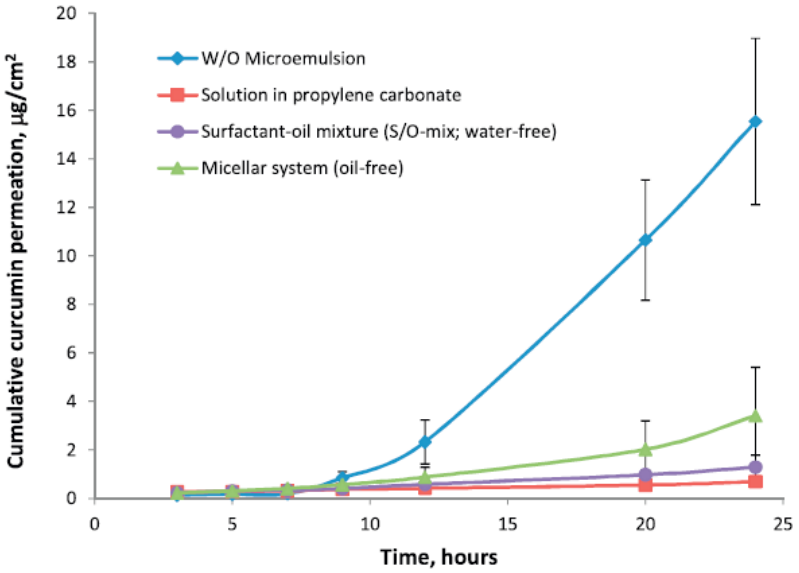

Figure 1.14: *Cumulative curcumin permeation (µg/cm^2) into rat skin following its application from a w/o microemulsion, micellar system, surfactant-oil mixture and plain solution in propylene carbonate, all formulations contained 1% w/w of curcumin with n = 4. Adapted from Sintov C.A. [219].*

Three types of microemulsion (oil in water, water in oil and bicontinous) can be formed depending on the proportion of their components as shown in Figure 1.15. When the oil content in the microemulsion is low, an o/w microemulsion is produced (Fig. 1.15a), conversely a w/o microemulsion is formed when the

ratio of water phase is low (Fig. 1.15c) and a bicontinuous microemulsion is produced when the amounts of water and oil are similar (Fig. 1.15b) [204, 205].

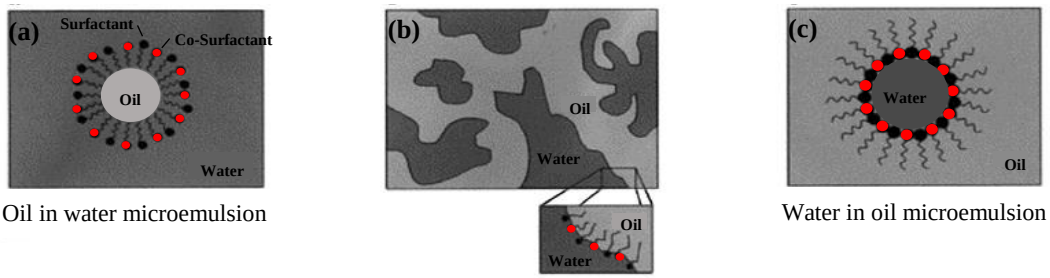

Figure 1.15: *Microemulsion types showing: (a) oil in water microemulsion, (b) bicontinuous microemulsion and (c) water in oil microemulsion. Adapted from Lawrence et al.* [205].

1.8.1.1 Microemulsions properties

The shape of the microemulsion droplets are usually represented as spheres (micelles) but they may also show asymmetrical shape such as a prolate ellipsoid or cylinder-like form [205, 220]. Microemulsions are transparent due to their small droplet size which is generally less than 100 nm in diameter and therefore they do not refract or scatter light. These nanodroplets create a large interfacial area and thus they need a large amount of surfactant/co-surfactant (S/Co-S) mixture to stabilise them approximately between 10%-40% [221]. The spontaneous formation of microemulsions and their high thermodynamic stability is a consequence of the very low interfacial tension ($<10^{-3}$ mN/m) at the oil/water interface which results in a very low free energy of the system and spontaneous emulsification of oil in water or water in oil [204, 221]. The great reduction in the interfacial tension is achieved by the addition of the co-surfactants [204, 207]. Co-surfactants provide the appropriate flexibility or fluidity of the surfactant film at the interface between oil and water phases by permitting the long hydrophobic tails of the surfactant to move freely at the interface and thus allow a greater penetration of the oil molecules into this region leading to a further decrease in the interfacial tension between the water

and oil phases [205, 207, 221]. A comparison between the properties of emulsions and microemulsions is shown in Table 1.1.

Table 1.1: *A comparison between the properties of emulsions and microemulsions. Adapted from Santos et al*. [204].

Property	Emulsions	Microemulsions
Droplet size	0.2-10 μm	<100 nm
Appearance	cloudy	transparent
Preparation	requires energy input	spontaneous formation
Stability	thermodynamically unstable	thermodynamically stable
Interfacial energy	high	very low

It is noteworthy that the term microemulsion (10^{-6}) is somewhat confusing because it describes a system containing droplets at nanosize diameter (10^{-9}). This confusion is a result of the historical development of the colloidal science since the first article to use the term microemulsion was published in 1961 before the growing interest in nano-technology field during the last decade [220].

1.8.1.2 Microemulsions components

1.8.1.2.1 Oil phase

Saturated and unsaturated fatty acids can be used as the oil phase of microemulsions with skin penetration enhancing effects demonstrated for a variety of drugs [222]. They have the ability to enter the hydrophobic bilayer of the *stratum corneum* and cause perturbation of the lipid arrangement to create separate domains for enhancing permeation [223]. For example, oleic acid showed a 28 fold increase in the flux of salicylic acid and a 56 fold increase in 5-fluorouracil flux through *ex vivo* human skin [4, 224]. Other oils that have been used as microemulsion oil phase are isopropyl myristate (IPM) [225], triacetin [218], isostearyl isostearate [226] and Miglyol 812 [227].

1.8.1.2.2 Surfactants

Non-ionic surfactants are widely utilised in topical formulations as emulsifying and solubilising agents. In addition, it was reported that they may influence the barrier properties of the *stratum corneum* [222, 228]. They either increase the fluidisation of the *stratum corneum* lipids or facilitate the partition of polar molecules across the barrier [222]. Tween 80 showed an improvement in the permeation of hydrocortisone [229] and lidocaine [230]. Similarly, Tween 20 enhanced 5-fluorouracil permeation through mouse skin [231]. In comparison with ionic surfactants, non-ionic surfactants have been reported to cause a minimum degree of skin irritation and toxicity [4, 204, 205]. Additionally, they are insensitive to pH and electrolyte concentration as ionic surfactants but they are more sensitive to temperature because of the decrease in their solubility with increasing temperature [205].

1.8.1.2.3 Co-surfactants

Short and medium chain alcohols such as ethanol and butanol are commonly used as co-surfactants to lower the interfacial tension required for the microemulsion formation [222]. Furthermore, they have skin permeation enhancing effects as ethanol and butanol have been shown to enhance the flux of estradiol and levonorgestrel respectively [232, 233]. However, the presence of alcohols as co-surfactants may cause additional skin irritation [204]. Chen *et al.* demonstrated that alcohol free microemulsions are less irritant to the skin [234]. Propylene glycol (PG) is used as a co-surfactant for microemulsions with permeation enhancing properties [222]. It increases the permeation of drugs by enhancing drug solubility in the *stratum corneum* in addition to the solvent drag effect [235]. Furthermore, it was reported that PG does not cause skin irritation [236]. The other component of microemulsions is the aqueous phase in which water is generally used [222].

1.8.1.3 Construction of pseudo-ternary phase diagrams

Phase diagrams are generally used as a means to delineate the area of existence of the microemulsion region [204, 221]. A pseudo-ternary phase diagram contains 3 axes and since there are 4 components in the microemulsion, frequently one of the axes is designated as a fixed ratio of two components (usually surfactant/co-surfactant). The other two axes represent the water and oil phases. Firstly, the surfactant and the co-surfactant are mixed together at a certain ratio to form the surfactant/co-surfactant (S/Co-S) mixture. The S/Co-S mixture is then mixed with the oil phase at varying ratios from 1:9 to 9:1 in multiple glass vials and titrated step by step with water using water titration method [237] while the mixture is being stirred by a magnetic stirrer at a moderate speed. Following each addition, the microemulsion is inspected visually for transparency and the proportion of each component is calculated and recorded. The different proportions of the microemulsion components at which microemulsion was formed are plotted to generate the microemulsion region within a pseudo-ternary phase diagram [221].

1.8.1.4 Characterisation of microemulsions

In addition to microemulsion formation, the mixture of oil, water, surfactants and co-surfactants can form other colloidal structures such as emulsions or liquid crystals depending on the ratio of each component. These other structures can be distinguished from microemulsions by visual examination or with the aid of the polarised light microscope since they are not isotropic as microemulsions [204, 207]. Emulsions can be easily recognised because they are non-transparent cloudy liquids and the liquid crystalline hexagonal, cubic or lamellar structures show solutions of higher viscosity and under the polarised light they are anisotropic structures [207]. Other tests that can assist in the characterisation of microemulsions are dynamic light scattering, viscosity and conductivity measurements in addition to freeze-fracture TEM that permits the direct visualisation of the microemulsion structure [204, 205].

1.8.1.5 Limitations of microemulsions

Some of the limitations of microemulsions are due to the fact that the evaluation of their efficacy and safety is mostly carried out on animal skin which may be not quite representative and predictive of the human skin. Other issues include irritation and toxicity offered by the use of high concentration of S/Co-S mixture required for microemulsion formulation [204] (i.e. excipient acceptability is a significant problem associated with microemulsions formulation) [205].

Due to the numerous advantages offered by microemulsions as a drug delivery system, they have been widely used as an enhancement strategy to improve skin permeation for variety of hydrophilic and lipophilic drugs. However, their potential role to enhance skin permeation of imiquimod to treat BCC lesions has not yet explored.

1.8.2 Microneedles

Since the passive methods of skin permeation enhancement showed a limited efficiency in improving drug permeation, particularly for the delivery of large drug molecules and vaccines, physical methods like microneedles have been developed and show great promise in this field [201]. Microneedles provide a minimally invasive means to transport drug molecules into and across the skin. Microneedles are composed of small micron sized needles (50-900 μm in height) which pierce the skin to create microchannels through which the drug molecules can be more easily transport [238-240]. Microneedles combine the simple and easy use of a transdermal patch with the efficiency of delivery accomplished by conventional hypodermic syringe [202]. They have the advantages of bypassing the *stratum corneum* and penetration into the viable epidermis layer avoiding nerves and blood vessels located in the dermis and therefore they are generally considered by many research groups to be painless [241-243]. This can improve patient compliance and adherence to the treatment. However, the degree of pain is related to the height of microneedles applied, the greater the height of microneedles the greater the sensation of pain.

Thus, microneedle height should be optimised to minimise the pain and at the same time enhance the drug delivery across the skin [244]. Unlike hypodermic injections, microneedles are minimally invasive injections and generally do not cause bleeding or require trained personnel for administration and can be applied by patients themselves (i.e. self-administration) [202, 245] since they are fabricated as a microneedle patch which can be applied using thumb pressure or they can be applied by a microneedle applicator [246].

Several studies reported the efficacy of microneedles to deliver a wide range of drugs into and through the skin, ranging from low molecular weight drugs such as alendronate [247] and ibuprofen [248] to macromolecules such as insulin [249, 250], desmopressin [251], low molecular weight heparins [252], gene therapies [253, 254] and vaccines [255]. For example, microneedles have been investigated by Donnelly *et al.* [256] for their potential role to enhance intradermal delivery of the porphyrin precursor 5-aminolevulinic acid (5-ALA) used in the topical photodynamic therapy of BCC. They used silicon microneedle arrays *in vivo* to enhance skin penetration of 5-ALA into mice skin. They found that microneedle pre-treatment could induce a significant higher level of the photosensitiser protoporphyrin IX (PpIX) in the skin compared to intact skin untreated with microneedles as illustrated in Figure 1.16.

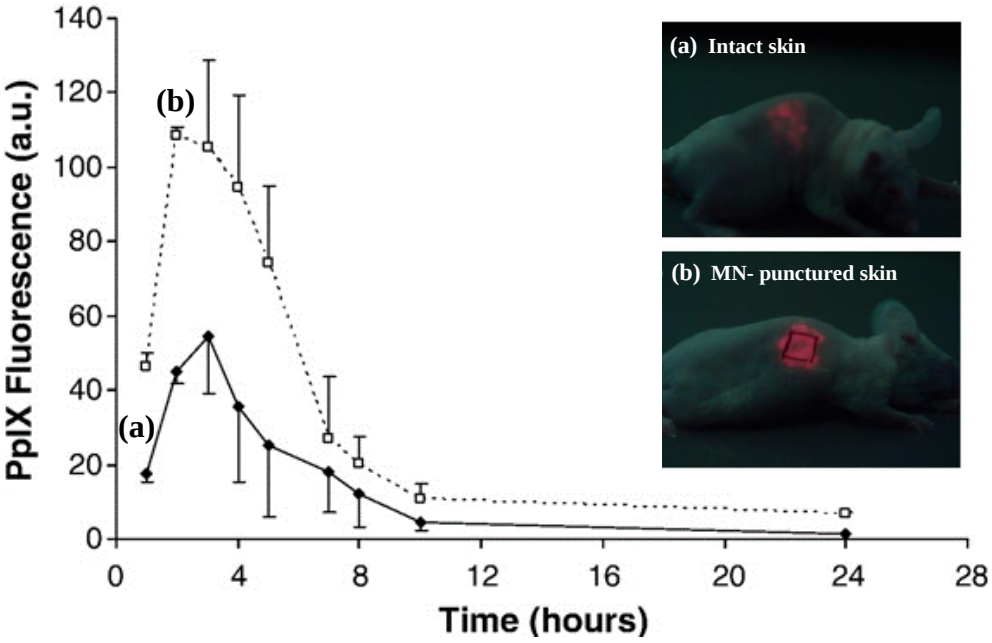

Figure 1.16: *Protoporphyrin IX (PpIX) fluorescence intensity and accumulation in murine skin at the site of application after 1 hr. application of bioadhesive patch containing 5 mg of 5-ALA to (a) intact skin (◆) and (b) MN-punctured skin (□). Mean ± SD, n = 3. Adapted from Donnelly et al.* [256].

1.8.2.1 Types of microneedles

Microneedles can be divided into four types, as shown in Figure 1.17, depending on the way they deliver drugs into the skin [201, 202, 245, 257], these are:

1. Solid microneedles (‘poke and patch’) can be used as a skin pre-treatment. The skin is punctured by intact solid microneedles followed by the application of a drug formulation.

2. Coated microneedles (‘coat and poke’) where the microneedles are coated with a drug formulation with a subsequent dissolution of the formulation after insertion into the skin. This approach solves the problem of two-step application of solid microneedles but has limitation in drug loading and delivery owing to the small dimensions of the microneedle tip.

3. Dissolving microneedles (‘poke and release’) where the drugs are encapsulated within a dissolving biodegradable microneedle array. This strategy has the advantages of elimination of the need for sharps disposal and the likelihood of accidental reuse of microneedles.

4. Hollow microneedles (‘poke and flow’) for infusion of a liquid drug solution through microneedles into the skin. Delivery of drug solutions through the microneedles into the skin can be achieved by a syringe.

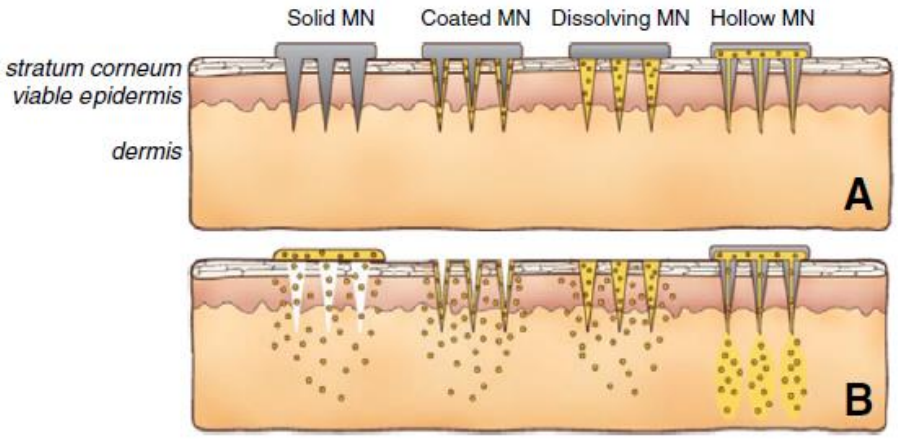

Figure 1.17: *Types of microneedles and methods of drug delivery into the skin using microneedles, showing (A) microneedles types applied on the skin and (B) delivery of drugs from these microneedles. Adapted from Kim et al.* [201].

1.8.2.2 Microneedles fabrication

The majority of microneedles are made from silicon or metal [258]. However, some of them are made from glass [259], dextrin [260], maltose [261] and polymers [262, 263]. Microneedles can be fabricated at different lengths, diameters, shapes and needle density [258, 264]. A microneedle array of an area less than 1 cm^2 can be fabricated to contain hundreds of microneedles [1]. The different fabrication methods used to manufacture microneedles are based on the microfabrication techniques such as photolithography, etching methods, laser cutting, metal electroplating and micromolding [201, 245].

1.8.2.3 Factors affecting microneedles efficacy

To obtain effective skin penetration capable of improving drug delivery, the microneedles should be sharp, robust and have the ability to withstand the lateral forces experienced by the skin during microneedle insertion but with some degree of flexibility (i.e. the microneedles should show sufficient strength to penetrate the skin without bending or breaking and to counteract the skin elasticity) [258]. The performance of the microneedles is dictated by the needle height, thickness, shape, tip-radius, base diameter, geometry and density of the array in addition to the force and method of application. These factors determine the overall insertion and breaking force of the microneedles. For effective and safe use of the microneedles, microneedles should be fabricated with a low insertion force and high fracture force (high margin of safety) [258, 265]. The margin of safety is the ratio of the fracture force to the insertion force and microneedles can be inserted without breaking if they show margin of safety values of greater than one [239, 266]. A noteworthy point is that the most important feature in microneedle design which leads to efficient insertion of microneedles is the tip-radius. A microneedle with a smaller tip radius is sharper and therefore penetrates the skin more smoothly and efficiently than one with a larger tip radius [267].

1.8.2.4 Techniques used to detect microneedle insertion

There are several techniques that have been used to demonstrate successful microneedle insertion and formation of the microconduits within skin [268]. Staining of microneedles treated skin with dyes such as gentian violet [269, 270], methylene blue [254, 271] or trypan blue [272, 273], measurement of the electrical impedance [274] and transepidermal water loss (TEWL) monitoring [275] are usually techniques used to detect the skin disruption caused by microneedle treatment. However, these techniques cannot provide information regarding the insertion depth of the microneedles as well as the dimensions of the created microchannels [268]. Therefore, other techniques have been utilized to overcome these difficulties including the histological examination of the stained cryo-sectioned skin samples following microneedles treatment

[276], the use of confocal laser scanning microscopy (CLSM) [277] and more recently the application of optical coherence tomography (OCT) [238, 278].

1.8.2.5 Limitations of microneedle therapy

Although, microneedles offer several advantages for enhancing drug permeation into or through the skin to produce local or systemic effects respectively, there are some challenges and safety issues that need to be addressed in order to make microneedles available for clinical use by patients. Microneedles limitations include the scale up production of microneedles to the industrial levels and the lack of specific quality standards, the irritation or skin trauma that may result from the long-term use of microneedles and pore closure following microneedle application as it relates to the microbial contamination and the risk of infections. In addition, there are some concerns about drug loading dose and the relevant therapeutic concentration of drugs achieved by microneedles application [202, 245, 279, 280].

Dermal and transdermal drug delivery using microneedles offers a great opportunity to enhance drug penetration into and across the skin. This is reflected by the increased number of studies that utilise microneedles as an enhancement strategy with some success demonstrated in clinical testing. However, to date there is no published data regarding the use of the microneedles to improve delivery of imiquimod into the skin to treat BCC lesions. Microneedle therapy can provide a promising approach to directly deliver imiquimod at appropriate therapeutic concentration to the basal layer of the epidermis where the tumour cells are located.

1.9 Tissue homogenisation methods

Tissue homogenisation or disruption is mostly used as an early and essential step in the process of isolation and quantification of proteins, DNA, RNA or analytes from intact tissue samples [281]. There are two main methods available for tissue disruption including chemical methods and

mechanical/physical methods. The choice of the method used is largely dependent upon the researcher's objectives (the method type should be dictated by the characteristics of the final homogenate). For example, if active proteins are required especially those which are affected by heat, then any step or process which leads to heat generation should be eliminated from the homogenisation protocol [282]. Another factor which may play a role in method selection is the sample throughput. A high throughput method is desirable to process hundreds of samples, but in turn, this may require a trade-off with the homogenisation effectiveness because a multi-step method may be more effective than the high throughput one step process [281].

1.9.1 Chemical methods

A chemical method is often preferred for the disruption of cultured cells in which the cellular components are liberated using either lysis buffers, detergents (surfactants) or lytic enzymes [282]. Intact hard tissues and solid samples are not efficiently homogenised by a chemical method alone. Therefore, a combination of chemical and mechanical methods are used in order to be more effective which has been demonstrated in studies requiring the homogenisation of lung, heart [283] and skin [284].

1.9.2 Mechanical methods

In mechanical homogenisation methods, tissue disruption occurs by applying an external force to the samples such as grinding, shearing, beating and shocking. Mechanical methods have the advantage of not introducing unwanted chemical molecules into the sample. Additionally, many proteins remain unaffected and intact after liberation from the cell which is useful for the isolation of proteins and enzymes assay [282]. Tissue homogenisation by mechanical methods can be carried out by mortar and pestle, Dounce homogenisers, rotor-stator homogenisers, beads beating homogenisers and sonication methods [281, 282]. Combined mechanical methods or multi-step homogenisation approaches offer a powerful strategy to obtain a uniform tissue homogenate with the liberation of nearly all analytes of interest [281]. The

initial step in this process involves reduction of the intact tissue size into smaller parts, whereas the second step is further disruption of these parts to release all cell components. The balance between the high efficiency of the two or multi-step process to liberate the key analytes and the increased processing time per sample should be dictated by the researcher's objectives [282].

Skin is a tough fibrous tissue with resilient properties and as such is relatively difficult to homogenise by a single method or in a one step process [282, 285]. Therefore, combined methods, or multi-step methods, are needed to obtain a uniform skin homogenate. Nirogi *et al.* reported the effectiveness of using a combination of lytic enzymes and mechanical methods to liberate and quantify analytes within skin. In this work by Nirogi *et al.* rat skin exposed to diclofenac gel was first incubated with collagenase enzymes at concentration of 0.25% w/v for 16 hours, then homogenised by beads in a beater mixer mill for 5-10 minutes and rotor-stator homogeniser for 30 seconds, followed by liquid-liquid extraction with methyl tert butyl ether (MTBE) solvent to quantify diclofenac in skin by LC-MS [284]. Although, this method achieved a uniform skin homogenate, the addition of chemicals or enzymes as a first step to aid in the homogenisation process may influence the chemistry of skin or introduce new chemical groups which may interfere with the ion signal of a compound of interest when analysed by ToF-SIMS. Therefore, it is thought that the development of another skin homogenisation method without the addition of enzymes is required for skin samples analysed by ToF-SIMS.

1.10 Microarray printing

The transfer of a liquid onto a solid surface to form microscopic spots in a particular pattern is called microarray printing [286]. Microarray technology allows a rapid and cost-effective screening of thousands of materials in a single analysis session by printing micron scale spots on a solid substrate [286]. A microarray can be produced by various surface patterning techniques, such as photolithography, electron beam lithography, soft lithography, nanolithography and direct-writing (robotic spotting) [287, 288]. Of these techniques, the most

common one is the direct-writing technique due to its simplicity, high throughput, flexibility in patterns design and suitability to wide range of samples [288, 289]. In direct-writing, thousands of different solutions can be removed from a well plate using a moving print head containing either a print pin or nozzle to be positioned onto a substrate at the desired location. Direct-writing can be divided into direct contact printing and non-contact (ink-jet) printing [286, 288] as illustrated in Figure 1.18.

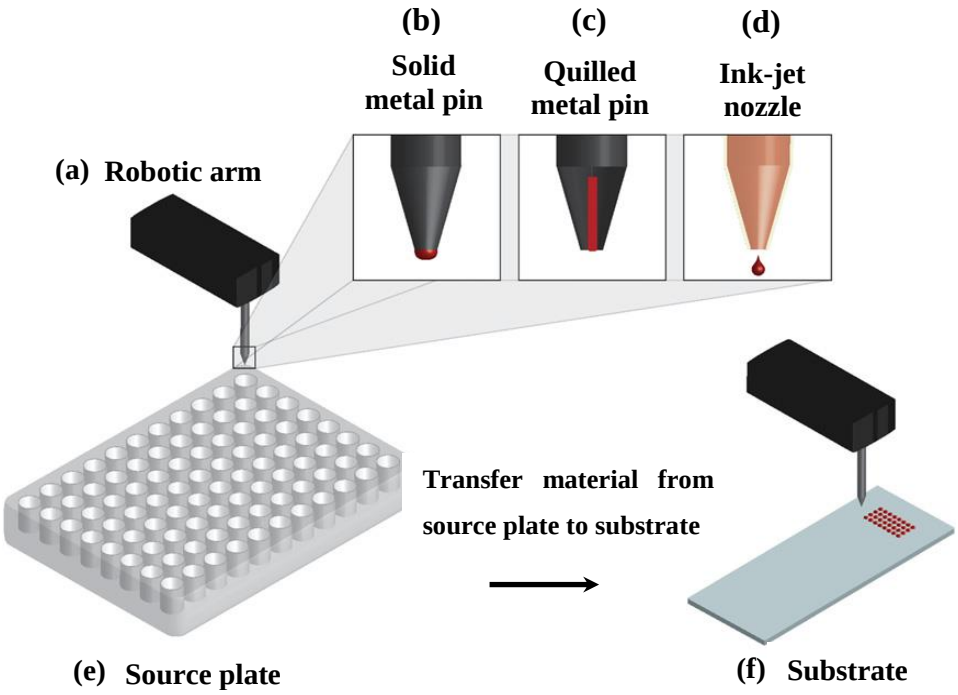

Figure 1.18: *A schematic of the formation of a microarray using direct contact and non-contact printing. The solid pin (b) and quilled pin (c) used for direct contact printing, whereas ink-jet nozzle (d) used for non-contact printing. Adapted from Hook et al.*[289].

1.10.1 Direct contact printing

As shown in Figure 1.18, microarrays formed by direct contact printing involve the use of a robot arm (a) connected to a pin (b or c) which first dips the pin into a solution in a well plate (e), then spots onto the substrate surface (f) at a desired location by making contact. The pin can be either a solid (Fig. 1.18b) or quill pin (Fig. 1.18c) (containing a slit or groove) [286, 288-290] and is

usually fabricated from stainless steel or tungsten for strength and durability [291]. A solid pin has the advantage of easier washing, most appropriate for printing viscous solutions [290] and no variation in the deposition volume during printing (the last spot can be exactly printed as the first spot) because the pin revisits a sample well plate after each spotting. However, this revisiting of the well plate results in lowering printing speed and increasing time required to complete array printing. Another issue associated with a solid pin is the evaporation of a captured liquid droplet before spotting when using volatile solutions or working in an evaporative environment [291].

A quill pin that has a slit reservoir is able to draw up a solution and produce more spots from a single dip before a refill is required, leading to faster printing [288, 289]. Additionally, this reservoir protects the sample from air, thus the evaporation of a liquid droplet from the tip is less severe than a solid pin [291]. A quill pin is more difficult to clean and susceptible to slit clogging by viscous and sticky samples. Therefore, it is not preferred to use for viscous solutions. Otherwise, efficient washing steps are required to prevent slit blocking [288, 291] which can be time consuming and ineffective. Control of the printing environment such as temperature and humidity is also important to obtain high quality, consistent and reproducible arrays [291]. The size of the printed spot in direct contact method is dependent on the pin shape, size and diameter [289, 291].

In general, the direct contact printing method provides a powerful tool for research applications due to its adaptability to a wide range of sample types, spot reproducibility and an easy cleaning system owing to the absence of an aperture (required for ink-jet printing) that may become blocked. Some limitations associated with direct contact printing include that the volume of a solution removed and deposited by a pin is not easily adjustable and that surface damage can result from the direct contact with a pin especially on delicate surfaces, such as 3D gels and nitrocellulose [286, 291]. Direct contact microarray printing has been successfully applied for the formation of DNA

[292], protein [293], polymer [294] and cell microarrays [295]. An example of a protein microarray is illustrated in Figure 1.19 in which green fluorescent proteins (GFP) were printed at specific concentrations on activated slides. Following incubation, fluorescence intensities were determined for each standard to generate a calibration curve [296]. However, to date it is not known if the microarray printing of a homogenised skin tissue with drug solutions to generate a calibration curve can be achieved.

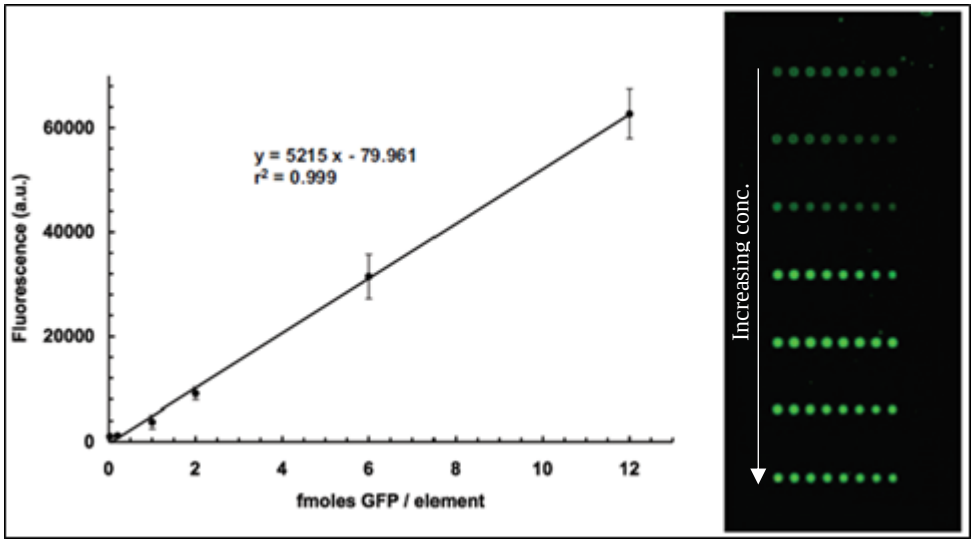

Figure 1.19: *Calibration curve of green fluorescent protein (GFP) generated from the printed microarray used for the determination of unknown protein amounts. Adapted from Zarate et al.* [296].

1.10.2 Non-contact printing

Non-contact (ink-jet) printing also uses a robotic arm but in this case to move a nozzle (Fig. 1.18d) that draws up the determined volume of a solution from a well plate and then ejecting nanolitre or even picolitre volumes at the specified location onto a substrate surface [286]. The spot size is determined by the droplet volume and the surface energy of the printed solution and the substrate [289]. This technique has several advantages in avoiding the issues that occur with pins, such as contamination of the tips due to insufficient cleaning, substrate damage because of the direct contact with a pin and variations in the spot volume [286, 288]. Ink-jet printers are less suitable for high viscosity

samples due to blockage of the nozzle orifice by material aggregates. In addition, rapid evaporation of a solvent form the printed picolitre sized spot can result in uneven distribution of the deposited material [286, 289]. Ink-jet printing has been successfully used to produce microarrays for drug screening purposes [297], high throughput cell patterning [287] and hydrogel microarray formation from polymers [298].

1.11 Aims of this thesis

The 1st aim of this thesis is to investigate the potential role of ToF-SIMS to map the permeation depth and visualise the spatial distribution of drugs permeated into the skin with a quantification aspect using imiquimod and chlorhexidine as model drugs.

The 2nd aim is to enhance imiquimod permeation into the lower epidermal layers of the skin, specifically the basal layer using microemulsions and microneedles enhancing strategies.

The objectives of the 1st aim are:

- To assess skin permeation of imiquimod from Aldara™ cream and from simple solvent systems in DMSO and oleic acid using Franz diffusion cells, skin tape stripping and skin cross-sectioning with subsequent analysis by HPLC and ToF-SIMS.
- To investigate the effect of concentration, type of vehicle and application time on chlorhexidine permeation into the skin using *in vivo* tape stripping of human volunteers and *ex vivo* porcine skin with subsequent ToF-SIMS analysis.
- To quantify ToF-SIMS data in the test samples depending on calibration curves generated by microarray printing of a skin homogenate with drug solutions at different concentrations.

The objectives of the 2nd aim are:

- To formulate, characterise and investigate the permeation enhancing ability of microemulsions of imiquimod to improve delivery of imiquimod over Aldara™ cream.
- To determine the ability of stamp pen microneedles to penetrate the skin and to enhance delivery of imiquimod when they are used as skin pre-treatment followed by the application of microemulsions or Aldara™ cream.

2 Chapter Two: Quantifying ToF-SIMS Data Using Microarray Printing of Drugs with Skin Homogenate

2.1 Introduction

As discussed in Chapter 1, Section 1.7.6, ToF-SIMS possesses several advantages which can be utilised for drug detection and mapping in biological samples, these advantages include relatively high spatial resolution of 1 μm, a large mass range > 7000 with high chemical specificity and sensitivity at ng/mL levels [170, 181, 182]. In addition, samples do not require laborious preparation, fluorescent tags or radio-labels [163, 183]. However, the major limitation of ToF-SIMS is its inability to produce quantitative results due to the matrix effects [170, 299] as detailed in Chapter 1, Section 1.7.5. Matrix effects can be overcome by assessing the ionisation of drug molecules within an identical or similar chemical environment [171, 175]. This is achieved by adding known amounts of a drug of interest at different concentrations to a tissue or model matrix to generate a calibration curve used in the quantification process [175]. For example, dextran has been used as a model matrix to quantify boron concentration in cell cultures. Dextran was selected because of its matrix similarity to cells and tissue matrices since it composed of long chain hydrocarbons containing carbon, hydrogen and oxygen [300, 301]. Henss *et al.* investigated the quantification of calcium in bone using ToF-SIMS and concluded that calcium quantification is possible when standards of calcium hydroxyapatite collagen scaffold were used as calibration reference samples. The use of this scaffold, which is similar in its composition to bone tissue, results in negligible matrix effect differences between the standards and bone [176]. To quantify ToF-SIMS data for a drug within skin, skin homogenate represents the ideal matrix for this purpose due to its identity and relevance to real skin tissue. The available method which was developed by Nirogi *et al.* [284] (discussed in Chapter 1, Section 1.9.2) used a combination of lytic enzymes and mechanical methods to obtain skin homogenate. It is thought that the addition of chemicals or enzymes as a first step to aid in the homogenisation process may influence the chemistry of skin or introduce new

chemical groups which may interfere with the ion signal of a compound of interest when analysed by ToF-SIMS. Therefore, the work in this chapter involves the development of a multi-step mechanical method for skin homogenisation without the need of enzymes addition. The work also manages for the first time to microarray print skin homogenate with known concentrations of imiquimod and chlorhexidine solutions to investigate the concentration effect on ion intensity (discussed in Chapter 1, Section 1.10.1).

2.2 Chapter Aims

The aim of this chapter is to quantify drug concentration within skin for samples analysed by ToF-SIMS. This can be achieved by microarray printing of a mixture of a drug at known concentrations with skin homogenate to generate a calibration curve used in the quantification process. Using this method any matrix effects could be overcome as the ion intensities of compounds of interest are measured from the identical matrix (skin homogenate) as the analysed material (skin tape strips and cross-sections). In addition, the microarray printing approach is not only high throughput in sample generation, thereby making multiple sample repeats obtainable, but is amenable to a high throughput analysis of many samples simultaneously. This work represents the first attempt or a 'proof of concept' for the quantification of a drug within skin when analysed by ToF-SIMS.

2.3 Materials and Methods

2.3.1 Materials

Imiquimod was purchased from Bioscience Life Sciences, UK. Chlorhexidine gluconate 20% w/v aqueous solution was ordered from Alfa Aesar, USA. Oleic acid, DMSO and IPA were purchased from Sigma-Aldrich, UK. Acetone was obtained from Fisher Scientific, UK. Teepol solution (Multipurpose detergent) was ordered from Scientific Laboratory Supplies, UK. Deionised water was obtained from an ELGA reservoir, PURELAB® Ultra, ELGA, UK. All reagents were of analytical grade, unless otherwise stated.

2.3.2 Skin preparation

Skin was prepared from pig ears obtained from a local abattoir, animals were aged approximately 6 months and the skin was acquired prior to any steam cleaning process. The skin was washed with distilled water and dried using tissue. Hair was carefully cut with scissors and the skin's subcutaneous fatty layer was removed using a scalpel in preparation for the homogenisation process.

2.3.3 Skin homogenisation

Several mechanical methods were investigated to obtain skin homogenate, including mortar and pestle, Dounce homogeniser, Retsch® mixer mill and rotor-stator homogeniser as illustrated in Figure 2.1.

2.3.3.1 Mortar and pestle

In cryogenic grinding by mortar and pestle (Fig. 2.1a), a piece of skin (1 × 1 cm^2) was snap frozen in liquid nitrogen to make it brittle and easy to fracture. It was then placed in a clean porcelain mortar and pressed by a pestle in a circular motion with downward pressure to fragment the skin into smaller pieces.

2.3.3.2 Dounce homogeniser

A Dounce homogeniser (GPE Limited) (Fig. 2.1b) was applied to a section of skin tissue (1 × 1 cm^2) alongside 3 mL of deionised water in a long tube and a pestle was inserted and pressed down and then lifted to shear the skin tissue.

2.3.3.3 Retsch® Mixer Mill

A Retsch® mixer mill (MM301, Germany) (Fig. 2.1c) was used which involves crushing tissue with beads. The skin was snap frozen in liquid nitrogen and placed with stainless steel grinding balls inside a tube which was again snap frozen in liquid nitrogen and rapidly shaken by back and forth motion at a vibrational frequency of 5 Hz /second for 10 minutes.

2.3.3.4 Rotor-stator Homogeniser

A Rotor-stator homogeniser (Ultra-Turrax, T25, IKA, Germany) (Fig. 2.1d) was used for skin homogenisation. Sections of skin tissue (1 × 1 cm^2) were cut with scissors into very small pieces in an aluminium foil covered petri dish. After that, they were carefully transferred into a clean plastic test tube and 2 mL of distilled water was added to them. Samples were left in water for approximately 1 hour and then homogenised using a rotor-stator homogeniser at full speed (24000 rpm) for 15 minutes. Following this, the uniform mass of skin homogenate was poured into a clean petri dish and left to air dry for approximately 2 hours at ambient temperature to be used further in the next steps of microarray printing.

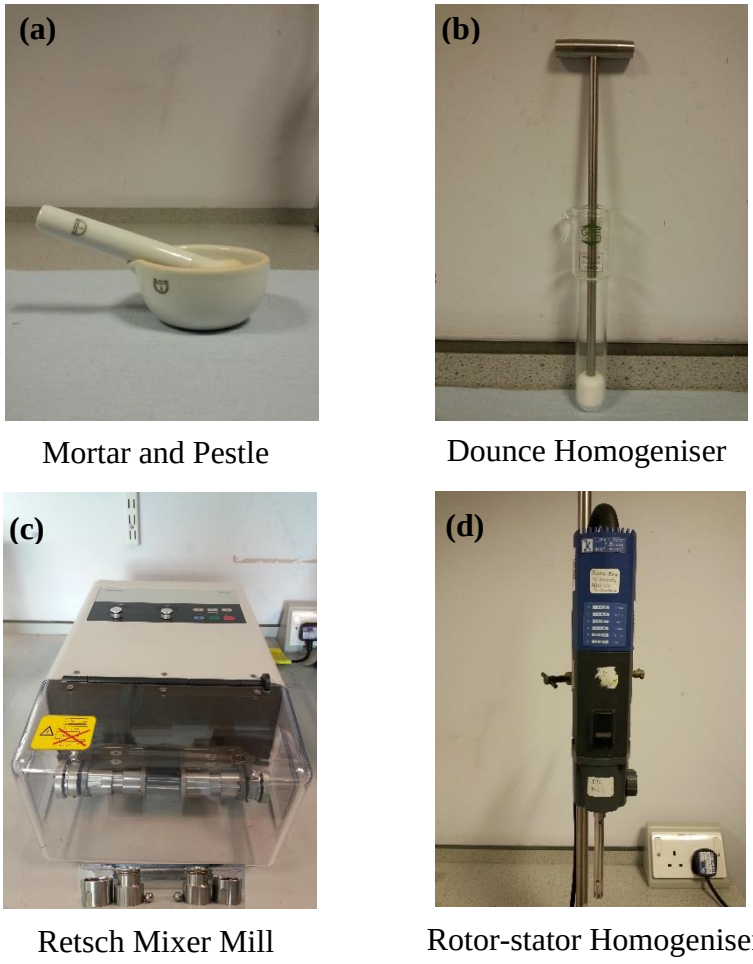

Figure 2.1: *Images of the instruments used in the development of skin homogenisation, specifically: (a) mortar and pestle, (b) Dounce homogeniser, (c) Retsch mixer mill and (d) rotor-stator homogeniser.*

2.3.4 Preparation of drug solutions

Stock solutions of imiquimod in DMSO at a concentration of 3 mg/mL and in oleic acid at concentrations of 20 mg/mL and 4 mg/mL were prepared by dissolving accurately weighed amounts of imiquimod in a specified volume of each solvent using volumetric flasks. For chlorhexidine gluconate (CHG), stock solutions in water and IPA 70% v/v were prepared at concentration of 2 mg/mL from the standard solution of 20% w/v. Following this, diluted solutions from each stock solution were prepared at different concentrations to make a calibration curve in each solvent. For imiquimod in DMSO, the concentrations prepared were 0.3, 0.6, 0.9, 1.2, 1.5, 1.8, 2.1, 2.4, 2.7 and 3.0 mg/mL. For imiquimod in oleic acid the concentrations prepared were 2, 4, 6,

8, 10, 12, 14, 16, 18, and 20 mg/mL from the 20 mg/mL stock solution and 0.05, 0.1, 0.2, 0.4, 0.6, 0.8, 1.0, 1.2, 1.4, 1.6, 1.8, 2.0, 2.5, 3, 3.5 and 4.0 mg/mL from the 4 mg/mL stock solution. For the first printing attempt of CHG in water and IPA 70% v/v (sonication bath trial), the concentrations were 0.2, 0.4, 0.6, 0.8, 1.0, 1.2, 1.4, 1.6, 1.8 and 2.0 mg/mL, the other attempt (probe sonication) was done with lower range of concentrations of 0.0078, 0.0156, 0.0312, 0.0625, 0.125, 0.25, 0.50, 0.75, 1.00, 1.25, 1.50, 1.75 and 2.00 mg/mL.

2.3.5 Mixing of drug solutions with skin homogenate

A consistent amount of dried skin homogenate was weighed on a balance (approximately 50 mg ± 1%) and placed in an Eppendorf vial, then 250 µL of each drug solution (imiquimod or CHG) at a specific concentration was added and sonicated to obtain a uniform dispersion of skin homogenate with a drug solution. In the first attempts, the vials containing skin homogenate and drug solutions were sonicated in a sonication bath (Fisher Scientific FB 15050, Germany) for 30 minutes. Further attempts employed a probe sonicator (BANDELIN Sonoplus, Germany) which was used for 2 minutes to mix drug solutions with skin homogenate instead of the sonication bath. The probe was cleaned with water and acetone following each run. Drug concentration was expressed as µg of a drug in mg of skin homogenate.

2.3.6 Microarray printing of drugs with skin homogenate

From Eppendorf vials containing uniform dispersions of skin homogenate with a drug, 100 µL were pipetted and transferred into polypropylene well plates ready for microarray printing. Microarray printing was carried out using a contact printer (BIODOT) with micro spotting quill pin (ArrayIt®, Catalog ID = 946MP6B). In the initial printing trials, acetone was used alone to clean the printing pin. Subsequent trials employed a triple washing method with detergent (Teepol® 3% v/v solution), water and acetone. Five repeats from each drug concentration solution were printed, in addition to a skin control and solvent blank. Following printing, slides were snap frozen in liquid nitrogen and placed in a freeze dryer (VirTis SP scientific, Sentry 2, USA) for one hour

at a temperature of -60 ^{o}C and vacuum pressure of 14 mT prior to ToF-SIMS analysis. Temperature and humidity were kept constant during printing at 21 ^{o}C and 41% respectively.

In addition to printing with a quill pin (containing a slit inside), a customised solid pin (without any slit) was made at the Medical Engineering workshop, The University of Nottingham and used in the microarray printing of the dispersion of skin homogenate with a drug during trials to improve the printing quality. The dimensions of the pin are as follows: the pin length is 22 mm with a diameter of Ø1.55 mm. The length of the base surrounding the pin is 7.30 mm with a diameter of 3.07 mm as illustrated in Figure 2.2.

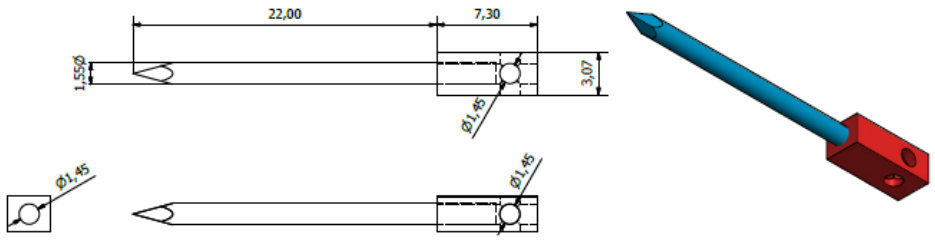

Figure 2.2: *An illustration showing the dimensions of the customised solid pin.*

2.3.7 ToF-SIMS analysis

ToF-SIMS analysis was performed using a ToF-SIMS IV instrument (IONTOF, GmbH) with a Bi_3^+ cluster source. A primary ion energy of 25 keV was used, the primary ion dose was preserved below 1×10^{12} per cm^2 to ensure static conditions. The area scanned encompassing the entire microarray region was varied from 15 × 14 mm to 7 × 25 mm and 6 × 14 mm according to the microarray area and were analysed in the 'high-current bunched' mode. The resolution was 100 pixels/mm and charge compensation was applied in the form of a low energy (~ 20 eV) electron flood gun. Data was acquired and analysed using SurfaceLab6 (IONTOF GmbH) instrument software. All peak intensities were normalised to the total ion count of the spectra.

2.4 Results and Discussion

2.4.1 Skin homogenisation

As discussed in Chapter 1, Section 1.9.2, skin is a tough fibrous tissue with resilient properties and as such is relatively difficult to homogenise by a single method or in a one step process [282, 285]. Thus, to obtain a uniform skin homogenate, a multi-step mechanical method was developed. Mechanical methods have the advantage of avoiding the introduction of chemicals into skin tissue that may interfere with the ToF-SIMS signal obtained from the compound of interest.

Cryogenic grinding by mortar and pestle is simple and easy to perform but was unsuccessful in breaking down skin tissue into small fragments. Hence, a Dounce homogeniser, which homogenises tissue by shearing forces, was attempted. The repeated up and down movement should result in tissue shearing but this was not the case for the skin. The skin was still intact without any fragmentation after a period of 15 minutes. Therefore, a beating method was attempted using Retsch® Mixer Mill and after a 10 minute homogenisation period it was observed that the skin tissue was still unfragmented suggesting that this method was unfeasible.

Finally, a rotor-stator homogeniser (Ultra-Turrax) was used and it was able to produce a uniform skin homogenate (Fig. 2.3c). In this trial, skin sections (Fig. 2.3a) were cut with scissors into very small pieces (Fig. 2.3b) to facilitate their passage into the slots of the homogeniser and following cutting they were left with 2 mL of distilled water for hydration and softening before homogenisation. During the homogenisation process, the plastic test tube containing hydrated skin pieces was placed in a glass beaker filled with ice to eliminate any heat generated during the homogenisation that may adversely affect both the skin and the homogeniser. The images of skin pre and post homogenisation by rotor-stator homogeniser are shown in Figure 2.3.

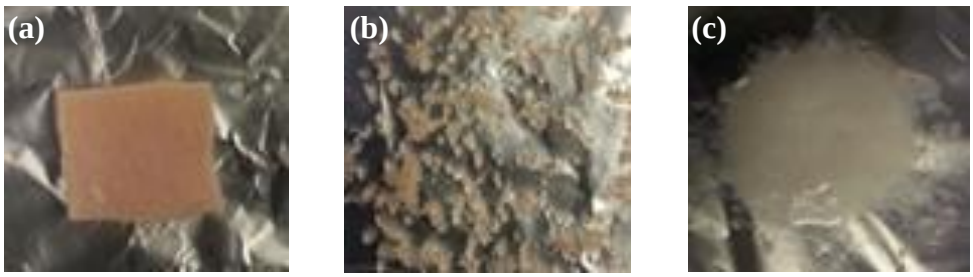

Figure 2.3: *Images of skin (a) pre-processing, (b) following cutting with scissors into very small pieces and (c) post rotor-stator homogenisation.*

The assessment of homogeneity of skin homogenate following the homogenisation by a rotor stator homogeniser was carried out grossly by pressing a spatula on skin homogenate to examine if there is any granulated non-homogenised material that may require further homogenisation.

This developed multi-step (cutting, hydrating and homogenisation) mechanical method was efficient in producing a uniform skin homogenate in approximately 2-3 hours without the need of chemicals or enzyme addition. Therefore, it seems to be appropriate for skin samples analysed by ToF-SIMS since there is no interference with an ion signal obtained from the compound of interest. As previously detailed in Chapter 1, Section 1.9.2, Nirogi *et al.* reported the effectiveness of using a combination of lytic enzymes and mechanical methods to liberate and quantify analytes within skin when analysed by LC-MS [284]. In comparison to Nirogi *et al.* method, the developed multi-step mechanical method (Section 2.3.3.4) is able to produce a uniform skin homogenate without the need of enzyme addition, with a reduced equipment requirement and reduced time (skin homogenate can be obtained in approximately 2-3 hours compared to more than 16 hours in Nirogi *et al.* method). This results in a high throughput and cost effective method.

During the skin homogenisation process using a rotor-stator homogeniser, it should be noted that heat is generated due to homogenisation at high speed and skin samples should always be kept in an ice beaker during homogenisation to compensate for this effect. Additionally, the cleaning of the homogeniser shaft should be done immediately after finishing the homogenisation process by washing with water and methanol several times, otherwise it becomes difficult to clean since the remaining skin homogenate sticks on the shaft and inside the slots and needs the use of a fine tweezer to remove.

The minimum time required to obtain a uniform skin homogenate is 15 minutes (tested experimentally) and it depends upon the size of skin pieces that are cut by scissors in the previous step. The finer the pieces, the shorter the time required for homogenisation. After homogenisation, skin homogenate was left to dry in air at ambient temperature for approximately two hours to allow the remaining water in skin to evaporate and not influence the weight of skin (i.e. to obtain a constant weight) when mixed with drug solutions in the next step. The summary of the steps of skin homogenisation, mixing with drug solutions and subsequent microarray printing and ToF-SIMS analysis is shown in Table 2.1.

Table 2.1: *Summary of the steps of skin homogenisation, mixing with drug solutions and subsequent microarray printing and ToF-SIMS analysis to finally generate a calibration curve for a drug in skin tissue.*

Step No.	Process
1	Skin sections removed from porcine ear (1 cm × 1 cm)
2	Cutting of skin with scissors into very small pieces
3	Mixing of skin tissue with 2 mL of deionised water
4	Homogenisation using Rotor-stator homogeniser
5	Obtaining skin homogenate
6	Drying at ambient temperature
7	Mixing of skin homogenate with drug solutions at different conc.
8	Sonication using probe sonicator
9	Microarray printing
10	Freeze drying
11	ToF-SIMS analysis

2.4.2 Microarray printing of imiquimod with skin homogenate (sonication bath attempt)

Microarray printing was performed using a BIODOT contact printer with a quill pin rather than non-contact (ink-jet) printer because of the high viscosity of the printed solutions (drug solutions with skin homogenate) which can cause blockage of the nozzle orifice of the ink-jet printer. One of the limitations of the ink-jet printer is that it cannot print viscous solutions [286, 289] (discussed in Chapter 1, Section 1.10.2) and was deemed suitable to investigate.

For the initial printing attempts, a sonication bath was used to mix imiquimod solutions with skin homogenate in order to obtain a homogeneous mixture, where vials containing the samples were sonicated for 30 minutes. In these attempts the printing pin was washed with acetone to prevent the 'carryover' effect and clogging of the slit by the dispersed tissue during the printing process. DMSO and oleic acid were chosen as solvents to dissolve imiquimod because of the higher solubility of imiquimod in these solvents rather than water or organic solvents [59].

ToF-SIMS data for imiquimod was collected in positive polarity for the molecular ion $[M+H]^+$ ($C_{14}H_{17}N_4^+$) at m/z = 241. Details regarding the selection of this particular ion and the choice of polarity will be discussed in Chapter 3, Section 3.4.1.3.1. In addition, (CH_4N^+) ion at m/z = 30 was selected as being indicative of skin in data acquisition and analysis.

ToF-SIMS ion images of the printed microarray of skin homogenate with imiquimod in DMSO and in oleic acid at different concentrations are shown in Figure 2.4. The upper section (i.e. upper 5 rows of spots) of the images shows spots printed in DMSO, while the lower section (i.e. lower 5 rows of spots) is in oleic acid (OA). Figure 2.4 illustrates the total ion image (Fig. 2.4a), the skin marker (CH_4N^+) image (Fig. 2.4b) which represents the printed skin spots and the molecular ion $[M+H]^+$ of imiquimod ($C_{14}H_{17}N_4^+$) image (Fig. 2.4c) which represents the imiquimod. Five repeats from each drug concentration, in addition to skin control and solvent blank are printed and can be observed in Figure 2.4c. An assessment of the skin marker image shows that skin spots are unevenly printed for DMSO solutions and printed with very low intensity for oleic acid solutions (Fig. 2.4b). The $[M+H]^+$ secondary ion image of imiquimod in DMSO (Fig. 2.4c) suggests that the imiquimod is only observable at the lowest concentration which is counterintuitive. It is proposed that the imiquimod might have precipitated in the well plates during the printing process leading to just printing spots of skin homogenate with the exception of the first spots printed at 10 µg/mg. These printing limitations are

likely due to improper mixing of drug solutions with skin homogenate or clogging of the printing pin due to inefficient washing method.

The spots of the $[M+H]^+$ of imiquimod in oleic acid are quite clearly printed at the range of concentrations used with an increase in ion intensity from the lower to higher concentrations. Intensity scale represents the intensity of the detected ions where the lighter the colour the higher the ion intensity. Ion intensity values obtained from these spots are calculated by finding regions of interest (ROI) around these spots. These intensity values are normalised to the total ion intensity value to overcome any differences due to spot size or fluctuation in ion beam current. Following this, these values are used to generate a calibration curve relating concentration of imiquimod in skin (µg of imiquimod per mg of skin) with the normalised ion intensity as shown in Figure 2.5.

2.4.3 Calibration curve of imiquimod in oleic acid with skin homogenate (sonication bath attempt)

Normalised ion intensity values of the $[M+H]^+$ for imiquimod in oleic acid obtained from the printed microarray are plotted versus imiquimod concentration in skin (µg of imiquimod per mg of skin) to generate a calibration curve as shown in Figure 2.5. It can be seen that there is a linear correlation between imiquimod concentration at the range of 10-80 µg/mg and the spots ion intensity (R-squared value of 0.94). However, the linearity of the curve disappeared at higher concentration points of 90 and 100 µg/mg.

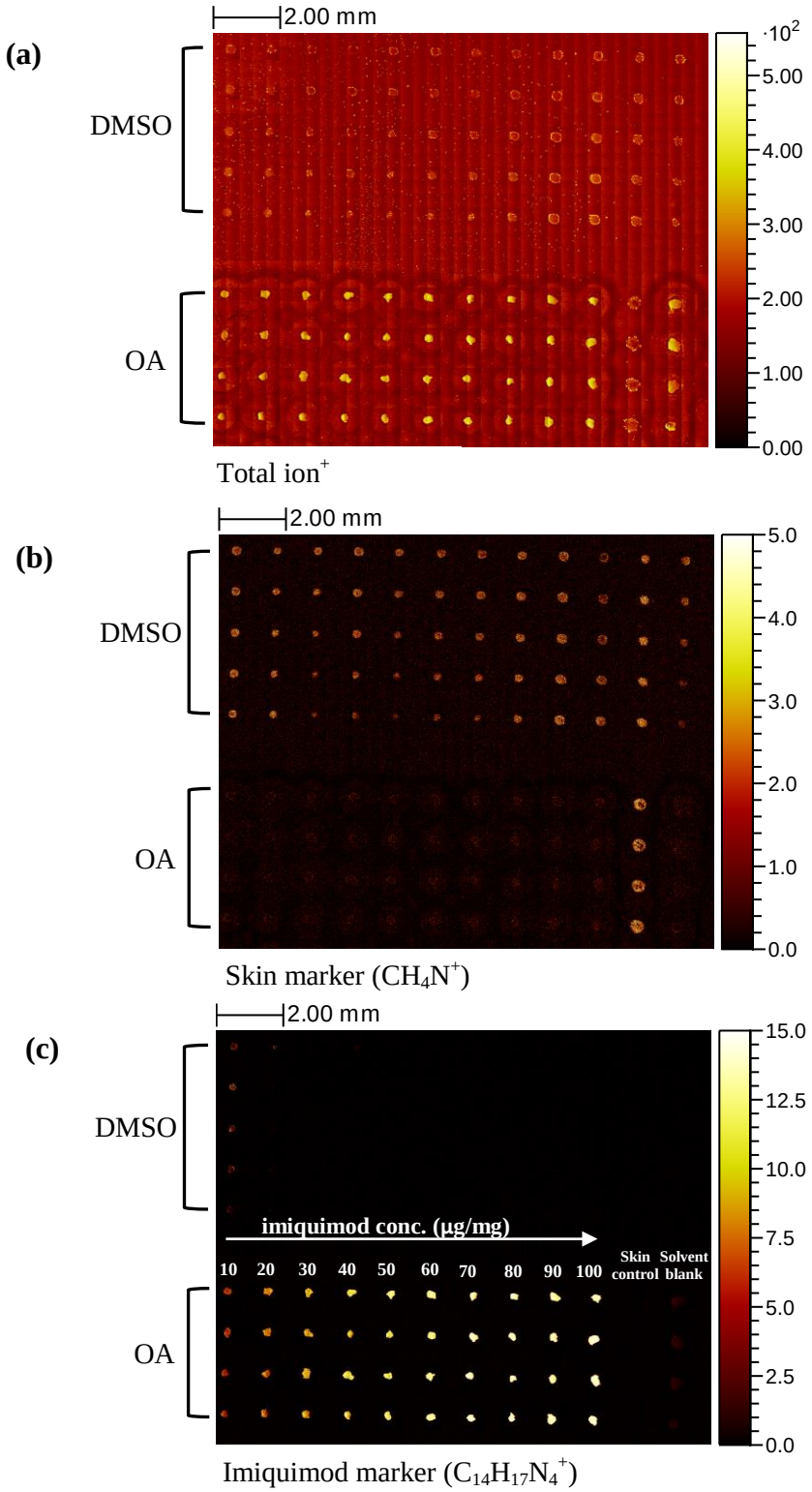

Figure 2.4: *ToF-SIMS ion images of the printed microarray of imiquimod in DMSO and oleic acid solutions with skin homogenate (sonication bath attempt) showing: (a) the total ion⁺, (b) the skin marker CH_4N^+ which represents the printed skin spots and (c) the imiquimod marker $C_{14}H_{17}N_4^+$ which represents the printed imiquimod spots. Five repeats (rows) from each drug concentration were printed, in addition to skin control and a solvent blank are shown in these images. These findings were representative for three repeats.*

In addition, at this range of the applied concentrations, the normalised ion intensity values are vary between 0.01 and 0.03 which are much higher than the normalised ion intensity of the future test samples informed by the *ex vivo* work (Chapter 3). Moreover, the intensity data of some printed spots such as those at 40, 60, 90 and 100 µg/mg show high standard deviation values of ± 0.0031, ± 0.0036, ± 0.0066 and ± 0.0051 of the ion intensities 0.0195, 0.0227, 0.0262 and 0.0290 respectively. This is attributed to the poor mixing of drug solutions with skin homogenate which results in a non-uniform mixture. Therefore, a second printing attempt with amendments in the mixing and printing conditions was carried out to address these limitations and generate a more reliable calibration curve.

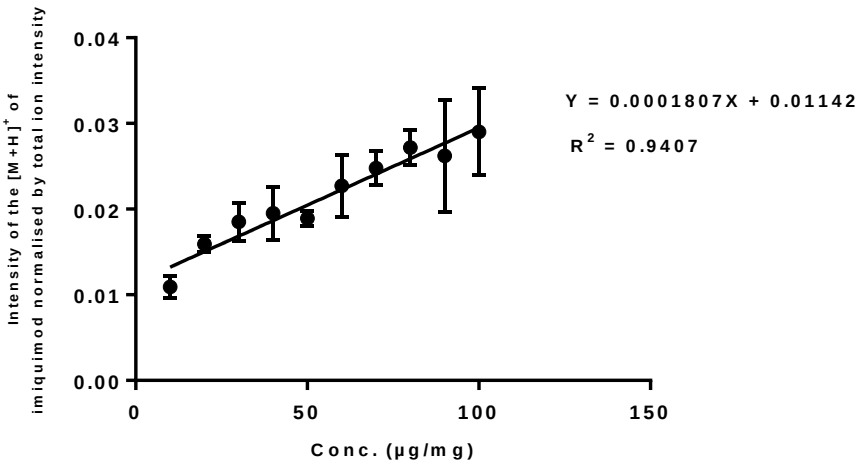

Figure 2.5: *Calibration curve of imiquimod in oleic acid with skin homogenate (sonication bath attempt) in which imiquimod concentration is plotted versus normalised molecular ion intensity. Data is presented as the mean ± SD (n = 5).*

2.4.4 Microarray printing of imiquimod with skin homogenate (probe sonication attempt)

In this attempt, some amendments were applied to improve the quality of printing. First, solutions of imiquimod in oleic acid were mixed with skin homogenate using a probe sonicator for 2 minutes instead of a sonication bath for 30 minutes, this yielded a more uniform and homogeneous mixture in a

shorter time period. A probe sonicator produces higher ultrasound energy with greater localised intensity in comparison to a sonication bath. This leads to higher efficiency of the sonication process [302, 303]. Second, a triple washing method with detergent (Teepol® 3% v/v solution), water and acetone was used rather than just washing with acetone. This ensures the cleaning of a printing quill pin and prevents clogging by the dispersed tissue during the printing process. In this attempt, imiquimod solutions in oleic acid were prepared and printed at lower range of concentrations (0.25-20 µg/mg) as shown in (Fig. 2.6c) to match the anticipated low ion intensity of the test samples.

Printing of imiquimod in DMSO was not repeated this time, since imiquimod spots in DMSO were not adequately printed from the previous sonication bath trial. In addition, oleic acid is more similar to the composition to the existing delivery systems of imiquimod such as Aldara® cream. Accordingly, the microarray of imiquimod in oleic acid with skin homogenate can be used to generate a calibration curve for quantification purposes.

ToF-SIMS ion images of the printed microarray of skin homogenate with imiquimod in oleic acid at different concentrations are shown in Figure 2.6 which illustrates the total ion image, the skin marker (CH_4N^+) image and the molecular ion ($C_{14}H_{17}N_4^+$) image as shown in Figure 2.6a-c respectively. Five repeats from each drug concentration, in addition to skin control are printed and can be seen in Figure 2.6c. An assessment of the skin marker and the $[M+H]^+$ of imiquimod images (Fig. 2.6b and c) show that the spots are uniformly printed for both the skin and imiquimod and increase in imiquimod concentration is associated with an increase in the secondary ion intensity (Fig. 2.6c). The improvement of microarray printing quality is attributed to the improved mixing of imiquimod solutions with skin homogenate achieved by probe sonication. Further benefit is obtained from the triple washing method used here to clean the printing pin to prevent clogging. Spots of skin control are clearly printed with high intensity in a skin marker image (Fig. 2.6b) but with very low intensity in the $[M+H]^+$ image of imiquimod (Fig. 2.6c). This

verifies the high specificity of the ToF-SIMS instrument towards imiquimod analysis.

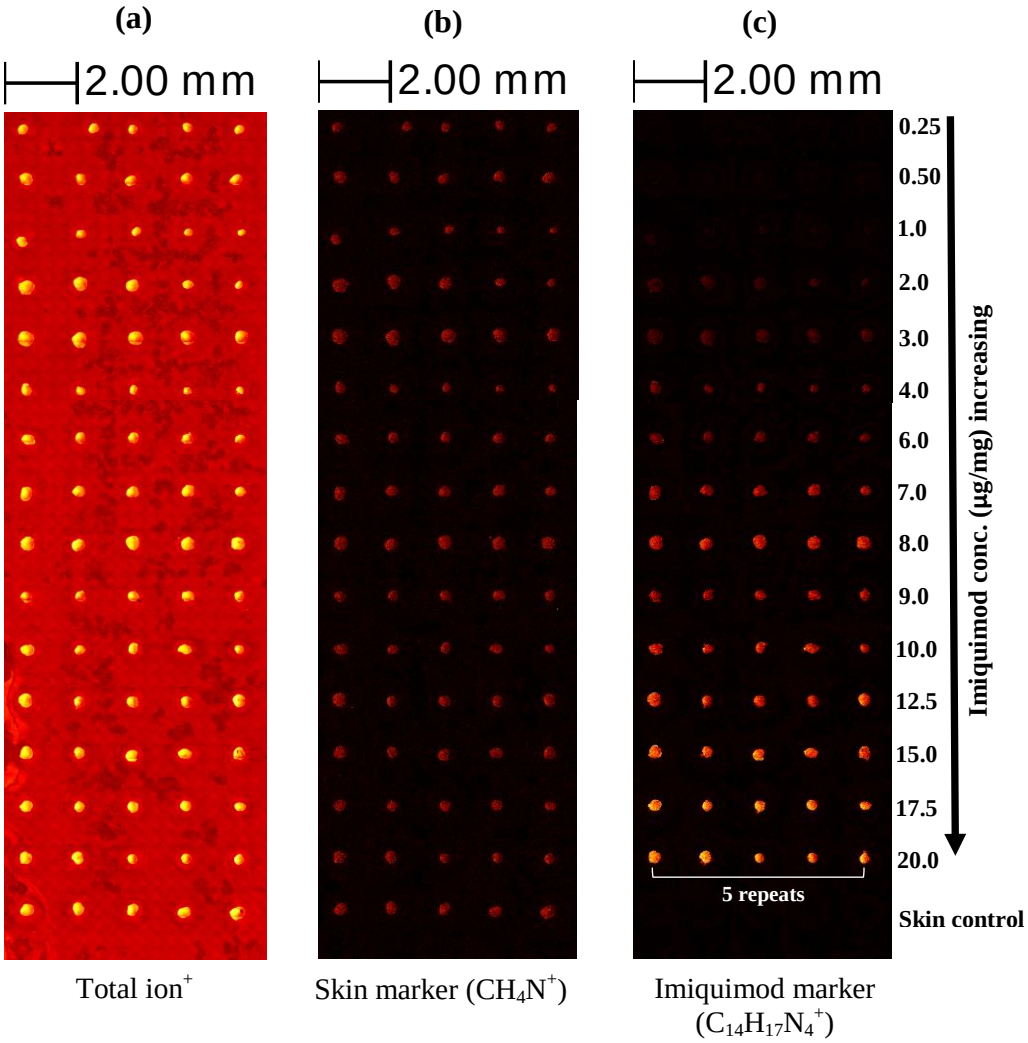

Figure 2.6: *ToF-SIMS ion images of the printed microarray of imiquimod in oleic acid solutions with skin homogenate (probe sonication attempt) showing: (a) the total ion*$^{+}$*, (b) the skin marker* CH_4N^+ *which represents the printed skin spots and (c) the imiquimod marker* $C_{14}H_{17}N_4^+$ *which represents the printed imiquimod spots. Five repeats from each drug concentration, in addition to skin control are shown in these images. These findings were representative for three repeats.*

2.4.5 Calibration curve of imiquimod in oleic acid with skin homogenate (probe sonication attempt)

A calibration curve of imiquimod in oleic acid with skin homogenate is generated by plotting imiquimod concentrations in skin (µg of imiquimod in mg of skin) versus normalised ion intensity values as illustrated in Figure 2.7. Data is presented as the mean of five repeats of each concentration with the error bars represent the standard deviation from the mean value. The concentration range (0.5-15 µg/mg) used in the generation of this probe sonication calibration curve is lower than that used in the previous sonication bath trial (10-100 µg/mg). This results in lower ion intensity values (0.001-0.006) that matches the ion intensity of the future test samples informed by the *ex vivo* work (Chapter 3). At the range of concentration used, a linear correlation between imiquimod concentration and the spots ion intensity is observed (R-squared value of 0.98). Therefore, this calibration curve can be applied for quantification purposes. The limit of detection (LoD) was found to be at 0.5 µg/mg and it was calculated by comparing the imiquimod $[M+H]^+$ intensity to the skin control ion intensity. The limit of quantification (LoQ) is determined where imiquimod concentration could be quantified with acceptable accuracy and precision at a coefficient of variation (CV) of less than 20% [304] and it is found to be at 1 µg/mg.

Furthermore, it was observed that the standard deviation of the ion intensity values is less than that obtained from the previous imiquimod calibration curve of the sonication bath attempt (Fig. 2.5). The highest standard deviation value is ± 0.0006 of the ion intensity 0.00628 at a concentration of 17.5 µg/mg in comparison to ± 0.006 of the ion intensity 0.026 at a concentration of 90 µg/mg from the previous sonication bath trial. This suggests the appropriate homogenisation of the printed samples (imiquimod solutions with skin homogenate) was achieved by the use of a probe sonicator which results in this reduction in the standard deviation values.

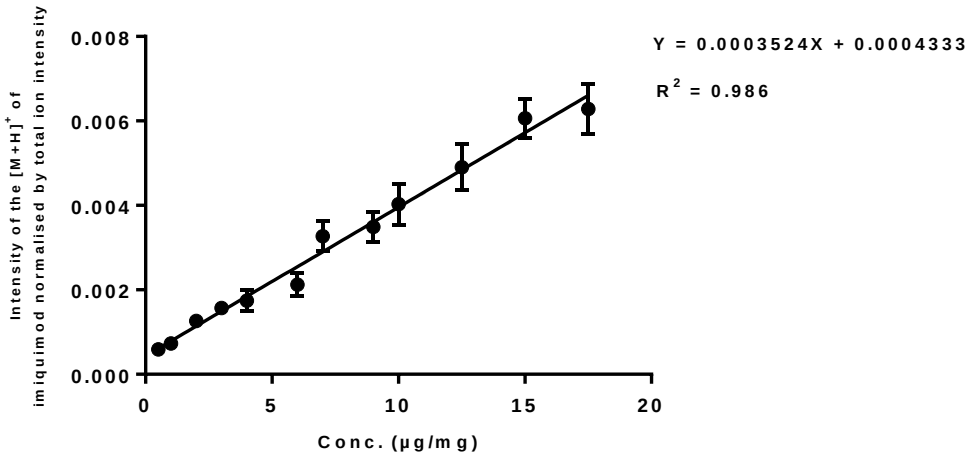

Figure 2.7: *Calibration curve of imiquimod in oleic acid with skin homogenate (probe sonication attempt) in which imiquimod concentration is expressed as µg of drug per mg of skin and plotted versus normalised molecular ion intensity. Data is presented as the mean ± SD (n = 5).*

2.4.6 Microarray printing of chlorhexidine gluconate (CHG) with skin homogenate (sonication bath attempt)

Microarray printing of CHG in water and in isopropyl alcohol (IPA 70% v/v) with skin homogenate is achieved using the same printing conditions as in the imiquimod microarray sonication bath attempt (Section 2.4.2), in which CHG solutions in water and IPA at different concentrations were mixed with skin homogenate using a sonication bath for 30 minutes and printed using a quill pin with a single washing method by acetone. Water and IPA were used as vehicles because of the miscibility of CHG standard solution (20% w/v aqueous solution) with these solvents. Additionally, the commercial products of chlorhexidine (test solutions) such as HiBiScrub® and ChloraPrep® which are available in water and IPA vehicles respectively. ToF-SIMS data for CHG was collected in negative polarity for the fragment ion ($C_7H_4N_2Cl^-$) at m/z = 151. Details regarding the selection of this particular ion and the choice of polarity will be discussed in Chapter 5, Section 5.4.1. In addition, the (CNO^-) ion at m/z = 42 was selected as being indicative of skin marker in data acquisition and analysis.

ToF-SIMS ion images of the printed microarray of skin homogenate with CHG in water and IPA at different concentrations are shown in Figure 2.8. The upper section (i.e. upper 5 rows of spots) of the images shows spots printed in water, while the lower section (i.e. lower 5 rows of spots) is in IPA. Figure 2.8 illustrates the total ion image (Fig. 2.8a), the skin marker (CNO^-) image (Fig. 2.8b) which represents the printed skin spots and the fragment ion ($C_7H_4N_2Cl^-$) image (Fig. 2.8c) which represents the CHG marker. Five repeats from each drug concentration, in addition to skin control are printed and can be observed in Figure 2.8c.

An examination of the skin marker (CNO^-) and the CHG marker ion ($C_7H_4N_2Cl^-$) images (Fig. 2.8b and c) reveal that skin spots and CHG spots are unevenly printed in both water and IPA with missing spots for IPA solutions. This might be due to improper mixing of skin homogenate with drug solutions or clogging of the quill pin during the printing process due to an insufficient washing method. Therefore, the generation of a reliable calibration of CHG in IPA is unfeasible due to this inappropriate printing of CHG spots in IPA (many missing spots) and a calibration curve can only be generated for CHG in water as shown in Figure 2.9.

It was observed that the sonication of skin homogenate with solutions of CHG in IPA results in non-homogeneous mixture which might lead to this inadequate printing, this is likely due to coagulation and precipitation of skin proteins by IPA. Zellner *et al.* demonstrated the ability of ethanol to precipitate proteins from water-ethanol mixture by decreasing the dielectric constant of water and causing dehydration of proteins leading to a reduction in their solubility and precipitation [305]. Some spots of skin control were printed showing high intensity skin marker (CNO^-) image (Fig. 2.8b) but with very low intensity in a CHG marker ($C_7H_4N_2Cl^-$) image (Fig. 2.8c). This suggests the high ion specificity of the ToF-SIMS instrument towards CHG analysis.

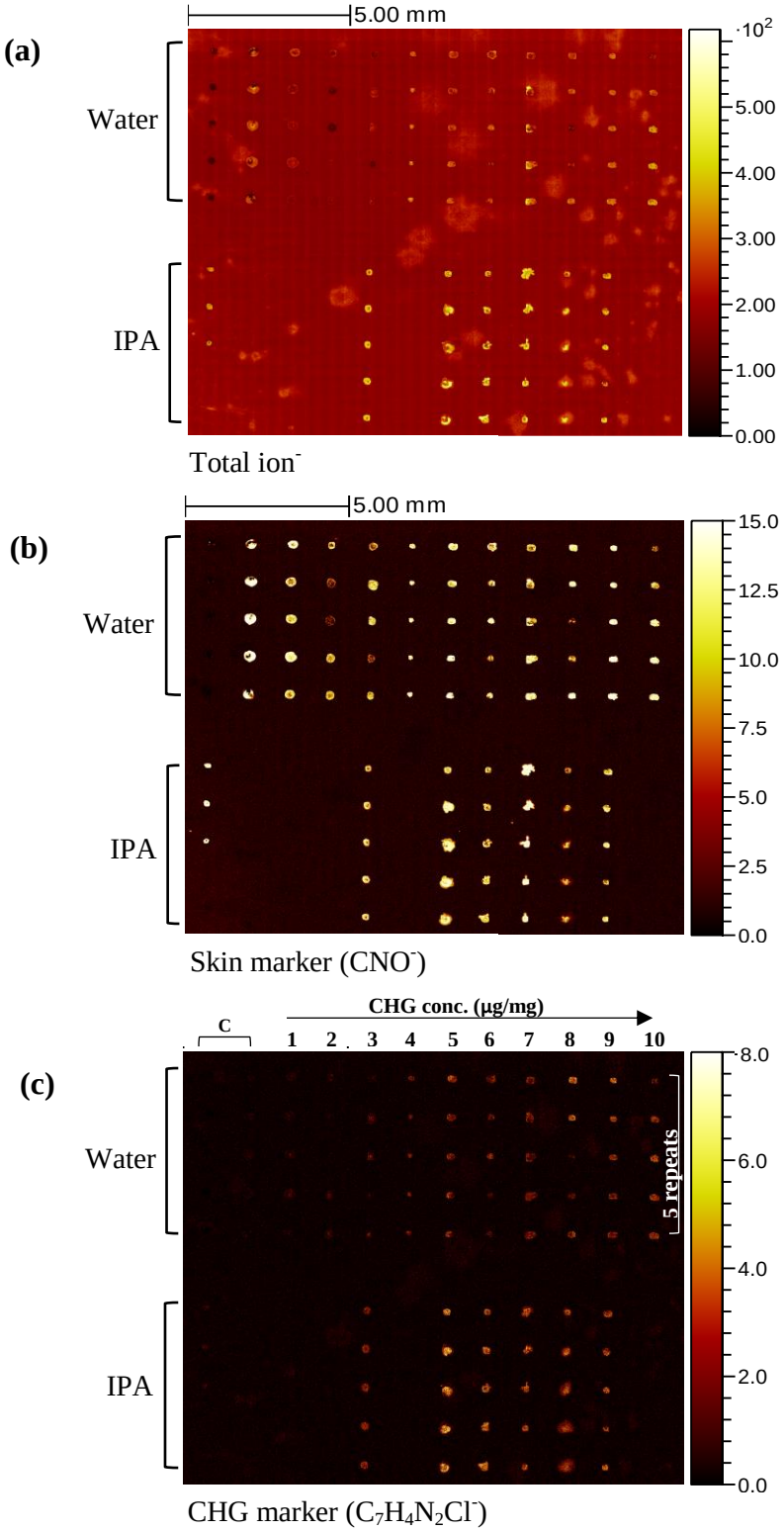

Figure 2.8: *ToF-SIMS ion images of the printed microarray of CHG in water and IPA solutions with skin homogenate (sonication bath attempt) showing: (a) the total ion⁻, (b) the skin marker (CNO^-) which represents the printed skin spots and (c) the CHG marker ($C_7H_4N_2Cl^-$) which represents the printed CHG spots. Five repeats from each drug concentration, in addition to skin control are shown in these images. These findings were representative for three repeats.*

2.4.7 Calibration curve of CHG in water with skin homogenate (sonication bath attempt)

A calibration curve of CHG in water with skin homogenate is generated by plotting CHG concentrations in skin (µg of CHG in mg of skin) versus normalised ion intensity values of a CHG marker ion ($C_7H_4N_2Cl^-$) as illustrated in Figure 2.9. Data is presented as the mean of five repeats of each concentration with the error bars represent the standard deviation from the mean value. A linear correlation between concentration at the range of (1-9 µg/mg) and the normalised ion intensity (R-squared value of 0.92) can be observed. However, there are some spots not adequately printed and showing high standard deviation values such as those at concentrations of 6 and 8 µg/mg in which the standard deviation values are ± 0.001 and ± 0.0012 of the ion intensity 0.0030 and 0.0041 respectively. This might be as mentioned earlier (Section 2.4.3) due to inadequate mixing of CHG solutions with skin homogenate which results in a non-homogeneous mixture.

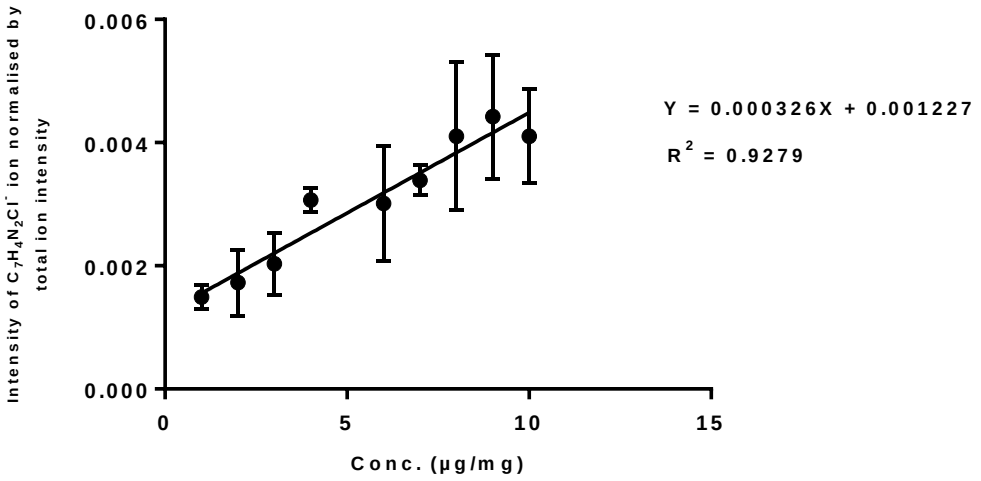

Figure 2.9: *Calibration curve of CHG in water with skin homogenate (sonication bath attempt) in which CHG concentration is expressed as µg of drug per mg of skin and plotted versus normalised CHG marker ion intensity. Data is presented as the mean ± SD (n = 5).*

2.4.8 Printing with a solid pin

In an attempt to further improve the quality of the printed microarray of CHG solutions with skin homogenate, a solid pin instead of a quill pin was used. A solid pin has several advantages (discussed in Chapter 1, Section 1.10.1) including easier cleaning, suitability for use with viscous solutions and less variation in the deposition volume during printing because it re-dips the well plate after each spotting [290, 291]. Therefore, it has been utilised for a further series of microarray printing. A customised solid pin was made at the Medical Engineering workshop, The University of Nottingham to be used in the printing process. It was made from stainless steel with approximately similar dimensions and measurements of a quill pin but without the slit inside. The microscopic images of both quill pin and solid pin used in the printing of microarrays are shown in Figure 2.10a and b respectively.

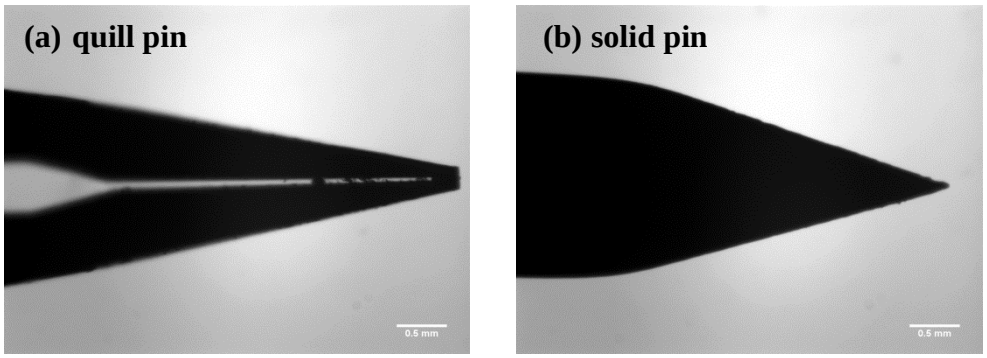

Figure 2.10: *Microscopic images of (a) quill pin and (b) solid pin used in the printing of microarrays of drug solutions with skin homogenate.*

CHG solutions in water were prepared and mixed uniformly with skin homogenate and then transferred to the well plate for printing according to the method previously used (Section 2.4.6). When the robotic arm started dipping the solid pin into solutions in the well plate and then spotting on a glass slide surface, it was apparent that there were no spots on the surface. It is thought that pin fabrication was imperfect causing failure in microarray printing and an amendment of the pin tip was required to improve the quality of printing. As illustrated in Figure 2.10b, the tip of the solid pin is very sharp and pointed in

comparison to the quill pin, this creates a difficulty for the solid pin to catch a liquid drop from the sample well plate in order to transfer and spot onto the substrate surface (a liquid drop slips from the pin tip prior to contact with the substrate). This can lead to a failure in microarray formation. Thus, the sharp tip of the solid pin was amended (cut) to be similar to a quill pin tip and utilised to print a new microarray. Figure 2.11 shows a CHG microarray printed after amendment of the solid pin.

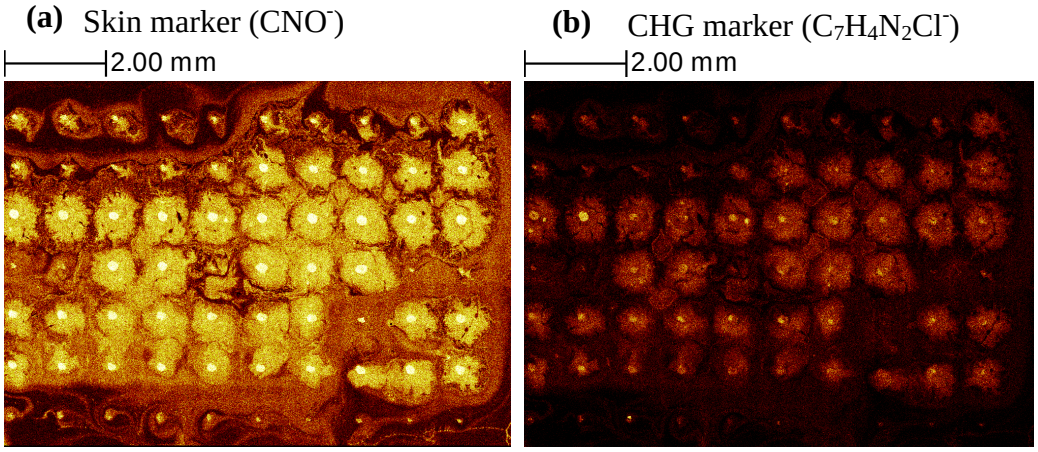

Figure 2.11: *ToF-SIMS ion images of the printed microarray of CHG in water with skin homogenate printed by a solid pin showing: (a) the skin marker (CNO^-) and (b) the CHG marker ($C_7H_4N_2Cl^-$).*

An assessment of the skin marker and CHG marker images (Fig. 2.11a and b respectively), demonstrate that some spots are printed on the glass slide but the quality of the printing is very poor (issues with printing consistency). The spots of skin and of CHG marker ion are printed in an uneven manner and with irregular shape. It is thought that the pin, even after amendment, is still unable to adequately print microarrays in an appropriate way. Therefore this solid pin was omitted from microarray printing due to its inefficiency in producing high quality microarrays. It was apparent that the fabrication of a pin with dimensions of few hundred microns is quite challenging and needs advanced machining technology that may not be available at an 'in house' workshop.

2.4.9 Microarray printing of CHG with skin homogenate (probe sonication attempt)

In this series of work the setting of the robotic printer arm connected to the quill pin has been modified to enable it to print as a solid pin. In this way, the pin revisits the sample well plate after each spotting which results in less variation in the deposition volume during printing to achieve a more even microarray. In addition, the probe sonicator and the triple washing method that has been used in imiquimod printing (probe sonication attempt, Section 2.4.4) was also used here to ensure optimised mixing and cleaning of the printing pin. Printing of CHG in IPA with skin homogenate was not repeated this time because of the inadequate mixing of the CHG in IPA solutions with skin homogenate achieved even with probe sonication which may result in improper microarray printing and unreliable calibration curve. Therefore, the microarray formation and calibration curve generation was only performed for solutions of CHG in water.

Figure 2.12 illustrates the ToF-SIMS ion images of the printed microarray of CHG in water at different concentrations with skin homogenate. Five repeats from each CHG concentration, in addition to skin control are printed and can be observed in Figure 2.12b. An assessment of the skin marker (CNO^-) image (Fig. 2.12a) shows that the skin spots are appropriately printed throughout the slide. This indicates that the mixing by probe sonicator and the use of the triple washing method to clean the pin after printing each drug concentration are more efficient in producing a uniform and even microarray than the previous sonication bath attempt (Section 2.4.6). Again, the specificity of ToF-SIMS instrument towards CHG analysis is confirmed by detecting spots of the skin control with a high intensity in skin marker (CNO^-) image (Fig. 2.12a) but with a very low intensity in CHG marker ion ($C_7H_4N_2Cl^-$) image (Fig. 2.12b).

An examination of CHG marker ion image (Fig. 2.12b) reveals that the CHG spots are adequately printed with a decreasing ion intensity from the higher to lower drug concentration. This suggests a direct relationship between CHG

concentration and ion intensity. Furthermore, at each particular CHG concentration, the repeats have approximately a similar spot size. This can be attributed to the modification in the setting of the robotic printer arm which made a quill pin to print as a solid pin. Thus, it revisits a sample well plate after each spotting leading to less difference in the volume deposited each time. Nevertheless, the time required to complete printing was longer [291], approximately one hour which is double the time of the previous sonication bath trial (Section 2.4.6) but it is still a reasonable time to obtain an improved quality of microarray. In addition, there is a difference in the size of the printed spots at the different CHG concentrations, this is likely related to the difference in the viscosity of the printed solutions. However, this difference in spot size will not influence the ion intensity values obtained from them when analysed by ToF-SIMS because each value is normalised to the total ion intensity and in this way the effect of spot size will be negated.

2.4.10 Calibration curve of CHG in water with skin homogenate (probe sonication attempt)

A calibration curve of CHG in water with skin homogenate is generated by plotting CHG concentrations in skin (µg of CHG in mg of skin) versus normalised ion intensity values of CHG marker ion as illustrated in Figure 2.13. Data is presented as the mean of five repeats of each concentration with the error bars represent the standard deviation from the mean value. The concentration range of 0.039-8.75 µg/mg results in ion intensity values between 0.001 and 0.008. This range of ion intensity is informed by the future *in vivo* and *ex vivo* CHG test samples (Chapter 5). A linear correlation between CHG concentration and ion intensity is observed with an R-squared value of 0.97. However, by careful examination of the curve it is apparent that the linearity of the curve disappeared at higher concentration points of 6.25, 7.5 and 8.75 µg/mg. This is attributed to saturation of the detector of the ToF-SIMS instrument. Nevertheless, the lower part of the curve at the concentration range of 0.039-3.75 µg/mg still shows higher linearity with an R-squared value

of 0.99 as shown in Figure 2.13. Therefore, this calibration curve can be applied for quantification purposes instead of the whole curve.

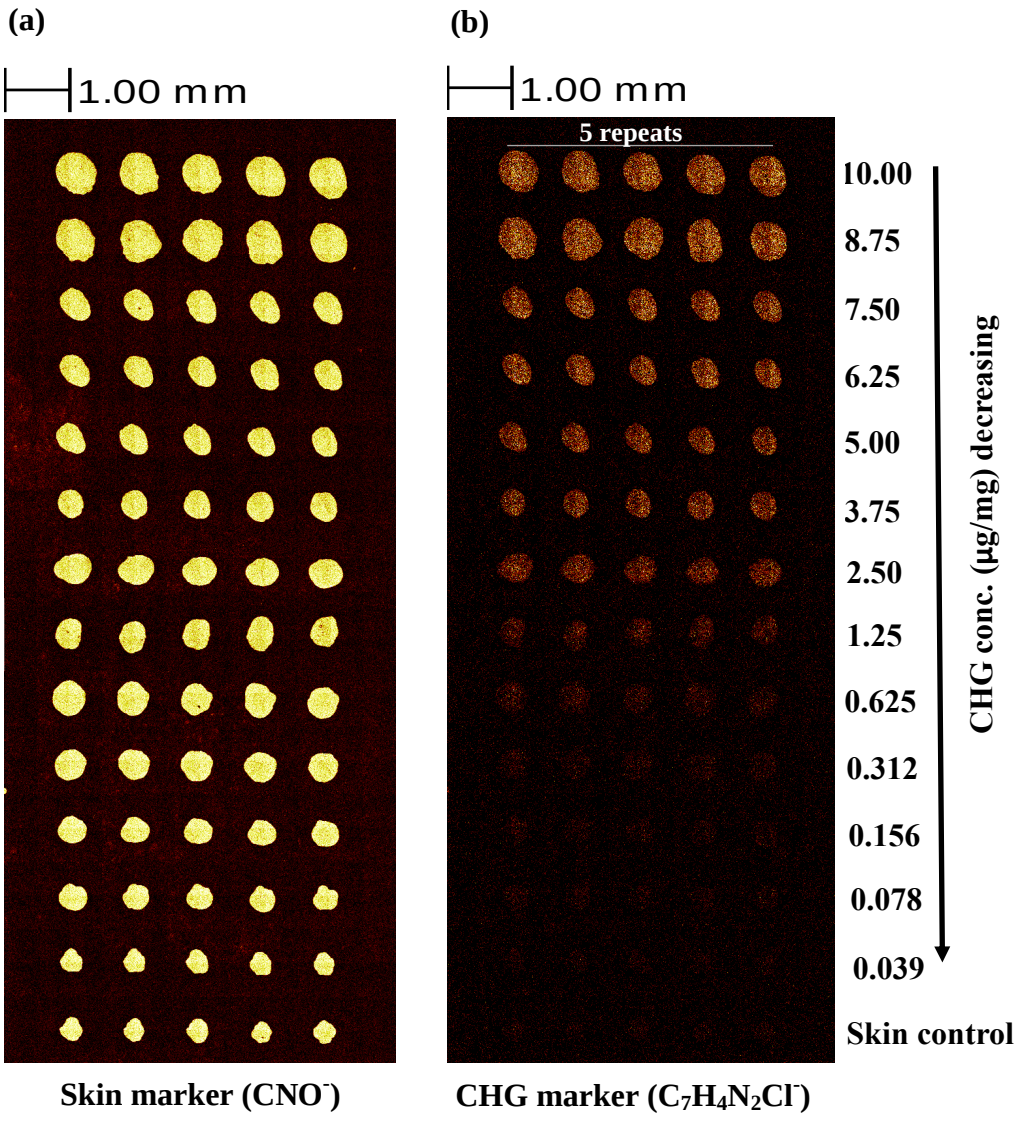

Figure 2.12: *ToF-SIMS ion images of the printed microarray of CHG in water with skin homogenate (probe sonication attempt) showing: (a) the skin marker (CNO^-) which represents the printed skin spots and (b) the CHG marker ($C_7H_4N_2Cl^-$) which represents the printed CHG spots. Five repeats from each drug concentration, in addition to skin control are shown in these images. These findings were representative for three repeats.*

The limit of detection (LoD) and the limit of quantification (LoQ) are found to be at 0.078 µg/mg. The limit of detection is calculated by comparing the intensity of CHG marker ion to the skin control ion intensity. The limit of quantification is determined where CHG concentration can be quantified with acceptable accuracy and precision at coefficient of variation (CV) of less than 20% [304]. Although, the application of this calibration curve for the determination of concentrations higher than 3.75 µg/mg will be inaccurate, it shows appropriate accuracy and precision at the lower concentrations necessary to compare the CHG concentration in the tape strips with the minimum bactericidal concentration of CHG (Chapter 5).

In addition, Figure 2.13 illustrates that the standard deviation at each concentration point is less than that obtained from the previous CHG calibration curve of the sonication bath attempt (Fig. 2.9). The highest value of the standard deviation is ± 0.00034 of the ion intensity 0.005 at concentration of 3.75 µg/mg in comparison to ± 0.0012 of the ion intensity 0.0041 at concentration of 8 µg/mg from the previous sonication bath attempt. This indicates the homogeneity of the printed samples (CHG solutions with skin homogenate) resulting in less variability of data around the mean value and confirms the significant role of the probe sonicator on the mixing uniformity of the printed samples.

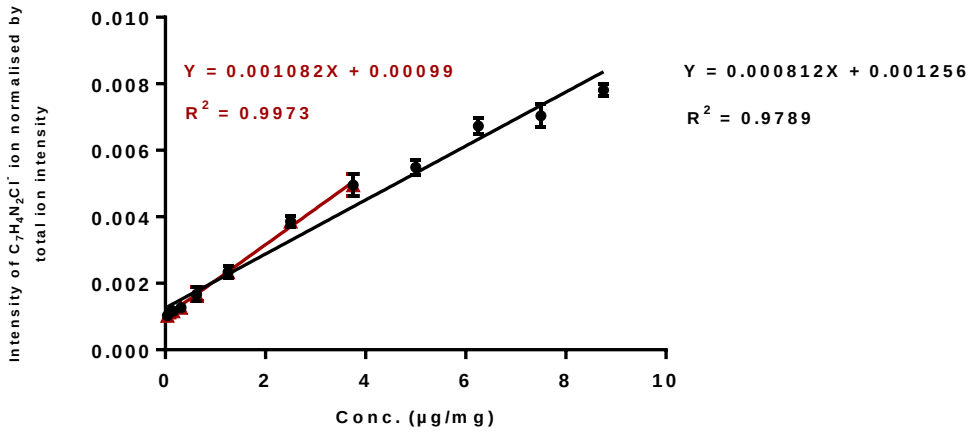

Figure 2.13: *Calibration curves of CHG in water with skin homogenate (probe sonication attempt) in which CHG concentration is expressed as µg of drug per mg of skin and plotted versus normalised ion intensity. The calibration curve at the lower concentration range of 0.039-3.75 µg/mg (red line) shows higher linearity than the whole curve (black line). Data is presented as the mean ± SD (n = 5).*

2.5 Conclusions

Quantification of ToF-SIMS data is a challenging task due to the matrix effects that influence the secondary ion yield. Therefore, to address this issue, quantification from an identical or similar model matrix is required to generate a calibration curve used in the quantification of the unknown concentration of a drug within skin. To quantify ToF-SIMS data for a drug within skin, skin homogenate represents the ideal matrix due to its identity and relevance to real skin tissue. The work in this chapter demonstrates the development of a mechanical method with a multi-step process that is efficient in producing skin homogenate in an acceptable time limit and without introducing any chemicals that may interfere with the signal obtained from an analyte within skin when analysed by ToF-SIMS. In addition, the microarray printing approach provides a high throughput technique to generate and analyse many samples simultaneously. The homogeneity of the mixture of drug solutions with skin homogenate, the type of pin used and pin washing method have a great impact on the quality of the printed microarray and consequently on the generated calibration curve. Calibration curves of imiquimod and chlorhexidine were successfully generated with acceptable linearity, accuracy and precision which can be used to determine their concentration in the test samples for example in the tape strips. This is believed to be the first time that a mechanical method for skin homogenisation with microarray printing of skin homogenate has been applied to enable quantification of ToF-SIMS data within skin. This method represents the first attempt or a proof of concept for the quantification of ToF-SMIS data within skin which can be further improved to be more reliable and pertinent.

3 Chapter Three: Assessment of Imiquimod Permeation into *ex vivo* Skin Tissue by HPLC and ToF-SIMS Analysis

3.1 Introduction

As detailed in Chapter 1, Section 1.5.1.1, the majority of skin permeation testing uses *in vitro* experiments due to the legal and ethical constraints [4, 306, 307], in addition to the difficulties associated with *in vivo* clinical trials including the high variability, costly and long experiments enrolling large number of subjects [122, 308]. The usefulness of Franz diffusion cells in predicting the *in vivo* percutaneous absorption, comparing permeation from different formulations and in risk assessment has been proven for wide range of drugs and chemicals [309-313]. The detection of a permeant traversing through the skin in Franz cell experiments is mostly achieved by the conventional chromatographic methods (usually HPLC). However, the HPLC has several drawbacks (discussed in Chapter 1, Section 1.6.1). Visualising distribution of a permeant within skin can be achieved by imaging techniques such as ToF-SIMS. Recently, ToF-SIMS has been used to map permeation and visualise distribution of drugs within skin as in the case of the antiseptic drug chlorhexidine digluconate [83], topically applied drug molecules (roflumilast, tofacitinib and ruxolitinib) [161] and cosmetics [314] as discussed in Chapter 1, Section 1.7.6.

To date, there is a gap in the in the available information regarding the exact depth of permeation and the spatial distribution of imiquimod when delivered from Aldara™ cream. The previous studies assessed the skin permeation of imiquimod from Aldara™ cream showed limitations in the analytical methodology employed. A study conducted by Stein *et al.* to compare permeation of imiquimod from a new formulated imiquimod containing emulsion gel (IMI-Gel) with Aldara™ cream across mouse skin found that 11.5% of imiquimod from Aldara™ permeated across the skin and only 19% remained on the skin surface when analysed by HPLC [61]. This high imiquimod permeability from Aldara™ cream can be attributed to the use of

mouse skin, since it is thinner and much more permeable than human or pig skin (up to 10 times) [131, 315]. These results are therefore not a relevant comparison to this work and highlight the necessity to use an appropriate skin type for permeation testing. Another study conducted by Rehman *et al.* reported a comparison of the imiquimod permeation from a formulated fish oil-carbopol bigel containing 5% imiquimod with Aldara™ cream into mouse skin. This study demonstrated that the tape strips and the remaining skin samples contained a higher amount of imiquimod permeated from Aldara™ cream than from the bigel formulation. The imiquimod content in the tape strips from Aldara™ cream and the bigel formulation was found to be 1.57 ± 0.5 mg/cm^2 and 0.93 ± 0.05 mg/cm^2 respectively. These values are equivalent to 59.66% and 35.34% of the mean % recovered amount. Similarly, the content in the remaining skin from Aldara™ cream and the bigel formulation was 0.85 ± 0.34 mg/cm^2 and 0.30 ± 0.04 mg/cm^2 respectively which are equivalent to 32.3% and 11.4% of the mean % recovery. In this study in addition to the use of mouse skin, the authors have used cetrimide (cationic surfactant) as a receptor fluid and the skin was wiped with a cotton swab dipped in IPA during the skin preparation step [62]. All these factors may influence the skin integrity which may give rise to a higher permeation rate. It is believed that the difference between the results presented here and the results from Stein and Rehman work [61, 62] which show a greater permeation of imiquimod from Aldara™ cream can be attributed to the variation in the experimental conditions used including the type of skin, receptor fluid and the HPLC analysis method.

Therefore, in this chapter, the permeation of imiquimod into *ex vivo* porcine skin from Aldara™ cream and from simple solvent systems in DMSO and oleic acid has been investigated using Franz diffusion cells with subsequent analysis by HPLC and ToF-SIMS. Imaging of skin tape strips and cryo-sectioned skin samples were conducted by ToF-SIMS to map permeation and visualise the distribution of imiquimod within skin tissue.

3.2 Chapter Aims

The key aim of this chapter is to evaluate the permeation of imiquimod from the commercial product Aldara™ cream into *ex vivo* porcine skin using a combination of conventional experimental method of Franz diffusion cells, skin tape stripping and HPLC analysis as well as advanced ToF-SIMS imaging technique. The expectation is to glean a presently unavailable insight into the exact depth of permeation and the spatial distribution of this drug within skin. Moreover, since published clinical trials showed the limited ability of Aldara™ cream to efficiently treat deep nodular BCC lesions, an investigation of the permeation of imiquimod from DMSO and oleic acid solutions (penetration enhancers) was carried out to examine if imiquimod could penetrate deeper skin layers. This is believed to be, the first time that the permeation of imiquimod from Aldara™ cream has been studied at this level of detail.

3.3 Materials and Methods

3.3.1 Materials

Imiquimod was purchased from Bioscience Life Sciences, UK. Aldara™ 5% cream, MEDA Company, Sweden was purchased from Manor pharmacy, UK. DMSO, oleic acid, HCl, sodium acetate and isopentane were purchased from Sigma-Aldrich, UK. Acetonitrile (HPLC grade), glacial acetic acid were obtained from Fisher Scientific, UK. Teepol solution (Multipurpose detergent) was ordered from Scientific Laboratory Supplies, UK. D-Squame standard sampling discs (adhesive discs) were ordered from CUDERM corporation, USA. OCT compound were obtained from VWR International Ltd. Belgium. Deionised water was obtained from an ELGA reservoir, PURELAB® Ultra, ELGA, UK. All reagents were of analytical grade, unless otherwise stated.

3.3.2 Permeation study of Aldara™ cream

All *in vitro* permeation experiments within this chapter were carried out using the following regulatory protocols as a guide:

- OECD Guideline for the Testing of Chemicals, Skin Absorption: *in vitro* Method, No. 428 (2004), [316].
- OECD Guidance Document for the Conduct of Skin Absorption Studies, No. 28 (2004), [136].

These guidelines are accepted as a reliable standard for conducting *in vitro* permeation experiments.

3.3.2.1 Skin preparation

Porcine skin was used in Franz cell experiments due to the limited availability and difficulties associated with the use of *ex vivo* human skin [317]. In addition, porcine skin has similar thickness, histological and permeability properties as human skin [132, 318]. Samples of dermatomed porcine skin were prepared from the flank of five month old pigs obtained from a local abattoir prior to any steam cleaning process. The skin was washed with distilled water and dried using tissue. Hair was carefully cut by scissors to avoid any damage to the *stratum corneum.* The subcutaneous fatty layer was removed using a scalpel and then the skin was dermatomed to approximately 400 µm thickness by an electrical dermatome (Zimmer electric dermatome 8821, USA). After that, skin samples were wrapped in aluminium foil and stored frozen at -20 °C. Skin samples were used within six weeks of being frozen [319].

3.3.2.2 Skin integrity test

The dermatomed skin was checked for skin integrity before performing the permeation study. The skin was placed in Franz cells with the *stratum corneum* facing upwards. The receptor chamber and the donor chamber were filled with 10 mL and 2 mL of 0.9% w/v sodium chloride solution respectively, then the Franz cells were placed in a stirring water bath (Cleaver Scientific Ltd., UK) at

37 °C for 30 minutes to equilibrate. Thereafter, the transepithelial electric resistance (TEER) was measured using a modified form of EVOM2 Voltohmmeter (World Precision Instruments, USA). Skin samples passed the skin integrity test if they showed TEER reading ≥ 3 KΩ [319].

3.3.2.3 Assembly of diffusion cells

Franz diffusion cells with an exposed surface area of 0.64 cm^2 were used for the permeation study of Aldara™ cream. Skin samples were mounted on Franz cells with the *stratum corneum* facing upwards. The receptor chamber was filled with 10 mL of 0.1N HCl used as receptor fluid to keep sink conditions because of the high solubility of imiquimod (basic compound) in this acidic medium 9.5 mg/mL (tested experimentally). Franz cells were then placed in a stirring water bath (Cleaver Scientific Ltd., UK) at 37 °C for 30 minutes to equilibrate before applying the formulation. The skin was dosed with 50 mg of Aldara™ cream and the experiment run time was 24 hours. The receptor fluid was stirred continuously by a small Teflon-coated magnetic stirrer bar at 600 rpm and it was analysed for imiquimod content by HPLC at 24 hours after cream application. Data was collected from 12 Franz cells (6 analysed by HPLC and other 6 by ToF-SIMS).

3.3.2.4 Measurement of mass balance

When the Franz cell experiments were completed (after 24 hours), the excess formulation was removed from the surface of the skin by careful application of a combination of very soft dry and moistened sponges with 3% v/v Teepol® detergent solution. The sponges were combined and analysed for imiquimod by HPLC as a total skin wash. In addition, any cream on the donor chamber inner surface was also removed by the sponges and analysed for imiquimod by HPLC as a donor chamber wash.

3.3.2.5 Tape stripping

After removing the excess cream from the skin surface, the skin was dismantled from the Franz cell assembly and left to air dry at ambient temperature for approximately 2 hours. Following this, a tape stripping technique was employed using adhesive tapes (D-Squame, Standard Sampling Discs, USA) with a diameter of 22 mm. The adhesive tapes were applied and removed successively from the same treated skin area for up to 20 strips with the aid of a roller to press the adhesive tape 10 times onto the skin surface to stretch it to avoid the effects of furrows and wrinkles on the tape stripping procedure [107]. Adhesive tapes were removed from the skin surface by tweezers in one swift motion [107] which were then placed in Eppendorf vials and stored at -20 °C until required for analysis. Tape strips obtained from 6 Franz cells were analysed by HPLC in which the tape strips from each cell were pooled together for analysis, the remaining skin after tape stripping (i.e. stripped skin without *stratum corneum* layer) was also reserved for HPLC analysis. In addition, tape strips from 3 Franz cells were analysed individually by ToF-SIMS in which the tape strips were attached to glass slides with a double sided adhesive tape where the removed *stratum corneum* facing upwards. Following this, the slides were placed in plastic petri dishes and liquid nitrogen was carefully poured into the petri dish to freeze tape strips on the slides, then the frozen slides were kept in a freeze dryer for 1 hour prior to ToF-SIMS analysis.

3.3.2.6 OCT embedding and skin cryo-sectioning

Skin samples removed from 3 Franz cells were placed in a plastic block containing optimum cutting temperature (OCT) gel (VWR International Ltd., Belgium) which is an inert mounting medium for cryotomy that solidifies upon rapid cooling. Therefore, the plastic block containing skin immersed in OCT was placed in a beaker of isopentane pre-cooled with liquid nitrogen to solidify. After solidification, the OCT blocks were wrapped in aluminum foil, placed in an airtight plastic bag and stored at -80 °C. Cryo-sectioning of skin samples was carried out by placing the OCT block in a cryostat chamber

(Thermo Cryotome™, UK) at a temperature of -20 °C. The block was allowed to equilibrate within the cryostat chamber for 30 minutes and then sectioned using a steel blade into vertical cross sections of 20 µm thickness. Following this, the cryo-sections were mounted onto clean polysine microscope adhesion slides (ThermoFisher Scientific) and freeze dried for 1 hour prior to ToF-SIMS analysis.

3.3.2.7 HPLC analysis

HPLC analysis was carried out using an Agilent 1100 series instrument (Agilent Technologies, Germany) equipped with degasser, quaternary pump, column thermostat, autosampler and UV detector. System control and data acquisition were performed using Chemostation software. The details of the HPLC chromatographic conditions are as follows: column C18 (75 × 4.6 mm) ACE5/ ACE-HPLC Hichrom Limited, mobile phase of acetate buffer pH 3.7: acetonitrile (70:30 v/v), flow rate of 1 mL/minute, UV detection at λ max. 239 nm, injection volume of 10 µL and column temperature at 25 °C.

3.3.2.7.1 Preparation of the calibration curves of imiquimod by HPLC

Two stock solutions of imiquimod, one in the extraction solvent MeOH mixture (MeOH 90%:Water 9%:0.1N HCl 1%) and the other one in 0.1N HCl (receptor fluid) were prepared at concentration of 10 µg/mL. Then solutions of different concentrations (0.039, 0.078, 0.156, 0.3125, 0.625, 1.25, 2.5, 5.0 and 10 µg/mL) were obtained by appropriate dilution from the stock solutions.

3.3.2.7.2 Determination of the percentages of imiquimod recovered by HPLC

The amount of imiquimod from the different Franz cell elements (skin wash, donor chamber wash, pooled tape strips and remaining skin after tape stripping) was extracted by the addition of 20, 10, 5 and 3 mL of the extraction solvent (MeOH mixture) respectively. They were then vortexed for 2 minutes and left overnight. Following this, they were sonicated for 30 minutes, filtered

through a 0.45 μm syringe filter and injected into the HPLC system where they were analysed using the method described in Section 3.3.2.7. Receptor fluid samples were filtered through a 0.22 μm centrifuge tube filter and injected directly into the HPLC system without any dilution.

3.3.2.8 ToF-SIMS analysis

ToF-SIMS was used to analyse individual tape strips and cryo-sectioned skin samples obtained from Franz cell testing. ToF-SIMS analysis was done using the same instrument and analysis conditions detailed in Chapter 2, Section 2.3.7. The area scanned of the tape strips samples was (9 mm × 9 mm) encompassing the entire skin area exposed to Aldara™ cream during Franz cell diffusion experiments. For the cryo-sectioned skin samples the scanned area was (6 mm × 6 mm) or (10 mm × 4 mm) depending on the section size. All the samples were analysed at a resolution of 100 pixels/mm. The tape strips and cryo-sectioned skin samples were placed in a freeze dryer for 1 hour prior to ToF-SIMS analysis to remove any moisture present in the samples. An ion representing biological material and therefore indicative of skin (skin marker) was identified as CH_4N^+ and was used to threshold the data sets. After that, the data was reconstructed to remove the data from the adhesive tape material found between the fissures in the stripped skin (removing the substrate data) and therefore the data was only analysed from the skin material. Following this, each image of the individual tape strip (9 mm × 9 mm) was divided into four smaller data sets of (4.5 mm × 4.5 mm) which results in four repeats (n = 4) for each sample and their intensities were normalised to the total ion intensity. All peak intensities were normalised to the total ion count of the spectra.

3.3.3 Skin permeation of imiquimod from DMSO and oleic acid solutions

Solutions of imiquimod in DMSO and oleic acid at concentration of 100 µg/mL were prepared and dosed onto porcine skin during Franz cell experiments, subsequently the tape strips and cryo-sectioned skin samples were analysed by ToF-SIMS. Porcine skin preparation, Franz diffusion cell experiment conditions, skin tape stripping, skin cryo-sectioning and ToF-SIMS analysis conditions were the same as mentioned previously in Section 3.3.2. However, before performing this experiment, a preliminary study was carried out to determine the concentration at which ToF-SIMS could detect imiquimod in DMSO and oleic acid solutions. This was achieved by spiking 1 µL of imiquimod in these solutions at concentrations of 1, 10 and 100 µg/mL onto tape strips obtained from porcine skin with subsequent analysis by ToF-SIMS.

3.3.4 Statistical analysis of the data

The statistical tests used to compare ion intensities were one way ANOVA with Tukey's multiple comparisons test or t-test. All data is presented as the mean ± SD of n = 4 with P values of ≤ 0.05 being regarded as significant using GraphPad Prism 7 software (USA). Prior to statistical analysis all data was tested for normality using Shapiro-wilk normality test.

3.4 Results and Discussion

3.4.1 Permeation study of Aldara™ cream

3.4.1.1 HPLC chromatograms and calibration curves of imiquimod

Imiquimod shows a sharp, well separated peak which is present at approximately two minutes in both MeOH mixture (extraction solvent) and in 0.1N HCl (receptor fluid) as illustrated in the HPLC chromatograms Figures 3.1 and 3.2 respectively.

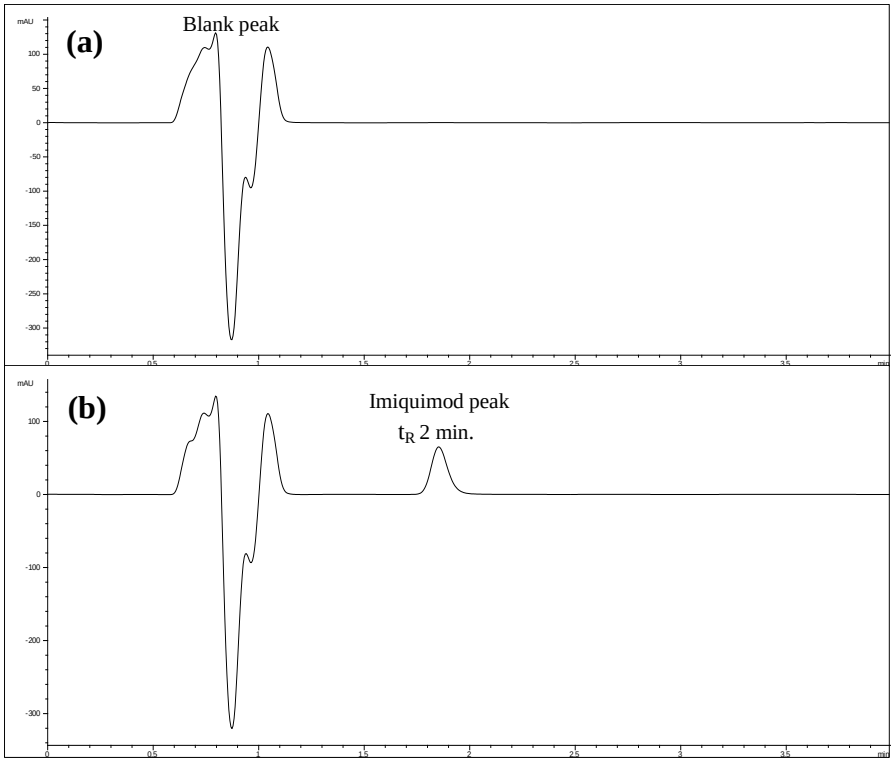

Figure 3.1: *HPLC chromatograms of imiquimod in MeOH mixture (extraction solvent) showing (a) blank chromatogram and (b) imiquimod chromatogram.*

The calibration curves of imiquimod in MeOH mixture and in 0.1N HCl generated by HPLC are shown in Figure 3.3a and b respectively which are observed to be linear at the range of concentration used with an R-squared value of 0.99 in both media. Therefore, a reliable measurement for the area under the curve can be obtained within this range of concentration. The limit of detection (LoD) and limit of quantitation (LoQ) are determined experimentally

according to the signal/noise ratio and CV% methods [304]. For imiquimod in a MeOH mixture, the LoD and LoQ were found to be at a concentration of 0.346 µg/mL. For 0.1N HCl, the LoD and LoQ were found at 0.151 µg/mL and 0.303 µg/mL respectively.

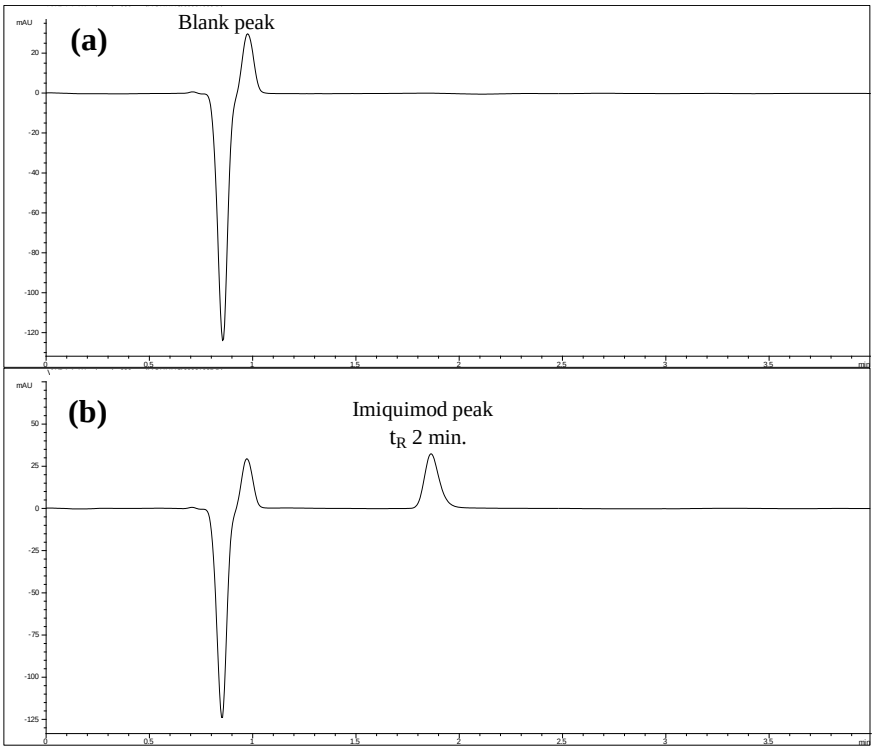

Figure 3.2: *HPLC chromatograms of imiquimod in 0.1N HCl (receptor fluid) showing (a) blank chromatogram and (b) imiquimod chromatogram.*

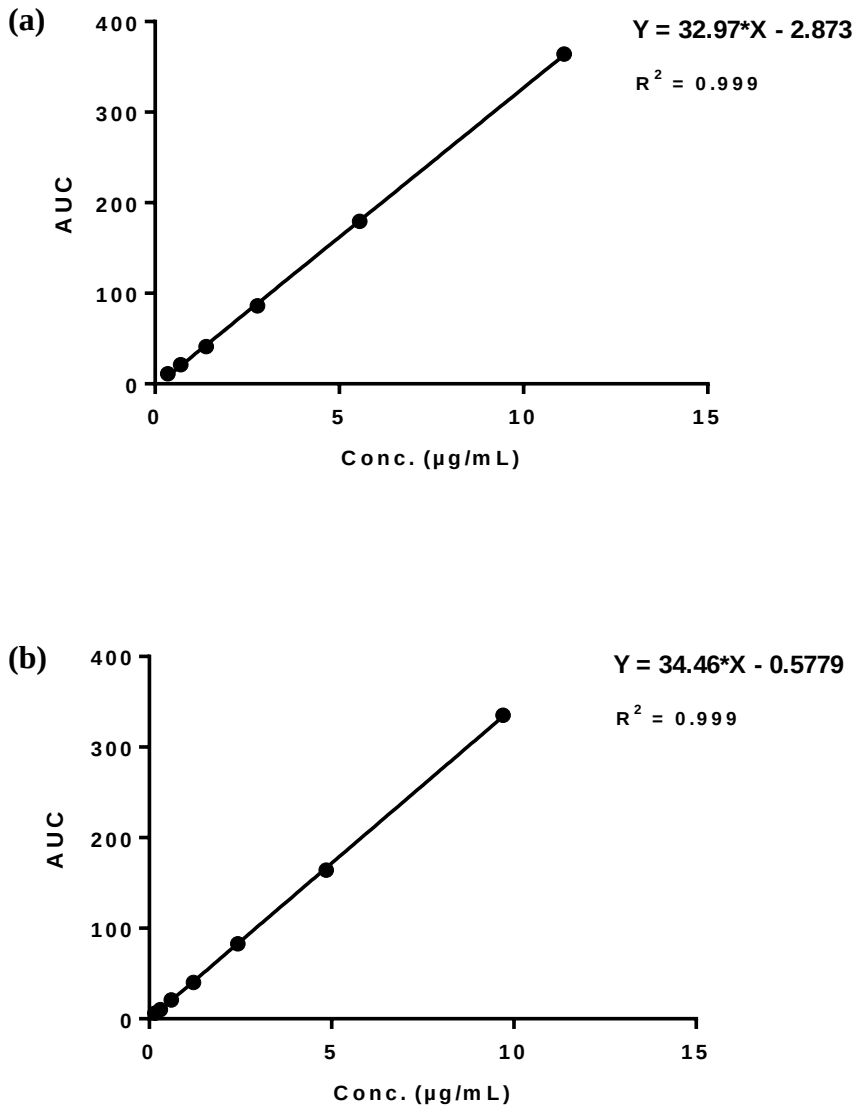

Figure 3.3: *Calibration curves of imiquimod in (a) MeOH mixture (extraction solvent) and (b) in 0.1N HCl (receptor fluid) by HPLC. Data is presented as the mean ± SD (n = 3).*

3.4.1.2 Determination of the percentage of imiquimod recovered from Aldara™ cream permeation study by HPLC

The percentage of imiquimod recovered from the different Franz cell elements (donor chamber wash, skin wash, tape strips, remaining skin and receptor fluid) of the permeation study of Aldara™ cream when analysed by HPLC are reported in Table 3.1 and graphically illustrated in Figure 3.4. The recovery percentage of imiquimod is highest in the skin wash as compared to other

elements indicating that Aldara™ cream has limited permeation into the skin with most of the imiquimod being recovered from the skin wash (mean recovery percentage is 90%) with a very minor amount (< 1%) recovered from the remaining skin. The recovery percentage of imiquimod from the tape strips is also low (1.18% ± 0.69) which indicates the existence of imiquimod in the *stratum corneum* at low concentration. The receptor fluid also shows a low recovery percentage of imiquimod (0.89% ± 0.19) which highlights the limited permeation of imiquimod across the skin to reach the receptor fluid compartment. The sum of the mean recovery percentage of imiquimod from the different Franz cell elements is approximately 95%. The 5% difference is thought to be lost during the extraction process prior to HPLC analysis. This data suggests that skin permeation of Aldara™ cream is very superficial and is consistent with the FDA approval specification and clinical trials that showed the efficacy of Aldara™ cream only for the treatment of superficial BCC lesions [45, 53].

The high lipophilicity and low aqueous solubility of imiquimod suggests that it exhibits more permeation into the *stratum corneum* layer compared with the more aqueous viable epidermis and therefore it may remain stored within the *stratum corneum* since the next layer (the viable epidermis) has high water content. Several studies have shown that lipophilic drugs and lipophilic sunscreens tend to be preferably located, or accumulated, on the skin surface and in the superficial layers of the *stratum corneum* [208, 320].

Table 3.1: *Recovery percentage of imiquimod from the different Franz cell elements of the permeation study of Aldara™ cream by HPLC.*

	Franz cells number							
Analysed element	**1**	**2**	**3**	**4**	**5**	**6**	**Mean recovery %**	**SD**
Donor wash	0.48	3.96	2.51	1.39	0.78	1.57	2.04	± 1.23
Skin wash	94.55	79.81	88.32	95.12	89.77	93.52	90.18	± 5.75
Tape strips	0.63	2.55	0.96	1.17	0.89	0.91	1.18	± 0.69
Remaining skin	0.45	1.47	1.08	0.92	0.81	0.75	0.91	± 0.34
Receptor fluid	0.75	0.93	1.24	0.67	0.86	0.91	0.89	± 0.19
	% Recovered							

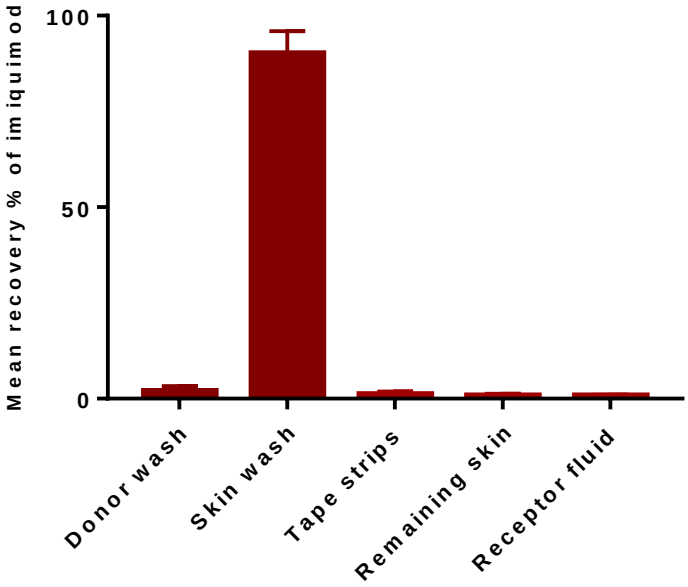

Figure 3.4: *Mean recovery percentage of imiquimod from the different Franz cell elements (donor chamber wash, skin wash, tape strips, remaining skin and receptor fluid) of the permeation study of Aldara™ cream when analysed by HPLC. Data is presented as the mean ± SD (n = 6).*

3.4.1.3 ToF-SIMS analysis

Due to several advantages offered by ToF-SIMS (discussed in Chapter 1, Section 1.7.6), it is used in these studies to detect and image imiquimod in tape stripped and cryo-sectioned skin samples obtained from the Aldara™ cream permeation and from DMSO and oleic acid experiments. Prior to ToF-SIMS analysis of the tape strips and cryo-sectioned skin samples, some preliminary ToF-SIMS experiments of the reference imiquimod material were performed to establish secondary ions representative of the imiquimod chemistry.

3.4.1.3.1 ToF-SIMS analysis of imiquimod reference on silicon wafer

ToF-SIMS survey spectra of imiquimod reference on silicon wafer in both positive and negative polarity are shown in Figure 3.5a and b.

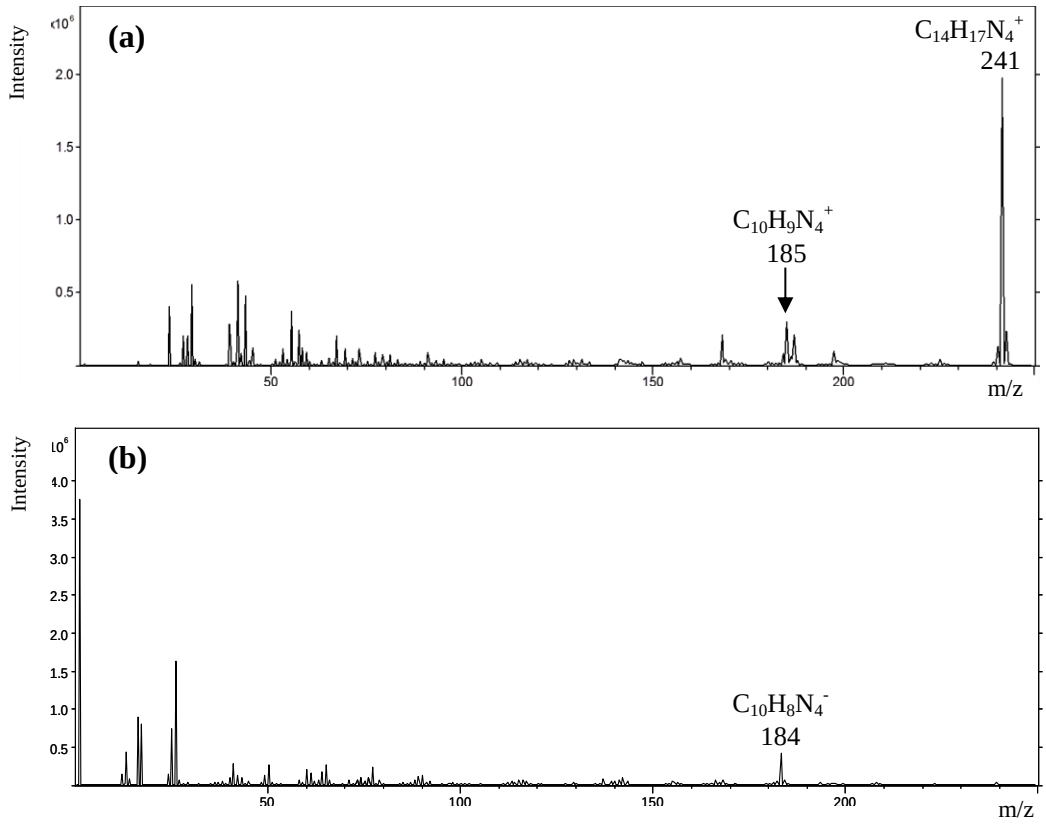

Figure 3.5: *ToF-SIMS spectra of imiquimod reference in (a) positive polarity and (b) negative polarity.*

As shown in Figure 3.5a, two secondary ion peaks relevant to imiquimod are observed in the positive polarity spectra, the molecular ion $[M+H]^+$ peak of imiquimod ($C_{14}H_{17}N_4^+$) at m/z = 241 and the fragment ion peak ($C_{10}H_9N_4^+$) at m/z = 185. The $[M+H]^+$ of imiquimod ($C_{14}H_{17}N_4^+$) which resulted from the ionisation of the whole imiquimod molecule $C_{14}H_{16}N_4$ (MW 240) is more intense than the fragment ion peak. Figure 3.5b shows the negative polarity data which highlights the fragment ion peak ($C_{10}H_8N_4^-$) at m/z = 184. The positive ion mode is therefore considered to be more informative than the negative ion mode due to the presence of the $[M+H]^+$ at a relatively high intensity which provides unambiguous identification of imiquimod. Therefore, the ToF-SIMS data of imiquimod will be presented in the positive polarity only. (CH_4N^+) peak at m/z = 30 which is generally considered as a generic marker for organic material in positive polarity, used in this work as a skin marker to indicate the regions on the sample containing skin tissue (i.e. it represents the skin pattern). The (CH_4N^+) peak shows a higher normalised ion intensity in the skin control sample than in the imiquimod reference material (Fig. 3.6). This verifies the appropriate use of (CH_4N^+) peak as a skin marker.

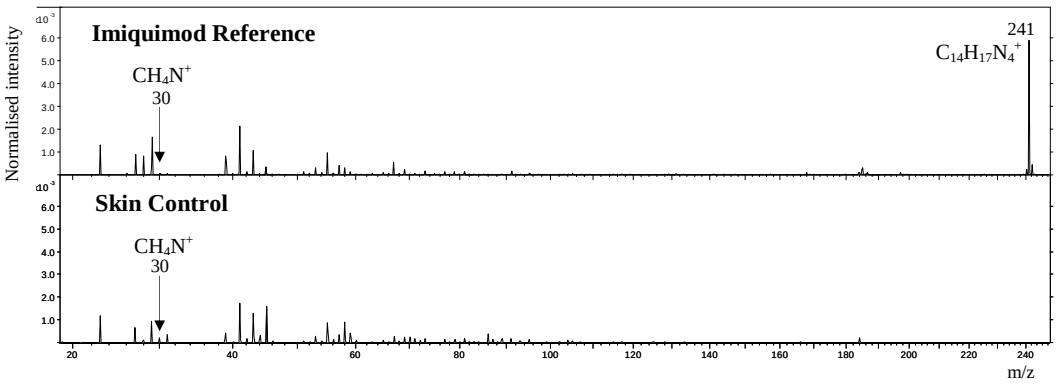

Figure 3.6: *Stacked ToF-SIMS spectra of imiquimod reference material and skin control sample showing the peak of skin marker ion (CH_4N^+) at m/z = 30.*

3.4.1.3.2 ToF-SIMS analysis of Aldara™ cream on silicon wafer

The ToF-SIMS survey spectrum of Aldara™ cream placed on silicon wafer is shown in Figure 3.7. Although the peak of the $[M+H]^+$ of imiquimod in Aldara™ cream is not very intense (relative to an analysis of pure imiquimod

reference material (Fig. 3.5a)), it is clearly resolved suggesting that ToF-SIMS can be used to identify imiquimod in Aldara™ cream.

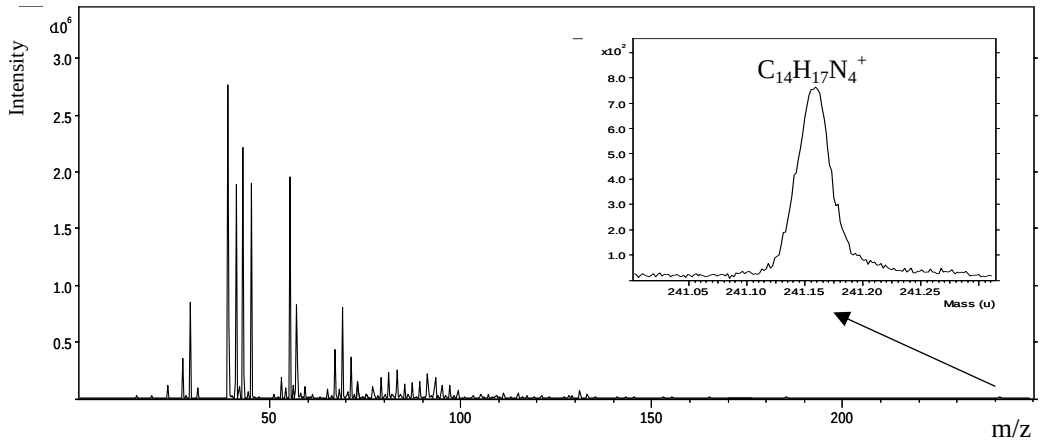

Figure 3.7: *ToF-SIMS survey spectrum of Aldara™ cream, where the inset spectrum shows the peak of the [M+H]$^+$ of imiquimod at m/z = 241.*

3.4.1.3.3 ToF-SIMS analysis of Aldara™ cream tape strips

To assess the exact permeation of imiquimod and visualise its distribution within the *stratum corneum*, tape strips obtained from Franz cell experiments were analysed by ToF-SIMS. Spectra showing the [M+H]$^+$ of imiquimod in Aldara™ cream tape strips are shown in Figure 3.8 (specifically showing strips 1, 2, 6, 12 and 18), in which the [M+H]$^+$ of imiquimod is detected throughout the series of 18 tape strips. A decreasing ion intensity is observed from the outer surface of the skin (TS 1) to the inner layers of the *stratum corneum* (TS 18). The ability of ToF-SIMS to analyse single tape stripped skin samples (layer by layer level analysis) to map the permeation of imiquimod within the *stratum corneum* has not been previously observed and this study provides new insight into the exact depth of permeation achieved with this drug. This work represents the first time use of the ToF-SIMS to assess the permeation of imiquimod from the Aldara™ cream into the skin as a function of depth.

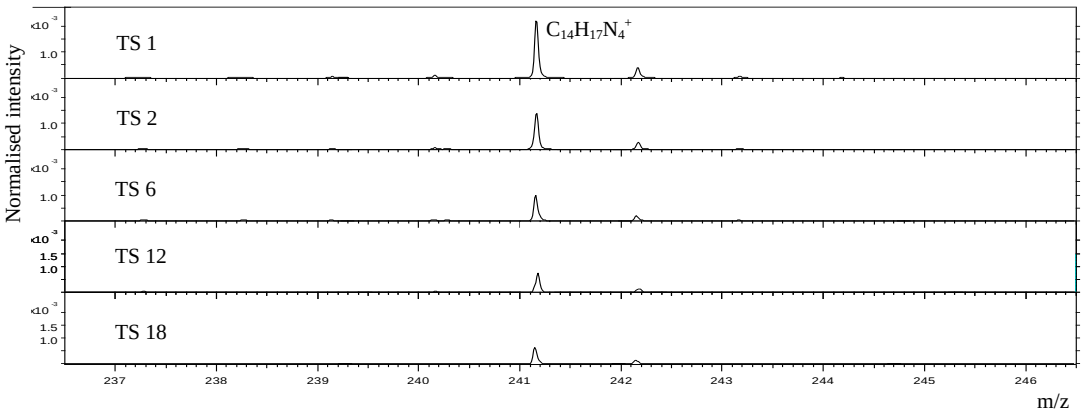

Figure 3.8: *Stacked ToF-SIMS spectra of the $[M+H]^+$ of imiquimod in Aldara™ cream tape strips showing the peak of the $[M+H]^+$ of imiquimod ($C_{14}H_{17}N_4^+$) at m/z = 241.*

Figure 3.9 illustrates the ion intensity values of the $[M+H]^+$ of imiquimod from the different tape strips normalised to total ion intensity following the removal of the substrate (adhesive tape background) plotted versus tape strip number. This data confirms the reduction in ion intensity values from TS 1 to TS 18 ($p \leq 0.05$) observed in Figure 3.8.

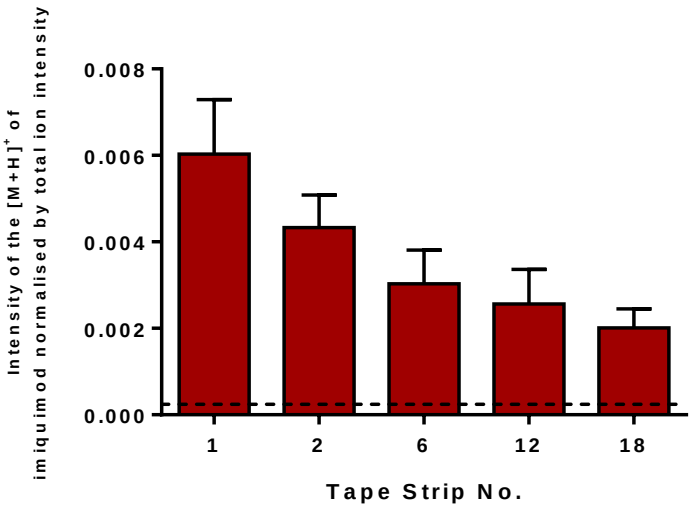

Figure 3.9: *Ion intensity values of the $[M+H]^+$ of imiquimod in Aldara™ cream tape strips normalised by total ion intensity. Data is presented as the mean ± SD (n = 4). The dotted black line represents the ion intensity obtained from the control skin samples.*

The tape stripping process was only confined to 20 tape strips. However, it is observed that the ion intensity of the $[M+H]^+$ of imiquimod at TS 18 is still significantly higher compared to the skin control ion intensity ($p \leq 0.05$). This indicates that the removed 20 tape strips did not achieve complete removal of the *stratum corneum* layer and imiquimod may remain at the lower layers of the *stratum corneum*.

The decreasing permeation of imiquimod at the inner layers of the *stratum corneum* is consistent with the HPLC results that demonstrated a limited permeation of imiquimod into the deeper skin layers (less than 1% recovered from the remaining skin specimen, Section 3.4.1.2). However, importantly, ToF-SIMS has shown enhanced sensitivity in the detection of imiquimod in the tape strips as compared to HPLC analysis to the extent that imiquimod within single tape strips can be successfully analysed throughout the entire *stratum corneum*.

As well as enhanced sensitivity compared to HPLC, ToF-SIMS also has an imaging capability. Visualisation of imiquimod's spatial distribution within skin layers can be achieved by ion beam rastering (scanning) of the tape strips obtained from the permeation study. ToF-SIMS ion images of the entire tape strip area, which represents the whole exposed area of the skin to Aldara™ cream during Franz cell diffusion experiment, are illustrated in Figure 3.10. Figure 3.10 illustrates the total ion image (Fig. 3.10a), the skin marker (CH_4N^+) image (Fig. 3.10b) and the $[M+H]^+$ of imiquimod ($C_{14}H_{17}N_4^+$) image (Fig. 3.10c).

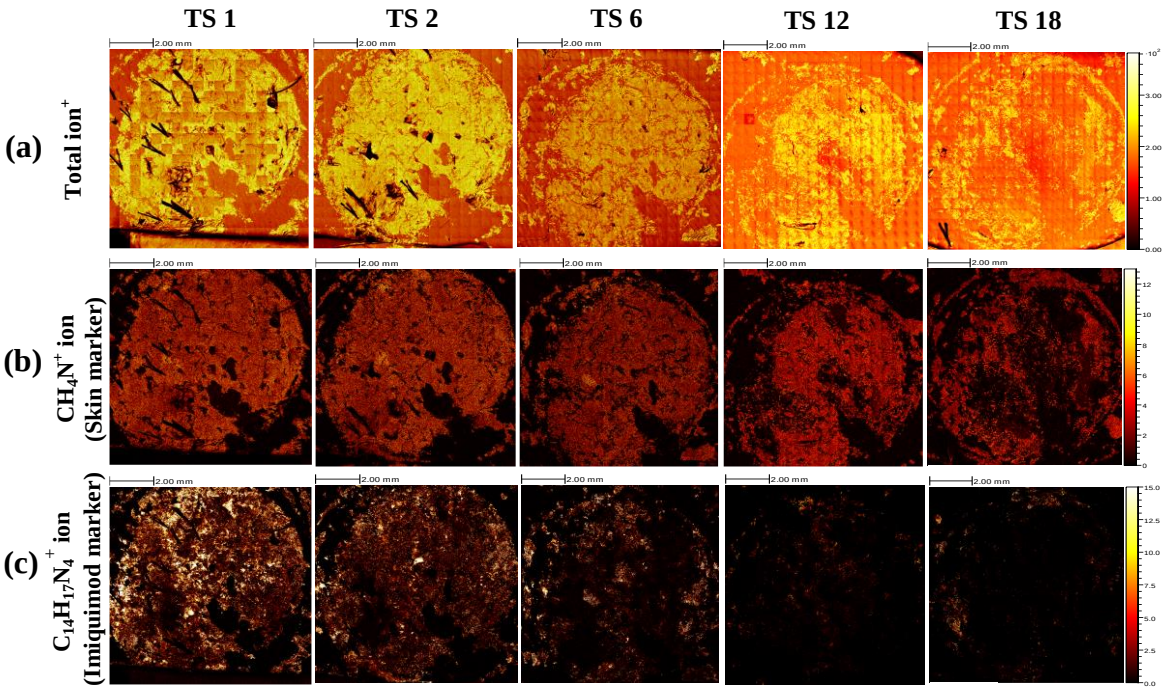

Figure 3.10: *ToF-SIMS ion images of Aldara™ cream tape strips showing: (a) the total ion$^+$, (b) the skin marker (CH_4N^+) and (c) the imiquimod marker ($C_{14}H_{17}N_4^+$). The scanned area is (9 mm × 9 mm).*

An examination of the skin marker, CH_4N^+ (Fig. 3.10b), shows that the amount of skin (corneocytes) attached per tape strip is reduced moving from the outer skin surface (TS 1) towards the inner layers of the *stratum corneum* (TS 18). Similar observations of decreasing skin amount from the upper to lower tape strips have been reported by other studies when corneocytes on tape strips were determined by different methods such as the weighing method, protein assay method and UV/visible method. This is due to the increased cohesion between the cells at the deeper *stratum corneum* layers compared to the outer layers which results in reduced amounts of skin being removed by a tape strip [106, 116, 321]. This higher cohesion at the deeper *stratum corneum* layers can be attributed to the increased number of corneosomes (*stratum corneum* desmosomes) from the skin surface towards the inner layers [322]. Furthermore, the ion intensity of the $[M+H]^+$ of imiquimod (Fig. 3.10c) which represents a reflection of the imiquimod spectra is also observed to decrease from the uppermost layer (TS 1) towards the deeper layer of the *stratum*

corneum (TS 18) with a non-uniform pattern of distribution within the *stratum corneum* layers where some skin areas shows spots of higher imiquimod density than the others. This is thought to be related to the pathway by which imiquimod in Aldara™ cream permeates through the skin (i.e. the existence of a particular constituent such as fatty acids that may facilitate the permeation of imiquimod into the skin) which is influenced by the physicochemical properties of imiquimod, the vehicle and formulation type.

The distribution of curcumin (lipophilic fluorescent dye) within the *stratum corneum* from different formulations has been studied by other researchers. They analysed tape strips removed from human volunteers using laser scanning microscopy (LSM) [208] or fluorescent microscopy [323] and demonstrated that the distribution and localisation of a particular dye is influenced by the physicochemical properties of the dye and the type of vehicle used which affects the pathway of penetration.

To investigate the effect of experimental conditions such as drying effect on the spatial distribution of imiquimod within skin, samples of skin homogenate were spiked with imiquimod dissolved in DMSO. Some of these samples were snap frozen immediately by liquid nitrogen and others left to air dry for 2 hrs prior to freeze drying. Both samples show a similar spatial distribution of imiquimod when analysed by ToF-SIMS (Fig. 3.11). This highlights that the non-uniform distribution of imiquimod within skin is not related to the experimental conditions. Furthermore, as shown in Figure 3.10c the non-uniform distribution is more pronounced at lower tape strips TS 6, 12 and 18 than TS 1 and 2. Thus, if the experimental conditions influence the distribution, they should affect all tape strips to the same extent. This condition is also applied for CHG tape strips (Chapter 5, Fig. 5.4) in which CHG is more uniformly distributed at TS 2 than other tape strips.

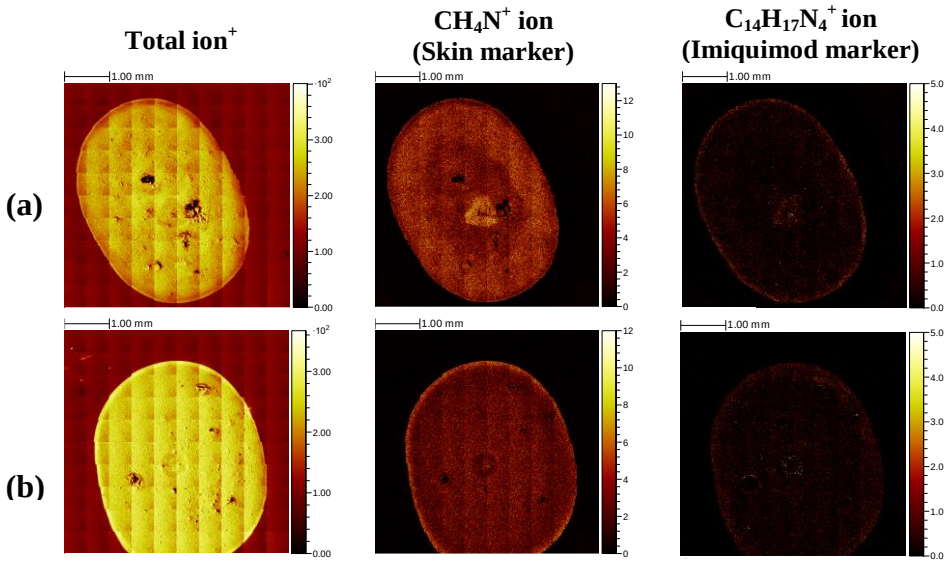

Figure 3.11: *ToF-SIMS ion images of drops of skin homogenate spiked with imiquimod in DMSO where (a) frozen immediately by liquid nitrogen and (b) left to air dry for 2 hrs prior to freeze drying.*

This non-uniform distribution of imiquimod within skin can decrease the efficacy of Aldara™ cream to uniformly treat whole BCC lesions. The pattern of drug distribution within the skin layers is very important in BCC because the whole lesion area should be treated uniformly at the effective concentration to increase the cure rate and prevent recurrence. Therefore, the ability to assess this is of great importance, since the topical treatment of BCC lesions with Aldara™ cream has shown higher recurrence rate in comparison to surgery [56], particularly tumours with a thickness of > 0.4 mm [48]. This is believed to be the first attempt to visualise the localisation of imiquimod within skin permeated from Aldara™ cream in a large scanned area of (9 mm × 9 mm) by ToF-SIMS. This provides information regarding the uniformity of imiquimod within skin which may assist to improve the design of imiquimod's formulations in the future.

3.4.1.3.4 ToF-SIMS analysis of Aldara™ cream cryo-sectioned samples

ToF-SIMS analysis of cryo-sectioned skin samples (prepared as described in Section 3.3.2.6) is used to map imiquimod permeation within different skin layers. Skin cross-sectioning can be used as a complementary tool to the tape stripping technique to follow and visualise drug permeation within skin. Skin sections were prepared by the OCT embedding method rather than the formalin-fixed paraffin embedding (FFPE) method to avoid the introduction of different solvents used in FFPE method such as paraformaldehyde, ethanol and xylene into the skin that may 'wash out' imiquimod from the tissue and influence the chemistry of samples. In addition, it has been reported that tissue sections prepared by FFPE can be covered with a layer of paraffin and this overlayer of paraffin can influence tissue signals when analysed by ToF-SIMS [324]. Although, this paraffin layer could be removed by short sputtering with C_{60} cluster ion but it may induce sample damage. Another issue associated with FFPE is that the formalin which is used as a fixative agent and the clearing agent xylene can extract lipids from tissue sections affecting the analysis results [324, 325]. Malm *et al.* compared the influence of different methods used in the fixation and drying of cells on the chemical structure and morphology of human fibroblasts when analysed by ToF-SIMS and they concluded that cryofixation and freeze drying can be utilised as a general preparation protocol to prepare cells for ToF-SIMS analysis with a preserved cell morphology and retained distribution of the diffusible ions [326]. In this work, sections of a thickness of 20 μm were found to be more appropriate for ToF-SIMS analysis in terms of how flat the sections were and clarity of the images compared to 10 or 30 μm thickness samples.

Figure 3.12 illustrates the ToF-SIMS spectra of the skin control and Aldara™ cream cryo-sectioned skin samples. The ion intensity of the $[M+H]^+$ of imiquimod is at the background or noise level for the skin control samples (Fig. 3.12a) while, it is at higher intensity for Aldara™ cream sections (Fig. 3.12b). Although, this intensity is not very high it is clearly resolved.

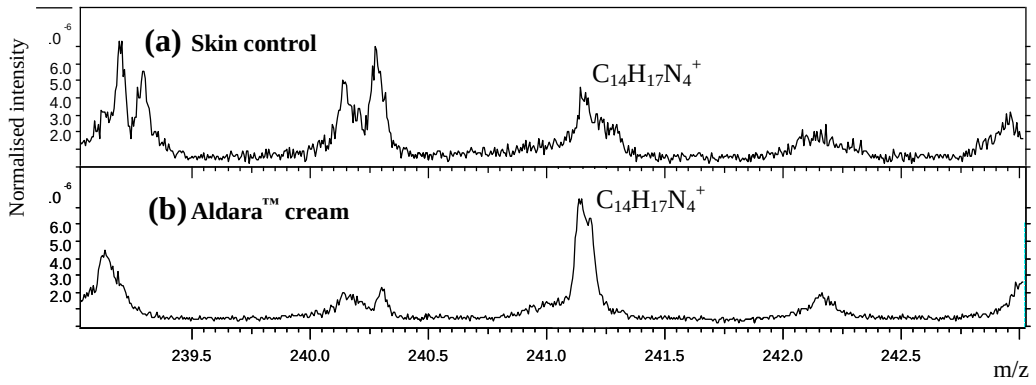

Figure 3.12: *Stacked ToF-SIMS spectra of the cryo-sectioned samples for (a) skin control and (b) Aldara™ cream, showing the peak of the [M+H]$^+$ of imiquimod ($C_{14}H_{17}N_4^+$) at m/z = 241.*

ToF-SIMS ion images of the cryo-sectioned samples for the skin control and Aldara™ cream are shown in Figure 3.13 which illustrates the total ion image (Fig. 3.13a), the skin marker (CH_4N^+) image (Fig. 3.13b) and the [M+H]$^+$ of imiquimod image (Fig. 3.13c). An examination of the total ion image and the skin marker image (Fig. 3.13a and b) indicates that the skin is adequately sectioned using the conditions mentioned in Section 3.3.2.7. ToF-SIMS ion images are strongly dependent on the quality of the cross-sectioned skin samples. The samples should be well sectioned and quite flat in order to minimise sample topography and obtain clear ToF-SIMS images. However, the identification of the different skin layers within a skin section such as the *stratum corneum*, viable epidermis and dermis is not straightforward and require the matching of a ToF-SIMS image to a microscope image to recognise the different skin layers. Therefore, an examination of the cryo-sectioned samples under a light microscope was carried out to identify the *stratum corneum* layer prior to ToF-SIMS analysis. An assessment of the [M+H]$^+$ of imiquimod image (Fig. 3.13c) shows the absence of imiquimod from the skin control section and its existence in Aldara™ cream sectioned samples at a low intensity in the *stratum corneum*. Therefore, this image further confirms the limited availability of imiquimod at the deeper skin layers but does illustrate its permeation into the *stratum corneum*.

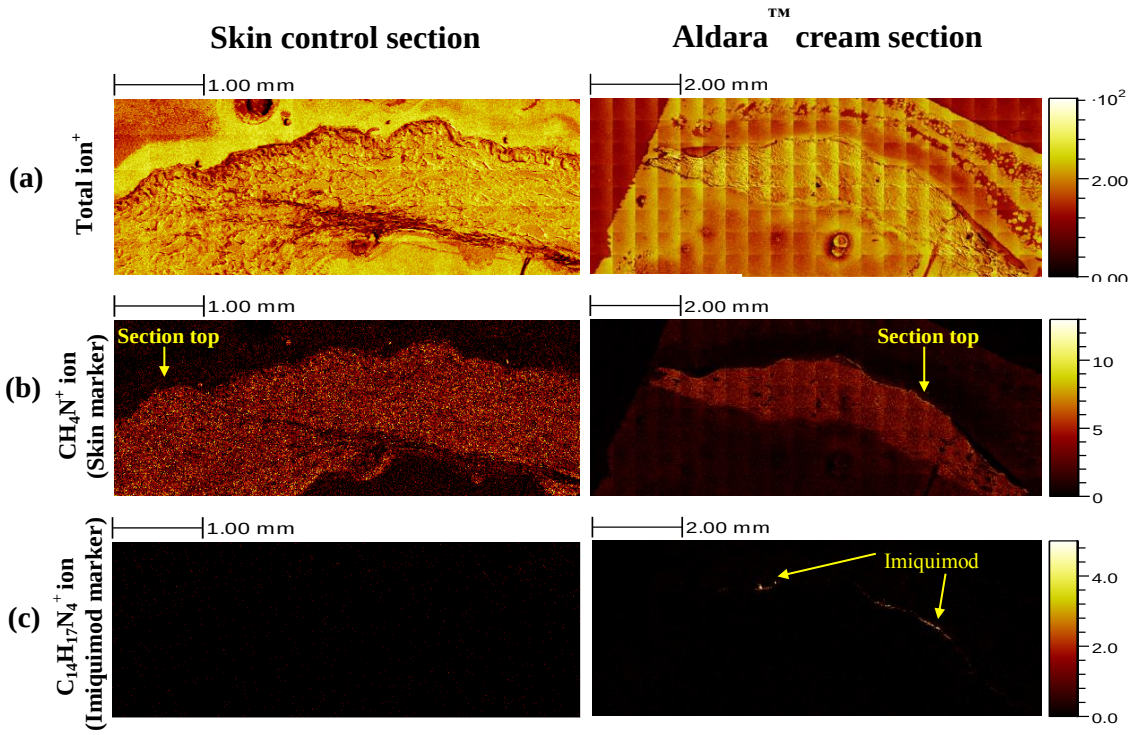

Figure 3.13: *ToF-SIMS ion images of the cryo-sectioned samples for the skin control and Aldara™ cream showing (a) the total ion$^+$, (b) the skin marker (CH_4N^+) and (c) the imiquimod marker ($C_{14}H_{17}N_4^+$).*

3.4.2 Skin permeation of imiquimod from DMSO and oleic acid solutions

As the HPLC and ToF-SIMS results for Aldara™ cream have shown the limited permeability of imiquimod into the skin and since greater permeation is anticipated from DMSO and oleic acid solutions (chemical penetration enhancers) [203, 327, 328], solutions of imiquimod in DMSO and oleic acid at concentration of 100 µg/mL were prepared and dosed onto porcine skin during Franz cell experiments to investigate the permeability of imiquimod into the deeper skin layers from these simple solutions before moving to more sophisticated formulations such as microemulsions.

3.4.2.1 Determination of imiquimod concentration in DMSO and oleic acid solutions detected by ToF-SIMS

A preliminary experiment was carried out to determine the concentration at which ToF-SIMS could detect imiquimod in DMSO and oleic acid solutions. It was observed that the $[M+H]^+$ of imiquimod is more intense at the concentration of 100 than 10 or 1 µg/mL as shown in Figure 3.14. Therefore, the concentration of 100 µg/mL is applied for imiquimod in DMSO and oleic acid Franz cell diffusion experiments.

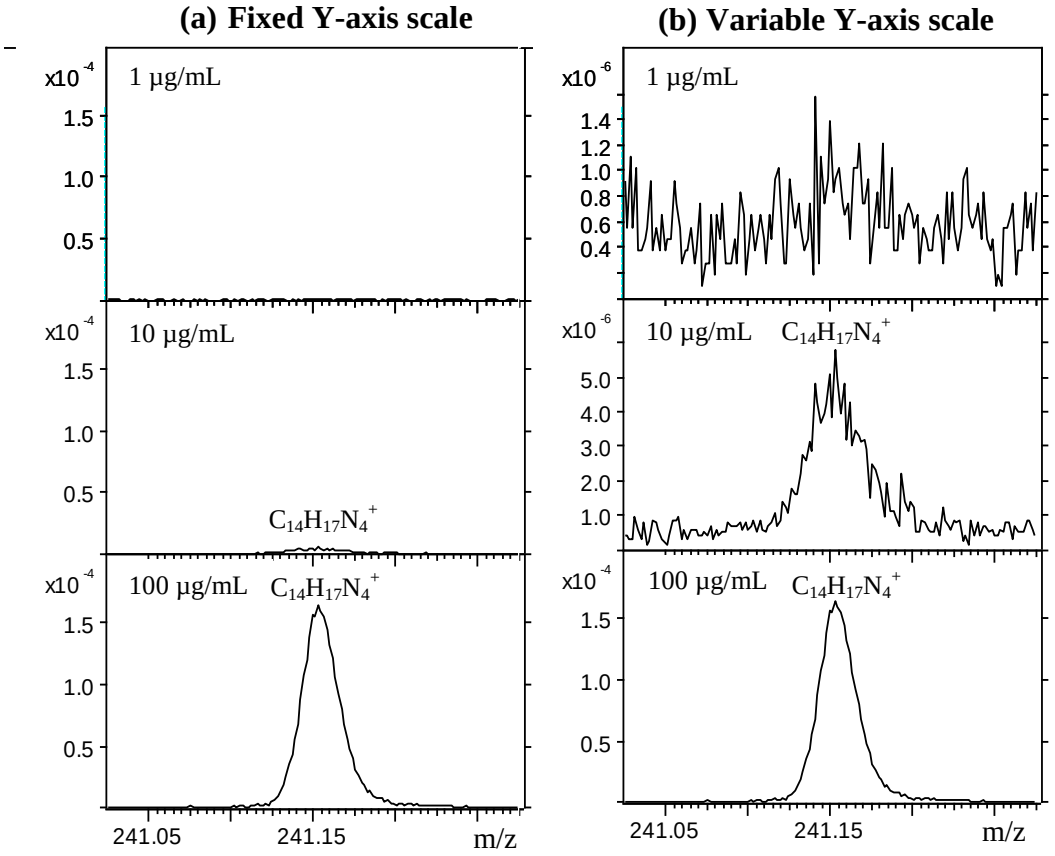

Figure 3.14: *ToF-SIMS spectra of imiquimod in DMSO at concentrations of (1, 10 and 100 µg/mL) spiked on tape strips showing the peak of the $[M+H]^+$ of imiquimod $C_{14}H_{17}N_4^+$ at m/z = 241, where (a) ion intensity at fixed Y-axis scale and (b) at variable Y-axis scale.*

3.4.2.2 ToF-SIMS analysis of the tape strips of imiquimod in DMSO solution

ToF-SIMS ion images of the tape strips of imiquimod in DMSO solution are shown in Figure 3.15. Due to the aggressive nature of DMSO as a solvent, tape strip one (TS 1) is observed to remove most of the *stratum corneum* layer with very little amount being removed by the second tape strip (Fig. 3.15b). Therefore, it is thought that the tape stripping in this condition is unreliable and skin cross-sectioning could provide the more relevant and reliable method to map imiquimod permeation from the DMSO solution.

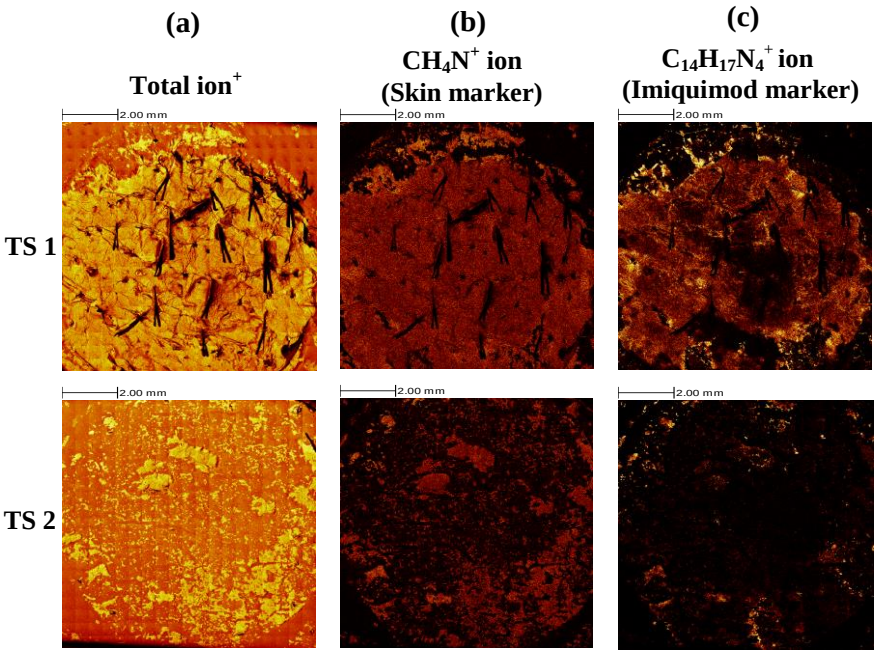

Figure 3.15: *ToF-SIMS ion images of imiquimod in DMSO tape strips 1 and 2 showing: (a) the total ion$^+$, (b) the skin marker (CH_4N^+) and (c) the imiquimod marker ($C_{14}H_{17}N_4^+$).*

3.4.2.3 ToF-SIMS analysis of the cryo-sectioned skin samples of imiquimod in DMSO solution

A ToF-SIMS spectrum (showing the 241 m/z region) of the cryo-sectioned skin samples of imiquimod in DMSO solution is illustrated in Figure 3.16. The $[M+H]^+$ of imiquimod could be clearly detected at m/z = 241. Additionally, an assessment of the $[M+H]^+$ image (Fig. 3.17c) shows the presence of imiquimod

in the skin section, most apparently at the *stratum corneum*. This suggests the limited ability of the penetration enhancer DMSO to enhance permeation of imiquimod into the deeper skin layers and the requirement of using another approach to achieve improvement in permeation.

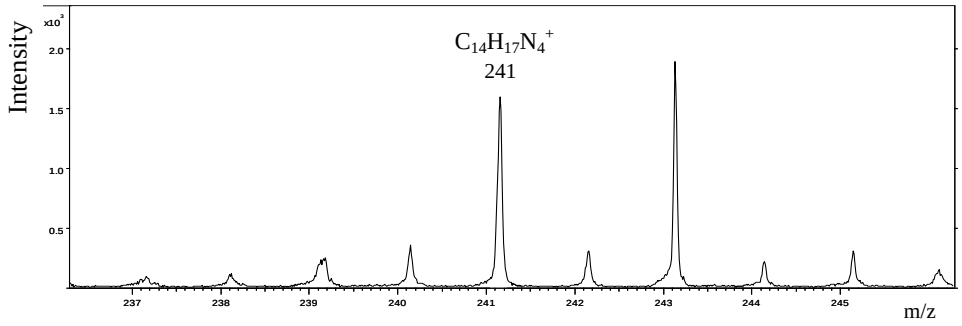

Figure 3.16: *ToF-SIMS spectrum of the cryo-sectioned skin samples of imiquimod in DMSO solution showing the peak of the $[M+H]^+$ of imiquimod ($C_{14}H_{17}N_4^+$) at m/z = 241.*

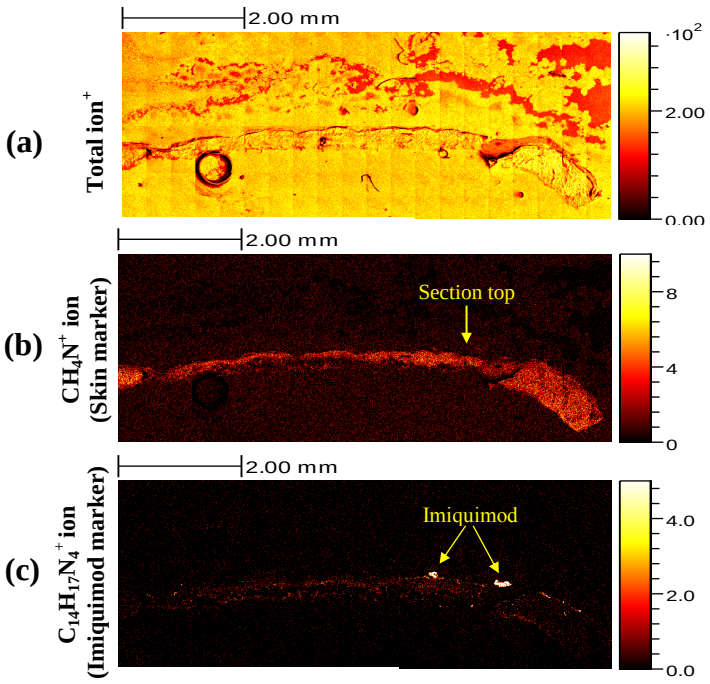

Figure 3.17: *ToF-SIMS ion images of the cryo-sectioned skin samples of imiquimod in DMSO solution showing (a) the total ion$^+$, (b) the skin marker (CH_4N^+) and (c) the imiquimod marker ($C_{14}H_{17}N_4^+$).*

3.4.2.4 ToF-SIMS analysis of the tape strips of imiquimod in oleic acid solution

Figure 3.18 shows the ToF-SIMS spectra of the $[M+H]^+$ of imiquimod in the different oleic acid tape strips, where the $[M+H]^+$ of imiquimod is detected at tape strip one (TS 1) to tape strip twenty (TS 20) with a decreasing ion intensity. Rationally, the removed amount of skin and a drug content is higher in the first tape strip than the other tape strips [107] but in the case of oleic acid, the removed amount of skin and the ion intensity of the $[M+H]^+$ of imiquimod in tape strip one is slightly less than tape strip two (Fig. 3.19). However, this difference is not significant at ($p \leq 0.05$).

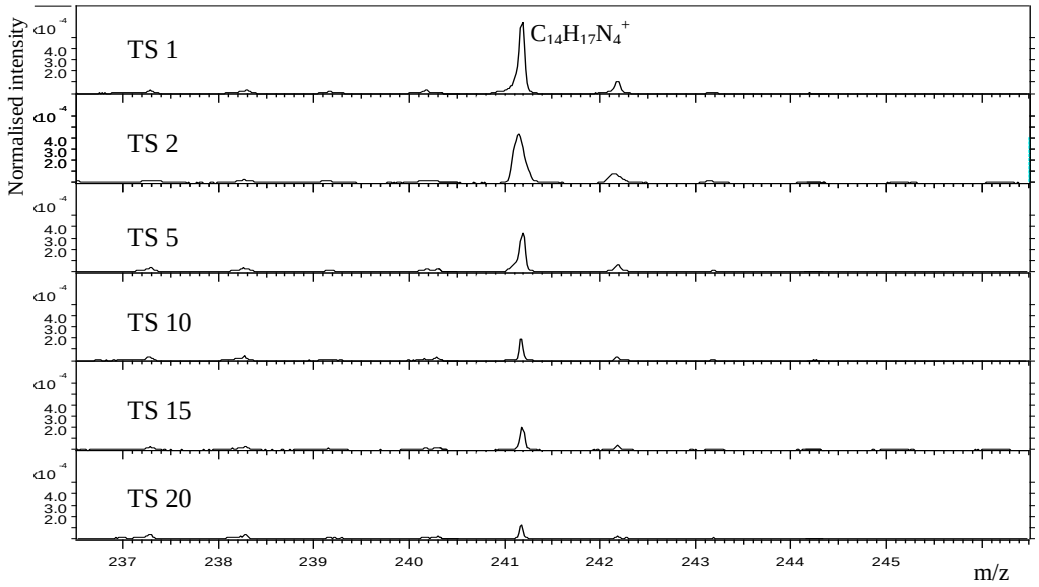

Figure 3.18: *stacked ToF-SIMS spectra of the $[M+H]^+$ of imiquimod in oleic acid tape strips showing the peak of the $[M+H]^+$ of imiquimod ($C_{14}H_{17}N_4^+$) at m/z = 241.*

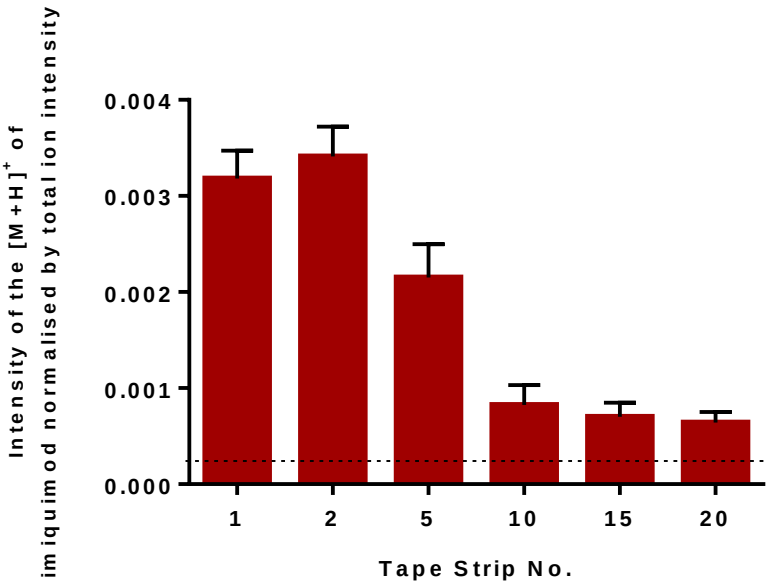

Figure 3.19: *Ion intensity values of the $[M+H]^+$ of imiquimod in oleic acid tape strips normalised by total ion intensity. Data is presented as the mean ± SD (n = 4). The dotted black line represents the ion intensity obtained from the control skin samples.*

Figure 3.20 illustrates ToF-SIMS ion images of the tape strips of imiquimod in oleic acid solution showing the total ion image (Fig. 3.20a), the skin marker (CH_4N^+) image (Fig. 3.20b) and the imiquimod marker image (Fig. 3.20c). An examination of the skin marker (CH_4N^+) image (Fig. 3.20b) demonstrates that there is a decrease in the amount of skin removed by a tape strip from the outer skin surface (TS 1) towards the inner layers of the *stratum corneum* (TS 20). However, it seems that tape strip one has removed less skin than tape strip two due to the oily nature of oleic acid which reduces the tackiness of the first tape strip. In addition, it is observed that the amount of skin removed by the lower tape strips (TS 15 and TS 20) is significantly reduced which may result in an unreliable determination of imiquimod concentration at these lower tape strips. An assessment of the images of the $[M+H]^+$ of imiquimod (Fig. 3.20c) which represents a reflection of the imiquimod spectra shows that the ion intensity of the $[M+H]^+$ is also decreased from the outer to the inner layers of the *stratum corneum* with a non-uniform distribution of imiquimod within these layers.

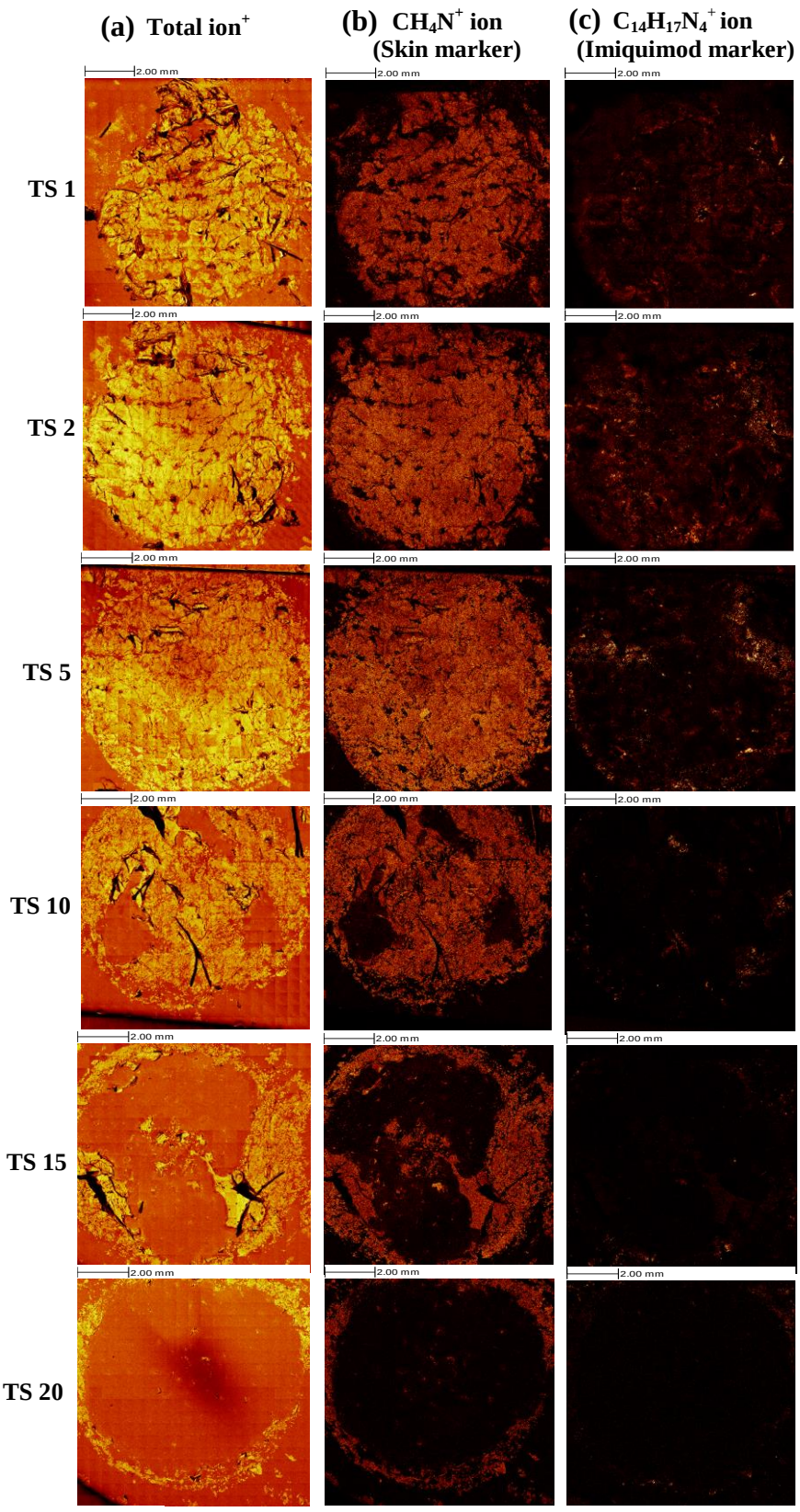

Figure 3.20: *ToF-SIMS ion images of imiquimod in oleic acid tape strips showing: (a) the total ion$^+$, (b) the skin marker (CH_4N^+) and (c) the imiquimod marker ($C_{14}H_{17}N_4^+$).*

3.4.2.5 ToF-SIMS analysis of the cryo-sectioned skin samples of imiquimod in oleic acid solution

Although, the intensity of the $[M+H]^+$ of imiquimod is not as intense as for DMSO cryo-sectioned samples, it is still detected at m/z = 241 as illustrated in Figure 3.21. The secondary ion image of the $[M+H]^+$ of imiquimod also shows the existence of imiquimod at the *stratum corneum* layer (Fig. 3.22c).

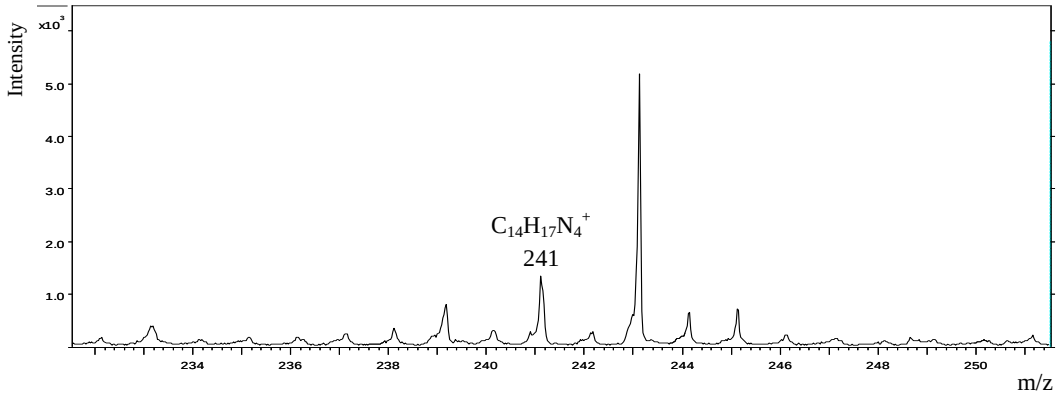

Figure 3.21: *ToF-SIMS spectrum of the cryo-sectioned skin samples of imiquimod in oleic acid solution showing the peak of the $[M+H]^+$ of imiquimod ($C_{14}H_{17}N_4^+$) at m/z = 241.*

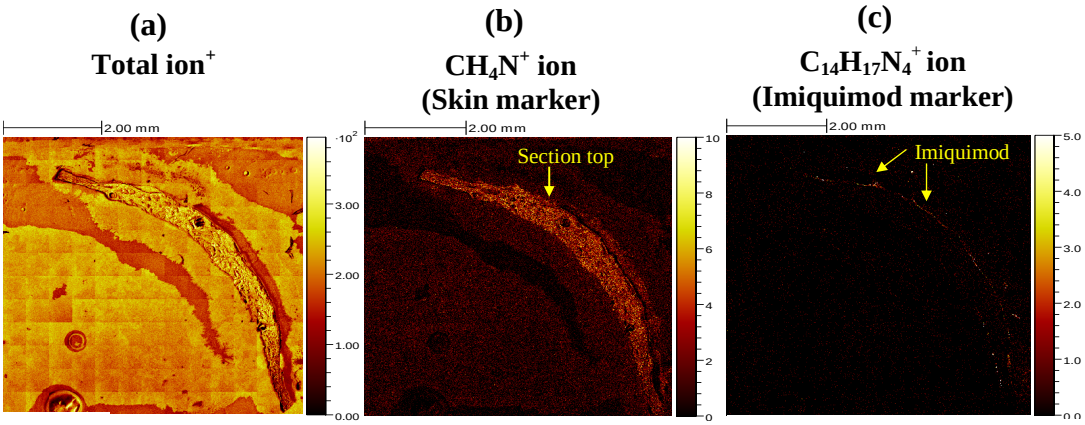

Figure 3.22: *ToF-SIMS ion images of the cryo-sectioned skin samples of imiquimod in oleic acid solution showing (a) the total ion$^+$, (b) the skin marker (CH_4N^+)and (c) the imiquimod marker ($C_{14}H_{17}N_4^+$).*

3.4.3 Quantification of imiquimod in the tape strips of Aldara™ cream and oleic acid solution

Determination of imiquimod concentration in the tape strips obtained from the permeation study of Aldara™ cream and oleic acid solution can be carried out employing the calibration curve generated for imiquimod with skin homogenate (Fig. 2.7). This calibration curve has been used as a reference to quantify imiquimod concentration in the tape strips. The normalised ion intensity from each tape strip is compared to the intensity of the calibration curve to determine the corresponding concentration. Values of the calculated concentration of imiquimod in the tape strips of Aldara™ cream and of oleic acid solution are shown in Tables 3.2 and 3.3 respectively and graphically illustrated in Figure 3.23. The concentration of imiquimod in tape strips is expressed as μg of imiquimod in mg of skin.

Table 3.2: *Determination of imiquimod concentration in Aldara™ cream tape strips.*

Tape strip No.	Normalised ion intensity	Conc. of imiquimod as calculated from the calibration curve (μg/mg)
1	0.00603	15.88
2	0.00433	11.05
6	0.00303	7.36
12	0.00256	6.03
18	0.00201	4.47

Table 3.3: *Determination of imiquimod concentration in oleic acid tape strips.*

Tape strip No.	Normalised ion intensity	Conc. of imiquimod as calculated from the calibration curve (μg/mg)
1	0.00318	7.79
2	0.00341	8.44
5	0.00215	4.87
10	0.000825	1.11
15	0.000701	below LoQ
20	0.000643	below LoQ

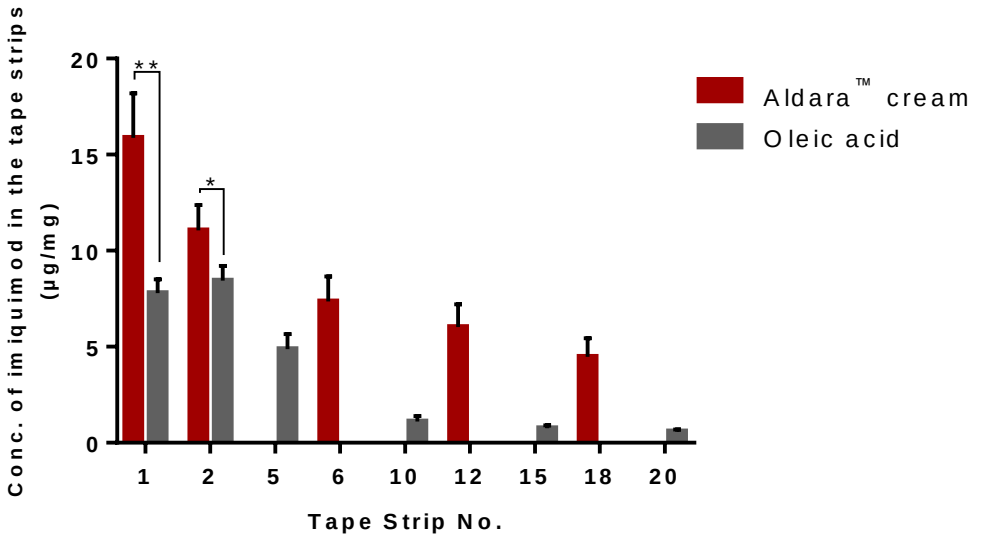

Figure 3.23: *Comparison of the imiquimod's concentration in Aldara™ cream and oleic acid tape strips as shown in Tables 3.2 and 3.3. Data is presented as the mean ± SD (n = 4).*

Tables 3.2, 3.3 and Figure 3.23 show that the concentration of imiquimod is decreased from the uppermost layer (TS 1) to the deepest layer (TS 18 or 20) and the imiquimod's concentration is higher in Aldara™ cream tape strips than oleic acid tape strips. This indicates that Aldara™ cream delivers more imiquimod into the *stratum corneum* than oleic acid.

The importance of the determination of imiquimod concentration at the different tape strips is to identify if the concentration at a particular tape strip is below or above the minimum effective concentration (MEC) of imiquimod. A previous study conducted by Miller *et al.* reported that the MEC of imiquimod required to release cytokines from corneocytes under *in vitro* conditions is 1 µg/mL [329]. According to the calculations used to generate imiquimod's calibration curve with skin homogenate (Chapter 2, Sections 2.3.4 and 2.3.5) this MEC of 1 µg/mL is equivalent to 0.005 µg of imiquimod in 1 mg of skin (0.005 µg/mg). Therefore, the calculated concentrations for imiquimod at the different tape strips from both Aldara™ cream and oleic acid solution shown in Tables 3.2 and 3.3 are higher than the MEC of imiquimod required to induce

release of cytokines to treat BCC lesions. Although, these values represent the concentration of imiquimod at a particular tape strip, it cannot be applied to the whole tape strip area because of the non-homogeneous distribution of imiquimod within the tape strip as established from ToF-SIMS ion images particularly at the lower tape strips. This variation in the ion intensity and hence in the concentration of imiquimod within the same strip may result in areas with a concentration lower than the MEC leading to treatment failure with a high tumour recurrence rate.

Additionally, the determination of imiquimod concentration at the *stratum basale* (the basal layer at which the tumour cells are originated) from the cross-sectioned skin samples is not likely possible due to the limited magnification capability of the camera of the ToF-SIMS instrument which cannot clearly differentiate between the different viable epidermis layers. Furthermore, the ion intensity of imiquimod obtained from the current analysis of the cross-sectioned samples is below the quantification limit of the calibration curve of imiquimod. Therefore, an improvement in the calibration curve sensitivity may help to determine the imiquimod concentration in these samples.

3.5 Conclusions

The work in this chapter demonstrates a novel application of Franz diffusion cells, skin tape stripping and skin cryo-sectioning with subsequent analysis by HPLC and ToF-SIMS to map and visualise the distribution of imiquimod into the skin from the commercial product Aldara™ cream as well as from the simple solvent systems of DMSO and oleic acid. This work also shows the valuable complementary role of ToF-SIMS technique in the analysis and imaging of imiquimod permeation into the skin with high sensitivity and chemical specificity without the need of fluorescent tags or radiolabels. The HPLC and ToF-SIMS results highlighted the most detailed assessment yet of the permeation of imiquimod from Aldara™ cream. This work, specifically the ToF-SIMS analysis, has evidenced that imiquimod does actually permeate into the *stratum corneum* but has limited permeation into the deeper skin layers which is consistent with the FDA approval and clinical trials for the treatment of superficial BCC. The ToF-SIMS ion images of Aldara™ cream tape strips illustrated a non-uniform distribution of imiquimod within skin which may result in a reduction the efficacy of the cream to uniformly treat whole BCC lesions giving rise to the likelihood of tumour recurrence. Quantification of the imiquimod concentration by ToF-SIMS to determine its concentration at individual tape strip was achieved using the calibration curve of imiquimod with skin homogenate. It was found that the concentration of imiquimod at the different tape strips from both Aldara™ cream and oleic acid solution is higher than the MEC of imiquimod determined under *in vitro* conditions required to elicit an immunological response. However, this concentration value cannot be applied to the whole tape strip area because of the non-homogeneous distribution of imiquimod within the tape strips. ToF-SIMS analysis of the Aldara™ cream cross-sections and the cross-section from the penetration enhancers DMSO and oleic acid solutions showed the existence of imiquimod is primarily at the *stratum corneum* layer. Indeed, penetration enhancers (DMSO and oleic acid) have not improved the permeation of imiquimod into the deeper skin layers and other techniques are needed to enhance delivery of imiquimod. This work represents the first instance that the permeation of imiquimod from Aldara™ cream has been explored at this level of detail

yielding new insights into its permeation characteristics. Importantly, this approach could be applied to enable the development of enhanced permeation delivery systems to treat BCC.

4 Chapter Four: Enhancement of Imiquimod Permeation into the Skin Using Microemulsions and Microneedles

4.1 Introduction

Since Aldara™ cream has shown some limitations in the treatment of BCC such as the high recurrence rate of superficial lesions [48, 56] as well as the cream's inability to deliver imiquimod into the deeper more invasive nodular lesions [45] (detailed in Chapter 1, Section 1.4.1.3.2), an enhancement of imiquimod permeation was thought to be useful to overcome these limitations. As shown in Chapter 1, Figure 1.13, there are several passive and active methods available for the enhancement of drug permeation into the skin [203, 330]. The selection of a particular method depends on the physicochemical properties of the drug and on the method's efficacy, safety and the availability of the materials and equipment required to achieve this permeation enhancement. Microemulsions and microneedles have numerous advantages and they have shown successful enhancement of drug permeation into and across the skin for various types of drugs (discussed in Chapter 1, Sections 1.8.1 and 1.8.2). However, to date they have not been explored to improve imiquimod permeation into the skin. Therefore, the work in this chapter is an attempt to enhance delivery of imiquimod into the skin using microemulsions and microneedles strategies as they have the potential for permeation enhancement.

4.2 Chapter Aims

The aim of this chapter is to improve the permeation of imiquimod into the skin (i.e. achieving higher permeated amounts of imiquimod in the viable epidermis layer) to overcome the limitations associated with the Aldara™ cream topical application. Therefore, oil in water (o/w) microemulsions of imiquimod were formulated, characterised and then tested for skin permeation enhancement. Additionally, solid microneedles were used as skin pre-treatment followed by the application of the formulated microemulsions as well as Aldara™ cream to investigate the effect of microneedles in enhancing delivery

of imiquimod from these formulations. Skin permeation enhancement experiments were performed using *ex vivo* porcine skin mounted in Franz diffusion cells with samples analysis carried out by HPLC and ToF-SIMS. This is thought to be, the first time that the microemulsions and microneedles have attempted to enhance imiquimod delivery into the skin.

4.3 Materials and Methods

4.3.1 Materials

Imiquimod was purchased from Bioscience Life Sciences, UK. Aldara™ 5% cream, MEDA Company, Sweden was purchased from Manor pharmacy, UK. DMSO, oleic acid, HCl, isopropyl myristate (IPM), Tween 20, Tween 85, propylene glycol (PG), Cremophore RH 40, methyl orange, methylene blue, isopropyl alcohol (IPA), absolute ethanol, butanol, isopentane, perchloric acid, triethylamine (HPLC grade), ammonia water, paraformaldehyde, haematoxylin, eosin and DPX were purchased from Sigma-Aldrich, UK, Germany and USA. Acetonitrile (HPLC grade), limonene D (+), industrial methylated spirit and xylene were obtained from Fisher Scientific, UK. Tween 80 and triacetin were purchased from Fluka, Switzerland. Sodium 1-octanesulfonate and OCT compound were obtained from VWR International Ltd. England and Belgium. Cremophore HS 15 was purchased from BASF, Germany. Gentian violet 1% w/v solution was obtained from De La Cruz products, USA. Isostearic acid (Prisorine 3505), Labrasol and Miglyol 812 N were kindly donated from CRODA, Netherland, GATTEFOSSE, France and CREMER OLEO, Germany respectively. Teepol solution (Multipurpose detergent) was ordered from Scientific Laboratory Supplies, UK. D-Squame standard sampling discs (adhesive discs) were ordered from CUDERM corporation, USA. Deionised water was obtained from an ELGA reservoir, PURELAB® Ultra, ELGA, UK. All reagents were of analytical grade, unless otherwise stated.

4.3.2 Microemulsions

4.3.2.1 Determination of imiquimod saturated solubility in different oils, surfactants and co-surfactants

Imiquimod saturated solubility in different oils (oleic acid, isostearic acid, triacetin, isopropyl myristate, Miglyol 812 N and limonene), surfactants (Tween 80, Tween 85, Tween 20 and Labrasol), co-surfactants (propylene glycol, ethanol, butanol, cremophore HS 15 and cremophore RH 40) and deionised water was determined by dissolving an excess amount of imiquimod in 3 mL of each solvent using a magnetic stirrer (IKA, Germany) with a speed of 600 rpm at 25 °C for 72 hours. Following this, the mixtures were centrifuged at 10000 rpm for 15 minutes and the supernatant was then filtered through a 0.45 µm syringe filter. Thereafter, filtrate was appropriately diluted in the same solvent and mixed with the methanol mixture (MeOH 90%:Water 9%:0.1N HCl 1%) at ratio of 1:3 before injection into the HPLC system. Calibration curves of imiquimod in each solvent were also performed by HPLC to be used in the determination of the unknown imiquimod concentration obtained from the solubility study. Excipients (oils, surfactants and co-surfactants) that showed the highest imiquimod solubility were used for further experiments.

4.3.2.2 Optimisation of HPLC method for imiquimod analysis

The HPLC analysis method for imiquimod was modified to the following chromatographic conditions: column C_{18} (150 × 4.6 mm) ACE3/ACE-HPLC Hichrom Limited, UK. Mobile phase of buffer:acetonitrile (70:30 v/v), the buffer is of 0.005 M sodium 1-octanesulfonate in water containing 0.1% triethylamine adjusted with dilute perchloric acid to pH of 2.2, flow rate of 0.8 mL/minute, UV detection at λ max. 226 nm, injection volume of 10 µL and column temperature at 25 °C. This method was used to determine imiquimod solubility in different oils, surfactants and co-surfactants in addition to the determination of the recovered imiquimod amount from the different Franz cell elements and it was validated for the accuracy, precision, linearity, LoD and LoQ.

4.3.2.3 Construction of pseudo-ternary phase diagrams

The oil, surfactant (S) and co-surfactant (Co-S) that showed the highest imiquimod solubility were used in the construction of the pseudo-ternary phase diagrams. As discussed in Chapter 1, Section 1.8.1.3, pseudo-ternary phase diagrams were constructed using water titration method [237]. The surfactant (Tween 80 or Tween 20) was mixed with the co-surfactant (propylene glycol, PG) at different ratios of 1:1, 2:1, 3:1, 4:1 and 1:2 to make the S/Co-S mixture. The S/Co-S mixture at a particular ratio was then mixed with the oil phase (oleic acid) at different ratios from 1:9 to 9:1 in multiple glass vials. Following this, the components of each vial (oil and S/Co-S mixture) at each ratio were slowly titrated with water. The water amount was added at approximately 5% increments using a micropipette for the step by step addition while the mixture was being stirred by a magnetic stirrer at a moderate speed of 300 rpm at 25 °C. The mixtures of oil, S/Co-S and water were prepared at weight basis (w/w %). Visual observation was made after each 5% water addition to determine the formation of a transparent, easily flowable o/w microemulsion and the end point of the titration process was when the solution turned turbid. These observations were plotted on a pseudo-three components phase diagram consisting of three axes representing the aqueous phase, oil phase and S/Co-S mixture. A separate phase diagram was constructed for each S/Co-S mixture ratio and the ratio that showed the largest microemulsion region in the pseudo-ternary phase diagram was used to select the microemulsion formulas. CHEMIX School 5 software was used to draw the ternary phase diagrams.

4.3.2.4 Formulation of microemulsions

Nine microemulsion formulas containing different oil (oleic acid) percentages 1%, 3% and 5% w/w and different S/Co-S mixture (Tween 20/PG) percentages were selected from the microemulsion region in the pseudo-ternary phase diagram of Tween 20/PG at ratio of 3:1 as shown in Table 4.1. Microemulsions were prepared by mixing the specified amounts of the oleic acid and the Tween 20/PG mixture on a weight basis in a glass vial using a magnetic stirrer (IKA, Germany) for 1 minute at a moderate speed of 300 rpm at 25 °C. The specified

water amount was then added gradually to the vial with continuous stirring until the formation of a transparent microemulsion. Microemulsions were allowed to equilibrate for 1 hour under moderate magnetic stirring. Following the preparation of microemulsions, they were then subjected to the characterisation tests.

Table 4.1: *Formulas of the microemulsions selected from the microemulsion region in the pseudo-ternary phase diagram of Tween 20/PG at ratio of 3:1.*

Formula No.	Oil% w/w	S/Co-S% w/w	Water% w/w
1	1	10	89
2	1	12	87
3	1	14	85
4	3	28	69
5	3	30	67
6	3	32	65
7	5	43	52
8	5	45	50
9	5	47	48

4.3.2.5 Characterisation of microemulsions

4.3.2.5.1 Visual inspection and determination of the microemulsion type

Formulated microemulsions were inspected visually to examine their appearance and clarity versus a black background. In order to determine the microemulsion type, three drops from a 1% w/v solution of water soluble dye (methyl orange) was added to the microemulsions to verify the microemulsion type.

4.3.2.5.2 Determination of the isotropic nature of microemulsions

A polarised light microscope (PriorLux POL, Prior Scientific Instrument Ltd., UK) was used to distinguish between the isotropic nature of the microemulsions and the anisotropic liquid crystals or lamellar phases. In this test, a drop of a particular microemulsion was placed on a clean microscope glass slide and tested against the polarised light. An image was captured to check if there was any refraction in the polarised light originating from the drop.

4.3.2.5.3 Microemulsions stability test

The microemulsion formulas were subjected to the thermodynamic stability test to identify the presence of the metastable formulas prior to performing any other characterisations. The stability was studied via the determination of clarity and phase separation of the microemulsions. The stability test consist of two steps [237], the first step was the centrifugation of the microemulsions at high speed of 14000 rpm for 30 minutes (Eppendorf AG, centrifuge 5430, Germany). Following this, the microemulsion formulas that did not show any phase separation were moved to the second step of cooling and heating cycles. In this step, six cycles of cooling at a temperature of 4 °C and heating at 45 °C for 48 hours were performed. Formulas that showed appropriate stability at the end of this stability test were used for imiquimod loading. The test was repeated again for the imiquimod loaded formulas to investigate if the addition of imiquimod influenced the stability of microemulsions. Chemical stability of imiquimod loaded microemulsions was determined monthly by HPLC, for the content of imiquimod, for up to 3 months.

4.3.2.5.4 Imiquimod loading into the microemulsion formulas

Imiquimod was loaded into the microemulsion formulas that showed appropriate stability. Formulas F3, F6 and F9 (Table 4.1) were loaded with 0.1%, 0.3% and 0.5% w/w of imiquimod respectively according to the following procedure: A stock solution of imiquimod in oleic acid was prepared

at a concentration of 10% w/w (100 mg/g) or (0.1 mg/mg) and used to load imiquimod into the various microemulsions to prepare a final volume of 10 g (10000 mg) as shown in Table 4.2. For loading F3 formula (1% oleic acid, 14% Tween 20/PG mixture and 85% water) with 0.1% w/w imiquimod, 100 mg of the stock solution was mixed with 1400 mg of the S/Co-S mixture and titrated with 8500 mg of water. F6 formula (3% oleic acid, 32% Tween 20/PG mixture and 65% water) was loaded with 0.3% w/w imiquimod using 300 mg of the stock solution mixed with 3200 mg of the S/Co-S mixture and titrated with 6500 mg of water. For loading F9 formula (5% oleic acid, 47% Tween 20/PG mixture and 48% water) with 0.5% w/w imiquimod, 500 mg of the stock solution was mixed with 4700 mg of the S/Co-S mixture and titrated with 4800 mg of water.

Table 4.2: *Quantities of the stock solution of imiquimod in oleic acid at a concentration of 0.1 mg/mg used to load the various microemulsion formulas.*

Formula No.	Stock solution of imiquimod in oleic acid (0.1 mg/mg) quantity	Tween 20/PG quantity	Water quantity	Total quantity
F3	100 mg	1400 mg	8500 mg	10000 mg
F6	300 mg	3200 mg	6500 mg	10000 mg
F9	500 mg	4700 mg	4800 mg	10000 mg

4.3.2.5.5 Droplet size and charge measurement

A zetasizer (Nano-Zs, Malvern, UK) was used to determine the size of the droplets of the microemulsions by dynamic light scattering (DLS). First, the microemulsions were filtered through a 0.2 mm filter. Following this, 100 µL of the microemulsion was added to 900 µL of deionised water and mixed together for 30 seconds using a vortex mixer (Fisherbrand, Italy). The mixture was then pipetted into a clean cuvette previously rinsed with methanol and deionised water and placed in the instrument for measurement (n = 3). Light

scattering was carried out at 173° angle at 25 °C. For zeta potential measurement, dilutions were performed with 10 mM NaCl. A sample was then injected into a flow through cell and analysed repeatedly (n = 3) before removal.

4.3.2.6 Microemulsions permeation study

The three microemulsion formulas F3, F6 and F9 loaded with 0.1%, 0.3% and 0.5% w/w of imiquimod respectively were used in the permeation study.

4.3.2.6.1 Skin preparation

Skin samples were prepared from the dorsal side of pig ears of six month old obtained from a local abattoir prior any steam cleaning process. The skin was washed with distilled water and dried using tissue. Hair was carefully cut by scissors to avoid any damage to the *stratum corneum* and the subcutaneous fatty layer was removed using a scalpel. After that, the skin samples were wrapped in aluminium foil and stored at -20 °C. Skin samples were used within six weeks of being frozen. A skin integrity test was performed as detailed in Chapter 3, Section 3.3.2.2.

4.3.2.6.2 Assembly of diffusion cells

Franz diffusion cell experiments conditions were the same as previously mentioned in Chapter 3, Section 3.3.2.3. The microemulsion formulas F3, F6 and F9 were tested in comparison to Aldara™ cream in the same run using the same piece of skin (n = 6). Microemulsions were dosed on the weight basis of 1000 mg. The measurement of mass balance was the same as previously described in Chapter 3, Section 3.3.2.4. In addition, F9 microemulsion formula was tested with an additional 6 Franz cells for ToF-SIMS analysis.

4.3.3 Microneedles

4.3.3.1 Microneedle application device and application conditions

A derma stamp electric pen (ZJchao, China) as shown in Figure 4.1 was used to pierce the skin by vibrational motion prior to the application of microemulsions or Aldara™ cream. The stamp pen contains 12 solid (metal) micron sized needles of 32 gauge (230 μm diameter). The length of the microneedles used was 0.25 mm (minimum length) with a minimum speed of vibration of 1000 turn per minute (green colour light). The application time was kept to 1 minute with a mild pressure application (thumb pressure). These application conditions were used throughout all microneedles experiments. This stamp pen is commercially available and mostly used in cosmetics to rejuvenate the skin through the stimulation of collagen production.

Figure 4.1: *Derma stamp electric pen (ZJchao) image showing the 12 solid (metal) micro sized needles.*

4.3.3.2 Insertion and staining protocol of microneedles

To demonstrate the penetration efficiency of the stamp pen, an insertion and staining protocol with *en face* imaging by a light microscope was followed. In this protocol, the porcine skin was prepared as previously mentioned in Section 4.3.2.6.1. Thereafter, the skin was pinned onto a flat cork board to stretch the skin and the stamp pen was applied vertically on the skin according to the application conditions mentioned in Section 4.3.3.1. Several drops of gentian

violet 1% or methylene blue 1% w/v dyes were subsequently applied to cover the treated area and left for 10 minutes. Afterwards, the excess of the dye was removed from the skin surface by a tissue towel and Azo wipes (70% v/v IPA, Synergyhealth, UK). The treated skin area was then examined under a light microscope (Leica optical microscope model EC3, Leica Microsystems Ltd., Switzerland) to capture an *en face* image of the microneedles treated skin area.

4.3.3.3 Histological examination of microneedle treated skin

Following the *en face* imaging of the skin area treated with microneedles by a light microscope, a histological examination was carried out to assess the penetration depth achieved by microneedles. OCT embedding and cryo-sectioning of the skin were performed as previously discussed in Chapter 3, Section 3.3.2.6 but in this work, the slides containing skin sections were stained with haematoxylin and eosin instead of freeze drying and ToF-SIMS analysis. Untreated skin samples with microneedles (blank skin) were also subjected to cryo-sectioning, staining and examination under light microscope.

4.3.3.3.1 Haematoxylin and Eosin (H&E) staining protocol

Staining and mounting of the skin sections were performed as follows: First, the skin sections were fixed in 4% v/v paraformaldehyde for 2 minutes and then rinsed in deionised water for 5 minutes. Thereafter, they were immersed in haematoxylin for 2 minutes and washed in tap water for 3 minutes. Following this, they were dipped for 15 seconds in 1% industrial methylated spirit and 10% ammoniated water. The slides were then rinsed in deionised water for 1 minute and immersed in eosin for 4 minutes and rinsed again in tap water for 5 minutes and allowed to dry at room temperature. Following the end of the staining process, the sections were mounted on the slides. The slides were first dehydrated in an increasing gradient of ethanol 50%, 70%, 90% and 100% v/v for 5 minutes in each concentration and then cleared in xylene for additional 5 minutes and mounted using a synthetic resin DPX (slide mounting medium) and a glass coverslip.

4.3.3.4 Permeation study of microemulsions with microneedle pre-treatment

Skin preparation was performed as previously discussed in Section 4.3.2.6.1. Skin integrity test and Franz cell experimental conditions were the same as previously discussed in Chapter 3, Sections 3.3.2.2 and 3.3.2.3 respectively. However, in this experiment following the integrity checking of the skin samples, they were placed on a cork support and the stamp pen was applied vertically on the skin according to the conditions mentioned in Section 4.3.3.1. Thereafter, the skin samples were mounted on Franz cells (n = 6) with the *stratum corneum* facing upwards and dosed with 1000 mg of F3 microemulsion formula. The measurement of mass balance by HPLC was the same as previously discussed in Chapter 3, Section 3.3.2.4.

4.3.3.5 Permeation study of Aldara™ cream with microneedle pre-treatment

The permeation of Aldara™ cream into the skin following microneedle pre-treatment of the skin was investigated in a similar manner to the microemulsions. The skin samples were first pierced by a stamp pen followed by the application of 20 mg of Aldara™ cream. Microneedle treated skin samples (n = 12) were analysed by HPLC and ToF-SIMS (6 samples for each analysis method) and the data compared to that obtained from skin samples without microneedle pre-treatment in the same run from the same piece of porcine ear skin.

Tape stripping, skin cryo-sectioning, HPLC and ToF-SIMS analysis were performed as previously discussed in Chapter 3, Sections 3.3.2.5, 3.3.2.6, 3.3.2.7 and 3.3.2.8 respectively except that the HPLC analysis here was carried out by applying the chromatographic conditions of the modified HPLC method (Section 4.3.2.2). In ToF-SIMS analysis, all peak intensities were normalised to the total ion count of the spectra.

4.3.4 Statistical analysis of the data

The statistical tests used to compare ion intensities were one way ANOVA with Tukey's multiple comparisons test or t-test. All data is presented as the mean ± SD of (n = 4 or 6) with P values of ≤ 0.05 being regarded as significant using GraphPad Prism 7 software (USA). Prior to statistical analysis all data was tested for normality using Shapiro-wilk normality test.

4.4 Results and Discussion

4.4.1 Optimisation of HPLC method for imiquimod analysis

The HPLC method that was previously used in the determination of imiquimod recovered from the Aldara™ cream permeation study (Chapter 3, Section 3.3.2.7) was unable to obtain a sharp and symmetrical peak for imiquimod (Fig. 4.2) when analysed from the different oils used in the solubility study of imiquimod. Therefore, a modified HPLC method was optimised and used instead to achieve more accurate determination of imiquimod in these solvents. This method was modified from the USP's pending monographs guideline, version 1, 2011 used for the analysis of imiquimod powder (raw material) [331].

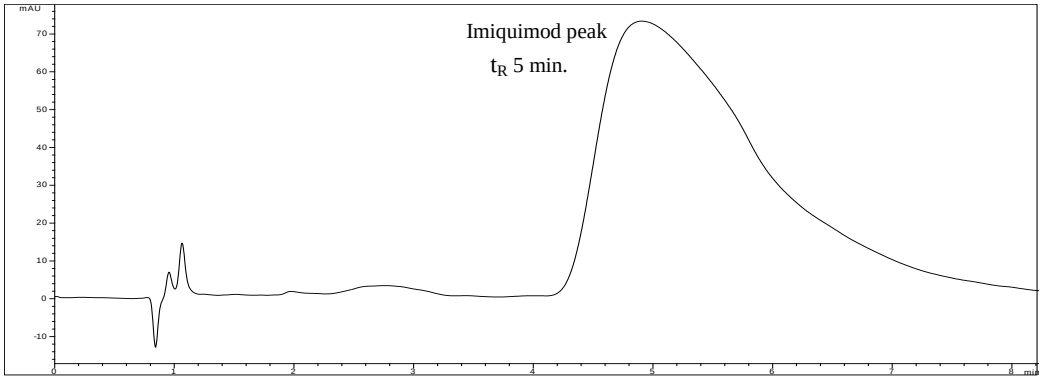

Figure 4.2: *HPLC chromatogram of imiquimod in oleic acid showing imiquimod peak at t_R 5 minutes when analysed by the previous HPLC method with a mobile phase (acetate buffer:ACN) ratio of 80:20 v/v.*

As shown in Figure 4.2, the imiquimod peak is very broad with an asymmetrical shape. The tailing factor (T) which is a measure of peak symmetry is 2.75 (recommended value ≤ 2) and the theoretical plate number (N) which represents the column efficiency for peak separation is 71 (recommended value > 2000, the larger the number the sharper the peak) [332]. This peak tailing affects the reliability of quantification, makes peak integration very difficult and interferes with accuracy and precision [333]. It is thought that the incompatibility between oleic acid (imiquimod's solvent) and

the mobile phase influences the partitioning of imiquimod between the mobile phase and the stationary phase leading to poor peak separation and peak tailing (i.e. the presence of oleic acid prevents the proper elution of imiquimod from the stationary phase). A study of the effect of sample solvent on the peak tailing showed that during the HPLC analysis of fat soluble vitamins (vitamins A, D3 and E) peak tailing was observed when the samples were dissolved in methanol rather than the mobile phase [334]. Hence, a modification of the current chromatographic conditions is required to produce a more powerful method capable of an efficient separation of imiquimod in the presence of oleic acid. Therefore, a new HPLC method was developed with multiple modifications to improve the elution of imiquimod from these oily solvents. In this modified method, the concept of ion-pairing chromatography was exploited to achieve an efficient separation of imiquimod. The sodium 1-octanesulfonate present in the mobile phase was used as an ion-pairing agent [335]. This ion pairing agent consists of two parts, a hydrophobic tail attached to the non-polar surface of the stationary phase of the column and a polar negatively charged head binds to the positively charged amine group of imiquimod, thereby improving the retention and separation of imiquimod. Moreover, the pH of the mobile phase was further reduced to 2.2 to ensure that the majority of the silanol groups (Si-OH) present on the surface of the stationary phase of the C_{18} column are unionized and less available for the interaction with the positively charged amine group of imiquimod, thereby reducing the likelihood of tailing. In addition, the presence of triethylamine (TEA) in the mobile phase help to reduce peak tailing by acting as a competing base [336] reducing the silanol groups availability to interact with imiquimod (i.e. saturates the available silanol groups).

In addition, the efficiency of separation of the imiquimod peak is increased by using a longer C_{18} column of 150 mm length packed with 3 μm particles instead of 75 mm length column packed with 5 μm particles as used in the previous HPLC method (Chapter 3, Section 3.3.2.7). Increasing column length and decreasing particle size of the packed material can result in more efficient separation and resolution of the analyte but with a longer retention time and an

increased pressure within the column [337]. The combination of these modifications in the mobile and stationary phases result in a sharp and symmetrical peak of imiquimod as shown in Figure 4.3b with a tailing factor of 1.1 and theoretical plate number of 17448. The retention time (t_R) is approximately at 12 minutes accompanied by a pressure of 220 bar at flow rate of 0.8 mL/min to keep the pressure within the column below the maximum allowable value of 275 bar. This moderate retention time of 12 minutes is a trade-off to obtain a sharp and symmetrical peak of imiquimod required for the quantification process.

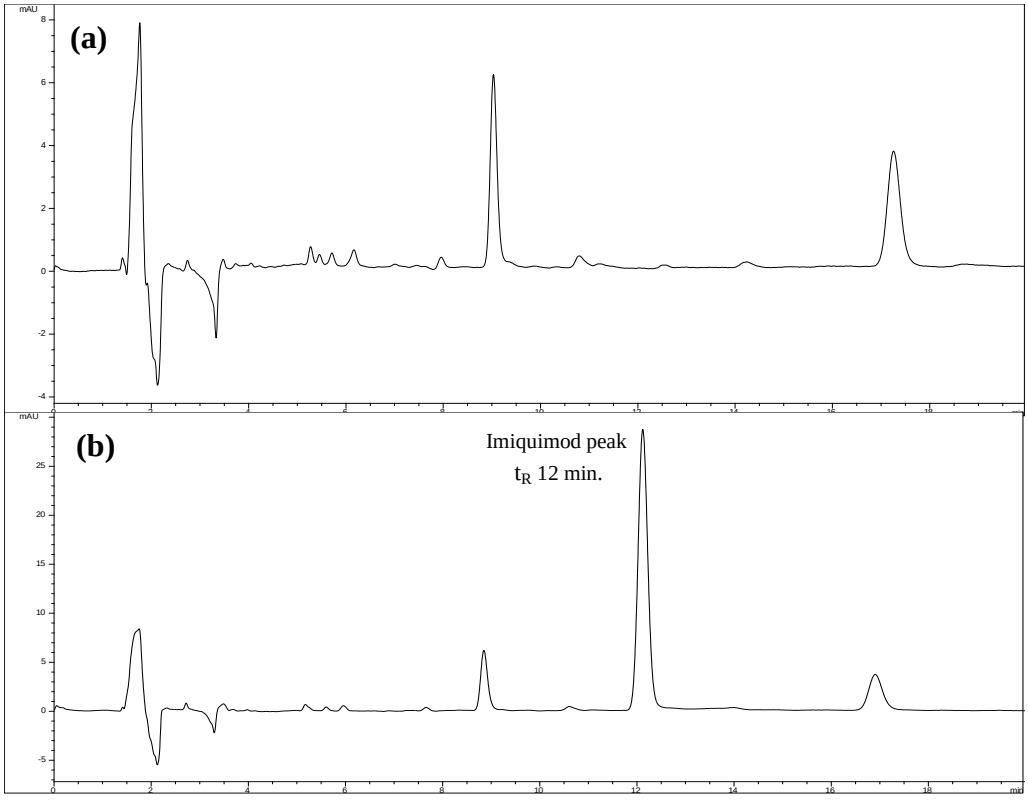

Figure 4.3: *HPLC chromatograms of imiquimod in oleic acid showing (a) blank chromatogram and (b) imiquimod chromatogram highlighting the imiquimod peak at t_R 12 minutes when analysed by the modified HPLC method.*

Paula *et al.* have demonstrated the development of a HPLC method for the determination of imiquimod from skin permeation studies using C_{18} column of 125 mm length packed with 5 μm particles and mobile phase of acetonitrile : acetate buffer pH 4:diethylamine at ratio 30:69.85:0.15 respectively. They

found that the use of these chromatographic conditions yielded a well separated peak of imiquimod (t_R of 4 minutes) without peak tailing when imiquimod was dosed from mixtures of propylene glycol and water at 1:1 ratio [139]. However, the use of these chromatographic conditions for solutions of imiquimod in oleic acid were insufficient to produce a sharp and symmetrical peak for imiquimod (tested experimentally). It is thought, that the lower pH value of 2.2 with the presence of the ion-pairing agent sodium 1-octanesulfonate in the mobile phase of the modified method provides additional advantages over the method applied by Paula *et al.* in obtaining a higher retention and more efficient separation for imiquimod peak with symmetrical shape.

4.4.2 Microemulsions

4.4.2.1 Determination of imiquimod saturated solubility in different oils, surfactants and co-surfactants

Since only the dissolved drug can permeate into the skin [338], it is important to discover the most appropriate solvents for imiquimod to be used in the microemulsion formulation. Imiquimod's saturated solubility in different oils, surfactants, co-surfactant and water (components of microemulsion) are reported in Table 4.3.

As shown in Table 4.3, imiquimod possesses the highest solubility for oils in oleic acid, for surfactants in Tween 80 and for co-surfactants in propylene glycol. Therefore, oleic acid, Tween 80 and propylene glycol were used to construct the pseudo-ternary phase diagrams to define the microemulsion region. In addition to the ability of these solvents to solubilise the highest amount of imiquimod, they have skin penetration enhancing properties with minimum irritation side effects reported [4, 236, 327, 328]. Oleic acid and propylene glycol showed synergistic effects in enhancing permeation of hydrophilic and lipophilic drugs [235, 339-341]. Tween 80 is a non-ionic surfactant with a minor enhancement effect reported to cause minimum skin irritation [4, 327].

Table 4.3: *Saturated solubility of imiquimod in different oils, surfactants, co-surfactants and water. Solubility is expressed as the mean ± SD (n = 3).*

	microemulsion components	Solubility (mg/mL) ± SD
Oils	Oleic acid	170 ± 8.38
	Prisorine 3505	84 ± 5.31
	Triacetin	0.096 ± 0.01
	Miglyol 812 N	0.027 ± 0.01
	IPM	0.0086 ± 0.002
	Limonene	0.0035 ± 0.001
Surfactants	Tween 80	0.618 ± 0.09
	Tween 20	0.416 ± 0.06
	Labrasol	0.373 ± 0.07
	Tween 85	0.180 ± 0.02
Co-surfactants	PG	0.490 ± 0.08
	Butanol	0.448 ± 0.09
	Cremophore HS 15	0.339 ± 0.07
	Ethanol	0.328 ± 0.02
	Cremophore RH 40	0.288 ± 0.05
	Water	0.0008 ± 0.0001

4.4.2.2 Construction of pseudo-ternary phase diagrams

As discussed in Chapter 1, Section 1.9.3, the construction of phase diagrams aid to delineate the boundaries of the microemulsion region. Therefore, a separate phase diagram was constructed for each S/Co-S mixture ratio according to the method discussed in Section 4.3.2.3. These will be used to determine the concentration range of the components of each microemulsion and the ratio that shows the largest microemulsion region in the pseudo-ternary phase diagram will be used for the microemulsion formula selection. Pseudo-ternary phase diagrams of Tween 80/PG at ratios of 1:1 and 2:1 are shown in Figure 4.4a and b respectively.

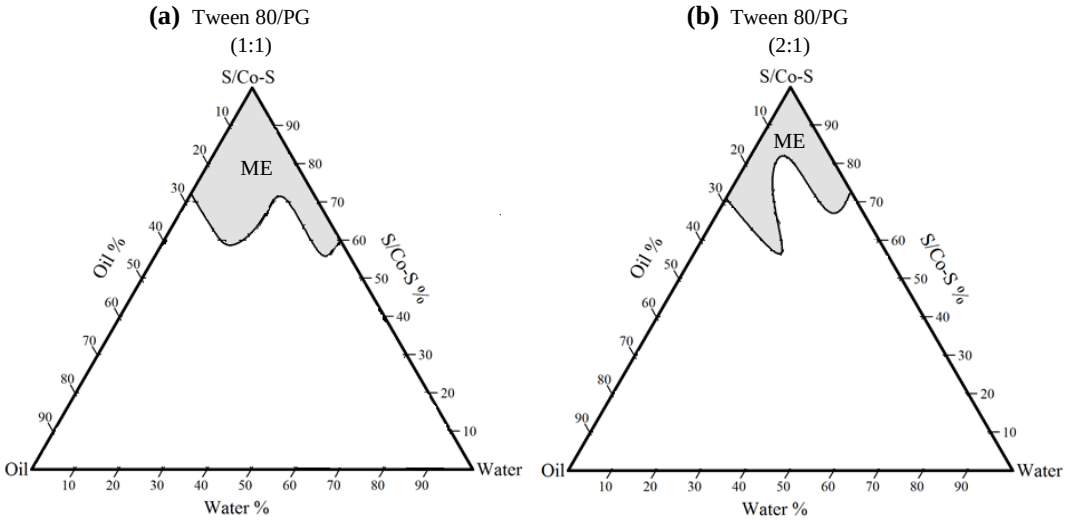

Figure 4.4: *Pseudo-ternary phase diagrams of the S/Co-S mixture (Tween 80/PG) at ratios of (a) 1:1 and (b) 2:1. The shaded area represents the microemulsion region.*

As illustrated in Figure 4.4a and b, the microemulsion region in the pseudo-ternary phase diagrams is relatively small and limited to the upper part of the diagram close to the S/Co-S apex where the concentration of S/Co-S mixture is high. This means the preparation of microemulsions from this region requires a high concentration of S/Co-S mixture (approximately minimum concentration of 60% w/w) which offers a greater potential for skin irritation. Therefore, in an attempt to enlarge the boundaries of the microemulsion region, the surfactant (Tween 80) with a hydrophilic-lipophilic balance (HLB) value of 15 [342] was replaced with Tween 20 (with HLB value of 16.7) [342] regardless the fact that imiquimod has higher solubility in Tween 80 than Tween 20 (Table 4.3). This replacement was carried out in order to make the HLB value of the surfactant closer to the required HLB value of the oleic acid of 17 [343] and thus being more compatible with the oil to produce a larger microemulsion region within the phase diagram. The pseudo-ternary phase diagrams of Tween 20/PG at ratios of 1:1, 2:1, 3:1, 4:1 and 1:2 are shown in Figure 4.5a, b, c, d and e respectively.

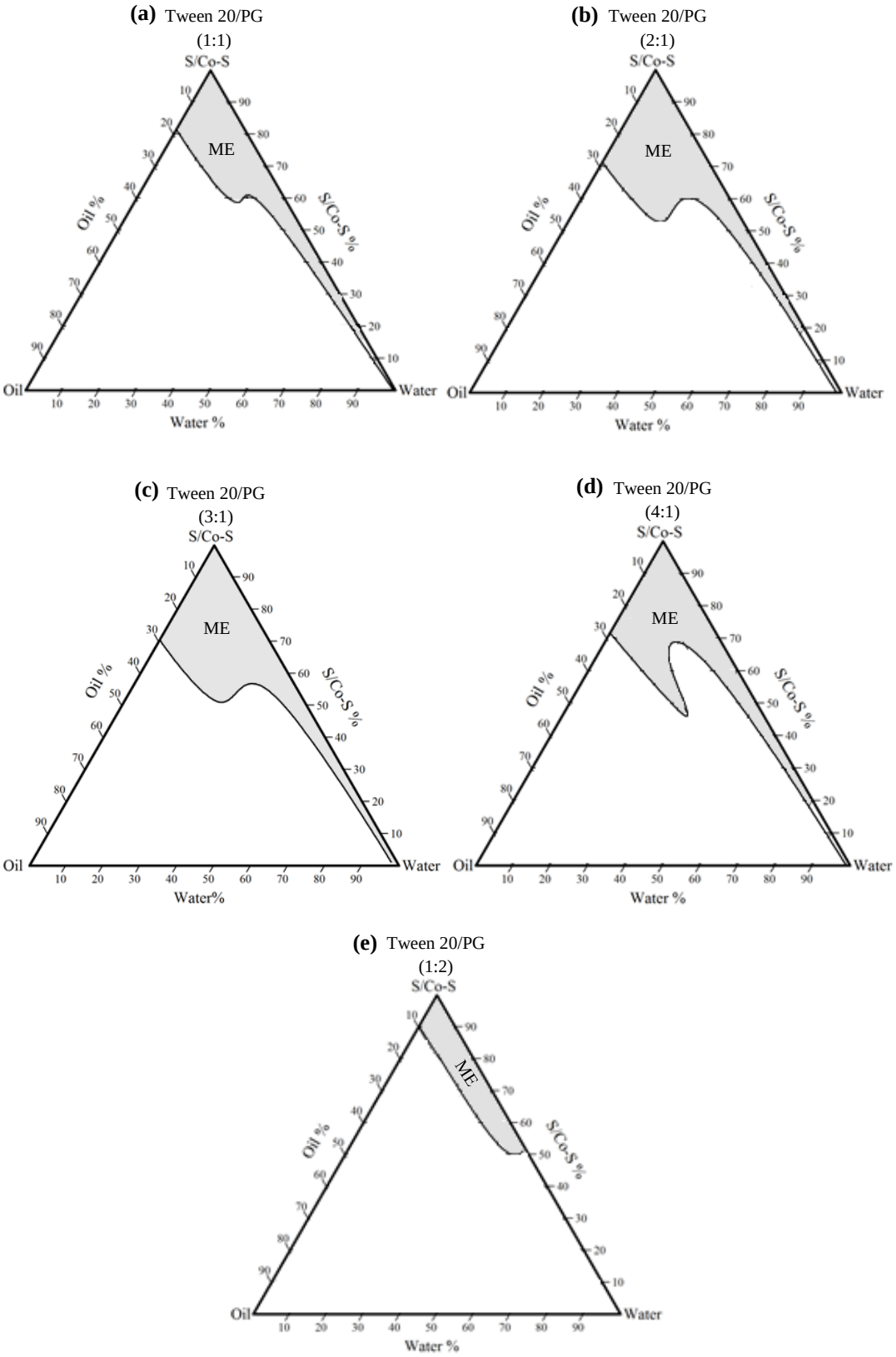

Figure 4.5: *Pseudo-ternary phase diagrams of the S/Co-S mixture (Tween 20/PG) at ratios of (a) 1:1, (b) 2:1, (c) 3:1, (d) 4:1 and (e) 1:2. The shaded area represents the microemulsion region.*

An examination of the pseudo-ternary phase diagrams shown in Figure 4.5a, b, c and d reveals that Tween 20 produces a larger microemulsion region than Tween 80 due to the higher proximity of its HLB (16.7) to the required HLB value of oleic acid (17) which results in higher compatibility between them. It was previously reported that the highest emulsification effect is obtained when the HLB value of a surfactant is equal to the required HLB value of an oil [338]. From the different Tween 20/PG ratios tested, it was observed that a 3:1 ratio (Fig. 4.5c) shows the largest microemulsion region within the phase diagrams and therefore it was used for the microemulsion formula selection. It is thought at this S/Co-S ratio the interaction between the surfactant (Tween 20) and the co-surfactant (PG) is higher than other ratios leading to an increase in the solubilisation capacity of the microemulsion and the formation of a larger single phase microemulsion region. It was reported that the formation of a microemulsion with maximum solubilisation capacity can be achieved by selecting the optimum S/Co-S ratio at which the co-surfactant is inserted properly into the cavities of the surfactant molecules at the oil/water interface [338, 344]. Additionally, it was observed that the increase in the co-surfactant concentration in relation to the surfactant concentration such as in the ratio of 1:2 of Tween 20/PG (Fig. 5.4e) resulted in a decrease in the microemulsion region. This can be due to reduction in the surfactant concentration which consequently reduces the solubilisation capacity of the microemulsion. Thus, this approach was omitted from further investigation.

4.4.2.3 Microemulsion formulas

The microemulsion formulas were selected from the microemulsion region in the pseudo-ternary phase diagram of Tween 20/PG at a 3:1 ratio to contain 3 different oleic acid percentages of 1%, 3% and 5% w/w as shown in Table 4.1. This selection was based on the fact that oleic acid is mostly effective as a penetration enhancer at low concentrations of less than 10% [4]. Rhee *et al.* reported that the permeation rates of ketoprofen into the skin from microemulsions containing different concentrations of oleic acid (3%, 6% and 12% w/w) were significantly different reaching a maximum at 6% [218]. Similarly, Nomura *et al*. found that the maximum enhancement of

indomethacin skin permeation was achieved at a concentration of 5% w/w, when oleic acid added to mixtures of fatty alcohol and propylene glycol bases at concentrations from 5%-30% [345]. In addition, it was reported that oleic acid in ethanol at a concentration of 10% can cause changes in the morphology with a decrease in density and dendricity of Langerhans cells located in the basal layer of the epidermis. [346]. Moreover, it was observed that the increase in oleic acid concentration is associated with an increase in S/Co-S mixture percentage required to solubilise the oil. This higher percentage of surfactants provides a greater opportunity for skin irritation [338]. Therefore, the maximum concentration of oleic acid in the selected formulas was fixed at 5% w/w to reduce the required percentage of the S/Co-S mixture. A microemulsion preparation depends on the relative quantities of the oil and surfactant mixture where the oil molecules are incorporated within the surfactant micelles until the saturation limit of the micelles. Following this, any further quantity of the oil added remains intact without incorporation and can result in separation of the oil phase [220]. As shown in Table 4.1, at each oil percentage (1%, 3% and 5%) three formulas of the microemulsions were prepared to contain different percentages of the S/Co-S mixture.

4.4.2.4 Characterisation of microemulsions

4.4.2.4.1 Visual inspection and dye test

The inspected microemulsion formulas showed a clear and transparent liquid with low viscosity which is characteristic of single phase system of a microemulsion. The water soluble dye (methyl orange) is distributed uniformly throughout the microemulsions which verify the o/w nature of the selected microemulsion formulas. It is proposed that the formulation o/w microemulsion of imiquimod is preferred over w/o type. In o/w microemulsion, the external phase is water which can pass more easily through the aqueous microchannels formed by microneedle pre-treatment than the less flowable external oil phase of w/o microemulsion. Additionally, dissolving imiquimod in the external oil phase of w/o microemulsion which is in a direct contact with

the skin can cause more irritation and it is not appropriate for the long term use from a safety perspective.

4.4.2.4.2 Determination of the isotropic nature of microemulsions

The images obtained from polarised light microscopy illustrate the isotropic nature of the selected microemulsion formulas since there is no refraction in the polarised light originated from the examined microemulsions drops as shown in Figure 4.6. In addition, the low viscosity of the microemulsion formulas further confirms their isotropic nature. It has been reported that the anisotropic crystalline cubic or lamellar structures have solutions of high viscosity [207].

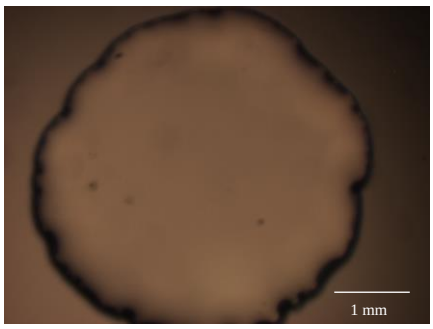

Figure 4.6: *Polarised light microscope image of a microemulsion drop showing the isotropic nature of the microemulsions.*

4.4.2.4.3 Microemulsions stability test

Microemulsion formulas F3, F6 and F9 (Table 4.1) show appropriate thermodynamic stability prior to and following loading with imiquimod when tested using the stability test described in Section 4.3.2.5.3. These microemulsion formulas successfully passed the centrifugation test and the heating cooling cycles and therefore they were subjected to further characterisation of droplet size determination as well as assessing their permeation into porcine skin. It is thought that F3, F6 and F9 microemulsion formulas remain stable at the end of the stability test because they contain higher amounts of the S/Co-S mixture than other microemulsion formulas. This

higher amount of the surfactant and co-surfactant is required to prevent phase separation of the microemulsion under different stress conditions. Degradation of imiquimod in microemulsion formulas is not observed since the concentration of imiquimod in microemulsions remains almost constant when analysed by HPLC during the 3 month period.

4.4.2.4.4 Imiquimod loading into the microemulsion formulas

Microemulsion formulas F3, F6 and F9 were loaded with imiquimod at lower concentrations of 0.1%, 0.3% and 0.5% w/w respectively (Table 4.2) in comparison with 5% w/w of imiquimod in Aldara™ cream. This is due to the solubility limit of imiquimod in the microemulsion components of each formula, specifically oleic acid percentage (i.e. imiquimod cannot be loaded at a higher concentration since low percentages of oleic acid were used in the formulation of microemulsions). These concentrations of imiquimod represent the maximum possible concentrations close to the saturated concentration of imiquimod in oleic acid which can be used to provide the highest thermodynamic activity but simultaneously maintaining appropriate stability of microemulsion formulas. It is well established that the thermodynamic activity of a drug in formulation is the driving force for permeation [234, 347] and it is regarded as the 'escaping tendency' for a drug from its vehicle [1]. Therefore, to achieve a strong thermodynamic drive for a drug to leave its formulation and ingress into the skin, the drug should be prepared at the saturation limit. However, saturated systems tend to be unstable and thus loading the drug at a concentration near saturation is considered as a successful compromise [1, 4].

4.4.2.4.5 Droplet size and charge measurement

The imiquimod loaded microemulsion formulas F3, F6 and F9 show an average droplet size of 10, 12 and 15 nm respectively when measured by DLS as illustrated in Figure 4.7. It was observed that the increase in oleic acid concentration in microemulsion formulas is associated with a minor increase in the average droplet size due to the expansion of the oil droplets by the further addition of oil. Other studies have also reported increases in droplet size of

microemulsions with increase of oil content [234, 338]. The polydispersity index (PDI) which describes the droplets size homogeneity exhibited values between 0.10 and 0.23. This result indicates the homogeneity of the droplets size since the PDI values are less than 0.5 [348].

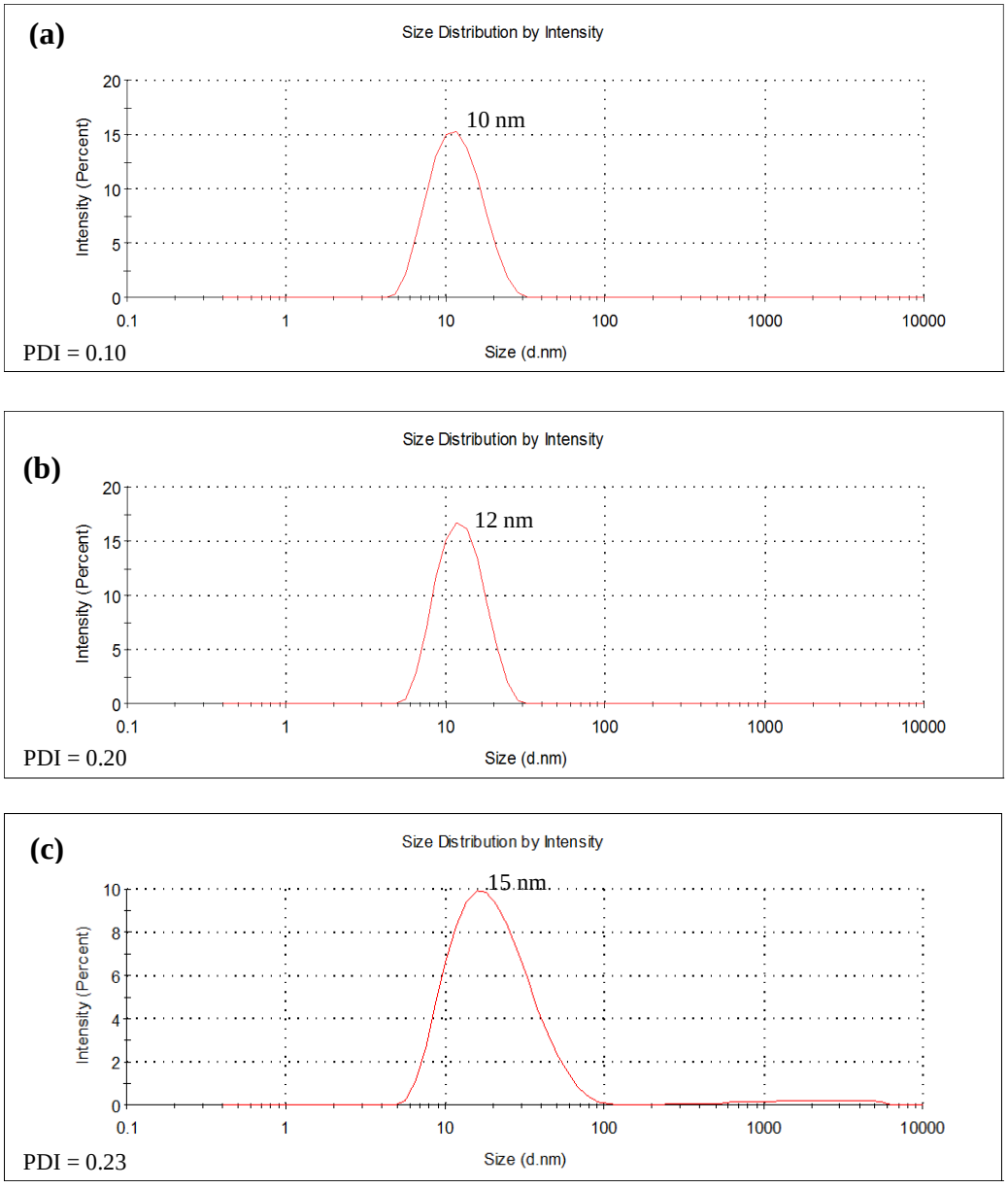

Figure 4.7: *Measurement of the average droplet size of imiquimod's microemulsion formulas by DLS, showing (a) F3 formula (b) F6 formula and (c) F9 formula.*

The measured zeta potential from microemulsion formulas is -20 mV (Fig. 4.8). This indicates that there is little chance for microemulsion droplets to form colloidal aggregates or interact with skin components as the skin also has a negative charge.

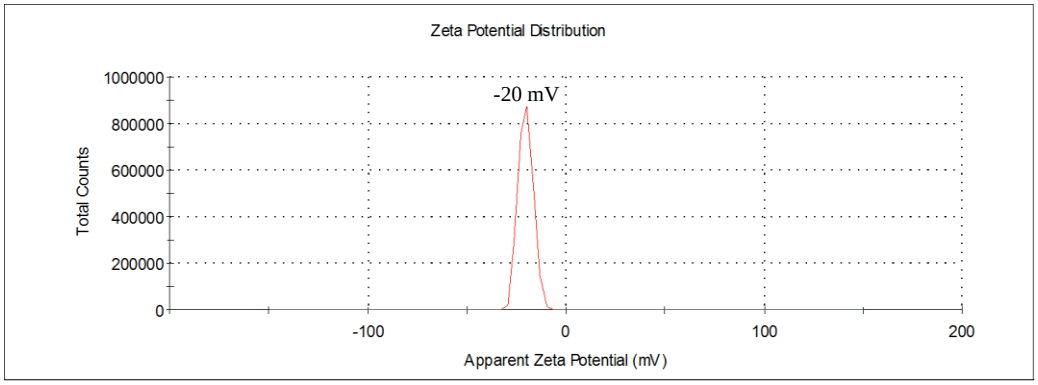

Figure 4.8: *Measurement of the average zeta potential of imiquimod's microemulsion droplets.*

4.4.2.5 Microemulsions permeation study

4.4.2.5.1 Calibration curves of imiquimod using the modified HPLC method

The calibration curves of imiquimod in MeOH mixture (extraction solvent) and in 0.1N HCl (receptor fluid) generated using the modified and previous HPLC methods are shown in Figure 4.9a and b respectively. The calibration curves show linearity at range of concentration used with R-squared values of 0.999 in both media. Therefore, a reliable measurement for the area under the curve (AUC) can be obtained within this range of concentrations. Furthermore, the comparison of the modified and previous HPLC methods (Fig. 4.9a and b) illustrates the higher sensitivity of the modified method. The slope of the regression line equations for the modified method is approximately double the slope value of the previous calibration curves (65 versus 32 and 34). A more sensitive measurement is obtained from a steeper line [349]. In addition, an assessment of the accuracy and precision measurement for the tested concentrations of imiquimod in both methanol mixture and in 0.1N HCl using the modified method shows values for the relative error of measurement (RE)

of less than ± 15% and RSD values of ≤ 15% which indicate excellent accuracy and precision [350]. The limit of detection (LoD) and limit of quantitation (LoQ) are determined experimentally according to the signal/noise ratio and CV% methods [304]. For imiquimod in a methanol mixture, the LoD and LoQ are found to be at a concentration of 0.086 µg/mL. For 0.1N HCl, the LoD and LoQ are found to be at 0.075 µg/mL and 0.151 µg/mL respectively. The lower values of the LoD and LoQ in comparison with the limits of the previous HPLC method (Chapter 3, Section 3.4.1.1) verifies the higher sensitivity of the modified method to detect a lower concentration of imiquimod in both media.

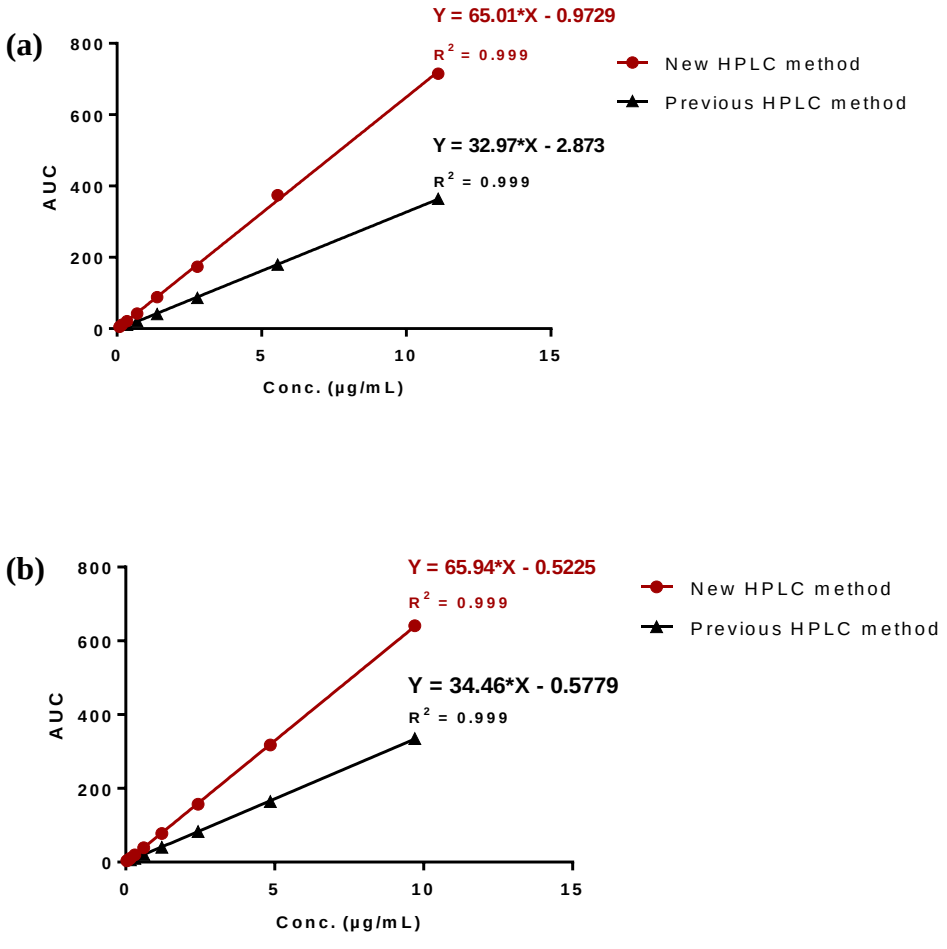

Figure 4.9: *Comparison of the calibration curves of imiquimod in (a) MeOH mixture (extraction solvent) and (b) in 0.1N HCl (receptor fluid) generated using the modified HPLC method (red colour line) and the previous HPLC method (black colour line). Data is presented as the mean ± SD (n = 5).*

4.4.2.5.2 Determination of the percentage of imiquimod recovered from microemulsions permeation study by HPLC

Imiquimod loaded microemulsion formulas F3, F6 and F9 which showed appropriate stability were used to assess the permeation of imiquimod from microemulsions into porcine skin in comparison with Aldara™ cream. The mean recovery percentage of imiquimod from the different Franz cell elements (donor solution, donor chamber wash, skin wash, tape strips, remaining skin and receptor fluid) of the permeation study of the microemulsions and Aldara™ cream are reported in Table 4.4. It is apparent from the data presented in Table 4.4, that the recovery percentage of imiquimod from microemulsion formulas is highest in the donor solution (the dosed microemulsion solution into the donor chamber recovered following completion of Franz cell run) as compared to other elements. In addition, very minor percentages are recovered from the tape strips, remaining skin and receptor fluid which are even less than the recovery percentages obtained from Aldara™ cream. This indicates the very limited permeation of imiquimod from these microemulsion formulas and suggests the inability of these microemulsion formulas to deliver more imiquimod into the skin compared to Aldara™ cream although they are formulated at a high thermodynamic activity of imiquimod and contain multiple ingredients regarded as penetration enhancers such as oleic acid, Tween 20 and propylene glycol.

The sum of the mean recovery percentage of imiquimod from the different Franz cell elements is not 100%. This is due to the loss of formulations that occurred during the removal of donor solution from the donor chamber following completion of the Franz cell run in addition to the formulations loss during the extraction process prior to HPLC analysis.

Table 4.4: *Mean recovery percentage of imiquimod from the different Franz cell elements of the permeation study of microemulsions in comparison with Aldara™ cream when analysed by HPLC. Data is presented as the mean % ± SD (n = 6). The donor solution represents the dosed microemulsion solution into the donor chamber recovered following completion of Franz cell run.*

Analysed Element	F3 microemulsion Formula	F6 microemulsion Formula	F9 microemulsion Formula	Aldara™ Cream
Donor solution	84.10 ± 3.42	88.17 ± 6.40	81.73 ± 5.40	
Donor wash	1.22 ± 0.53	2.76 ± 0.65	3.82 ± 0.90	6.41 ± 2.01
Skin wash	6.19 ± 0.58	4.27 ± 0.53	9.82 ± 0.30	87.48 ± 8.64
Tape strips	0.10 ± 0.07	0.08 ± 0.05	0.11 ± 0.09	0.95 ± 0.56
Remaining skin	**0.15 ± 0.08**	**0.18 ± 0.07**	**0.33 ± 0.08**	**0.99 ± 0.18**
Receptor fluid	0.14 ± 0.05	0.17 ± 0.04	0.28 ± 0.03	0.47 ± 0.29

An assessment of the mean recovery percentage of imiquimod in the remaining skin element from the different microemulsion formulas shows that the recovery percentage from the microemulsion formulas F3, F6 and F9 is significantly less than that of Aldara™ cream as illustrated in Figure 4.10. Moreover, the comparison among the different microemulsion formulas demonstrates that the recovery percentage of imiquimod from F9 formula (0.33% ± 0.08) is higher than F3 (0.15% ± 0.08) and F6 (0.18 ± 0.07) formulas. F6 formula, in turn yields a slightly higher recovery percentage than F3 formula. This can be attributed to the increase in oleic acid and Tween 20/PG mixture content from F3 to F9 formulas. However, these differences in the recovery percentage among the different microemulsion formulas are found to be non-significant as shown in Figure 4.10. It is apparent from the HPLC results, that microemulsion formulas F3, F6 and F9 do not have the capability to improve the delivery of imiquimod into the skin over Aldara™ cream.

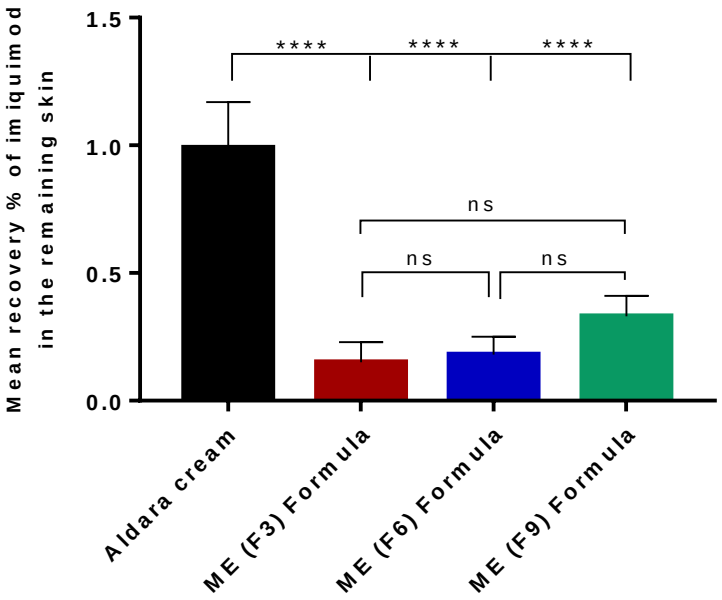

Figure 4.10: *Mean recovery percentage of imiquimod in the remaining skin obtained from the permeation study of microemulsion formulas F3, F6 and F9 in comparison with Aldara™ cream when analysed by HPLC. Data is presented as the mean ± SD (n = 6).*

4.4.2.5.3 ToF-SIMS analysis of microemulsion tape strips

The ToF-SIMS spectra that highlight the $[M+H]^+$ of imiquimod in tape strips 2 and 10 obtained from the permeation study of F9 microemulsion formula are shown in Figure 4.11. The $[M+H]^+$ of imiquimod is detected with a moderate intensity at TS 2 but with a very low ion intensity at TS 10. In addition, an examination of the ToF-SIMS ion image of the $[M+H]^+$ of imiquimod in TS 10 (Fig. 4.12c) which represents a reflection of the imiquimod spectra shows the presence of imiquimod at a very low intensity. These results indicate the very limited permeation of imiquimod into the *stratum corneum* from the F9 microemulsion formula which are in close agreement with the HPLC results.

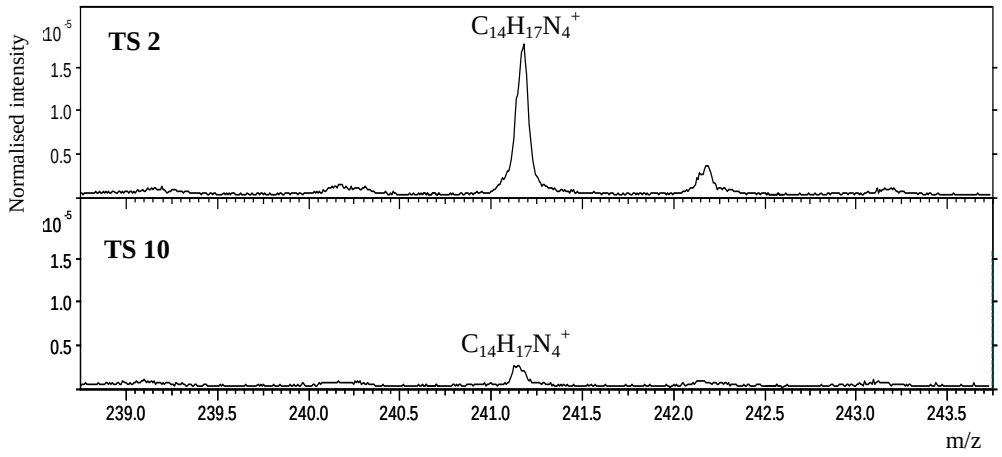

Figure 4.11: *Stacked ToF-SIMS spectra of the $[M+H]^+$ of imiquimod in tape strips 2 and 10 of F9 microemulsion formula, showing the peak of the $[M+H]^+$ of imiquimod ($C_{14}H_{17}N_4^+$) at m/z = 241.*

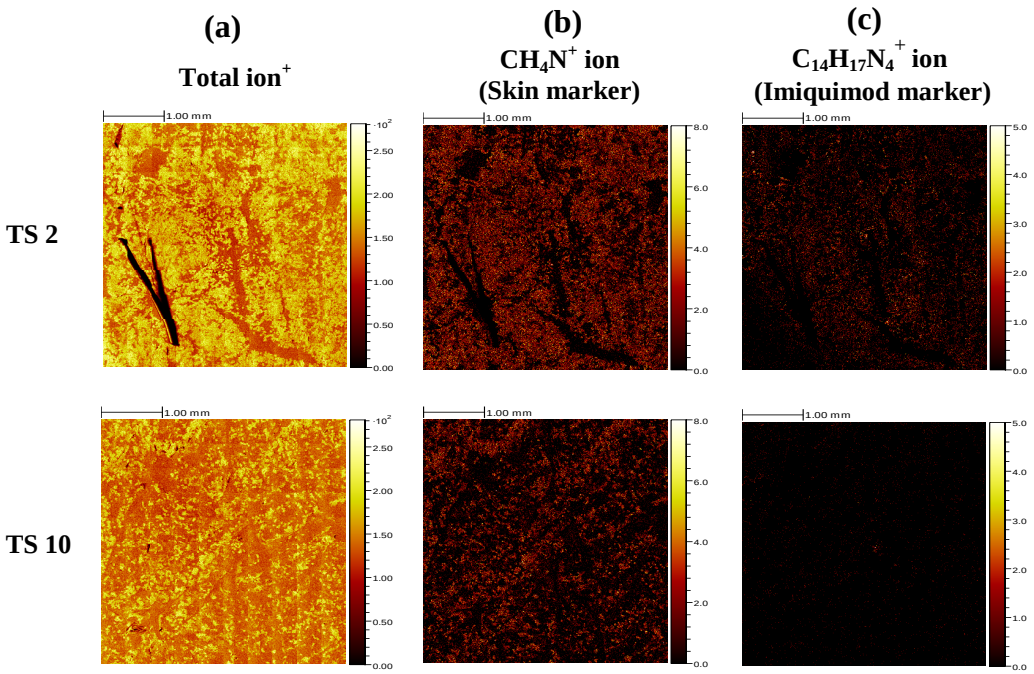

Figure 4.12: *ToF-SIMS ion images of tape strips 2 and 10 of F9 microemulsion formula, showing: (a) the total ion$^+$, (b) the skin marker (CH_4N^+) and (c) the imiquimod marker ($C_{14}H_{17}N_4^+$).*

4.4.2.5.4 ToF-SIMS analysis of microemulsion cryo-sectioned samples

The ToF-SIMS spectrum of the cryo-sectioned skin samples of F9 microemulsion formula is shown in Figure 4.13b, in which the normalised ion intensity of the $[M+H]^+$ of imiquimod is detected with a very low intensity close to the ion intensity of the skin control sample (Fig. 4.13a). This very low ion intensity is also observed in ToF-SIMS ion image of the $[M+H]^+$ of imiquimod (Fig. 4.14c) which illustrates the absence of imiquimod from the cross-sectioned samples.

The HPLC and ToF-SIMS results confirm the very limited permeation of imiquimod from microemulsions and suggest the requirement of an active device that has the ability to bypass the *stratum corneum* barrier to deliver microemulsions directly into the viable epidermis layer of the skin (e.g. microneedles).

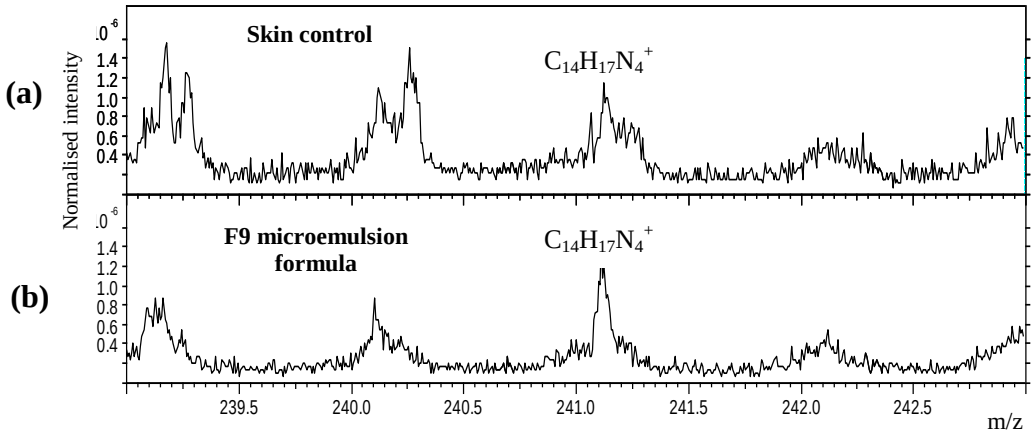

Figure 4.13: *stacked ToF-SIMS spectra of the cryo-sectioned samples for (a) skin control and (b) F9 microemulsion formula, showing the peak of the* $[M+H]^+$ *of imiquimod* ($C_{14}H_{17}N_4^+$) *at m/z = 241.*

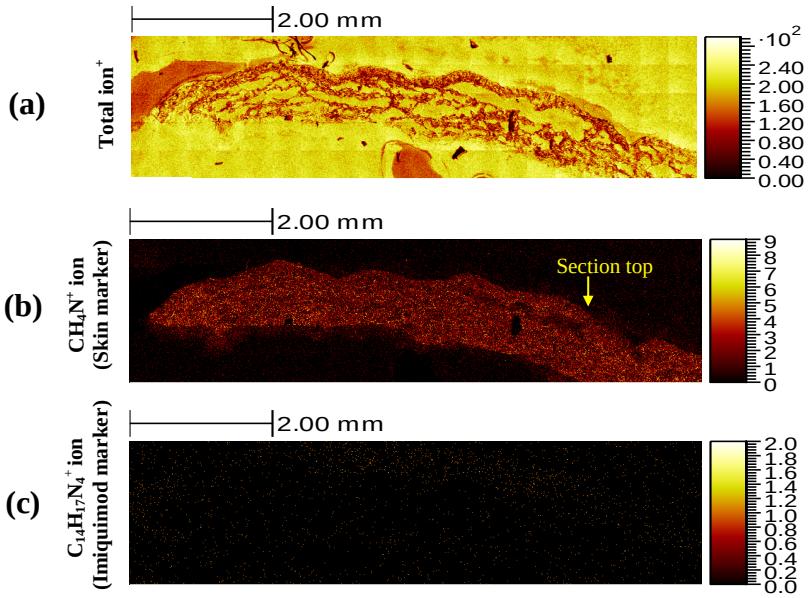

Figure 4.14: *ToF-SIMS ion images of the F9 microemulsion formula cryo-sectioned samples showing (a) the total ion$^+$, (b) the skin marker (CH_4N^+) and (c) the imiquimod marker ($C_{14}H_{17}N_4^+$).*

4.4.3 Microneedles

4.4.3.1 Histological examination of porcine skin samples

In order to deliver therapeutic agents into the epidermal layers using microneedles, it is essential first to determine the relative thickness of the skin layers. Therefore, porcine skin samples were examined by a light microscope following the cryo-sectioning and staining processes to highlight the different skin layers and measure their thickness. Light microscope images of porcine skin cross-sectioned samples (blank skin) stained with H&E showing the different skin layers at low and high magnifications are illustrated in Figure 4.15a and b respectively. The *stratum corneum* layer is the uppermost non-nucleated layer stained with a pink colour with a measured thickness of 14-32 µm. The next layer is the nucleated viable epidermis stained with a purple colour. This layer shows a great variability in thickness even within the same section as indicated by the white arrows (Fig. 4.15a) where the measured thickness varies from 33 to 139 µm. It was reported by Jenning *et al.* that the upper 100 µm section of the porcine skin represents the *stratum corneum* and

the upper layers of the viable epidermis, the second section which is between 100 and 200 µm basically represents the viable epidermis layer [351].

This variability in the thickness of the epidermal layer imposes a practical difficulty in delivering drugs to specifically target the viable epidermal layer and it should be considered during the design and use of microneedles for the localised delivery of drugs to this layer. Although, this measurement of the epidermal layer thickness is performed on pig's ear skin, it can be used as a prediction for the human skin due to the close structural similarity of porcine skin to human skin [132, 133, 318]. Additionally, it was reported that the thickness of the human skin epidermis varies in a similar range from 75 to 150 µm [325]. However, in BCC the *stratum corneum* becomes thicker because of the hyperkeratinisation associated with the tumour lesions [45]. Therefore, it is thought that the use of derma stamp electric pen microneedles at a length of 250-300 µm may be appropriate to deliver imiquimod into the basal layer of the epidermis to treat BCC lesions. The appropriate length of the microneedles used depends on the skin elasticity and the method of application [352].

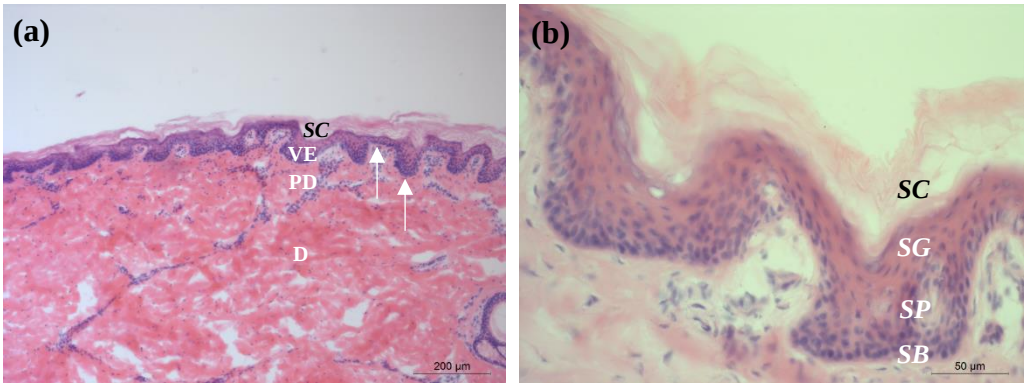

Figure 4.15: *Light microscope images of porcine skin cross-sections stained with H&E highlighting the skin layers at (a) low magnification (scale bar 200 µm) showing SC, VE, PD and D layers, the white arrows highlight the variability in the viable epidermis thickness and (b) high magnification (scale bar 50 µm) showing the multiple epidermal layers: SB, SP, SG and SC.*

4.4.3.2 *En face* light microscope imaging of porcine skin samples following microneedles application

The image of the 12 metal microneedles cartridge that is fixed in the derma stamp electric pen used to pierce the skin is shown in Figure 4.16a. The diameter of the base (circular shape) containing the 12 microneedles is 5 mm and the distance between each microneedle pin is approximately 1.5 mm. Figure 4.16b shows a microscopic lateral view of the microneedles highlighting the diameter of the microneedle pin of approximately 113 μm at the length of 250 μm used to pierce the skin. The base diameter of the needle is 258 μm, while the tip diameter is 12 μm.

To demonstrate the efficiency of the stamp pen to penetrate the uppermost layer of the skin, *en face* imaging by light microscopy was performed for the skin samples treated with the microneedles and stained with gentian violet and methylene blue dyes as illustrated in Figure 4.16c and d respectively. These images show that the dyes are appropriately retained in the microchannels formed by the microneedles. This indicates the capability of the microneedles to successfully pierce the skin. The stamp pen penetration efficiency is observed to occur in a reproducible manner throughout the tested skin samples which can be attributed to the fixed velocity used in the microneedle insertion provided by the electrical stamp pen applicator. Verbaan *et al*. demonstrated that the use of an electrical applicator for microneedles with 300 μm length at a certain velocity facilitates the insertion of the microneedles into the skin in a reproducible manner compared to manual application [353]. In another study, they found that piercing skin by slow manual application of short length microneedles of 300 μm was unsuccessful due to the elasticity of the skin that counteracted the penetration of the microneedles into the skin and makes the piercing unreproducible [354]. Therefore, the use of an impact electrical insertion device can circumvent the skin elasticity challenge [353].

Furthermore, it can be observed in Figure 4.16c and d that the measured diameter of the pores ranges from 300 to 500 μm. However, these values are in

contrast to the measured values from the cryo-sectioned samples (Fig. 4.17a) that showed the diameter of the pores between 40 and 95 μm. This overestimation of the pore size is thought to be due to the lateral diffusion of the dyes within tissue. An apparent limitation of the *en face* imaging method of visualising microneedles treated skin is the overestimation of the pore diameter because of the lateral diffusion of the dyes [268, 278]. A noteworthy point is that the microneedles cartridge fixed to stamp pen applicator is disposable and can be used just for one application and then has to be replaced with a new one for the next sample. From the clinical perspective, this eliminates any safety issue generated from the bending or breaking of the microneedles within skin from the repeated use of the microneedles.

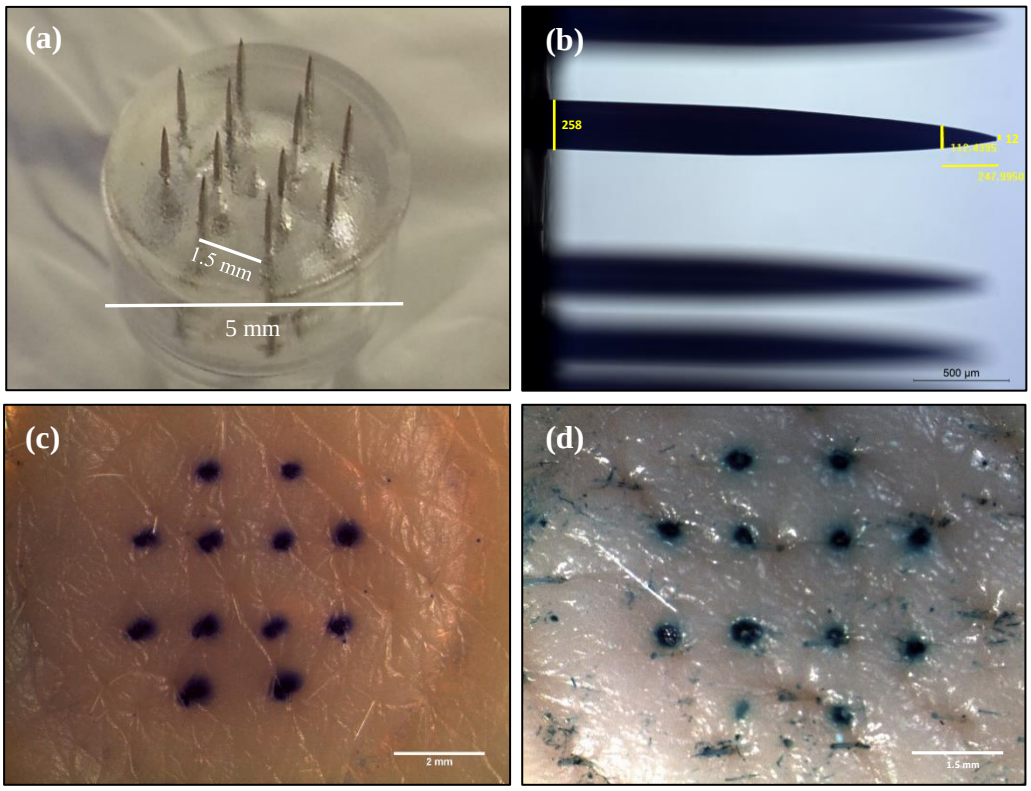

Figure 4.16: *En face images of (a) the microneedles cartridge fixed in the stamp pen used to pierce the skin, (b) the microscopic lateral view of the microneedles highlighting the diameter of the microneedle pin at the base, at the length of 250 μm and at the tip, (c) and (d) porcine skin following stamp pen treatment and staining with gentian violet and methylene blue respectively.*

4.4.3.3 Histological examination of porcine skin samples following microneedles application

Light microscope images of unstained and stained cross-sections of porcine skin following the treatment with microneedles are illustrated in Figure 4.17. The images of the unstained cryo-sections (Fig. 4.17a) show the penetration of gentian violet dye through the microchannels formed by the application of stamp pen which verifies the penetration efficiency of the microneedles. The measured depth and diameter of the microconduits are approximately 88-100 and 40-95 μm respectively. The stained cross-sections with H&E (Fig. 4.17b and c) identify the location of the microchannels within skin tissue and it can be observed that the microneedles penetrate the *stratum corneum* and viable epidermis to reach the papillary dermis (PD) layer (the layer located directly beneath the viable epidermis). However, a recent study conducted by Coulman *et al.* highlighted that the histological preparation of the skin can result in an overestimation of the dimensions of the microchannels [278]. This was observed when they compare histological images with the *in vivo* optical coherence tomography images. This overestimation can be due to the tissue processing through different steps of fixation, sectioning and staining which influence tissue hydration and elasticity in addition to the biomechanical (elastic) properties of the skin and its ability to constrict *in vivo* following the removal of microneedles [278].

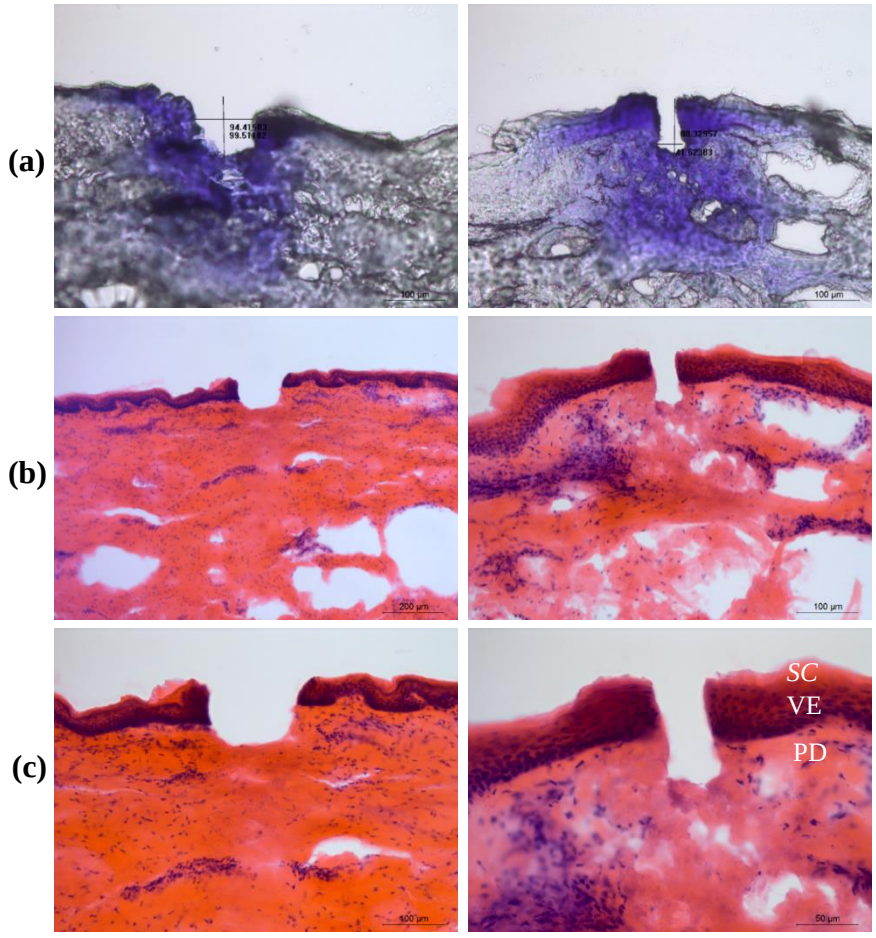

Figure 4.17: *Light microscope images of the microchannels created in porcine skin following stamp pen application showing (a) the unstained cross-sections highlighting the penetration of gentian violet dye through the microchannels created by microneedles, (b) H&E stained cross-sections identifying the location of the microchannels within skin tissue, and (c) H&E stained cross-sections but at a higher magnification.*

4.4.3.4 Permeation study of microemulsions with microneedle pre-treatment

The results obtained from the previous permeation study of the different microemulsion formulas (Section 4.4.2.5) showed the inability of these microemulsions to enhance permeation of imiquimod into the skin. Therefore, the strategy of using microneedle pre-treatment followed by application of microemulsions was investigated to improve the delivery of imiquimod into the epidermal layers. In this way, the microemulsions loaded with imiquimod can

pass through the microchannels created by microneedles to reach the epidermal layers. F3 microemulsion formula loaded with 0.1% w/w of imiquimod was selected to be applied on the skin following microneedle pre-treatment because it contains the highest water content of 84% w/w and the lowest S/Co-S concentration of 14% w/w. In addition, it was not significantly different from the other microemulsion formulas in terms of imiquimod skin permeation as shown previously in Figure 4.9.

4.4.3.4.1 Determination of the percentage of imiquimod recovered by HPLC

The mean recovery percentage of imiquimod from the different Franz cell elements of the permeation study of F3 microemulsion formula with and without microneedle pre-treatment are reported in Table 4.5. The reported data for F3 formula without microneedle pre-treatment in Table 4.5 is the same data obtained from the previous microemulsions permeation study (Table 4.4) and used here for the comparison with microneedle pre-treatment data.

Table 4.5: *Mean recovery percentage of imiquimod from the different Franz cell elements of the permeation study of F3 microemulsion formula with and without microneedle pre-treatment when analysed by HPLC. Data is presented as the mean % ± SD (n = 6).*

Analysed Element	F3 formula (alone) without microneedle pre-treatment (mean % recovery ± SD)	F3 formula with microneedle pre-treatment (mean % recovery ± SD)
Donor solution	84.10 ± 3.42	79.85 ± 5.61
Donor wash	1.22 ± 0.53	2.35 ± 1.33
Skin wash	6.19 ± 0.58	4.71 ± 1.67
Tape strips	0.10 ± 0.07	0.11 ± 0.09
Remaining skin	**0.15 ± 0.08**	**0.18 ± 0.13**
Receptor fluid	0.14 ± 0.05	0.16 ± 0.10

The data presented in Table 4.5, surprisingly shows that the mean recovery percentage of imiquimod in tape strips, remaining skin and receptor fluid for F3 microemulsion formula with microneedle pre-treatment are very low and similar to percentages recovered without microneedles application. The sum of the mean recovery percentage of imiquimod from the different Franz cell elements is not 100%. This is due to the loss of formulations that occurred during the removal of donor solution from the donor chamber following completion of the Franz cell run in addition to the formulations loss during the extraction process prior to HPLC analysis. In addition, Figure 4.18 statistically compares the mean recovery percentage of imiquimod in the remaining skin of F3 microemulsion formula with and without microneedle pre-treatment and shows that there is a non-significant difference between the two application conditions. This data suggests that there is an issue with the release of imiquimod from the microemulsion formula since with microneedle pre-treatment, the skin barrier integrity is reduced by the formation of microchannels through which the applied formulation can pass in a significant amount into the skin and receptor fluid compartment.

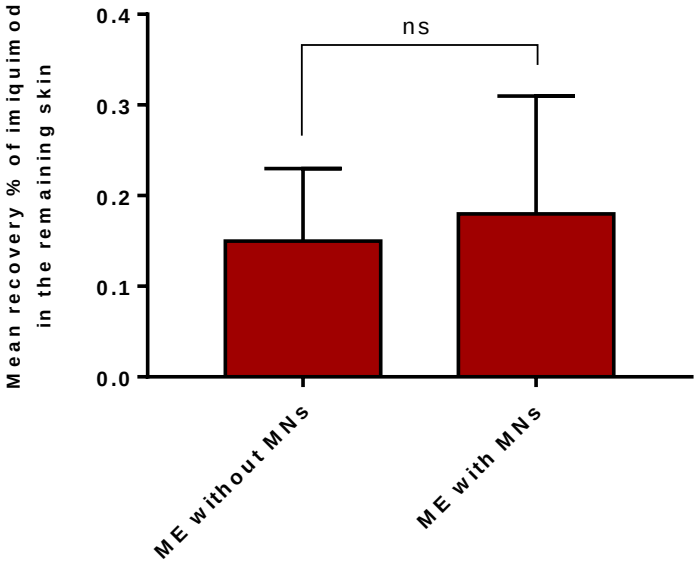

Figure 4.18: *Mean recovery percentage of imiquimod in the remaining skin of the permeation study of F3 microemulsion formula with and without microneedle pre-treatment when analysed by HPLC. Data is presented as the mean ± SD (n = 6).*

The drug release from the formulation should be at an optimum rate and encourage partitioning into the skin. This can be achieved by using a solvent in which the drug is only moderately soluble (the vehicle should allow some solubility of the drug but should not retain the drug) [1]. In the case of imiquimod's microemulsions, imiquimod is a lipophilic drug with a partition coefficient of 2.7 [60] which showed the highest solubility of 170 mg/mL in oleic acid. Therefore, it is proposed that the high solubility of imiquimod in oleic acid significantly decreases the release of imiquimod from the microemulsion formulations (i.e. oleic acid retains imiquimod and reduces its partition out to the skin). It was reported that the high affinity of a drug to its vehicle can inhibit skin permeation due to the slow release and transfer of the drug from the vehicle to the skin [355].

Takahashi *et al.* compared the skin permeation of diclofenac sodium delivered from different oils following the addition of 10% ethanol and 5% n-octanol to them to increase the solubility of diclofenac sodium in these oils and they found that the flux (*J*) from squalane vehicle and castor oil was 112.6 ± 14.7 and 1.3 ± 0.3 nmol/cm^2/h respectively. Similarly, they studied the release of diclofenac sodium from these vehicles using a cellophane membrane and they found that the release control factor (*k*) was 252.8 ± 10.9 and 66.3 ± 10 respectively. They revealed that these differences in the permeation and release profile can be attributed to the higher solubility of diclofenac sodium 38.8 mM in castor oil compared to 10.1 mM in squalane which resulted in a slower release and lower flux of diclofenac sodium from castor oil. They concluded that the higher affinity of a drug to the vehicle reduces the skin permeation because of the slow release and poor transfer of the drug from the vehicle to the skin [355]. Similar observations were also reported from the skin permeation of ketoprofen microemulsions, in which ketoprofen showed solubilities of 81 and 20 mg/mL in triacetin and oleic acid respectively. However, the highest permeation was in oleic acid 8.44 ± 0.86 μg/cm^2/h compared to 1.22 ± 0.29 μg/cm^2/h in triacetin [218].

Although, the high solubility of imiquimod in oleic acid can reduce the release and skin permeation of imiquimod from the microemulsion formulas, it is proposed that this is not the only factor which influences the poor release of imiquimod from the microemulsions. Imiquimod was previously detected in the tape strips and cryo-sectioned skin samples of oleic acid solution (Chapter 3, Sections 3.4.2.4 and 3.4.2.5) at a higher intensity compared to the tape strips and cryo-sectioned samples of imiquimod's microemulsions. Therefore, it is thought that the microstructure of the microemulsion and more specifically the presence of S/Co-S mixture surrounding or encapsulating oleic acid droplets may additionally impart a negative influence on the release of imiquimod from the microemulsions (i.e. make it more difficult for imiquimod to be released from the microemulsions). It was reported that in some cases that the drug may be held within microemulsion droplets leading to a reduction in its permeation into the skin [217]. Chen *et al*. studied the skin permeation of triptolide microemulsions using oleic acid as an oil phase, they found that the encapsulation of oleic acid by the S/Co-S mixture (Tween 80/PG) reduced the penetration of oleic acid into the *stratum corneum* [234]. In another study conducted by Paolino *et al*. they observed that there was no significant enhancing effect obtained by the addition of oleic acid to ketoprofen lecithin microemulsions due to the strong binding of oleic acid to the microemulsion structure [356].

It is possible that the high affinity of imiquimod for oleic acid and the encapsulation of oleic acid droplets by S/Co-S mixture results in retaining imiquimod within oleic acid droplets with a reduced ability to partition out that leads to the poor release and transfer of imiquimod from microemulsions to the skin. An optimisation of the microemulsions formulation is required as future work, perhaps focusing on areas such as changing the type of oil used to one in which imiquimod is just only moderately soluble to facilitate its release to the skin.

4.4.3.5 Permeation study of Aldara™ cream with microneedle pre-treatment

Application of Aldara™ cream following pre-treatment of porcine skin with the stamp pen microneedles was carried out to investigate if this approach can enhance permeation of imiquimod into the skin in comparison with the conventional application of Aldara™ cream alone. It has been proven that Aldara™ cream releases imiquimod in sufficient amounts to induce an immunological response [59] and the previous HPLC and ToF-SIMS results showed that the cream has limited permeation into the deeper skin layers and it mostly located at the *stratum corneum* layer (Chapter 3, Section 3.4.1). Therefore, the availability of microchannels created by microneedles provides an opportunity for the cream to pass through them to reach the deeper epidermal skin layers.

4.4.3.5.1 Determination of the percentage of imiquimod recovered by HPLC

The mean recovery percentage of imiquimod from the different Franz cell elements of the permeation study of Aldara™ cream with and without microneedle pre-treatment are reported in Table 4.6.

Table 4.6 shows that the mean recovery percentage of imiquimod from tape strips and remaining skin elements of Aldara™ cream with microneedle pre-treatment is approximately three times higher than the Aldara™ cream alone. This provides an increase opportunity for the cream to more effectively treat the whole superficial or nodular BCC lesions. In addition, the statistical comparison between the mean recovery percentages of imiquimod in the remaining skin shows that the recovery percentage of imiquimod with microneedle pre-treatment is significantly higher than the Aldara™ cream alone as illustrated in Figure 4.19.

Table 4.6: *Mean recovery percentage of imiquimod from the different Franz cell elements of the permeation study of Aldara™ cream with and without microneedle pre-treatment when analysed by HPLC. Data is presented as the mean % ± SD (n = 6).*

Analysed Element	Aldara™ cream (alone) without microneedle pre-treatment (mean recovery % ± SD)	Aldara™ cream with microneedle pre-treatment (mean recovery % ± SD)
Donor wash	7.11 ± 3.27	9.38 ± 4.59
Skin wash	81.72 ± 8.14	75.39 ± 12.02
Tape strips	0.67 ± 0.13	2.38 ± 1.40
Remaining skin	**0.81 ± 0.26**	**2.27 ± 0.39**
Receptor fluid	0.17 ± 0.08	1.89 ± 0.47

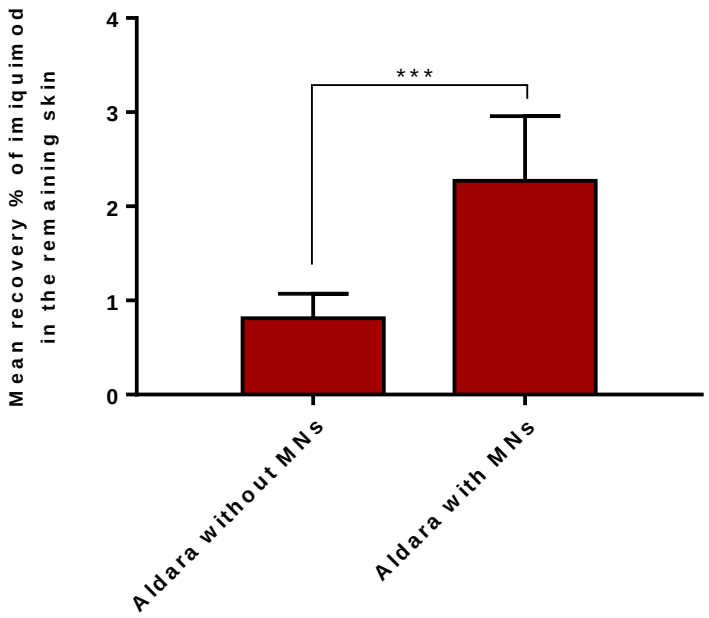

Figure 4.19: *Mean recovery percentage of imiquimod in the remaining skin of the permeation study of Aldara™ cream with and without microneedle pre-treatment when analysed by HPLC. Data is presented as the mean ± SD (n = 6).*

Furthermore, it is observed that with microneedle pre-treatment the mean recovery percentage of imiquimod in the receptor fluid is approximately ten times higher than the Aldara™ cream alone (Table 4.6). This increase in the recovery percentage of imiquimod in the receptor fluid is perhaps anticipated since the microchannels created by microneedles can reach the depth of papillary dermis layer as previously shown in Figure 4.17 and thus higher amounts of imiquimod bypass the skin barriers and presented in the receptor fluid. For *in vivo* conditions, this means higher percentage of imiquimod would be available for systemic circulation which may increase imiquimod's systemic adverse effects. However, in BCC patients the *stratum corneum* becomes thicker because of the hyperkeratinisation associated with the tumour lesions [45]. Therefore, the microchannels created by the stamp pen may not reach the depth of papillary dermis and hence less percentage of imiquimod would be available for systemic absorption. However, the control of microneedle penetration to target a specific skin layer such as basal layer in a consistent way is very difficult to achieve due to intra and inter-individual variability of the thickness of epidermal layer.

4.4.3.5.2 ToF-SIMS analysis of the tape strips of Aldara™ cream with microneedles

ToF-SIMS analysis of the tape strips of Aldara™ cream with and without microneedles highlights the significant increase in the ion intensity of the $[M+H]^+$ of imiquimod in tape strips 2, 5 and 10 of the Aldara™ cream with microneedle pre-treatment compared to Aldara™ cream alone as shown in Figure 4.20. This indicates that a higher amount of imiquimod is permeated into the *stratum corneum* following microneedles application which is in accordance with the HPLC results (Table 4.6). This comparison between the tape strips of Aldara™ cream with and without microneedles was performed using the same section of porcine ear skin and it is unrelated to the previous analysis of the tape strips of Aldara™ cream discussed in Chapter 3, Section 3.4.1.3.3 which was carried out using dermatomed pig's flank skin.

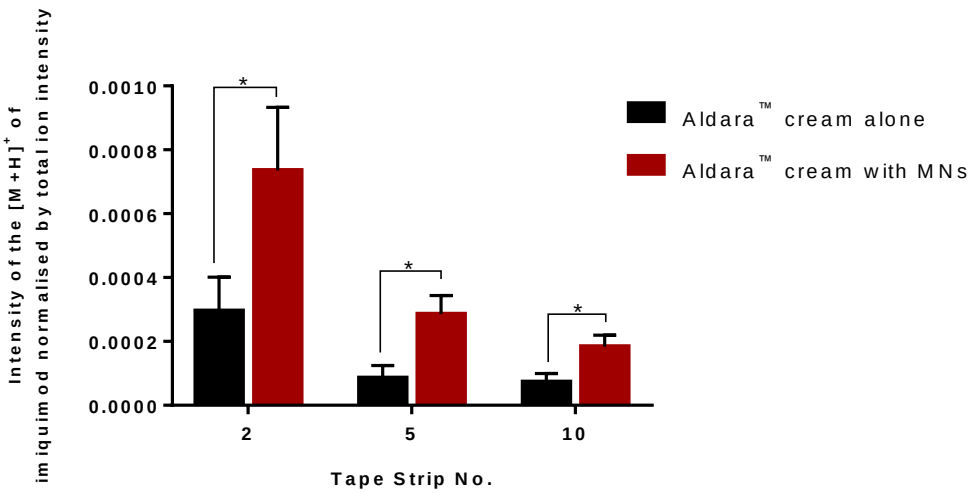

Figure 4.20: *Ion intensity values of the $[M+H]^+$ of imiquimod ($C_{14}H_{17}N_4^+$) in Aldara™ cream tape strips (2, 5 and 10) with and without microneedle pre-treatment normalised by total ion intensity. Data is presented at the mean ± SD (n = 4).*

ToF-SIMS ion images of tape strip two of Aldara™ cream with microneedle pre-treatment are shown in Figure 4.21. Figure 4.21b illustrates the $[M+H]^+$ of imiquimod ($C_{14}H_{17}N_4^+$) image which highlights the pattern of imiquimod distribution following stamp pen application. It was observed that imiquimod is mostly localised in the area disrupted by the application of the stamp pen (i.e. at a circular region in the middle of the tape strip which corresponds to the shape of the stamp pen cartridge). Additionally, Figure 4.21c which is the overlaid image of imiquimod and the skin where imiquimod is highlighted in a green colour and the skin in a brown colour, shows that imiquimod radiates out of the microchannels and distributes within skin tissue.

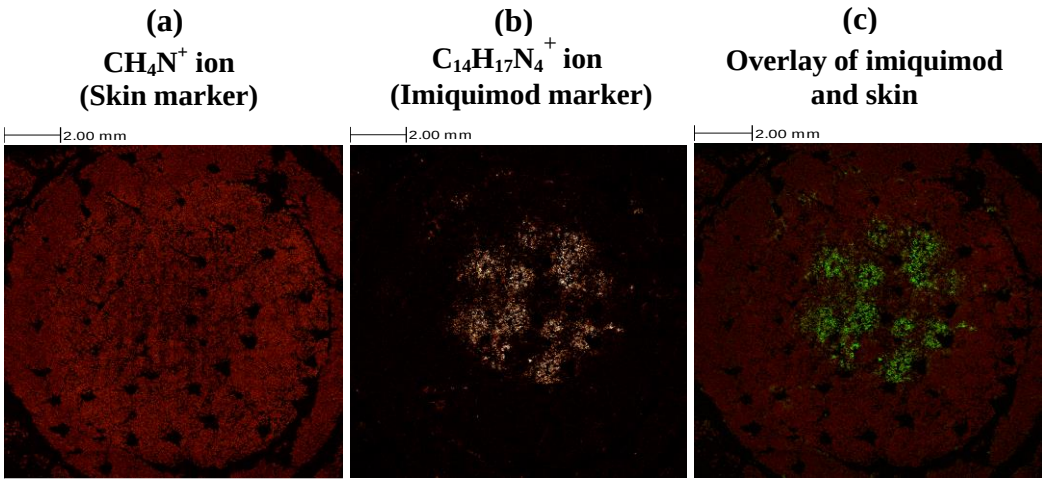

Figure 4.21: *ToF-SIMS ion images of tape strip two of Aldara™ cream with microneedle pre-treatment showing: (a) the skin marker (CH_4N^+), (b) the imiquimod marker ($C_{14}H_{17}N_4^+$), and (c) the overlaid image of imiquimod (green colour) and the skin (brown colour). The scanned tape strip area is of 12 × 12 mm^2.*

4.4.3.5.3 ToF-SIMS analysis of the cryo-sectioned skin samples of Aldara™ cream with microneedles

ToF-SIMS analysis of the cryo-sectioned skin samples shows that the ion intensity of the $[M+H]^+$ imiquimod from Aldara™ cream with microneedle pre-treatment is significantly higher than the ion intensity obtained from the samples without microneedle pre-treatment as shown from their overlaid spectra (Fig. 4.22). This higher ion intensity is also reflected in the ToF-SIMS ion images of the $[M+H]^+$ imiquimod from Aldara™ cream with microneedle pre-treatment as illustrated in Figure 4.23. It is proposed that the presence of the microchannels created by microneedle application, imiquimod penetration is not only restricted to the microchannel site but it radiates to the adjacent tissue (lateral distribution) which results in almost higher intensity of imiquimod localised at the upper part of the sections (Fig. 4.23).

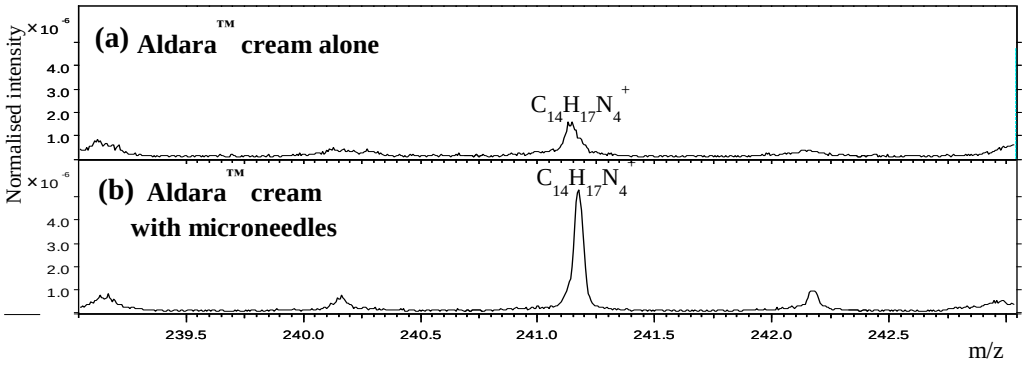

Figure 4.22: *Stacked ToF-SIMS spectra of the cryo-sectioned samples for (a) Aldara™ cream alone and (b) Aldara™ cream with microneedle pre-treatment, showing the peak of the [M+H]$^+$ of imiquimod ($C_{14}H_{17}N_4^+$) at m/z = 241.*

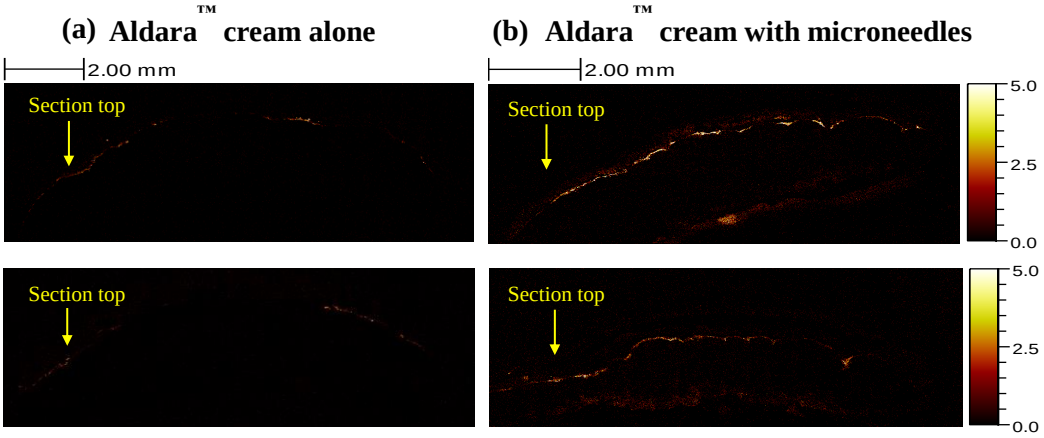

Figure 4.23: *ToF-SIMS ion images of the [M+H]$^+$ of imiquimod ($C_{14}H_{17}N_4^+$) from the cryo-sectioned skin samples for (a) Aldara™ cream alone without microneedle pre-treatment and (b) Aldara™ cream with microneedle pre-treatment.*

The whole ToF-SIMS ion images of the cryo-sectioned skin samples of Aldara™ cream with microneedle pre-treatment are illustrated in Figure 4.24 which show the total ion image (Fig. 4.24a), the skin marker (CH_4N^+) image (Fig. 4.24b) and the [M+H]$^+$ of imiquimod image (Fig. 4.24c). An examination of the total ion image (Fig. 4.24a) and the skin marker image (Fig. 4.24b) indicate the location of the microchannels within skin sections (white arrows) created by the application of microneedles. The image of the [M+H]$^+$ of imiquimod (Fig. 4.24c) highlights the distribution of imiquimod at the upper

layer of the skin sections in addition to its localisation in the microchannels. However, with ToF-SIMS ion images it is difficult to specify exactly the boundaries of the skin layers and therefore in order to obtain a clearer visualisation of imiquimod localisation within the different skin layers, the ToF-SIMS ion images are matched with their counterparts light microscopy images stained with H&E (Fig. 4.24d and e). It was observed that imiquimod is mostly located in the epidermal layer (*stratum corneum* and viable epidermis) and within the microchannels which penetrate down to the papillary dermis which make imiquimod available in this layer. This is believed to be the first time that ToF-SIMS has been used to detect and visualise drug penetration into the skin following microneedle pre-treatment and suggests its successful application in microneedle field especially in microneedles used for intra-dermal drug delivery to treat skin disorders or in vaccination therapy. In these cases, ToF-SIMS can be helpful to map the permeation and visulaise distribution of a drug within skin by analysis of a biopsy of treated skin.

The HPLC and ToF-SIMS results of Aldara™ cream with microneedle pre-treatment showed the capability of this approach to improve delivery of imiquimod into the epidermal skin layers and suggest its potential usefulness for more efficient treatment of both superficial and nodular BCC lesions. In addition, both the Aldara™ cream and the stamp pen are commercially available making them easily accessible. The use of commercial product Aldara™ cream in the permeation experiments is quite relevant to the real situation, since it is an approved product currently used in clinical setting to treat superficial BCC lesions. In addition, stamp pen is widely used in cosmetic therapy and can be easily obtained by patients. However, this study is preliminary and provides an early insight into the potential use of microneedles for improving imiquimod's skin penetration and further *ex vivo* and *in vivo* investigation on human skin with BCC lesions are required to optimise the final application conditions.

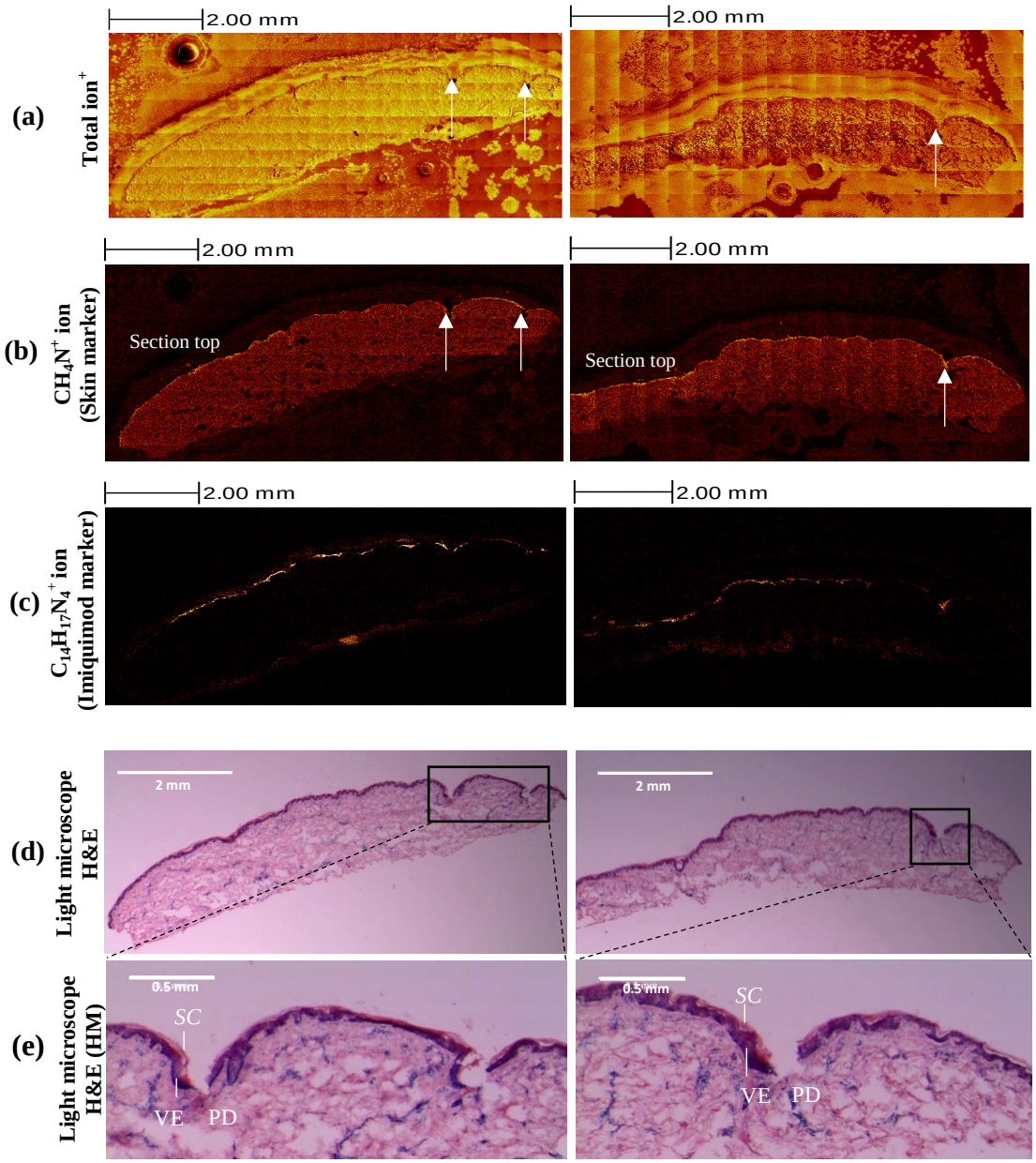

Figure 4.24: *ToF-SIMS ion images and light microscope images of Aldara™ cream with microneedles cryo-sectioned skin samples showing (a) the total ion$^+$, (b) the skin marker (CH_4N^+), (c) the imiquimod marker ($C_{14}H_{17}N_4^+$), (d) light microscope image stained with H&E and (e) light microscope image stained with H&E at higher magnification (HM) highlights the microchannels within skin cross-sections.*

4.5 Conclusions

The work in this chapter investigates the potential advantages of microemulsions and microneedles strategies to enhance delivery of imiquimod into the epidermal layers of the skin. A new HPLC method with higher accuracy and sensitivity than previously used HPLC method was successfully modified and used to determine the imiquimod solubility in different microemulsion components as well as to calculate the recovery percentage of imiquimod from the different Franz cell elements. The *en face* light microscope images of the microneedle treated skin samples demonstrated the penetration efficiency and reproducibility of the stamp pen to disrupt the skin barrier by forming pores through which the penetration of the dyes (gentian violet and methylene blue) was facilitated. In addition, the histological examination of the microneedle treated skin samples (unstained and stained samples) proved the ability of the stamp pen to create microchannels through the skin reach the depth of papillary dermis layer. The assessment of imiquimod permeation from the formulated microemulsion formulas alone and with microneedle pre-treatment using HPLC and ToF-SIMS showed the limited ability of the microemulsions to improve delivery of imiquimod over Aldara™ cream. This was attributed to the poor release of imiquimod from the microemulsion formulas due to the high affinity of imiquimod for the oil phase and the encapsulation of the oil droplets by the S/Co-S mixture. In contrast, Aldara™ cream with microneedle pre-treatment showed improved delivery of imiquimod into the skin. The recovery percentage of imiquimod in the tape strips and the remaining skin determined by HPLC is approximately three times higher than samples without microneedle pre-treatment. The ToF-SIMS ion images of the cryo-sectioned skin samples illustrated the existence of imiquimod in the microchannels and in the epidermal layer at higher ion intensity compared to Aldara™ cream alone. This work is the first known instance that demonstrates the enhancement of imiquimod delivery using microemulsions and microneedles and it may pave the way for future optimisation to develop more effective and safer treatments for BCC lesions. In addition, the high sensitivity and imaging capability offered by ToF-SIMS in producing chemical images for imiquimod distribution and localisation within

skin tissue following microneedle pre-treatment has not been previously observed and indicate the potential role of this instrument that may participate in microneedles field.

5 Chapter Five: *In vivo* and *ex vivo* Assessment of Chlorhexidine Permeation into the Skin from Commercial Products Using ToF-SIMS

5.1 Introduction

To prevent surgical site infections associated with the invasive procedures such as catheter insertion or surgery, efficient skin antisepsis is necessary. Skin is colonised by various microorganisms which are not only located on the skin surface but also inhabit the lower layers of the skin and hair follicles [63, 64] (detailed in Chapter 1, Section 1.4.2). These resident microorganisms may remain at the incision site following skin antisepsis and can cause infections when the skin barrier is ruptured during surgery. Thus, rapid and efficient permeation of the topically applied antiseptic into the deeper skin layers is required to prevent infections associated with the surgical procedures [77].

The antiseptic drug chlorhexidine gluconate (CHG) is widely used clinically for skin antisepsis prior to surgical incision or insertion of catheters [78, 85]. However, its permeation into the deeper skin layers is limited [77, 83-85]. This poor permeability of CHG can be attributed to the sub-optimal physicochemical properties of CHG for the skin delivery as it is an ionised compound [357] with high molecular weight (897.8 g/mol) [37] and low lipid solubility (log P = 0.037) [358]. As discussed in Chapter 1, Section 1.4.3, several researchers have studied the permeation of CHG into *ex vivo* human, rat or porcine skin either from aqueous or alcoholic solutions of CHG [83-85] but to date there is no published *in vivo* data investigating CHG permeation on human volunteers using commercial products. Therefore, the work in this chapter involves investigating the *in vivo* skin permeation of CHG on human volunteers using *in vivo* tape stripping with subsequent analysis by ToF-SIMS following the application of commercial CHG products currently used in hospitals within the UK. Additionally, these products have also been tested on *ex vivo* porcine skin in an attempt to compare with the *in vivo* data and see if there is a correlation between them. ToF-SIMS is a highly sensitive instrument

and offers the opportunity to analyse an individual tape strip (layer by layer analysis). Therefore, it was exploited here to follow CHG permeation as a function of the *stratum corneum* depth.

5.2 Chapter Aims

The aim of this chapter is to compare the *in vivo* skin permeation of CHG from commercial products of chlorhexidine (HiBiSCRUB® 4% w/v, CHG in aqueous vehicle) and (ChloraPrep® 2% w/v, CHG in IPA vehicle) using human volunteers and *ex vivo* porcine skin. The parameters investigated in this comparison are the effect of concentration (2% and 4%), the vehicle effect (water and IPA) and the application time effect (specifically 2, 5, 10, 15, 30 and 60 minutes). A comparison was carried out using the tape stripping technique with subsequent analysis of an individual tape strip by ToF-SIMS. This provides the ability to map the permeation and visualise the localisation of CHG within skin. This work demonstrates the first use of ToF-SIMS to compare the *in vivo* skin permeation of commercially available CHG products.

5.3 Materials and Methods

5.3.1 Materials

HiBiSCRUB® 4% w/v chlorhexidine gluconate, 500 mL solution, Molnlycke Health Care Ltd. UK and ChloraPrep® 2% w/v chlorhexidine gluconate in 70% IPA, 3 mL clear applicator, BD CareFusion, USA were purchased from www.amazon.co.uk. D-Squame standard sampling discs (adhesive discs) were ordered from CUDERM corporation, USA. Deionised water was obtained from an ELGA reservoir, PURELAB® Ultra, ELGA, UK.

5.3.2 *In vivo* study

Tape strips were collected from human volunteers following the application of CHG products in addition to a control skin site. Ethical approval for this study

was obtained from the University of Nottingham Research Ethics Committee (reference no. 003-2016).

5.3.2.1 Volunteer population

Six volunteers (3 male and 3 female) aged between 23-52 years from different ethnic groups participated in this study after providing their consent indicating that they did not possess any skin disorders or hypersensitivity towards adhesive tapes or chlorhexidine containing products. The volar forearm of each volunteer was selected as an application area which was first wiped with tissue to remove any dirt or sweat before products application. The application area was marked with a permanent pen and it was 4 cm away from either the wrist or the bend of the elbow.

5.3.2.2 Tested CHG products

Three products were used in this *in vivo* skin permeation comparison experiments, specifically HiBiSCRUB® 4% w/v (HS 4%) CHG in aqueous vehicle, HiBiSCRUB 2% w/v (HS 2%) CHG in aqueous vehicle (obtained by dilution of HS 4%) and ChloraPrep® 2% w/v (CP 2%) CHG in 70% IPA. This *in vivo* permeation comparison study consist of two steps as shown in Table 5.1. Step one is to investigate the concentration effect (2% and 4%) and the vehicle effect (water and IPA) on skin permeation of CHG. Therefore, 200 μL from each product was applied to a defined skin area of approximately 3 × 3 cm^2 of the volunteers' volar forearm for a 2 minute to mimic the clinical situation used prior to surgery [81, 359, 360]. Following this, the excess formulation was carefully wiped from the skin surface with a soft tissue ready for tape stripping. Step two is to study the application time effect on CHG skin permeation. Thus, the product which showed the highest permeation at the 2 minute time interval from step one was applied again at longer intervals of 5, 10, 15, 30 and 60 minutes. Tape strips were removed at each time interval for ToF-SIMS analysis.

Table 5.1: *Protocol for the in vivo skin permeation comparison experiments of CHG products: HS 4%, HS 2% and CP 2%. S 1 and S 2 represent step one and step two of the experiments.*

Investigated parameter		Products			Application time (minute)					
		HS 4%	HS 2%	CP 2%	2	5	10	15	30	60
S1	Conc. effect	✓	✓		✓					
	Vehicle effect		✓	✓	✓					
S 2	Application time effect	✓				✓	✓	✓	✓	✓

5.3.2.3 *In vivo* tape stripping

In vivo tape stripping was carried out using adhesive tape discs (D-Squame, standard sampling discs, USA) with a diameter of 22 mm. The tape strips were allowed to equilibrate in the laboratory overnight. Following removal of the test product from the skin surface, a template was applied over the product application site to ensure that all tape strips were removed from the same area. Tape strips were applied to the template, pressed down with the aid of a roller 10 times to stretch the skin surface to avoid the effects of furrows and wrinkles on the tape stripping procedure [105] and then removed in one quick movement (constant velocity) by tweezers for up to 20 strips. Samples were stored at -20 °C until required for analysis. Prior to ToF-SIMS analysis the tape strips were attached to glass slides with double sided adhesive tape with the removed *stratum corneum* facing upwards. Following this, the slides were placed in plastic petri dishes and liquid nitrogen was carefully poured into the petri dishes to freeze the tape strips with subsequent freeze drying for 1 hour prior to ToF-SIMS analysis. In addition to the collection of the tape strips from the 3 product application sites, tape strips were also collected from the control skin site.

5.3.3 *Ex vivo* study

5.3.3.1 Assembly of diffusion cells

Skin preparation was performed as previously discussed in Chapter 4, Section 4.3.2.6.1. The method of Franz diffusion cell experiments was carried out as previously detailed in Chapter 3, Section 3.3.2.3 with the exception of the receptor fluid used here which is PBS pH 7.4. The skin was dosed with 200 µL from each CHG product (HS 4%, HS 2% and CP 2%) and left for a 2 minute exposure time as with the *in vivo* experiments before wiping the skin surface with a soft tissue. Each product was tested on six Franz cells with additional skin control samples.

5.3.3.2 *Ex vivo* tape stripping

Skin tape stripping process was carried out as discussed previously in Chapter 3, Section 3.3.2.5. Tape strips were collected from six Franz cells for each CHG product in addition to the skin control sample where analysed individually by ToF-SIMS.

5.3.4 ToF-SIMS analysis

ToF-SIMS was used to analyse single tape stripped samples obtained from both *in vivo* and *ex vivo* studies. ToF-SIMS analysis was done using the same instrument and analysis conditions detailed in Chapter 2, Section 2.3.7 except that the data was acquired from negative polarity which was established as being more informative than the positive polarity data. The analysed area of the tape strips samples was (4 mm × 4 mm) acquired at a resolution of 100 pixels/mm. An ion representing the biological material and therefore indicative of skin (skin marker) in negative polarity was identified as (CNO^-) and it was used to threshold the data sets. Data was reconstructed using regions of interest to remove the data from the adhesive tape material found between the fissures in the stripped skin and hence the data was only analysed from the skin material. Following this, each image of the individual tape strip (4 mm × 4 mm) was divided into four smaller data sets of (2 mm × 2 mm) which resulted

in four repeats (n = 4) for each sample and their intensities were normalised to the total ion intensity.

5.3.5 Statistical analysis of the data

The statistical tests used to compare ion intensities were one way ANOVA with Tukey's multiple comparisons test or paired t-test. All data is presented as the mean ± SD of n = 4 with P values of ≤ 0.05 being regarded as significant using GraphPad Prism 7 software (USA). Prior to statistical analysis all data was tested for normality using Shapiro-wilk normality test.

5.4 Results and Discussion

5.4.1 Identification of the ions characteristics of chlorhexidine by ToF-SIMS

Ions which are distinctive of chlorhexidine have been previously demonstrated by Judd *et al.* during their ToF-SIMS analysis of porcine skin samples dosed with 2% w/v CHG aqueous solution [83, 361]. These ions are the chlorine ion (Cl^-) at m/z = 35 and 37, the fragment ion ($C_7H_4N_2Cl^-$) at m/z = 151 and the molecular ion $[M-H]^-$ ($C_{22}H_{30}N_{10}Cl_2^-$) at m/z = 505. The work in this chapter also uses these ions to detect chlorhexidine in the tape strips obtained from *in vivo* and *ex vivo* studies. Chlorine ion (Cl^-) might be anticipated as an ideal marker for chlorhexidine since its chemical structure contains two chlorinated aromatics. However, this is not the case because it was found that (Cl^-) is also abundant within skin tissue and it is not a unique marker for chlorhexidine (Fig. 5.1a). The $[M-H]^-$ of chlorhexidine at m/z = 505 (Fig. 5.1b) shows excellent chemical specificity, however with a very low intensity (around that of noise) in the CHG treated skin samples, it cannot be used as a reliable marker for chlorhexidine. Instead, the fragment ion, ($C_7H_4N_2Cl^-$) at m/z = 151 (Fig. 5.1c) exhibits chemical specificity whilst also demonstrating a relatively high ion intensity in the CHG treated skin samples and as such is regarded as a reliable marker for the presence of chlorhexidine. In addition, the (CNO^-) peak at m/z = 42 which is generally considered as a generic marker for organic material in negative polarity, was used in this work as a skin marker to indicate the regions on the sample containing skin tissue (i.e. represents the skin pattern). The (CNO^-) peak shows a higher normalised ion intensity in skin control samples than in the CHG reference material (Fig. 5.1d). This verifies the appropriate use of (CNO^-) peak as a skin marker.

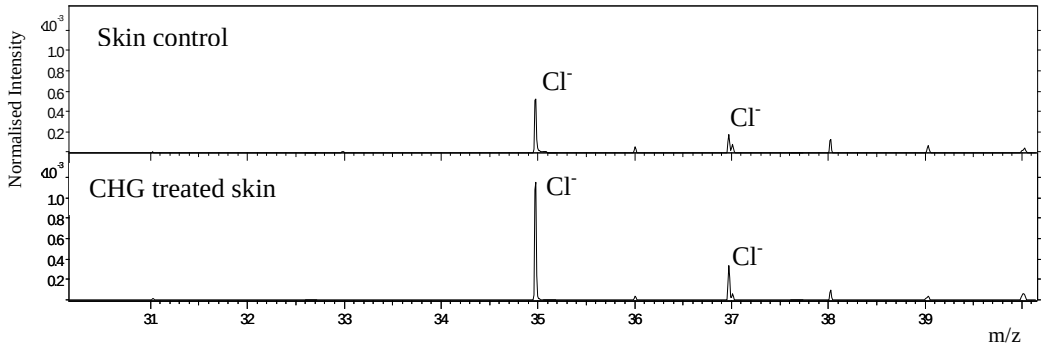

Figure 5.1 (a): *Stacked ToF-SIMS spectra of skin control and CHG treated skin showing the chlorine ion (Cl^-) peak at m/z = 35 and 37.*

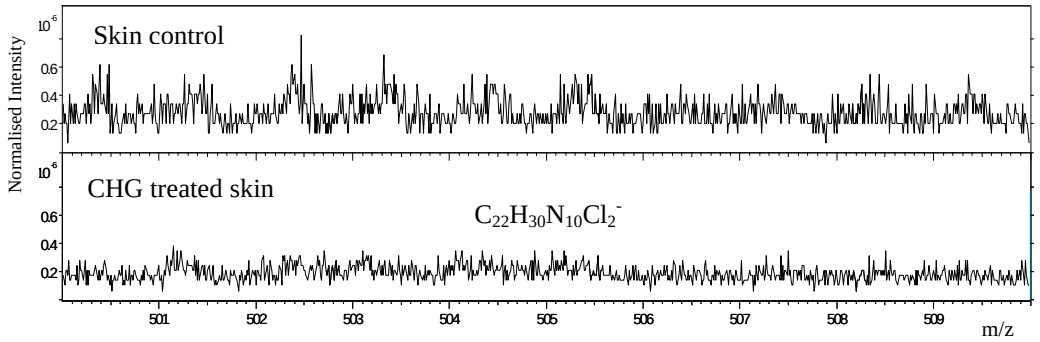

Figure 5.1 (b): *Stacked ToF-SIMS spectra of skin control and CHG treated skin showing the molecular ion ($C_{22}H_{30}N_{10}Cl_2^-$) peak at m/z = 505.*

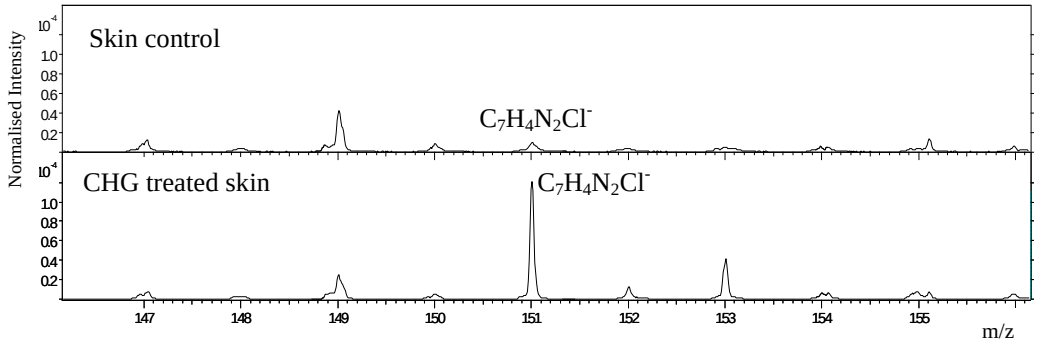

Figure 5.1 (c): *Stacked ToF-SIMS spectra of skin control and CHG treated skin showing the fragment ion ($C_7H_4N_2Cl^-$) peak at m/z = 151.*

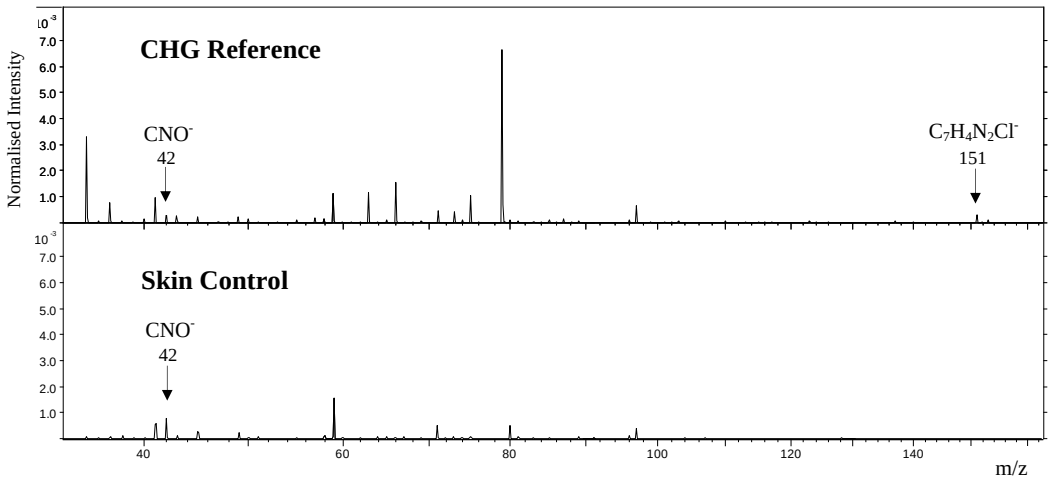

Figure 5.1 (d): *Stacked ToF-SIMS spectra of CHG reference material and skin control sample showing the peak of skin marker ion (CNO^-) at m/z = 42.*

5.4.2 *In vivo* study

5.4.2.1 Investigation of the effect of CHG concentration

The concentration effect on the skin permeation of CHG was investigated by comparing the *in vivo* skin permeation of three CHG products (HS 4%, HS 2% and CP 2%) in six human volunteers using *in vivo* tape stripping with subsequent ToF-SIMS analysis.

5.4.2.1.1 ToF-SIMS data from the 1st volunteer

ToF-SIMS spectra of CHG marker ion ($C_7H_4N_2Cl^-$) from the three CHG products in the tape strips removed from the 1st volunteer are shown in Figure 5.2, in which the marker ion is detected throughout the full series of tape strips, i.e. 2-20. There is, a decreasing ion intensity from the upper layer of the *stratum corneum* (TS 2) to the deeper layer (TS 20).

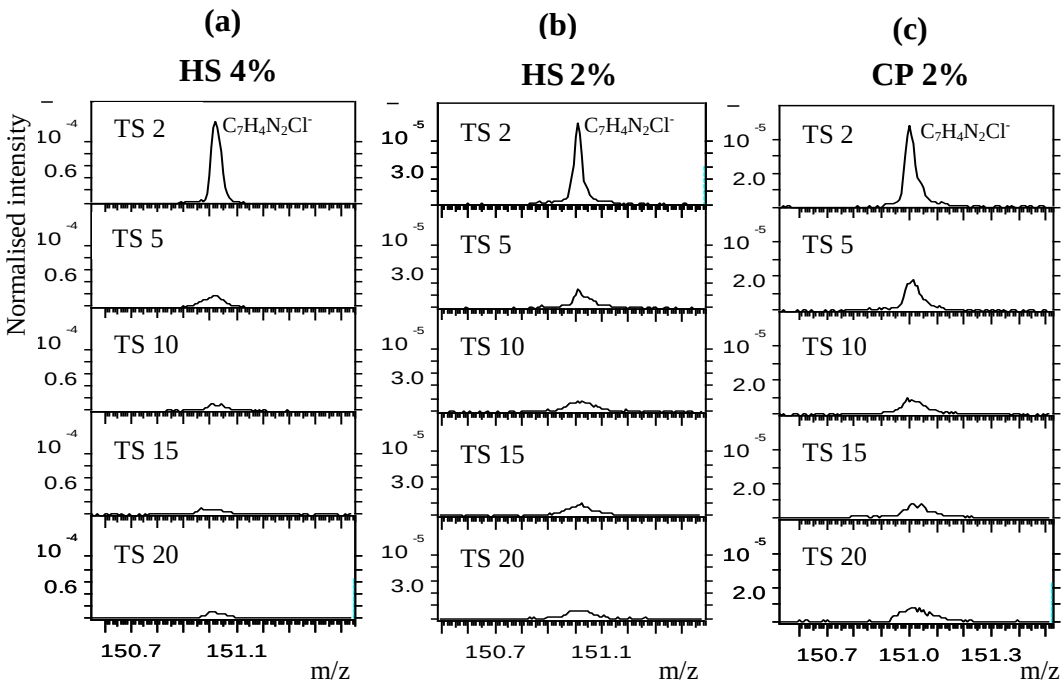

Figure 5.2: *Stacked ToF-SIMS spectra of CHG marker ion ($C_7H_4N_2Cl^-$) at m/z = 151 in the tape strips removed from the 1st volunteer after a 2 minute application time of three CHG products:(a) HS 4%, (b) HS 2% and (c) CP 2%.*

Comparison of the normalised ion intensities of CHG marker ion obtained from the skin control and the different CHG products is shown in Figure 5.3. In this 1st volunteer CP 2% shows a higher intensity than HS 2% and therefore it is used for the comparison purposes. Figure 5.3 shows that the ion intensity of the CHG marker ion is more intense from HS 4% than from the skin control or the CP 2% with a significant increase at TS 2 and 5. However, CP 2% is still showing a significant increase from the skin control at these tape strips. At TS 10, the ion intensity obtained from HS 4% is significantly higher from the skin control but it is not from CP 2%. Furthermore, at TS 15 and 20 there is no significant difference between the ion intensity from HS 4% and skin control.

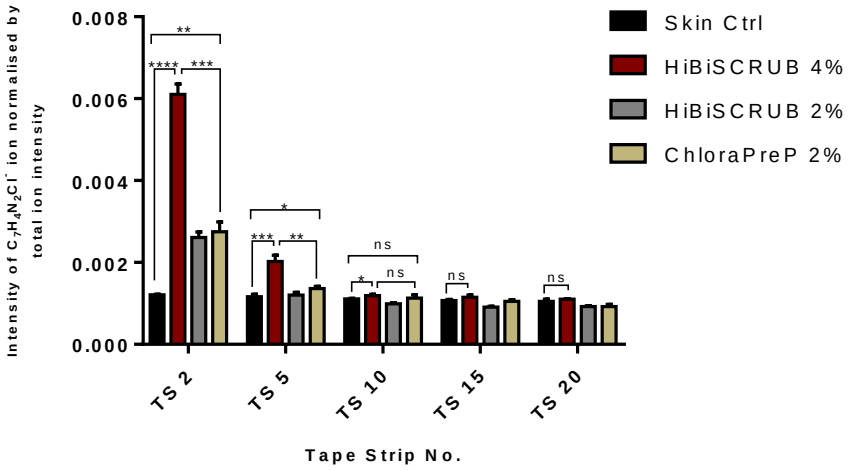

Figure 5.3: *Normalised ion intensity values of CHG marker ion in the 1st volunteer tape strips after a 2 minute application time of the three CHG products (HS 4%, HS 2% and CP 2%). Skin Ctrl represents the ion intensity obtained from the skin without any CHG products application. Data is presented as mean ± SD of n = 4 with p ≤ 0.05.*

This data indicates that more chlorhexidine has permeated into the *stratum corneum* from HS 4% than from CP 2% at TS 2 and 5 which may provide a better opportunity to eradicate more bacteria at this depth but at TS 10 there is no significant difference. In addition, there is a very limited amount (almost negligible) of CHG permeated from HS 4% at TS 15 and 20.

The determination of CHG concentration in the tape strips can be carried out by employing the calibration curve of CHG with skin homogenate (Chapter 2, Section 2.4.10), the calculated concentrations of CHG in HS 4% and CP 2% tape strips are reported in Table 5.2. This determination of CHG concentration at different tape strips is useful to compare with the minimum bactericidal concentration (MBC) of CHG required to eradicate the bacteria. This point will be discussed later after showing the data from all volunteers.

Table 5.2: *Determination of CHG concentration in HS 4% and CP 2% tape strips.*

Tape strip No.	Conc. of CHG (µg/mg) in HS 4% tape strips	Conc. of CHG (µg/mg) in CP 2% tape strips
TS 2	4.63	1.62
TS 5	0.95	0.34
TS 10	0.18	0.13

In addition to ion intensity data, ToF-SIMS secondary ion images can provide a detailed information regarding the spatial distribution of specified ions within skin by rastering the analysed area of the tape strip with an ion beam. ToF-SIMS secondary ion images of the tape strips removed from the 1st volunteer after the application of HS 4%, HS 2% and CP 2% products for 2 minutes are illustrated in Figures 5.4., 5.5 and 5.6 respectively.

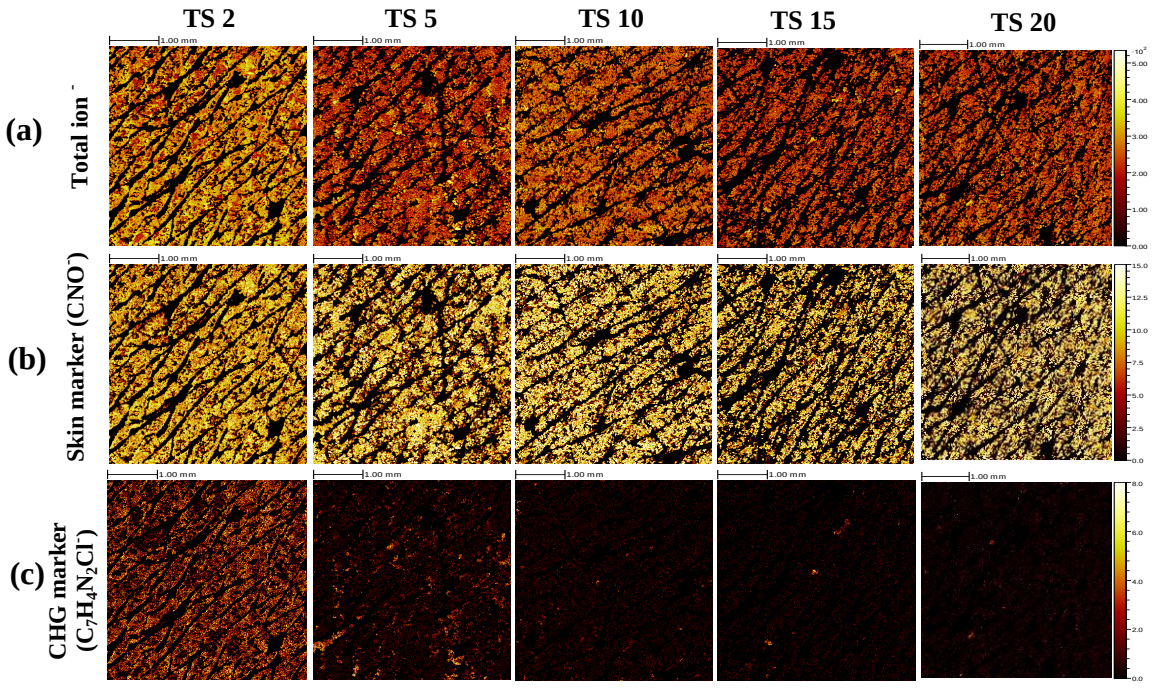

Figure 5.4: *ToF-SIMS ion images of tape strips removed from the 1st volunteer after a 2 minute application of HS 4% highlighting: (a) the total ion^{-} ,(b) the skin marker (CNO^{-}), and (c) the CHG marker ($C_7H_4N_2Cl^{-}$).*

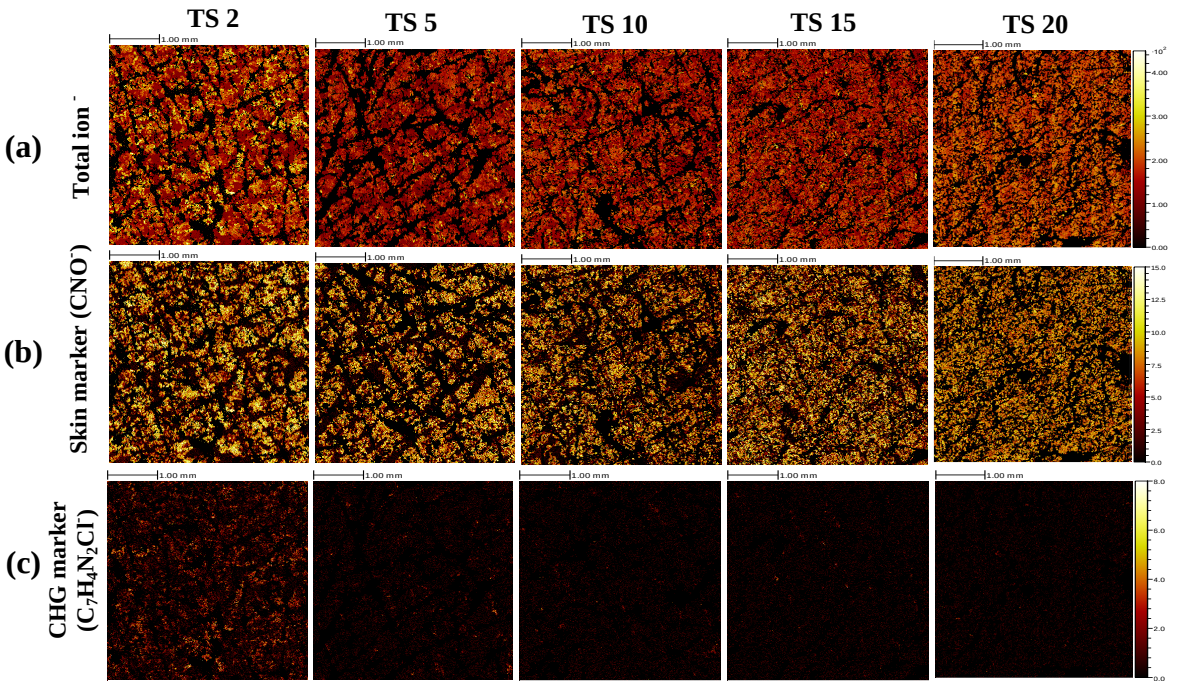

Figure 5.5: : *ToF-SIMS ion images of tape strips removed from the 1st volunteer after a 2 minute application of HS 2% highlighting: (a) the total ion- (b) the skin marker (CNO^-), and (c) the CHG marker ($C_7H_4N_2Cl^-$).*

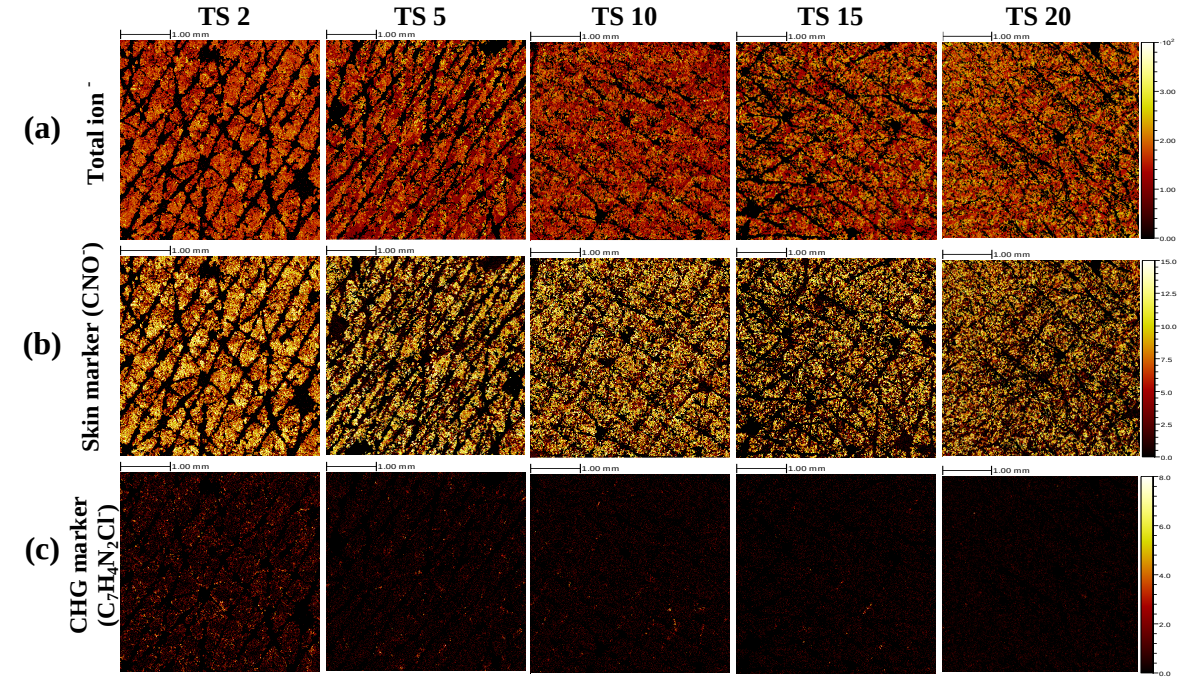

Figure 5.6: *ToF-SIMS ion images of tape strips removed from the 1st volunteer after 2 a minute application of CP 2% highlighting: (a) the total ion- ,(b) the skin marker (CNO^-), and (c) the CHG marker ($C_7H_4N_2Cl^-$).*

An examination of the skin marker (CNO^-) ion images from the different CHG products (Fig. 5.4b, Fig. 5.5b and Fig. 5.6b) demonstrates that the skin is adequately removed by the tape strips with a homogeneous distribution of the corneocytes throughout the tape stripped area. However, there is a reduction in the amount of skin attached per tape strip moving towards the deeper layers of the *stratum corneum*. This is as discussed earlier in Chapter 3, Section 3.4.1.3.3 due to the increased cohesion between the cells at the deeper *stratum corneum* layers compared to the outer layers [106, 116, 321]. Nonetheless, even at TS 20 there is still a relatively large amount of skin removed per strip.

An assessment of the CHG marker ion ($C_7H_4N_2Cl^-$) images (Fig. 5.4c, Fig. 5.5c and Fig. 5.6c) shows that the permeated CHG is decreased from the upper layer TS 2 towards the deeper layer of the *stratum corneum* TS 20. This reduction in the permeated amount of CHG represents the actual trend of the distribution profile of CHG within skin and not due to the reduction in skin amount per tape strip as the tape stripping process progresses deeper into the *stratum corneum* layers because the skin is still homogeneously covering the whole tape strips area (there are no large empty spaces within the tape strip area). In addition, the intensity of the fragment ion is normalised to the total ion intensity within the ROI (just the skin material within the tape strip) which accounts for the reduction of skin amount with increasing tape strip number. Regarding the homogeneity of the distribution of CHG within skin, the images of CHG marker ion (Fig. 5.4c, Fig. 5.5c and Fig. 5.6c) illustrate that CHG is distributed and localised non-uniformly within skin beyond TS 2 (patchy areas of CHG is recognised at TS 5, 10, 15 and 20). This may influence the ability of CHG to uniformly eradicate all the bacteria located beneath the skin surface.

The spatial distribution of CHG marker ion ($C_7H_4N_2Cl^-$) in the 1st volunteer tape strips from the three CHG products is illustrated in Figure 5.7. As shown previously in the data extracted from the ToF-SIMS spectra (Fig. 5.3), the examination of these ToF-SIMS ion images also clearly demonstrates that HS 4% shows higher ion intensity of CHG marker ion than either HS 2% or CP

2% at TS 2 and 5. The ion intensity at the deeper *stratum corneum* layers (TS 10, 15 and 20) is approximately similar from all products. In terms of the homogeneity of distribution, it is observed that CHG only shows a uniform distribution at TS 2 with a non-uniform distribution at the other tape strips.

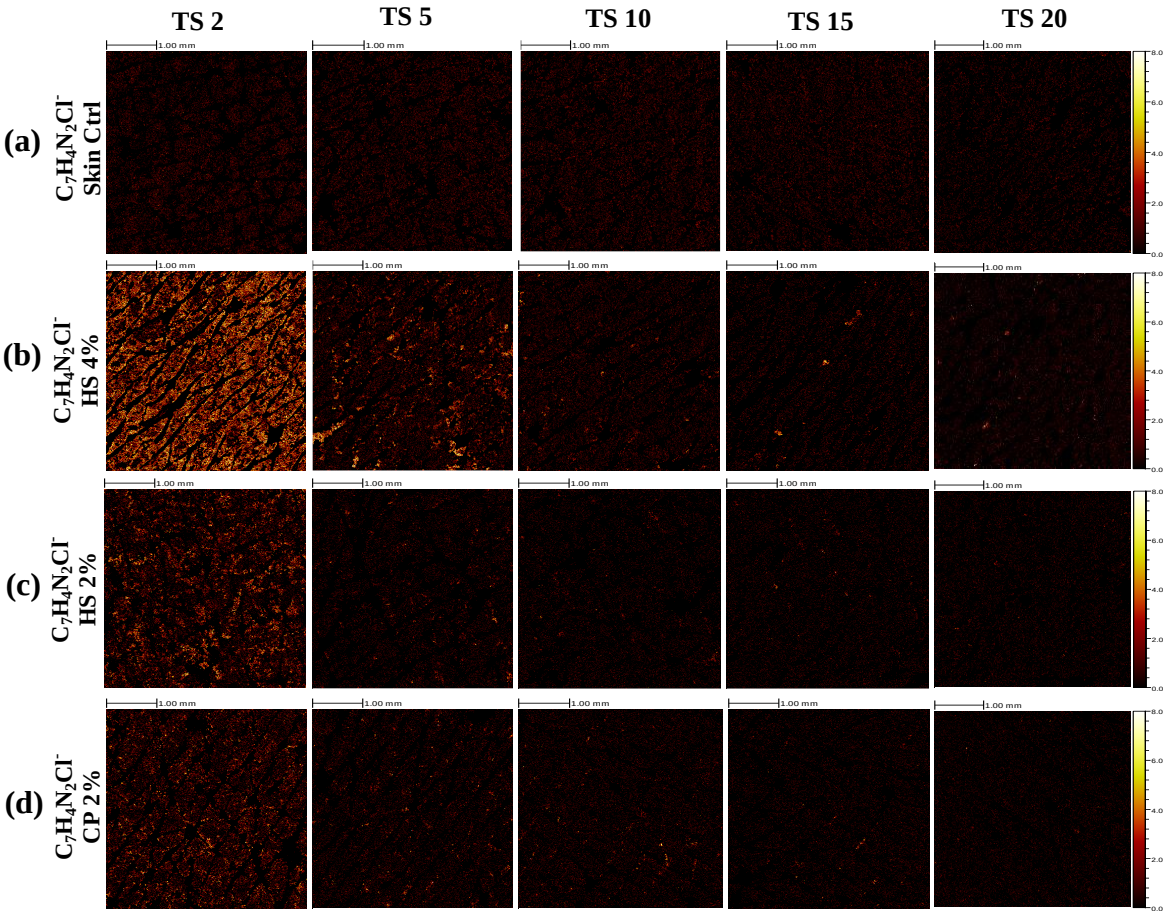

Figure 5.7: *ToF-SIMS ion images of the tape strips removed from the 1st volunteer highlighting the spatial distribution of CHG marker ion ($C_7H_4N_2Cl^-$) from (a) Skin Ctrl, (b) HS 4%, (c) HS 2%, and (d) CP 2%.*

These findings regarding the spatial distribution of the skin and CHG marker ions obtained from the tape strips of the 1st volunteer are also representative for the rest of volunteers. Therefore, only the data of the ion intensity of CHG marker ion from the different products will be presented here for the rest of volunteers. The ion intensity data for the full series of six *in vivo* analyses for CHG products treated volunteers is shown in Figure 5.8.

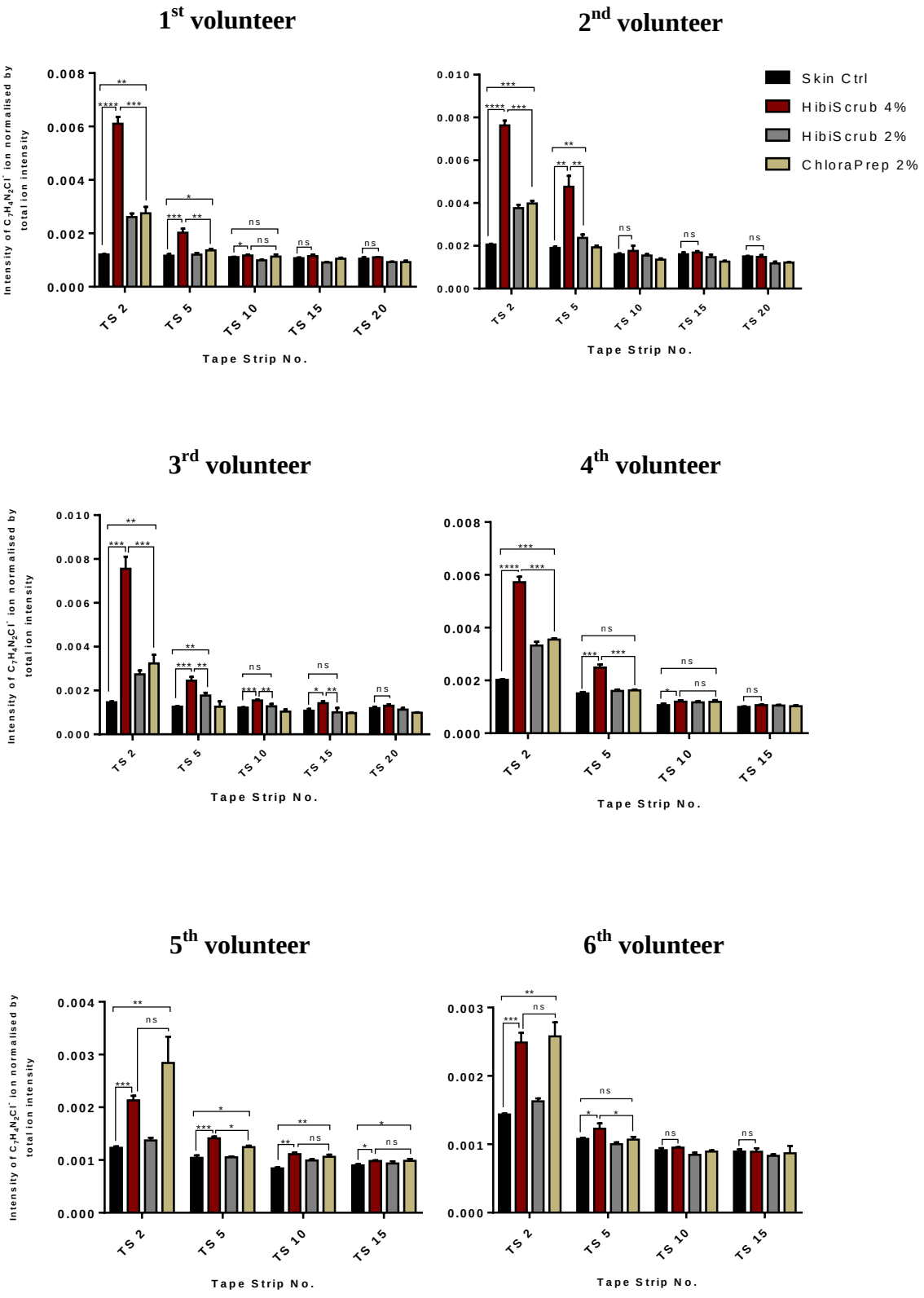

Figure 5.8: *A summary of the figures that show the comparison of the ion intensity of CHG marker ion ($C_7H_4N_2Cl^-$) in the six volunteers after a 2 minute application time of the three CHG products (HS 4%, HS 2% and CP 2%).*

As demonstrated in Figure 5.8, the overall results generally indicate that HS 4% delivers a greater amount of CHG into the *stratum corneum* layers than does either CP 2% or HS 2%. It is apparent that HS 4% at TS 2 shows a higher ion intensity of CHG marker ion ($C_7H_4N_2Cl^-$) with a significant increase from the skin control and CP 2% in four volunteers (1^{st}, 2^{nd}, 3^{rd} and 4^{th}). In the other two volunteers (5^{th} and 6^{th}) there is a non-significant difference between HS 4% and CP 2%. At TS 5, HS 4% shows a higher ion intensity with a significant increase from the skin control and the 2% CHG products (either HS 2% or CP 2%) in all volunteers. This higher ion intensity indicates that a greater concentration of CHG is available at a particular tape strip which is thought to be important to ensure that the CHG concentration exceeds the minimum bactericidal concentration (MBC) required to eradicate the bacteria. In addition, in the 4^{th} and 6^{th} volunteers, HS 4% shows to deliver CHG deeper at TS 5 than does CP 2% which in turn does not significantly differ from the skin control. This may provide an opportunity to efficiently kill more bacteria at the deeper *stratum corneum* layers.

It was found by previous studies that the minimum bactericidal concentration (MBC) of CHG required to eradicate the various types of bacteria commonly present in the skin is between 4 and 32 μg/mL under *in vitro* conditions [362-364]. According to the calibration curve of CHG generated by the microarray printing of CHG solutions with the skin homogenate (Chapter 2, Section 2.4.10), this MBC of CHG can approximately produce an ion intensity of 0.001 which is at or below the skin control ion intensity. Since both products HS 4% and CP 2% generally show an ion intensity that is significantly higher from the skin control which is in turn significantly higher from the MBC, it is thought that a microbiological experiment is required as a future work to substantiate if the more permeated concentration of CHG from HS 4% has the ability to kill more bacteria than CP 2% at a particular tape strip. At TS 10, the ion intensity obtained from HS 4% in most volunteers (1^{st}, 2^{nd}, 4^{th}, 5^{th} and 6^{th}) is either non-significantly different from the skin control or CP 2% ion intensities. At the deeper *stratum corneum* layers TS 15 and 20, HS 4% mostly shows a non-significant difference from the skin control. This indicates the limited

permeability of CHG into the deeper layers of the *stratum corneum.* This limited permeation may allow for the bacteria located at the deeper skin layers to survive and to cause local or systemic infections when the skin barrier is breached during surgery [77, 85].

5.4.2.2 Investigation of the vehicle effect

The vehicle effect on the skin permeation of CHG was investigated by comparing the *in vivo* skin permeation of HS 2% (a water based CHG treatment) and CP 2% (an IPA based CHG treatment) products in the six human volunteers using the same ToF-SIMS data obtained from the investigation of the concentration effect (Section 5.4.2.1). A summary of the data is shown in Figure 5.9 detailing the ion intensity of CHG marker ion in the six volunteers tape strips after a 2 minute application of both products. The statistical comparison is first carried out by comparing the ion intensity from either HS 2% or CP 2% (depending which one is showing higher ion intensity) to the ion intensity of the skin control and if it is significantly higher from it, the comparison is then accomplished between the two products.

In general, the results illustrated in Figure 5.9 show no superiority of one product over the other. In the 1st volunteer, there is a non-significant difference between the two products at TS 2 and 5. At TS 10, 15 and 20, the ion intensity from CP 2% and HS 2% is either equal or less than that of the skin control. The 2nd and 3rd volunteers show a non-significant difference between the two products at TS 2 but at TS 5, HS 2% demonstrates a higher ion intensity with a significant increase than CP 2%. The 4th volunteer shows a non-significant difference at the all tape strips. However, in the 5th and 6th volunteers CP 2% demonstrates a higher ion intensity with a significant increase than HS 2% at TS 2 and 5 (5th volunteer) and at TS 2 (6th volunteer). Therefore, the data obtained from the six volunteers does not clearly highlight the superiority of either HS 2% or CP 2% and generally it can be assumed that the type of the vehicle (water or IPA) which is used in the product formulation of HS 2% and

CP 2% respectively does not show a significant difference in the skin permeation of CHG.

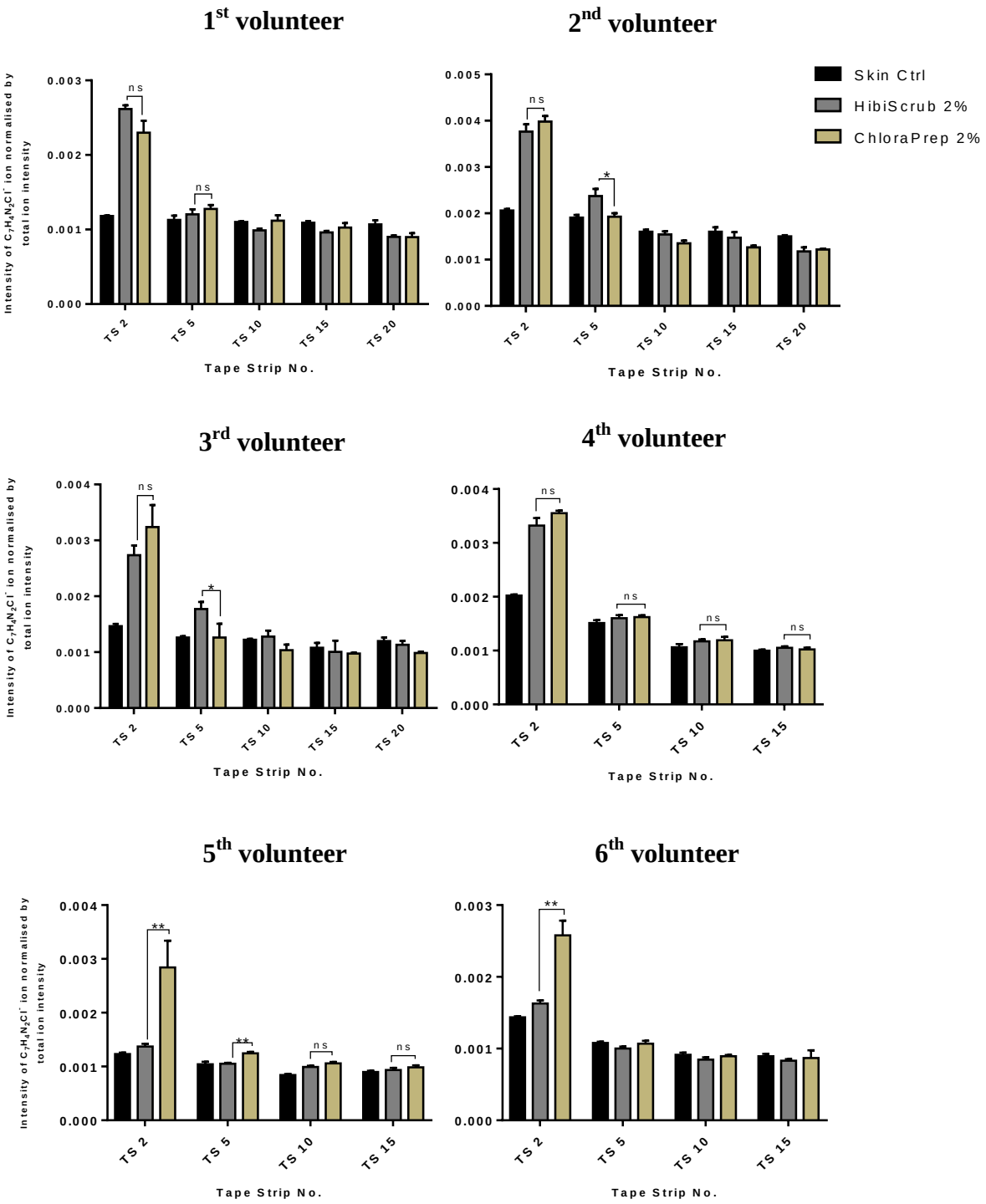

Figure 5.9: *A summary of the figures that show the comparison of the ion intensity of CHG marker ion ($C_7H_4N_2Cl^-$) in the six volunteers after a 2 minute application time of two CHG products HS 2% and CP 2%.*

Although, the Evidence-Based Practice in Infection Control (EPIC) guidelines recommends the use of 2% CHG in 70% IPA for skin antisepsis [78]. The data demonstrated in other studies show some contradiction regarding the superiority of aqueous or alcoholic CHG solutions. However, these studies are not comparative since they were performed using different approaches such as *in vitro* time-kill test, *ex vivo* permeation experiment or *in vivo* clinical study. Adams *et al.* showed that CP 2% has a greater efficacy than the 2% aqueous CHG solution when tested *in vitro* against *Staphylococcus epidermidis* using quantitative time-kill suspension and carrier tests [365]. This higher efficacy of CP 2% may be related to the rapid antimicrobial activity offered by the IPA as well [85].

In another study, Karpanen *et al.* compared the skin permeation of CHG from the 2% w/v aqueous and alcoholic CHG solutions using human skin mounted in Franz cells. They concluded that the concentration of the 2% CHG alcoholic solution recovered from the top 100 μm skin sections following a 2 minute application time was significantly less than that of the 2% CHG aqueous solution. Following 30 minutes application time, there was a non-significant difference between them [85]. Furthermore, one clinical study compared CP antimicrobial activity with 2% CHG aqueous solution in 106 healthy subjects using microbial counts of colony-forming units per square centimetre (CFU/cm^2) and it found that both products have demonstrated an equivalent immediate antimicrobial activity following 10 minute exposure [68]. Additionally, Valles *et al.* conducted a clinical study to compare the effectiveness of 2% aqueous CHG and 0.5% alcoholic solution for the prevention of catheter colonisation and they found that their activity is comparable [366]. The overall findings presented here in this section also highlight the no superiority of either HS 2% or CP 2% regarding CHG skin permeation.

5.4.2.3 Investigation of the application time effect

The influence of the product application time (2, 5, 10, 15, 30 and 60 minute) on the skin permeation of CHG in the six volunteers was also investigated. The rationale behind this investigation is to establish if the standard 2 minute application time of CHG products is optimal to allow an effective permeation of CHG into the deeper layers of the *stratum corneum*. Thus, longer application times are studied. In order to ensure the highest possibility of success the HS 4% which demonstrated the highest ion intensity (greater CHG permeation) in the study of the concentration effect (Section 5.4.2.1) was used in this study.

A summary of the data shows the comparison of the ion intensity of CHG marker ion at the different application times of HS 4% in the six volunteers, illustrated in Figure 5.10. In this study, the highest ion intensity value of CHG marker ion from the longer application times (in this case 5 and 10 minute) is compared to the 2 minute time ion intensity to determine if there is a significant difference between them. Since it is observed in the first three volunteers that there is a non-significant difference between the 2, 5 and 10 minutes ion intensities at TS 20 in addition to the very low ion intensity obtained at 60 minutes time interval, the tape stripping procedure is limited to 15 tape strips and an application time of 30 minutes in the remaining three volunteers.

As illustrated in Figure 5.10, the results for volunteers 1-4 generally show a non-significant difference in the ion intensity between the longer application times and 2 minutes and suggest no benefit of applying HS 4% for a longer period. However, volunteers 5 and 6 exhibit a different trend in that the ion intensity obtained from the 5 and 10 minute application time is higher than the 2 minute ion intensity with a significant difference at approximately all tape strips. The different results between the volunteers can be attributed to the inter-individual and inter-seasonal variations which can influence the permeation of CHG into the skin and the amount of the *stratum corneum* removed by the tape strips.

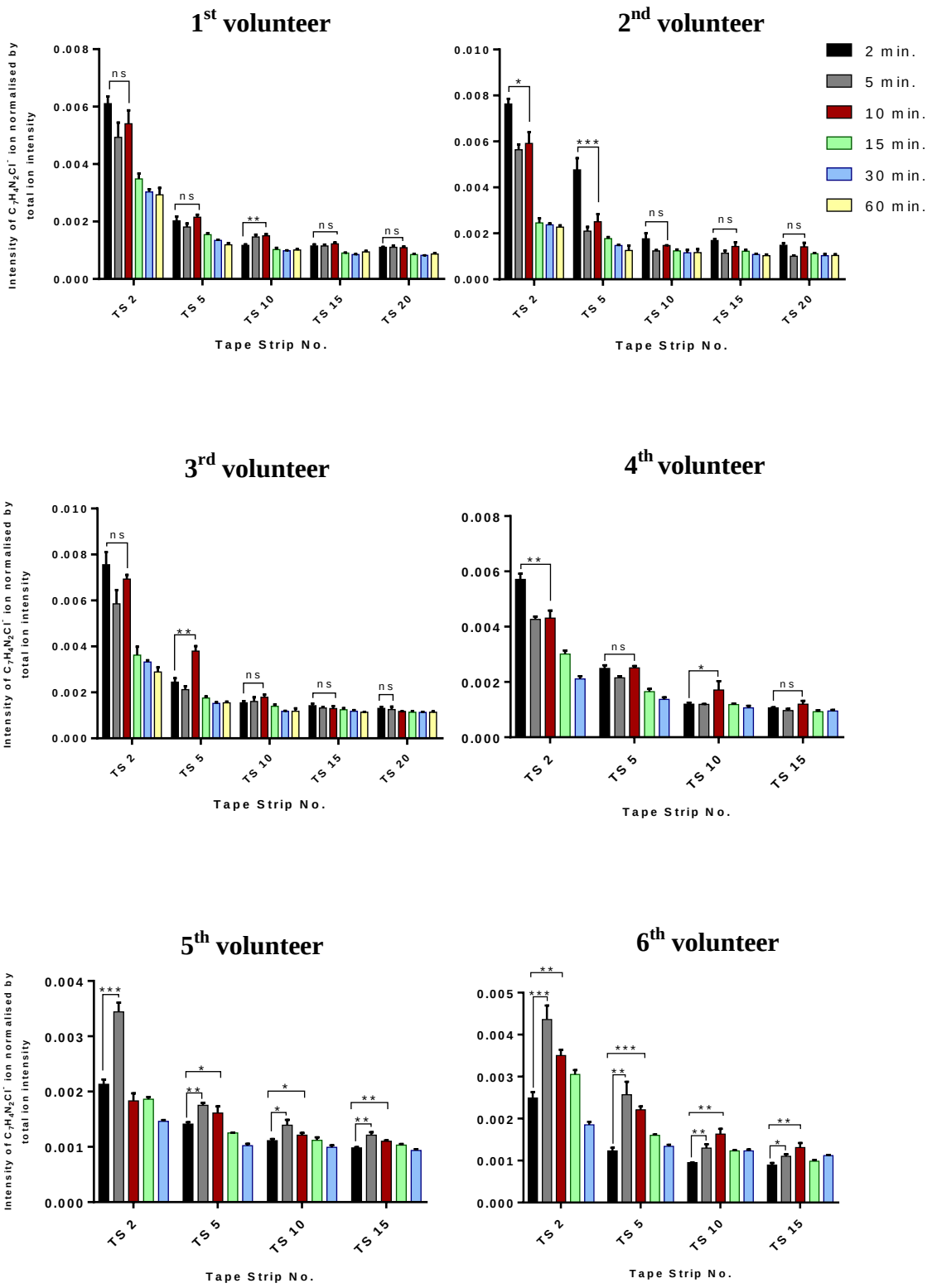

Figure 5.10: *A summary of the figures that show the comparison of the ion intensity of CHG marker ion ($C_7H_4N_2Cl^-$) at the different application times of HS 4% in the six volunteers.*

Furthermore, it is observed that at longer exposure times (15, 30 and 60 minutes), the ion intensity and hence the permeated CHG concentration is decreased with increasing application time throughout the different tape strips. This may be due to the evaporation and drying of the HS 4% solution over time, compromising the permeation of CHG into the skin. Karpanen *et al.* have demonstrated that the CHG concentration achieved within 100 μm skin sections following 30 minute application time is less than that following 2 minute (0.077 ± 0.015 μg/mg and 0.157 ± 0.047 μg/mg respectively) when they studied the permeation of CHG into *ex vivo* human skin using Franz cells [77]. The overall results indicate that there may be no advantage of increasing the application time of HS 4% to improve permeation of CHG into the *stratum corneum*.

The results presented here for the investigation of the concentration, vehicle and the application time effects on the skin permeation of CHG from different CHG products are preliminary and lay the foundation for further research in this area. A larger number of volunteers are required to be recruited to reduce the variability of the data and obtain more reliable results. In addition, to overcome the issue associated with the removal of variant amounts of the skin by the tape strips, it is more accurate to depend on the fraction of the *stratum corneum* removed by a tape strip rather than the tape strip number as discussed in Chapter 1, Section 1.5.1.2.

5.4.3 *Ex vivo* study

5.4.3.1 Investigation of the effect of CHG concentration

As in the *in vivo* study, the concentration effect on the skin permeation of CHG was investigated from the three CHG products (HS 4%, HS 2% and CP 2%) but in this case using *ex vivo* porcine skin mounted in Franz cells instead of the *in vivo* human volunteers. Comparison was carried out using the same technique of skin tape stripping with ToF-SIMS analysis. The ion intensity data of CHG marker ion ($C_7H_4N_2Cl^-$) in the 6 Franz cells after a 2 minute

application of the three CHG products (HS 4%, HS 2% and CP 2%) are illustrated in Figure 5.11.

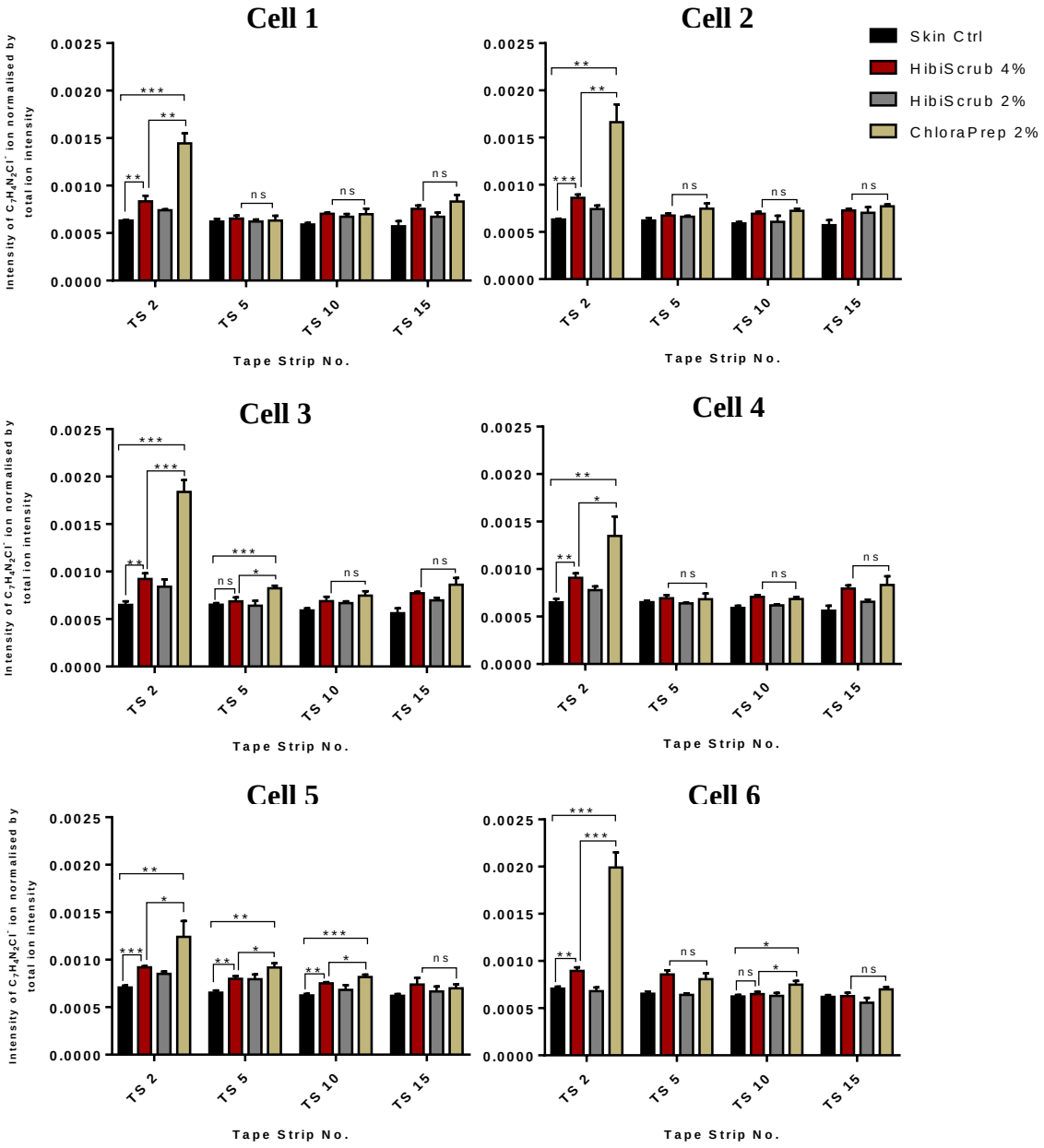

Figure 5.11: *A summary of the figures that show the comparison of the ion intensity of CHG marker ion in six Franz cells after a 2 minute application of the three CHG products (HS 4%, HS 2% and CP 2%) on porcine skin.*

As shown in Figure 5.11, CP 2% generally demonstrates a higher ion intensity than the skin control and HS 4% with a significant increase at TS 2 in all Franz cells. At the other tape strips there is mostly a non-significant difference between the two products. These results are in contrast to the *in vivo* results (Section 5.3.3.1) that showed the superiority of HS 4% over CP 2% in terms of CHG permeation. In addition, it is observed that the ion intensity of CHG marker ion obtained from the *ex vivo* data (maximum value 0.002) is less than that of the *in vivo* results.

The differences between the *ex vivo* and *in vivo* results (lack of correlation) can be attributed to the variation in the type of the skin used in the testing (excised pig ear skin versus viable *in vivo* human volar arm skin). Excretion of sweat, sebum and moisture on the skin surface represent *in vivo* physiological functions of the viable skin which is difficult to mimic in *in vitro* testing. It has been reported that the poor correlation in percutaneous permeation of compounds across species is because of the variations in skin thickness, in the composition of the *stratum corneum* lipids and in the number of hair follicles [367]. Netzlaff *et al*, have demonstrated that variations in the skin amount of free fatty acids and triglycerides as well as the number of hair shafts can cause differences in the skin barrier among species [368].

Although, porcine skin is quite similar to human skin [369, 370] and many compounds have shown a similar permeability in both with a correlation coefficient of 0.88, some dissimilarities are also exist between them [134]. Jung *et al.* demonstrated that for 25 compounds in 15 studies, there was a difference in the percutaneous permeability between pig and human skin. The degree of similarity varies with the compound chemical properties [134] i.e. permeant specific. The lack of correlation between *in vitro* and *in vivo* data for the skin permeation experiments of CHG products means that the *in vitro* data which is performed using porcine skin is not relevant or representative to reflect the actual permeation profile of CHG products on human volunteers. Extension of this finding of poor IVIV correlation of CHG to include

imiquimod's skin permeation data which was tested using porcine skin leads to the conclusion that imiquimod results will be poorly correlated to *in vivo* data. However, this may not be case for imiquimod because the IVIV correlation is greatly dependent on the chemical properties of the permeant; especially imiquimod has different chemical properties from CHG. The difference in skin permeability is compound specific and may vary from chemical to chemical [371]. Other factors that may lead to variation between *in vitro* and *in vivo* data are the daily application of multiple products on human skin including soaps, shower gels and hand creams in addition to the environmental conditions such as temperature and humidity that influence the permeability properties of the skin and may result in such differences.

It is believed that in order to achieve a reliable *in vitro in vivo* (IVIV) correlation for CHG, a new investigation using *ex vivo* human skin should be performed since it is considered the most reliable model for the *in vivo* human skin [129].

5.4.3.2 Investigation of the vehicle effect

The vehicle effect on the permeation of CHG into the porcine skin from HS 2% and CP 2% products was investigated using the same ToF-SIMS data obtained from the investigation of the concentration effect (Section 5.4.3.1). A summary of the data is shown in Figure 5.12 highlighting the ion intensity of CHG marker ion in the six Franz cells after a 2 minute application of HS 2% and CP 2%. CP 2% generally shows a higher ion intensity than the skin control and HS 2% with a significant increase at the most tape strips in the six Franz cells as illustrated in Figure 5.12. This means that CP 2% product and subsequently the vehicle IPA can deliver greater amount of CHG into the porcine skin. Again this result is dissimilar to the *in vivo* results (Section 5.4.2.2) that showed no superiority of one product over the other in terms of CHG permeation into the skin of human volunteers. The difference between the two results is probably related to the skin type used in the comparison study as previously discussed in the *ex vivo* investigation of the concentration effect (Section 5.4.3.1). The investigation of the application time effect in *ex vivo* porcine skin was omitted

because of the poor IVIV correlation obtained from the concentration and vehicle effects.

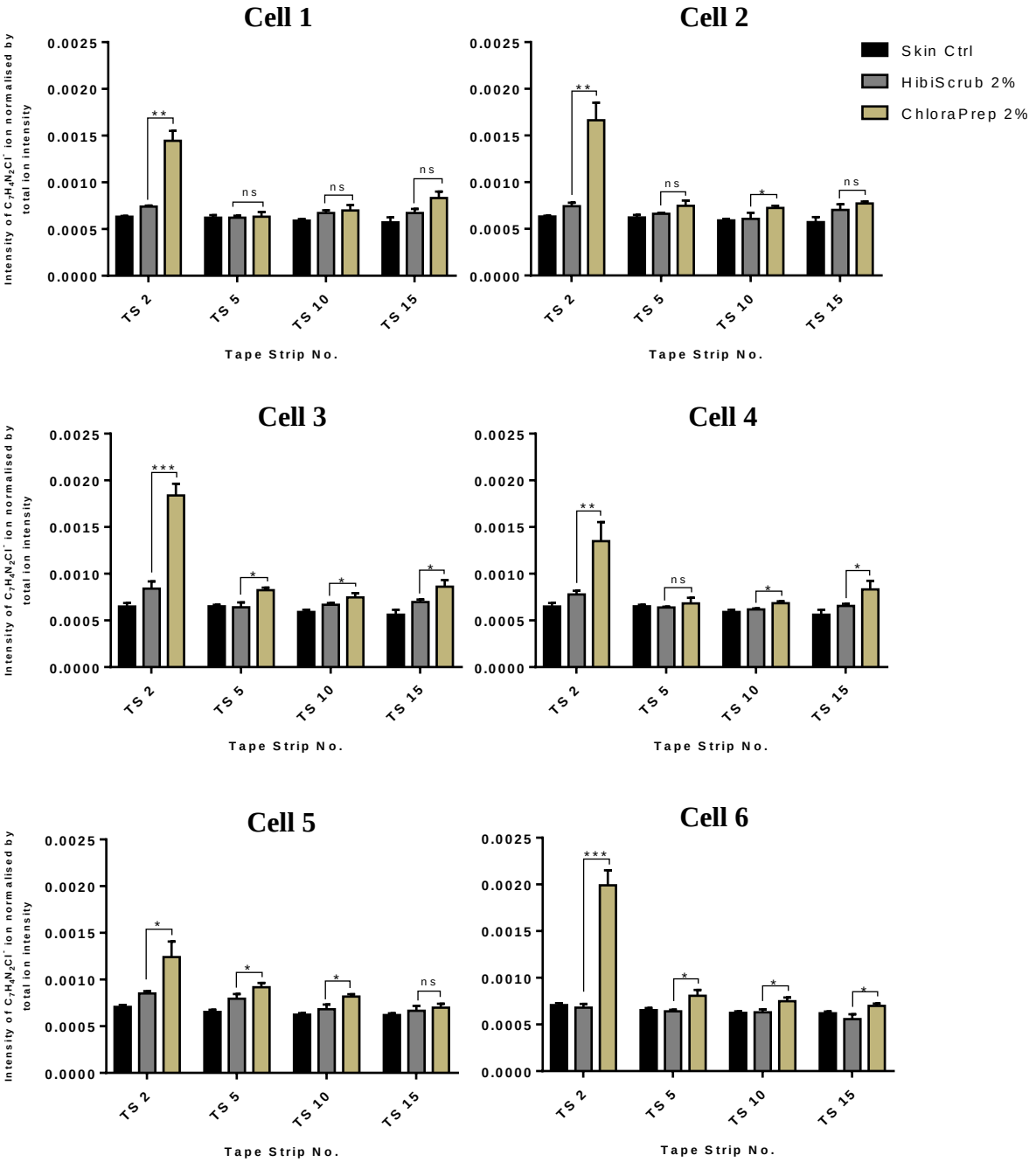

Figure 5.12: *A summary of the figures that show the comparison of the ion intensity of CHG marker ion ($C_7H_4N_2Cl^-$) in six Franz cells after a 2 minute application of HS 2% and CP 2% on porcine skin.*

5.5 Conclusions

The work in this chapter has exploited the high sensitivity of the ToF-SIMS to analyse individual tape strips removed from human volunteers to compare the skin permeation of CHG from commercial products currently used in hospitals within the UK for skin antisepsis before performing a surgery or catheter insertion. The comparison between the different products was carried out to investigate the influence of concentration, vehicle, and the application time on the skin permeation of CHG. An investigation of the concentration effect (2% and 4% w/v) in human volunteers after a 2 minute application of different products has shown that HS 4% produces a higher concentration of CHG in the upper *stratum corneum* (TS 2 and 5). However, at the deeper *stratum corneum* layers (TS 15 and 20) a very limited amount of CHG has been permeated. This finding of the limited permeation of CHG into the deeper *stratum corneum* layers achieved by the layer by layer analysis of the *stratum corneum* using ToF-SIMS confirms the already established knowledge of the limited permeation of CHG into the skin. Moreover, the ToF-SIMS secondary ion images have shown that CHG was distributed and localised non-uniformly within the skin beyond TS 2. This may affect the antiseptic activity of CHG to uniformly eradicate the bacteria located beneath the skin surface. The results from the investigation of the vehicle effect (water and IPA) on the skin permeation of CHG after a 2 minute application of HS 2% and CP 2% on the skin of human volunteers have not clearly shown the superiority of one product over the other in terms of the effect on CHG permeation. Additionally, investigating the effect of the different application times on the skin permeation of CHG from HS 4% in the human volunteers has demonstrated that no benefit of increasing the application time to achieve a greater permeation of CHG into the deeper *stratum corneum* layers. It is thought that an investigation on a larger number of volunteers is required to reduce the inter-individual variability and obtain more reliable data. In contrast to the *in vivo* results, *ex vivo* study using porcine skin has shown that a higher ion intensity of CHG is obtained from CP 2% rather than HS 4% at the upper *stratum corneum* layers (TS 2) with mostly a non-significant difference between the two products at the other tape strips. In addition, the investigation

of the vehicle effect, CP 2% has shown superiority over HS 2% in delivering CHG into the porcine skin *stratum corneum*. These differences between the *in vivo* and *ex vivo* results can be attributed to the difference in the skin type used in both studies. Therefore, it is believed that the use of *ex vivo* human skin may lead to an improvement in the IVIV correlation.

6 Chapter Six: General Conclusions and Future Work

6.1 General Conclusions

The assessment of drug permeation into/across the skin is traditionally performed using Franz diffusion cells with subsequent analysis of the different Franz cell elements by HPLC. Although, HPLC represents a quick, quantitative and versatile analysis method, it suffers from issues of low sensitivity and the requirement of an efficient sample extraction step with solvents prior to injection into the HPLC system. This increases the complexity of the method and the time needed for the analysis. Additionally, as the HPLC does not have any imaging capability, it is unable to identify the exact depth of permeation or provide information about the spatial distribution of a permeant within skin for the topically applied formulations.

ToF-SIMS offers numerous advantages of high sensitivity and chemical specificity that can be exploited for the analysis of biological samples without the need for fluorescent tags or radiolabels. However, to date there are only a small number of studies that utilise ToF-SIMS to explore drug permeation into the skin. Therefore, the 1st aim of this thesis was to investigate the potential complementary role of ToF-SIMS to map the permeation and visualise spatial distribution of imiquimod and chlorhexidine within skin with a quantification aspect.

ToF-SIMS is generally considered to provide semi-quantitative results due to matrix effects that influence the ionisation and secondary ion yield. The work in chapter 2 demonstrated the ability to manage the matrix effects and to quantify ToF-SIMS data using calibration curves generated by microarray printing of skin homogenate with drug solutions at different concentrations.

Skin homogenate represents the ideal matrix for this purpose due to its identity and relevance to real skin tissue. Therefore, a multi-step mechanical method was developed that is efficient in producing skin homogenate in an acceptable time limit and without introducing any chemicals that may interfere with the signal obtained from an analyte within skin when analysed by ToF-SIMS. In addition, the microarray printing approach provides a high throughput technique to generate and analyse many samples simultaneously. The homogeneity of the mixture of drug solutions with skin homogenate, the type of pin used and pin washing method have a great impact on the quality of the printed microarray and consequently on the generated calibration curve. Calibration curves of imiquimod and chlorhexidine were successfully generated with appropriate linearity, accuracy and precision and used in the subsequent chapters to determine their concentration in the test samples for example in the tape strips. Nevertheless, the quantification of ToF-SIMS data for imiquimod from the cross-sectioned skin samples was inapplicable as the ion intensity of imiquimod obtained from these samples was below the quantification limit of the calibration curve of imiquimod.

The novel approach of combining conventional and advanced analysis techniques to assess drug permeation into the skin was successfully shown in chapter 3. The work in this chapter provided complementary and detailed information regarding the permeated amounts of imiquimod, the permeation depth and the spatial distribution of imiquimod within skin. The HPLC and ToF-SIMS results highlighted the most detailed assessment yet of the permeation of imiquimod from Aldara™ cream. The results showed that imiquimod permeates into the *stratum corneum* but has limited permeation into the viable epidermis and dermis layers. These results are consistent with the FDA approval and clinical trials for the treatment of superficial BCC lesions. The imaging capabilities offered by ToF-SIMS provided a significant advantage over HPLC for visualising the spatial distribution of imiquimod in tape strips and cross-sectioned skin samples. The ToF-SIMS ion images of Aldara™ cream tape strips illustrated a non-uniform distribution of imiquimod within skin which may result in decreasing the efficacy of the cream to

uniformly treat whole BCC lesions giving rise to the likelihood of tumour recurrence. ToF-SIMS analysis of cross-sections obtained from the permeation study of penetration enhancers DMSO and oleic acid showed that the existence of imiquimod is primarily at the *stratum corneum* layer. Indeed, penetration enhancers (DMSO and oleic acid) have not improved the permeation of imiquimod into the deeper skin layers and other strategies are needed to enhance delivery of imiquimod. The complementary approach of analysis using conventional and advanced techniques may assist to improve the design of more effective formulations of imiquimod in the future to treat BCC lesions. Additionally, this approach was successfully utilised in chapter 4 to demonstrate if there was an enhancement of imiquimod permeation into the skin following microemulsions and microneedles application.

Furthermore, the high sensitivity offered by ToF-SIMS elucidated in unprecedented way the *in vivo* and *ex vivo* comparison of chlorhexidine permeation into the *stratum corneum* from commercial products (HS 4%, HS 2% and CP 2% w/v) by the analysis of individual tape strips removed from human volunteers or porcine skin. This work demonstrated the successful application of ToF-SIMS to monitor drug permeation into the *stratum corneum* and highlighted the potential of providing detailed information that cannot be obtained by conventional analysis methods. The comparison between the different products was carried out to investigate the influence of concentration, vehicle, and the application time on the skin permeation of CHG. An investigation of the concentration effect (2% and 4% w/v) in human volunteers after a 2 minute application has shown that HS 4% produces a higher concentration of CHG in the upper *stratum corneum* (TS 2 and 5). However, at the deeper *stratum corneum* layers (TS 15 and 20) a very limited amount of CHG has been permeated. Moreover, the ToF-SIMS secondary ion images have shown that CHG was distributed and localised non-uniformly within the skin beyond TS 2. This may influence the antiseptic activity of CHG to uniformly eradicate the bacteria located beneath the skin surface. The results from the investigation of the vehicle effect (water and IPA) on the skin permeation of CHG after a 2 minute application on the skin of human

volunteers have not clearly shown the superiority of one product over the other in terms of the effect on CHG permeation. Additionally, investigating the effect of the different application times on the skin permeation of CHG from HS 4% in the human volunteers has demonstrated that no benefit of increasing the application time to achieve a greater permeation of CHG into the deeper *stratum corneum* layers. In contrast to the *in vivo* results, *ex vivo* study using porcine skin has shown that a higher ion intensity of CHG is obtained from CP 2% than other products. These differences between the *in vivo* and *ex vivo* results can be attributed to the difference in the skin type used in both studies. Therefore, it is believed that the use of *ex vivo* human skin may lead to an improvement in the IVIV correlation.

As other studies have reported that Aldara™ cream has some limitations in the treatment of nodular BCC lesions due to the cream's inability to deliver imiquimod into the deeper more invasive nodular lesions, the 2nd aim of this thesis was to enhance imiquimod permeation into the skin to overcome these limitations. Therefore, an attempt to improve delivery of imiquimod into the viable epidermis layers of porcine skin using microemulsions and microneedles was investigated. Imiquimod microemulsions were formulated, characterised and then tested for skin permeation enhancement. However, the assessment of imiquimod permeation from the formulated microemulsions alone and with microneedle pre-treatment using HPLC and ToF-SIMS demonstrated a limited ability of the microemulsions to improve delivery of imiquimod over Aldara™ cream. This was attributed to the poor release of imiquimod from the microemulsion formulas due to the high affinity of imiquimod for the oil phase and the encapsulation of the oil droplets by the S/Co-S mixture. The *en face* light microscope images of the microneedle treated skin samples demonstrated the penetration efficiency and reproducibility of the stamp pen to disrupt the skin barrier by forming pores through which the penetration of the dyes (gentian violet and methylene blue) was facilitated. In addition, the histological examination of the microneedle treated skin samples (unstained and stained samples) proved the ability of the stamp pen to create microchannels through the skin reach the depth of papillary dermis layer. In contrast to

microemulsions, Aldara™ cream with microneedle pre-treatment using derma stamp electric pen showed improved delivery of imiquimod into the skin. The recovery percentage of imiquimod in tape strips and remaining skin determined by HPLC was approximately three times higher than samples without microneedle pre-treatment. In addition, the ToF-SIMS ion images of the cross-sectioned skin samples illustrated the existence of imiquimod in the microchannels and in the epidermal layer at a higher ion intensity compared to Aldara™ cream alone. This greater permeation of imiquimod into the epidermal layer may provide the opportunity for more efficient treatment of BCC lesions.

6.2 Future Work and Recommendations

The majority of the work in this study is the first of its kind and lays the foundation for further application of these approaches to assess the permeation into and across the skin following the administration of topical or transdermal formulations. However, there are some amendments and recommendations that can be carried out to further improve the quality of data and expand the scope of information gained.

For the quantification of ToF-SIMS data, this work demonstrated the ability to manage the matrix effects and to quantify ToF-SIMS data by generation of a calibration curve of a drug in skin homogenate using a high throughput method of microarray printing. Skin homogenate represents a similar chemical environment for the tested samples and therefore it can be used to assess the ionisation efficiency of drug molecules permeated into the skin. However, this skin homogenate consists of the different skin layers (*stratum corneum*, viable epidermis and dermis) which vary in the composition of their constituents such as the difference in the type of lipids in each layer. For example, phospholipids are absent in the *stratum corneum* layer but present in the viable epidermis. Thus, the presence of phospholipids may influence the ionisation of drugs to some extent and subsequently affect the calibration curve used in the quantification of a drug concentration in the tape strips containing only the removed *stratum corneum* layer. Therefore, it is thought that the extraction of

the *stratum corneum* layer from the other skin layers and its use as skin matrix to generate a calibration curve may be more relevant to the tested tape strips samples and can results in more accurate determination of a drug concentration. In addition, it is more relevant to make the correlation between the calibration curve and the tested samples using the same type of skin. For example, in the determination of CHG concentration in the tape strips removed from human volunteers, the comparison was made with a calibration curve using skin homogenate of porcine skin. Therefore, it is believed that the use of human skin to make the skin homogenate to generate the calibration curve will be more pertinent to the tested samples. Another point is to investigate the physical and chemical uniformity of the printed microarray spots using optical profilometry and ToF-SIMS depth profiling through the spots. Another recommendation regarding the microarray printing process is to use a solid pin manufactured by a specialised company and not by a small workshop to ensure the appropriate design of the pin tip which has a great influence on the quality and consistency of printing. This may further improve the printing outcome.

The assessment of imiquimod permeation into porcine skin from Aldara™ cream has provided previously unobserved insights into the permeation depth and the spatial distribution of imiquimod within skin. However, this assessment was carried out using porcine skin. This can only provide an initial idea or prediction about the delivery in living humans. Therefore, to obtain more relevant information it is recommended to assess the permeation of imiquimod using *ex vivo* human skin followed by *in vivo* experiments. In addition, imiquimod has demonstrated a non-uniform distribution within skin which may decrease the efficiency of Aldara™ cream to uniformly treat whole BCC lesions. Therefore, an investigation is required to explore the reason behind this non-uniform distribution which may be related to the existence of a particular constituent such as fatty acids that facilitated the permeation of imiquimod into the skin. i.e. further investigation is needed to elucidate the mechanism or the pathway of imiquimod skin permeation. One area for future work would be to develop a method to conduct the depth profiling through skin tissue using dynamic SIMS to investigate the permeation depth of imiquimod. This

provides an opportunity to map imiquimod permeation into skin without the need to perform a skin cross-sectioning. However, this requires the development of a method to monitor the sputter rate. In addition, the analysis area in this case is limited only to a small area of 200 μm.

The enhancement of imiquimod permeation into the skin using microemulsions and microneedles is thought to be useful to overcome some of the limitations associated with the topical treatment of BCC lesions by Aldara™ cream. However, the formulation of o/w microemulsions of imiquimod was unable to improve the delivery of imiquimod either alone or with microneedle pre-treatment. It is possible that the high affinity of imiquimod for oleic acid and the encapsulation of oleic acid droplets by S/Co-S mixture result in retaining imiquimod within oleic acid droplets. This reduced the ability to partition out that leads to the poor release and transfer of imiquimod from microemulsions to the skin. It is believed that an optimisation of the microemulsions formulation is required as a future work, perhaps focusing on areas such as changing the type of oil used to one in which imiquimod is only moderately soluble to facilitate its release to the skin. e.g. isostearic acid. On the other hand, the application of the stamp pen in conjugation with Aldara™ cream has shown promising results regarding the enhancement of imiquimod permeation into porcine skin. Therefore, it is recommended that the next step would be to repeat these series of experiments using *ex vivo* human skin. Further to this, clinical trials could be carried out to test this treatment method on patients suffering from BCC lesions to optimise the final application conditions. The 'poke and patch' concept (i.e. two-step process) used in the application of the solid microneedles may decrease patient compliance and the adherence to the treatment. Thus, the use of coated or dissolving microneedles with imiquimod at the tip of the needles or within the dissolved needles can address the issue of the two-step application and consequently increase patient compliance.

The *in vivo* comparison between the different commercial products of CHG used in skin antisepsis showed new insights into the depth and the spatial

distribution of CHG within skin as well as providing the foundation for the potential application of ToF-SIMS to assess the bioequivalence of topical products. However, this study has investigated the permeation of CHG from these products on only 6 volunteers and analysed 4-5 strips from each product. Therefore, a larger number of volunteers can be recruited in this study with the analysis of the whole set of the removed strips to reduce the variability of the results and obtain more detailed information regarding the permeation behaviour. The results demonstrated that CHG permeates at higher concentration from HS 4% than CP 2% at TS 2 and 5. However, the permeated concentration from both products HS 4% and CP 2% is significantly higher from the minimum bactericidal concentration (MBC) of CHG. Therefore, it is thought that a microbiological experiment is required to substantiate if the more permeated concentration of CHG from HS 4% has the ability to kill more bacteria than CP 2% at a particular tape strip. Additionally, it is more accurate to depend on the fraction of the *stratum corneum* removed by a tape strip rather than the tape strip number to overcome the issue associated with the removal of variant amounts of the skin by the tape strips. The *ex vivo* permeation comparison between the different CHG products has shown a poor correlation with the *in vivo* study. Therefore, it is recommended that the use human skin instead of porcine skin may have a tendency to improve the IVIV correlation.

7 References

[1] A. C. Williams, "Topical and Transdermal Drug Delivery," in *Aulton's Pharmaceutics: The Design and Manufacture of Medicines*, M. E. Aulton and K. M. G. Taylor, Eds., Fourth ed Edinburgh: Churchill Livingstone Elsevier, 2013, pp. 675-697.

[2] P. M. Elias and E. H. Choi, "Interactions among stratum corneum defensive functions," *Experimental Dermatology*, vol. 14, pp. 719-726, 2005.

[3] H. A. E. Benson, "Skin Structure, Function, and Permeation," in *Topical and Transdermal Drug Delivery: Principles and Practice*, H. A. E. Benson and A. C. Watkinson, Eds., First ed New Jersey: John Wiley & Sons, 2012, pp. 3-22.

[4] A. C. Williams, *Transdermal and Topical Drug Delivery Form Theory to Clinical Practice*, First ed. London: Pharmaceutical Press, 2003.

[5] A. Haake, G. A. Scott, and K. A. Holbrook, "Structure and function of the skin: overveiw of the epidermis and dermis," in *The Biology Of The Skin*, R. K. Freinkel and D. T. Woodley, Eds., ed New York: The Parthenon Publishing Group, 2001, pp. 19-45.

[6] S. M. Roberts and A. K. Walters, "The relationship between structure and barrier function of skin," in *Dermal Absorption and Toxicity Assessment*, S. M. Roberts and A. K. Walters, Eds., ed New York: Marcel Dekker, 1998, pp. 1-42.

[7] E. Fuchs, "Epidermal differentiation: the bare essentials," *The Journal of cell biology*, vol. 111, pp. 2807-2814, 1990.

[8] P. Kaur and A. Li, "Adhesive properties of human basal epidermal cells: an analysis of keratinocyte stem cells, transit amplifying cells, and postmitotic differentiating cells," *Journal of Investigative Dermatology*, vol. 114, pp. 413-420, 2000.

[9] L. Lajtha, "Stem cell concepts," *Differentiation*, vol. 14, pp. 23-33, 1979.

[10] R. Darlenski, J. Kazandjieva, and N. Tsankov, "Skin barrier function: morphological basis and regulatory mechanisms," *J. Clin. Med*, vol. 4, pp. 36-45, 2011.

[11] P. J. Caspers, G. W. Lucassen, E. A. Carter, H. A. Bruining, and G. J. Puppels, "In vivo confocal Raman microspectroscopy of the skin: noninvasive determination of molecular concentration profiles," *Journal of Investigative Dermatology*, vol. 116, pp. 434-442, 2001.

[12] P. Caspers, G. Lucassen, and G. Puppels, "Combined in vivo confocal Raman spectroscopy and confocal microscopy of human skin," *Biophysical journal*, vol. 85, pp. 572-580, 2003.

[13] R. A. Clark, K. Ghosh, and M. G. Tonnesen, "Tissue engineering for cutaneous wounds," *Journal of Investigative Dermatology*, vol. 127, pp. 1018-1029, 2007.

[14] R. J. Scheuplein and I. H. Blank, "Permeability of the skin," *Physiol Rev*, vol. 51, pp. 702-747, 1971.

[15] K. R. Feingold, "Thematic review series: skin lipids. The role of epidermal lipids in cutaneous permeability barrier homeostasis," *Journal of lipid research*, vol. 48, pp. 2531-2546, 2007.

[16] D. T. Downing, "Lipid and protein structures in the permeability barrier of mammalian epidermis," *Journal of lipid research*, vol. 33, pp. 301-313, 1992.
[17] P. M. Elias, "Epidermal lipids, barrier function, and desquamation," *Journal of Investigative Dermatology*, vol. 80, pp. 44-49, 1983.
[18] D. Beeckman, J. Campbell, K. Campbell, D. Denise Chimentão, R. Domansky, M. Gray, *et al.*, "Incontinence-associated dermatitis: moving prevention forward," *Wounds International*, 2015.
[19] G. W. Lu and G. L. Flynn, "Cutaneous and Transdermal Delivery─Processes and Systems of Delivery," in *Modern Pharmaceutics: Applications and Advances*, A. T. Florence and J. Siepmann, Eds., Fifth ed New York: Informa Healthcare, 2009, pp. 43-99.
[20] A. Rawlings and C. Harding, "Moisturization and skin barrier function," *Dermatologic therapy*, vol. 17, pp. 43-48, 2004.
[21] W. Montagna and P. F. Parakkal, *The Structure and Function of Skin*, Third ed. New york: Academic Press Inc., 1974.
[22] V. J. Hearing, "Biochemical control of melanogenesis and melanosomal organization," *Journal of Investigative Dermatology Symposium Proceedings*, vol. 4, pp. 24-28, 1999.
[23] M. Merad, M. G. Manz, H. Karsunky, A. Wagers, W. Peters, I. Charo, *et al.*, "Langerhans cells renew in the skin throughout life under steady-state conditions," *Nature Immunology*, vol. 3, pp. 1135-1141, 2002.
[24] T. Tachibana and T. Nawa, "Recent progress in studies on Merkel cell biology," *Anatomical science international*, vol. 77, pp. 26-33, 2002.
[25] T. P. Banning and C. M. Heard, "Binding of doxycycline to keratin, melanin and human epidermal tissue," *International Journal of Pharmaceutics*, vol. 235, pp. 219-227, 2002.
[26] B. Barry, "Mode of action of penetration enhancers in human skin," *Journal of Controlled Release*, vol. 6, pp. 85-97, 1987.
[27] M. A. Bolzinger, S. Briançon, J. Pelletier, and Y. Chevalier, "Penetration of drugs through skin, a complex rate-controlling membrane," *Current Opinion in Colloid & Interface Science*, vol. 17, pp. 156-165, 2012.
[28] V. V. Venuganti and O. P. Perumal, "Nanosystems for Dermal and Transdermal Drug Delivery," in *Drug Delivery: Nanoparticles Formulation and Characterization*, Y. Pathak and D. Thassu, Eds., First ed New York: Informa Healthcare, 2009, pp. 126-155.
[29] J. Hadgraft and W. J. Pugh, "The selection and design of topical and transdermal agents: a review," *Journal of Investigative Dermatology Symposium Proceedings*, vol. 3, pp. 131-135, 1998.
[30] N. Otberg, A. Patzelt, U. Rasulev, T. Hagemeister, M. Linscheid, R. Sinkgraven, *et al.*, "The role of hair follicles in the percutaneous absorption of caffeine," *British Journal of Clinical Pharmacology*, vol. 65, pp. 488-492, 2008.
[31] U. Blume-Peytavi, L. Massoudy, A. Patzelt, J. Lademann, E. Dietz, U. Rasulev, *et al.*, "Follicular and percutaneous penetration pathways of topically applied minoxidil foam," *European Journal of Pharmaceutics and Biopharmaceutics*, vol. 76, pp. 450-453, 2010.

[32] M. Tabbakhian, N. Tavakoli, M. R. Jaafari, and S. Daneshamouz, "Enhancement of follicular delivery of finasteride by liposomes and niosomes 1. In vitro permeation and in vivo deposition studies using hamster flank and ear models," *International Journal of Pharmaceutics*, vol. 323, pp. 1-10, 2006.

[33] H. Wosicka and K. Cal, "Targeting to the hair follicles: current status and potential," *J Dermatol Sci*, vol. 57, pp. 83-9, 2010.

[34] W. Craane-Van-Hinsberg, J. Coos Verhoef, L. J. Bax, H. E. Junginger, and H. E. Bodde, "Role of appendages in skin resistance and iontophoretic peptide flux: Human versus snake skin," *Pharmaceutical Research (New York)*, vol. 12, pp. 1506-1512, 1995.

[35] J. Lademann, H. Richter, M. C. Meinke, B. Lange-Asschenfeldt, C. Antoniou, W. C. Mak, *et al.*, "Drug delivery with topically applied nanoparticles: science fiction or reality," *Skin Pharmacol Physiol*, vol. 26, pp. 227-33, 2013.

[36] M. Roberts, W. Pugh, J. Hadgraft, and A. Watkinson, "Epidermal permeability-penetrant structure relationships: 1. An analysis of methods of predicting penetration of monofunctional solutes from aqueous solutions," *International journal of pharmaceutics*, vol. 126, pp. 219-233, 1995.

[37] J. D. Bos and M. M. Meinardi, "The 500 Dalton rule for the skin penetration of chemical compounds and drugs," *Experimental dermatology*, vol. 9, pp. 165-169, 2000.

[38] O. Pillai and R. Panchagnula, "Transdermal delivery of insulin from poloxamer gel: ex vivo and in vivo skin permeation studies in rat using iontophoresis and chemical enhancers," *Journal of controlled release*, vol. 89, pp. 127-140, 2003.

[39] Y. K. Song and C. K. Kim, "Topical delivery of low molecular weight heparin with surface charged flexible liposomes," *Biomaterials*, vol. 27, pp. 271-280, 2006.

[40] A. Naik, Y. N. Kalia, and R. H. Guy, "Transdermal drug delivery: overcoming the skin's barrier function," *Pharmaceutical science & technology today*, vol. 3, pp. 318-326, 2000.

[41] W. J. Pugh, "Relationship between H-bonding of penetrants to stratum corneum lipids and diffusion," *Drugs and the pharmaceutical sciences*, vol. 97, pp. 177-192, 1999.

[42] J. du Plessis, W. J. Pugh, A. Judefeind, and J. Hadgraft, "Physico-chemical determinants of dermal drug delivery: effects of the number and substitution pattern of polar groups," *European journal of pharmaceutical sciences*, vol. 16, pp. 107-112, 2002.

[43] M. Roberts, W. Pugh, and J. Hadgraft, "Epidermal permeability: penetrant structure relationships. 2. The effect of H-bonding groups in penetrants on their diffusion through the stratum corneum," *International journal of pharmaceutics*, vol. 132, pp. 23-32, 1996.

[44] T. Diepgen and V. Mahler, "The epidemiology of skin cancer," *British Journal of Dermatology*, vol. 146, pp. 1-6, 2002.

[45] S. F. Taveira and R. F. Lopez, "Topical administration of anticancer drugs for skin cancer treatment," in *Skin Cancers-Risk Factors, Prevention and Therapy*, C. L. Porta, Ed., ed: http://www.intechopen.com, 2011.

[46] M. Alam, L. H. Goldberg, S. Silapunt, E. S. Gardner, S. S. Strom, A. W. Rademaker, *et al.*, "Delayed treatment and continued growth of nonmelanoma skin cancer," *Journal of the American Academy of Dermatology,* vol. 64, pp. 839-848, 2011.
[47] V. Madan, J. T. Lear, and R. Szeimies, "Non-melanoma skin cancer," *The Lancet,* vol. 375, pp. 673-685, 2010.
[48] K. McKay, B. Sambrano, P. Fox, R. Bassett, S. Chon, and V. Prieto, "Thickness of superficial basal cell carcinoma (sBCC) predicts imiquimod efficacy: a proposal for a thickness-based definition of sBCC," *British Journal of Dermatology,* vol. 169, pp. 549-554, 2013.
[49] N. R. Telfer, G. B. Colver, and C. A. Morton, "Guidelines for the management of basal cell carcinoma," *Br J Dermatol,* vol. 159, pp. 35-48, 2008.
[50] J. Rippey, "Why classify basal cell carcinomas," *Histopathology,* vol. 32, pp. 393-398, 1998.
[51] J. T. Lear, "Evidence-based treatment for low-risk basal cell carcinoma," *The lancet oncology,* vol. 15, p. 12, 2014.
[52] A. I. Rubin, E. H. Chen, and D. Ratner, "Basal-cell carcinoma," *New England Journal of Medicine,* vol. 353, pp. 2262-2269, 2005.
[53] L. A. Skelton, "The effective treatment of basal cell carcinoma," *British Journal of Nursing,* vol. 18, p. 346, 2009.
[54] K. Peris, E. Campione, T. Micantonio, G. Clare Marulli, M. Concetta Fargnoli, and S. Chimenti, "Imiquimod Treatment of Superficial and Nodular Basal Cell Carcinoma: 12-Week Open-Label Trial," *Dermatologic surgery,* vol. 31, pp. 318-323, 2005.
[55] F. Lacarrubba, M. R. Nasca, and G. Micali, "Advances in the use of topical imiquimod to treat dermatologic disorders," *Therapeutics and clinical risk management,* vol. 4, p. 87, 2008.
[56] F. Bath-Hextall, M. Ozolins, S. J. Armstrong, G. B. Colver, W. Perkins, P. S. J. Miller, *et al.*, "Surgical excision versus imiquimod 5% cream for nodular and superficial basal-cell carcinoma (SINS): a multicentre, non-inferiority, randomised controlled trial," *The Lancet Oncology,* vol. 15, pp. 96-105, 2014.
[57] A. H. M. Arits, K. Mosterd, B. A. B. Essers, E. Spoorenberg, A. Sommer, M. J. M. De Rooij, *et al.*, "Photodynamic therapy versus topical imiquimod versus topical fluorouracil for treatment of superficial basal-cell carcinoma: a single blind, non-inferiority, randomised controlled trial," *The Lancet Oncology,* vol. 14, pp. 647-654, 2013.
[58] A. J. Wagstaff and C. M. Perry, "Topical Imiquimod," *Drugs,* vol. 67, pp. 2187-2210, 2007.
[59] J. L. Chollet, M. J. Jozwiakowski, K. R. Phares, M. J. Reiter, P. J. Roddy, H. J. Schultz, *et al.*, "Development of a topically active imiquimod formulation," *Pharmaceutical development and technology,* vol. 4, pp. 35-43, 1999.
[60] W.-R. Lee, S.-C. Shen, S. A. Al-Suwayeh, H.-H. Yang, C.-Y. Yuan, and J.-Y. Fang, "Laser-assisted topical drug delivery by using a low-fluence fractional laser: imiquimod and macromolecules," *Journal of Controlled Release,* vol. 153, pp. 240-248, 2011.

[61] P. Stein, K. Gogoll, S. Tenzer, H. Schild, S. Stevanovic, P. Langguth, *et al.*, "Efficacy of imiquimod-based transcutaneous immunization using a nano-dispersed emulsion gel formulation," *PloS one,* vol. 9, p. e102664, 2014.

[62] K. Rehman, M. F. F. M. Aluwi, K. Rullah, L. K. Wai, M. C. I. M. Amin, and M. H. Zulfakar, "Probing the effects of fish oil on the delivery and inflammation-inducing potential of imiquimod," *International journal of pharmaceutics,* vol. 490, pp. 131-141, 2015.

[63] E. A. Grice and J. A. Segre, "The skin microbiome," *Nature reviews. Microbiology,* vol. 9, p. 244, 2011.

[64] S. Selwyn and H. Ellis, "Skin bacteria and skin disinfection reconsidered," *Br Med J,* vol. 1, pp. 136-140, 1972.

[65] E. A. Grice, H. H. Kong, G. Renaud, A. C. Young, G. G. Bouffard, R. W. Blakesley, *et al.*, "A diversity profile of the human skin microbiota," *Genome research,* vol. 18, pp. 1043-1050, 2008.

[66] R. R. Roth and W. D. James, "Microbial ecology of the skin," *Annual Reviews in Microbiology,* vol. 42, pp. 441-464, 1988.

[67] I. Uckay, D. Pittet, P. Vaudaux, H. Sax, D. Lew, and F. Waldvogel, "Foreign body infections due to Staphylococcus epidermidis," *Annals of medicine,* vol. 41, pp. 109-119, 2009.

[68] J. S. Hibbard, G. K. Mulberry, and A. R. Brady, "A clinical study comparing the skin antisepsis and safety of ChloraPrep, 70% isopropyl alcohol, and 2% aqueous chlorhexidine," *Journal of Infusion Nursing,* vol. 25, pp. 244-249, 2002.

[69] C. Crosby, T. Elliott, P. Lambert, and D. Adams, "Preoperative skin preparation: a historical perspective," *British Journal of Hospital Medicine (17508460),* vol. 70, 2009.

[70] A. J. Mangram, T. C. Horan, M. L. Pearson, L. C. Silver, and W. R. Jarvis, "Guideline for Prevention of Surgical Site Infection, 1999," *Infection Control and Hospital Epidemiology,* vol. 20, pp. 250-280, 1999.

[71] D. E. Fry, "The surgical infection prevention project: processes, outcomes, and future impact," *Surgical Infections,* vol. 7, pp. s-17-s-26, 2006.

[72] D. Leaper, "Surgical-site infection," *British journal of Surgery,* vol. 97, pp. 1601-1602, 2010.

[73] T. Elliott and P. Lambert, "Surgical site infection: are we using the right skin preparation?," ed: MA Healthcare London, 2009.

[74] P. Silva, "The right skin preparation technique: a literature review," *Journal of perioperative practice,* vol. 24, pp. 283-285, 2014.

[75] A. Woods, "Key points in the CDC's surgical site infection guideline," *Advances in skin & wound care,* vol. 18, pp. 215-220, 2005.

[76] J. Tanner, D. Khan, C. Aplin, J. Ball, M. Thomas, and J. Bankart, "Post-discharge surveillance to identify colorectal surgical site infection rates and related costs," *Journal of Hospital Infection,* vol. 72, pp. 243-250, 2009.

[77] T. J. Karpanen, T. Worthington, B. R. Conway, A. C. Hilton, T. S. Elliott, and P. A. Lambert, "Penetration of chlorhexidine into human skin," *Antimicrobial agents and chemotherapy,* vol. 52, pp. 3633-3636, 2008.

[78] H. Loveday, J. Wilson, R. Pratt, M. Golsorkhi, A. Tingle, A. Bak, *et al.*, "epic3: national evidence-based guidelines for preventing healthcare-associated infections in NHS hospitals in England," *Journal of Hospital Infection,* vol. 86, pp. S1-S70, 2014.

[79] DH, "Department of Health: High impact intervention: care bundle to prevent surgical infections," ed, 2011, pp. 1-7.

[80] R. O. Darouiche, M. J. Wall Jr, K. M. Itani, M. F. Otterson, A. L. Webb, M. M. Carrick, *et al.*, "Chlorhexidine–alcohol versus povidone–iodine for surgical-site antisepsis," *New England Journal of Medicine,* vol. 362, pp. 18-26, 2010.

[81] G. W. Denton, "Cholrhexidine," in *Disinfection, Sterilization, and Preservation*, S. S. Block, Ed., 5th ed Philadelphia: Lippincott Williams & Wilkins, 2001, pp. 321-336.

[82] T. Kuyyakanond and L. B. Quesnel, "The mechanism of action of chlorhexidine," *FEMS Microbiology Letters,* vol. 100, pp. 211-215, 1992.

[83] A. M. Judd, D. J. Scurr, J. R. Heylings, K.-W. Wan, and G. P. Moss, "Distribution and Visualisation of Chlorhexidine Within the Skin Using ToF-SIMS: A Potential Platform for the Design of More Efficacious Skin Antiseptic Formulations," *Pharmaceutical research,* vol. 30, pp. 1896-1905, 2013.

[84] C. Lafforgue, L. Carret, F. Falson, M. Reverdy, and J. Freney, "Percutaneous absorption of a chlorhexidine digluconate solution," *International Journal of Pharmaceutics,* vol. 147, pp. 243-246, 1997.

[85] T. J. Karpanen, T. Worthington, B. R. Conway, A. C. Hilton, T. S. Elliott, and P. A. Lambert, "Permeation of chlorhexidine from alcoholic and aqueous solutions within excised human skin," *Antimicrobial agents and chemotherapy,* vol. 53, pp. 1717-1719, 2009.

[86] A. M. Holmes, D. J. Scurr, J. R. Heylings, K.-W. Wan, and G. P. Moss, "Dendrimer pre-treatment enhances the skin permeation of chlorhexidine digluconate: Characterisation by in vitro percutaneous absorption studies and Time-of-Flight Secondary Ion Mass Spectrometry," *European Journal of Pharmaceutical Sciences,* vol. 104, pp. 90-101, 2017.

[87] R. A. Weinstein, A. M. Milstone, C. L. Passaretti, and T. M. Perl, "Chlorhexidine: expanding the armamentarium for infection control and prevention," *Clinical Infectious Diseases,* vol. 46, pp. 274-281, 2008.

[88] A. Goon, I. White, R. Rycroft, and J. McFadden, "Allergic contact dermatitis from chlorhexidine," *Dermatitis: contact, atopic, occupational, drug,* vol. 15, pp. 45-47, 2004.

[89] R. Khan, T. Kazi, and B. O'Donohoe, "Near fatal intra-operative anaphylaxis to chlorhexidine—is it time to change practice?," *BMJ case reports,* vol. 2011, p. bcr0920092300, 2011.

[90] V. P. Shah, G. L. Flynn, A. Yacobi, H. I. Maibach, C. Bon, N. M. Fleischer, *et al.*, "Bioequivalence of topical dermatological dosage forms–methods of evaluation of bioequivalence," *Skin Pharmacology and Physiology,* vol. 11, pp. 117-124, 1998.

[91] M. Cambon, N. Issachar, D. Castelli, and C. Robert, "An in vivo method to assess the photostability of UV filters in a sunscreen," *Journal of cosmetic science,* vol. 52, pp. 1-11, 2001.

[92] U. Jacobi, H.-J. Weigmann, M. Baumann, A.-I. Reiche, W. Sterry, and J. Lademann, "Lateral spreading of topically applied UV filter substances investigated by tape stripping," *Skin pharmacology and physiology*, vol. 17, pp. 17-22, 2004.

[93] A. Teichmann, U. Jacobi, H.-J. Weigmann, W. Sterry, and J. Lademann, "Reservoir function of the stratum corneum: development of an in vivo method to quantitatively determine the stratum corneum reservoir for topically applied substances," *Skin pharmacology and physiology*, vol. 18, pp. 75-80, 2005.

[94] A. Gamer, E. v. Leibold, and B. Van Ravenzwaay, "The in vitro absorption of microfine zinc oxide and titanium dioxide through porcine skin," *Toxicology in vitro*, vol. 20, pp. 301-307, 2006.

[95] S. Wissing and R. Müller, "Solid lipid nanoparticles as carrier for sunscreens: in vitro release and in vivo skin penetration," *Journal of Controlled Release*, vol. 81, pp. 225-233, 2002.

[96] I. Alberti, Y. N. Kalia, A. Naik, J.-D. Bonny, and R. H. Guy, "In vivo assessment of enhanced topical delivery of terbinafine to human stratum corneum," *Journal of controlled release*, vol. 71, pp. 319-327, 2001.

[97] I. Alberti, Y. N. Kalia, A. Naik, J.-D. Bonny, and R. H. Guy, "Effect of ethanol and isopropyl myristate on the availability of topical terbinafine in human stratum corneum, in vivo," *International journal of pharmaceutics*, vol. 219, pp. 11-19, 2001.

[98] B. N'Dri-Stempfer, W. C. Navidi, R. H. Guy, and A. L. Bunge, "Improved bioequivalence assessment of topical dermatological drug products using dermatopharmacokinetics," *Pharmaceutical research*, vol. 26, p. 316, 2009.

[99] H. Lboutounne, J.-F. Chaulet, C. Ploton, F. Falson, and F. Pirot, "Sustained ex vivo skin antiseptic activity of chlorhexidine in poly (ϵ-caprolactone) nanocapsule encapsulated form and as a digluconate," *Journal of Controlled Release*, vol. 82, pp. 319-334, 2002.

[100] F. Schwarb, B. Gabard, T. Rufli, and C. Surber, "Percutaneous absorption of salicylic acid in man after topical administration of three different formulations," *Dermatology*, vol. 198, pp. 44-51, 1999.

[101] S. Bashir, F. Dreher, A. Chew, H. Zhai, C. Levin, R. Stern, *et al.*, "Cutaneous bioassay of salicylic acid as a keratolytic," *International journal of pharmaceutics*, vol. 292, pp. 187-194, 2005.

[102] J.-C. Tsai, S.-A. Chuang, M.-Y. Hsu, and H.-M. Sheu, "Distribution of salicylic acid in human stratum corneum following topical application in vivo: a comparison of six different formulations," *International journal of pharmaceutics*, vol. 188, pp. 145-153, 1999.

[103] S. Wiedersberg and S. Nicoli, "Skin Permeation Assessment: Tape Stripping," in *Topical and Transdermal Drug Delivery: Principles and Practice*, H. A. E. Benson and A. C. Watkinson, Eds., First ed New Jersey: John Wiley & Sons, 2012, pp. 109-130.

[104] V. Klang, J. C. Schwarz, B. Lenobel, M. Nadj, J. Auböck, M. Wolzt, *et al.*, "In vitro vs. in vivo tape stripping: validation of the porcine ear model and penetration assessment of novel sucrose stearate emulsions," *European Journal of Pharmaceutics and Biopharmaceutics*, vol. 80, pp. 604-614, 2012.

[105] J. Lademann, U. Jacobi, C. Surber, H. J. Weigmann, and J. W. Fluhr, "The tape stripping procedure - evaluation of some critical parameters," *Eur J Pharm Biopharm,* vol. 72, pp. 317-23, 2009.
[106] K. Trebilcock, J. Heylings, and M. Wilks, "In vitro tape stripping as a model for in vivo skin stripping," *Toxicology in vitro,* vol. 8, pp. 665-667, 1994.
[107] J. Lademann, U. Jacobi, C. Surber, H.-J. Weigmann, and J. Fluhr, "The tape stripping procedure–evaluation of some critical parameters," *European Journal of Pharmaceutics and Biopharmaceutics,* vol. 72, pp. 317-323, 2009.
[108] T. Jui-Chen, N. D. Weiner, G. L. Flynn, and J. Ferry, "Properties of adhesive tapes used for stratum corneum stripping," *International journal of pharmaceutics,* vol. 72, pp. 227-231, 1991.
[109] H.-J. Weigmann, J. Lademann, H. Meffert, H. Schaefer, and W. Sterry, "Determination of the horny layer profile by tape stripping in combination with optical spectroscopy in the visible range as a prerequisite to quantify percutaneous absorption," *Skin Pharmacology and Physiology,* vol. 12, pp. 34-45, 1999.
[110] J. T. Reed, R. Ghadially, and P. M. Elias, "Skin type, but neither race nor gender, influence epidermal permeability barrier function," *Archives of dermatology,* vol. 131, pp. 1134-1138, 1995.
[111] H. Löffler, F. Dreher, and H. Maibach, "Stratum corneum adhesive tape stripping: influence of anatomical site, application pressure, duration and removal," *British journal of dermatology,* vol. 151, pp. 746-752, 2004.
[112] M. Iguchi and H. Tagami, "Functional analysis of the stratum corneum of scalp skin: studies in patients with alopecia areata and androgenetic alopecia," *Archives of dermatological research,* vol. 292, pp. 605-611, 2000.
[113] A. Rougier, C. Lotte, and H. I. Maibach, "In vivo percutaneous penetration of some organic compounds related to anatomic site in humans: predictive assessment by the stripping method," *Journal of pharmaceutical sciences,* vol. 76, pp. 451-454, 1987.
[114] D. Bommannan, R. O. Potts, and R. H. Guy, "Examination of stratum corneum barrier function in vivo by infrared spectroscopy," *Journal of investigative dermatology,* vol. 95, pp. 403-408, 1990.
[115] Y.-C. E. Chao and L. A. Nylander-French, "Determination of keratin protein in a tape-stripped skin sample from jet fuel exposed skin," *Annals of Occupational Hygiene,* vol. 48, pp. 65-73, 2004.
[116] U. Jacobi, H. J. Weigmann, J. Ulrich, W. Sterry, and J. Lademann, "Estimation of the relative stratum corneum amount removed by tape stripping," *Skin Research and Technology,* vol. 11, pp. 91-96, 2005.
[117] J. Lademann, M. Meinke, S. Schanzer, H. Richter, M. Darvin, S. Haag, *et al.*, "In vivo methods for the analysis of the penetration of topically applied substances in and through the skin barrier," *International journal of cosmetic science,* vol. 34, pp. 551-559, 2012.
[118] A. Lavrijsen, I. Higounenc, A. Weerheim, E. Oestmann, E. Tuinenburg, H. Bnddé, *et al.*, "Validation of an in vivo extraction method for human stratum corneum ceramides," *Archives of dermatological research,* vol. 286, pp. 495-503, 1994.

[119] J. Lademann, S. Schanzer, H. Richter, M. C. Meinke, H.-J. Weigmann, and A. Patzelt, "Stripping Procedures for Penetration Measurements of Topically Applied Substances," in *Percutaneous Penetration Enhancers, Drug Penetration Into/Through the Skin, Methodology and General Considerations*, N. Dragicevic and H. I. Maibach, Eds., ed Berlin: Springer, 2017, pp. 205-214.

[120] S. Farahmand, L. Tien, X. Hui, and H. I. Maibach, "Measuring transepidermal water loss: a comparative in vivo study of condenser-chamber, unventilated-chamber and open-chamber systems," *Skin Research and Technology*, vol. 15, pp. 392-398, 2009.

[121] R. Holmgaard, J. B. Nielsen, and E. Benfeldt, "Skin Permeation Assessment: Microdialysis," in *Topical and Transdermal Drug Delivery: Principles and Practice*, H. A. E. Benson and A. C. Watkinson, Eds., First ed New Jersey: John Wiley & Sons, 2012, pp. 131-153.

[122] A. Yacobi, V. P. Shah, E. D. Bashaw, E. Benfeldt, B. Davit, D. Ganes, *et al.*, "Current challenges in bioequivalence, quality, and novel assessment technologies for topical products," *Pharmaceutical research*, vol. 31, pp. 837-846, 2014.

[123] P. G. Ortiz, S. H. Hansen, V. P. Shah, T. Menne, and E. Benfeldt, "The effect of irritant dermatitis on cutaneous bioavailability of a metronidazole formulation, investigated by microdialysis and dermatopharmacokinetic method," *Contact Dermatitis*, vol. 59, pp. 23-30, 2008.

[124] P. G. Ortiz, S. H. Hansen, V. P. Shah, T. Menné, and E. Benfeldt, "Impact of adult atopic dermatitis on topical drug penetration: assessment by cutaneous microdialysis and tape stripping," *Acta dermato-venereologica*, vol. 89, pp. 33-38, 2009.

[125] E. Benfeldt, S. H. Hansen, A. Vølund, T. Menné, and V. P. Shah, "Bioequivalence of topical formulations in humans: evaluation by dermal microdialysis sampling and the dermatopharmacokinetic method," *Journal of Investigative Dermatology*, vol. 127, pp. 170-178, 2007.

[126] R. N. O. Tettey-Amlalo, I. Kanfer, M. F. Skinner, E. Benfeldt, and R. K. Verbeeck, "Application of dermal microdialysis for the evaluation of bioequivalence of a ketoprofen topical gel," *european journal of pharmaceutical sciences*, vol. 36, pp. 219-225, 2009.

[127] J. Haigh and I. Kanfer, "Assessment of topical corticosteroid preparations: the human skin blanching assay," *International journal of pharmaceutics*, vol. 19, pp. 245-262, 1984.

[128] SCCS, "Basic criteria for the *in vitro* assessment of dermal absorption of cosmetic ingredients," vol. SCCS/1358/10, ed. Brussels, 2010.

[129] B. Finnin, K. A. Walters, and T. J. Franz, "In Vitro Skin Permeation Methodology," in *Topical and Transdermal drug delivery: Principles and Practice*, H. A. E. Benson and A. C. Watkinson, Eds., First ed New Jersey: John Wiley & Sons, 2012, pp. 85-108.

[130] A. M. Barbero and H. F. Frasch, "Pig and guinea pig skin as surrogates for human in vitro penetration studies: a quantitative review," *Toxicol In Vitro*, vol. 23, pp. 1-13, 2009.

[131] B. E. Vecchia and A. L. Bunge, "Animal models: a comparison of permeability coefficients for excised skin from humans and animals," in *Dermal Absorption Models in Toxicology and Pharmacology*, J. E. Riviere, Ed., First ed Boca Raton: CRC Press 2006, pp. 305-333.
[132] V. Vallet, C. Cruz, J. Licausi, A. Bazire, G. Lallement, and I. Boudry, "Percutaneous penetration and distribution of VX using in vitro pig or human excised skin validation of demeton-S-methyl as adequate simulant for VX skin permeation investigations," *Toxicology,* vol. 246, pp. 73-82, 2008.
[133] I. P. Dick and R. C. Scott, "Pig ear skin as an in-vitro model for human skin permeability," *Journal of pharmacy and pharmacology,* vol. 44, pp. 640-645, 1992.
[134] E. C. Jung and H. I. Maibach, "Animal models for percutaneous absorption," *Journal of Applied Toxicology,* vol. 35, pp. 1-10, 2015.
[135] P. A. Lehman, S. G. Raney, and T. J. Franz, "Skin Permeation Assessment in Man: In Vitro-In Vivo Correlation," in *Topical and Transdermal Drug Delivery: Principles and Practice*, H. A. E. Benson and A. C. Watkinson, Eds., First ed New Jersey: John Wiley & Sons, 2012, pp. 167-182.
[136] OECD, "Guidance Document for the Conduct of Skin Absorption Studies, Number 28," ed. Paris, 2004.
[137] H. Wagner, K.-H. Kostka, C.-M. Lehr, and U. F. Schaefer, "Drug distribution in human skin using two different in vitro test systems: comparison with in vivo data," *Pharmaceutical research,* vol. 17, pp. 1475-1481, 2000.
[138] N. Dragicevic-Curic, D. Scheglmann, V. Albrecht, and A. Fahr, "Temoporfin-loaded invasomes: development, characterization and in vitro skin penetration studies," *Journal of Controlled Release,* vol. 127, pp. 59-69, 2008.
[139] D. D. Paula, C. A. Martins, and M. V. L. B. Bentley, "Development and validation of HPLC method for imiquimod determination in skin penetration studies," *Biomedical Chromatography,* vol. 22, pp. 1416-1423, 2008.
[140] N. Hasler-Nguyen, D. Shelton, G. Ponard, M. Bader, M. Schaffrik, and P. Mallefet, "Evaluation of the in vitro skin permeation of antiviral drugs from penciclovir 1% cream and acyclovir 5% cream used to treat herpes simplex virus infection," *BMC dermatology,* vol. 9, p. 3, 2009.
[141] D. Verma, S. Verma, G. Blume, and A. Fahr, "Liposomes increase skin penetration of entrapped and non-entrapped hydrophilic substances into human skin: a skin penetration and confocal laser scanning microscopy study," *European Journal of Pharmaceutics and Biopharmaceutics,* vol. 55, pp. 271-277, 2003.
[142] C. S. Campbell, L. R. Contreras-Rojas, M. B. Delgado-Charro, and R. H. Guy, "Objective assessment of nanoparticle disposition in mammalian skin after topical exposure," *Journal of Controlled Release,* vol. 162, pp. 201-207, 2012.

[143] F. S. De Rosa, J. M. Marchetti, J. A. Thomazini, A. C. Tedesco, and M. V. L. B. Bentley, "A vehicle for photodynamic therapy of skin cancer: influence of dimethylsulphoxide on 5-aminolevulinic acid in vitro cutaneous permeation and in vivo protoporphyrin IX accumulation determined by confocal microscopy," *Journal of Controlled Release*, vol. 65, pp. 359-366, 2000.

[144] R. Alvarez-Román, A. Naik, Y. Kalia, H. Fessi, and R. H. Guy, "Visualization of skin penetration using confocal laser scanning microscopy," *European Journal of Pharmaceutics and Biopharmaceutics*, vol. 58, pp. 301-316, 2004.

[145] R. Mendelsohn, C. R. Flach, and D. J. Moore, "Determination of molecular conformation and permeation in skin via IR spectroscopy, microscopy, and imaging," *Biochimica et Biophysica Acta (BBA)-Biomembranes*, vol. 1758, pp. 923-933, 2006.

[146] I. Notingher and R. E. Imhof, "Mid-infrared in vivo depth-profiling of topical chemicals on skin," *Skin Research and Technology*, vol. 10, pp. 113-121, 2004.

[147] C. Marcott, M. Lo, K. Kjoller, Y. Domanov, G. Balooch, and G. S. Luengo, "Nanoscale infrared (IR) spectroscopy and imaging of structural lipids in human stratum corneum using an atomic force microscope to directly detect absorbed light from a tunable IR laser source," *Experimental dermatology*, vol. 22, pp. 419-421, 2013.

[148] G. Zhang, D. J. Moore, K. B. Sloan, C. R. Flach, and R. Mendelsohn, "Imaging the prodrug-to-drug transformation of a 5-fluorouracil derivative in skin by confocal Raman microscopy," *Journal of Investigative Dermatology*, vol. 127, pp. 1205-1209, 2007.

[149] M. Tosato, D. Orallo, S. Ali, M. Churio, A. Martin, and L. Dicelio, "Confocal Raman spectroscopy: In vivo biochemical changes in the human skin by topical formulations under UV radiation," *Journal of Photochemistry and Photobiology B: Biology*, vol. 153, pp. 51-58, 2015.

[150] Y. Pyatski, Q. Zhang, R. Mendelsohn, and C. R. Flach, "Effects of permeation enhancers on flufenamic acid delivery in Ex vivo human skin by confocal Raman microscopy," *International journal of pharmaceutics*, vol. 505, pp. 319-328, 2016.

[151] C. W. Freudiger, W. Min, B. G. Saar, S. Lu, G. R. Holtom, C. He, *et al.*, "Label-free biomedical imaging with high sensitivity by stimulated Raman scattering microscopy," *Science*, vol. 322, pp. 1857-1861, 2008.

[152] B. G. Saar, L. R. Contreras-Rojas, X. S. Xie, and R. H. Guy, "Imaging drug delivery to skin with stimulated Raman scattering microscopy," *Molecular pharmaceutics*, vol. 8, pp. 969-975, 2011.

[153] K. Park, "Confocal Raman spectroscopy to study in vivo skin penetration of retinol," *Journal of Controlled Release*, vol. 138, p. 1, 2009.

[154] P. J. Caspers, A. C. Williams, E. A. Carter, H. G. Edwards, B. W. Barry, H. A. Bruining, *et al.*, "Monitoring the penetration enhancer dimethyl sulfoxide in human stratum corneum in vivo by confocal Raman spectroscopy," *Pharmaceutical research*, vol. 19, pp. 1577-1580, 2002.

[155] B. Enthaler, M. Trusch, M. Fischer, C. Rapp, J. K. Pruns, and J.-P. Vietzke, "MALDI imaging in human skin tissue sections: focus on various matrices and enzymes," *Analytical and bioanalytical chemistry,* vol. 405, pp. 1159-1170, 2013.

[156] C. S. Macedo, D. M. Anderson, B. M. Pascarelli, J. M. Spraggins, E. N. Sarno, K. L. Schey, *et al.*, "MALDI imaging reveals lipid changes in the skin of leprosy patients before and after multidrug therapy (MDT)," *Journal of mass spectrometry,* vol. 50, pp. 1374-1385, 2015.

[157] P. J. Hart, S. Francese, E. Claude, M. N. Woodroofe, and M. R. Clench, "MALDI-MS imaging of lipids in ex vivo human skin," *Analytical and bioanalytical chemistry,* vol. 401, pp. 115-125, 2011.

[158] M. Lagarrigue, M. Becker, R. Lavigne, S.-O. Deininger, A. Walch, F. Aubry, *et al.*, "Revisiting rat spermatogenesis with MALDI imaging at 20-μm resolution," *Molecular & Cellular Proteomics,* vol. 10, p. M110. 005991, 2011.

[159] J. Bunch, M. R. Clench, and D. S. Richards, "Determination of pharmaceutical compounds in skin by imaging matrix-assisted laser desorption/ionisation mass spectrometry," *Rapid communications in mass spectrometry,* vol. 18, pp. 3051-3060, 2004.

[160] J. D'Alvise, R. Mortensen, S. H. Hansen, and C. Janfelt, "Detection of follicular transport of lidocaine and metabolism in adipose tissue in pig ear skin by DESI mass spectrometry imaging," *Analytical and bioanalytical chemistry,* vol. 406, pp. 3735-3742, 2014.

[161] P. Sjövall, T. M. Greve, S. K. Clausen, K. Moller, S. Eirefelt, B. r. Johansson, *et al.*, "Imaging of Distribution of Topically Applied Drug Molecules in Mouse Skin by Combination of Time-of-Flight Secondary Ion Mass Spectrometry and Scanning Electron Microscopy," *Analytical chemistry,* vol. 86, pp. 3443-3452, 2014.

[162] J. C. Vickerman, "Molecular Surface Mass Spectrometry by SIMS," in *Surface analysis: the principal techniques*, J. C. Vickerman and I. Gilmore, Eds., 2nd ed West Sussex: John Wiley & Sons, 2009, pp. 113-206.

[163] C. Bich, D. Touboul, and A. Brunelle, "Biomedical studies by TOF-SIMS imaging," *Biointerphases,* vol. 10, p. 018901, 2015.

[164] B. Hagenhoff, R. Kersting, and D. Rading, "Ion Beam Techniques: Time-of-Flight Secondary Ion Mass Spectroscopy (ToF-SIMS)," in *Handbook of surface and interface analysis: methods for problem-solving*, J. C. Rivière and S. Myhra, Eds., 2nd ed Florida: CRC press, 2009, pp. 65-96.

[165] Z. Postawa, B. Czerwinski, M. Szewczyk, E. J. Smiley, N. Winograd, and B. J. Garrison, "Microscopic insights into the sputtering of Ag {111} induced by C60 and Ga bombardment," *The Journal of Physical Chemistry B,* vol. 108, pp. 7831-7838, 2004.

[166] N. Winograd, "The magic of cluster SIMS," *Analytical chemistry,* vol. 1, pp. 143A-149A, 2005.

[167] J. Kozole and N. Winograd, "Cluster Secondary Ion Mass Spectrometry," in *Surface Analysis and Techniques in Biology*, V. S. Smentkowski, Ed., ed Switzerland: Springer, 2014, pp. 71-98.

[168] D. Weibel, N. Lockyer, and J. Vickerman, "C 60 cluster ion bombardment of organic surfaces," *Applied surface science,* vol. 231, pp. 146-152, 2004.
[169] Y. Yokoyama, S. Aoyagi, M. Fujii, J. Matsuo, J. S. Fletcher, N. P. Lockyer, *et al.*, "Peptide Fragmentation and Surface Structural Analysis by Means of ToF-SIMS Using Large Cluster Ion Sources," *Analytical chemistry,* vol. 88, pp. 3592-3597, 2016.
[170] A. M. Belu, D. J. Graham, and D. G. Castner, "Time-of-flight secondary ion mass spectrometry: techniques and applications for the characterization of biomaterial surfaces," *Biomaterials,* vol. 24, pp. 3635-3653, 2003.
[171] R. N. Sodhi, "Time-of-flight secondary ion mass spectrometry (TOF-SIMS):—versatility in chemical and imaging surface analysis," *Analyst,* vol. 129, pp. 483-487, 2004.
[172] I. Gilmore and M. Seah, "Electron flood gun damage in the analysis of polymers and organics in time-of-flight SIMS," *Applied surface science,* vol. 187, pp. 89-100, 2002.
[173] I. Gilmore and M. Seah, "Investigating the difficulty of eliminating flood gun damage in TOF-SIMS," *Applied surface science,* vol. 203, pp. 600-604, 2003.
[174] J. C. Vickerman, "Prologue: ToF-SIMS An evolving mass spectrometry of materials," in *ToF-SIMS: Materials Analysis by Mass Spectrometry*, J. C. Vickerman and D. Briggs, Eds., 2nd ed West Sussex: IM publications, 2013, pp. 1-37.
[175] A. M. Piwowar and N. Winograd, "Application of SIMS to study of biological systems," in *ToF-SIMS: Materials Analysis by Mass Spectrometry*, J. C. Vickerman and D. Briggs, Eds., 2nd Edition ed West Sussex: IM publications, 2013, pp. 553-582.
[176] A. Henss, M. Rohnke, S. Knaack, M. Kleine-Boymann, T. Leichtweiss, P. Schmitz, *et al.*, "Quantification of calcium content in bone by using ToF-SIMS–a first approach," *Biointerphases,* vol. 8, p. 31, 2013.
[177] R. L. Wilson and M. L. Kraft, "Quantifying the molar percentages of cholesterol in supported lipid membranes by time-of-flight secondary ion mass spectrometry and multivariate analysis," *Analytical chemistry,* vol. 85, pp. 91-97, 2012.
[178] C. Piantadosi and R. S. C. Smart, "Statistical comparison of hydrophobic and hydrophilic species on galena and pyrite particles in flotation concentrates and tails from TOF-SIMS evidence," *International journal of mineral processing,* vol. 64, pp. 43-54, 2002.
[179] E. Jones, N. Lockyer, and J. Vickerman, "Suppression and enhancement of non-native molecules within biological systems," *Applied surface science,* vol. 252, pp. 6727-6730, 2006.
[180] E. A. Jones, N. P. Lockyer, J. Kordys, and J. C. Vickerman, "Suppression and enhancement of secondary ion formation due to the chemical environment in static-secondary ion mass spectrometry," *Journal of the American Society for Mass Spectrometry,* vol. 18, pp. 1559-1567, 2007.

[181] D. C. Muddiman, A. I. Gusev, L. B. Martin, and D. M. Hercules, "Direct quantification of cocaine in urine by time-of-flight mass spectrometry," *Fresenius' journal of analytical chemistry,* vol. 354, pp. 103-110, 1996.

[182] D. C. Muddiman, A. I. Gusev, A. Proctor, D. M. Hercules, R. Venkataraman, and W. Diven, "Quantitative measurement of cyclosporin A in blood by time-of-flight mass spectrometry," *Analytical chemistry,* vol. 66, pp. 2362-2368, 1994.

[183] J. Chabala, K. Soni, J. Li, K. Gavrilov, and R. Levi-Setti, "High-resolution chemical imaging with scanning ion probe SIMS," *International journal of mass spectrometry and ion processes,* vol. 143, pp. 191-212, 1995.

[184] N. J. Starr, D. J. Johnson, J. Wibawa, I. Marlow, M. Bell, D. A. Barrett, *et al.*, "Age-related changes to human stratum corneum lipids detected using time-of-flight secondary ion mass spectrometry following in vivo sampling," *Analytical chemistry,* vol. 88, pp. 4400-4408, 2016.

[185] Y.-C. Wang and D. G. Castner, "Characterization of Protein G B1 Immobilized Gold Nanoparticles using Time of Flight Secondary Ion Mass Spectrometry and X-ray Photoelectron Spectroscopy," *Microscopy and Microanalysis,* vol. 22, pp. 346-347, 2016.

[186] R. N. Foster, E. T. Harrison, and D. G. Castner, "ToF-SIMS and XPS characterization of protein films adsorbed onto bare and sodium styrenesulfonate-grafted gold substrates," *Langmuir,* vol. 32, pp. 3207-3216, 2016.

[187] D. Touboul, S. Roy, D. P. Germain, P. Chaminade, A. Brunelle, and O. Laprévote, "MALDI-TOF and cluster-TOF-SIMS imaging of Fabry disease biomarkers," *International Journal of Mass Spectrometry,* vol. 260, pp. 158-165, 2007.

[188] P. Sjövall, B. Johansson, and J. Lausmaa, "Localization of lipids in freeze-dried mouse brain sections by imaging TOF-SIMS," *Applied Surface Science,* vol. 252, pp. 6966-6974, 2006.

[189] P. Malmberg, H. Nygren, K. Richter, Y. Chen, F. Dangardt, P. Friberg, *et al.*, "Imaging of Lipids in Human Adipose Tissue by Cluster Ion TOF-SIMS," *Microscopy research and technique,* vol. 70, pp. 828-835, 2007.

[190] P. Malmberg, K. Börner, Y. Chen, P. Friberg, B. Hagenhoff, J.-E. Månsson, *et al.*, "Localization of lipids in the aortic wall with imaging TOF-SIMS," *Biochimica et Biophysica Acta (BBA)-Molecular and Cell Biology of Lipids,* vol. 1771, pp. 185-195, 2007.

[191] H. Nygren, P. Malmberg, C. Kriegeskotte, and H. F. Arlinghaus, "Bioimaging TOF-SIMS: localization of cholesterol in rat kidney sections," *FEBS letters,* vol. 566, pp. 291-293, 2004.

[192] S. Mas, D. Touboul, A. Brunelle, P. Aragoncillo, J. Egido, O. Laprévote, *et al.*, "Lipid cartography of atherosclerotic plaque by cluster-TOF-SIMS imaging," *Analyst,* vol. 132, pp. 24-26, 2007.

[193] T. Kezutyte, N. Desbenoit, A. Brunelle, and V. Briedis, "Studying the penetration of fatty acids into human skin by ex vivo TOF-SIMS imaging," *Biointerphases,* vol. 8, p. 3, 2013.

[194] C. Bich, R. Havelund, R. Moellers, D. Touboul, F. Kollmer, E. Niehuis, *et al.*, "Argon cluster ion source evaluation on lipid standards and rat brain tissue samples," *Analytical chemistry,* vol. 85, pp. 7745-7752, 2013.
[195] H. Nygren, K. Börner, B. Hagenhoff, P. Malmberg, and J.-E. Månsson, "Localization of cholesterol, phosphocholine and galactosylceramide in rat cerebellar cortex with imaging TOF-SIMS equipped with a bismuth cluster ion source," *Biochimica et Biophysica Acta (BBA)-Molecular and Cell Biology of Lipids,* vol. 1737, pp. 102-110, 2005.
[196] A. N. Lazar, C. Bich, M. Panchal, N. Desbenoit, V. W. Petit, D. Touboul, *et al.*, "Time-of-flight secondary ion mass spectrometry (TOF-SIMS) imaging reveals cholesterol overload in the cerebral cortex of Alzheimer disease patients," *Acta neuropathologica,* vol. 125, pp. 133-144, 2013.
[197] P. Sjövall, B. Johansson, D. Belazi, P. Stenvinkel, B. Lindholm, J. Lausmaa, *et al.*, "TOF-SIMS analysis of adipose tissue from patients with chronic kidney disease," *Applied Surface Science,* vol. 255, pp. 1177-1180, 2008.
[198] D. Debois, M.-P. Bralet, F. o. Le Naour, A. Brunelle, and O. Laprévote, "In situ lipidomic analysis of nonalcoholic fatty liver by cluster TOF-SIMS imaging," *Analytical chemistry,* vol. 81, pp. 2823-2831, 2009.
[199] L. J. Gooren and M. C. Bunck, "Transdermal testosterone delivery: testosterone patch and gel," *World J Urol,* vol. 21, pp. 316-9, 2003.
[200] R. C. Wester and H. I. Maibach, "Regional Variation in Percutaneous Absorption," in *Topical Absorption of Dermatological Products*, R. L. Bronaugh and H. I. Maibach, Eds., First ed New York: Marcel Dekker, 2002, pp. 33-42.
[201] Y.-C. Kim, J.-H. Park, and M. R. Prausnitz, "Microneedles for drug and vaccine delivery," *Advanced drug delivery reviews,* vol. 64, pp. 1547-1568, 2012.
[202] A. Z. Alkilani, M. T. McCrudden, and R. F. Donnelly, "Transdermal drug delivery: Innovative pharmaceutical developments based on disruption of the barrier properties of the stratum corneum," *Pharmaceutics,* vol. 7, pp. 438-470, 2015.
[203] J. Hadgraft and M. E. Lane, "Skin: the ultimate interface," *Physical Chemistry Chemical Physics,* vol. 13, pp. 5215-5222, 2011.
[204] P. Santos, A. Watkinson, J. Hadgraft, and M. Lane, "Application of microemulsions in dermal and transdermal drug delivery," *Skin pharmacology and physiology,* vol. 21, pp. 246-259, 2008.
[205] M. J. Lawrence and G. D. Rees, "Microemulsion-based media as novel drug delivery systems," *Advanced drug delivery reviews,* vol. 64, pp. 175-193, 2012.
[206] I. Danielsson and B. Lindman, "The definition of microemulsion," *Colloids and Surfaces,* vol. 3, pp. 391-392, 1981.
[207] M. Kreilgaard, "Influence of microemulsions on cutaneous drug delivery," *Advanced Drug Delivery Reviews,* vol. 54, pp. S77-S98, 2002.

[208] A. Teichmann, S. Heuschkel, U. Jacobi, G. Presse, R. H. Neubert, W. Sterry, *et al.*, "Comparison of stratum corneum penetration and localization of a lipophilic model drug applied in an o/w microemulsion and an amphiphilic cream," *European Journal of Pharmaceutics and Biopharmaceutics,* vol. 67, pp. 699-706, 2007.
[209] L. Boltri, S. Morel, M. Trotta, and M. Gasco, "In vitro transdermal permeation of nifedipine from thickened microemulsions," *Journal de pharmacie de Belgique,* vol. 49, pp. 315-320, 1993.
[210] F. Bonina, L. Montenegro, N. Scrofani, E. Esposito, R. Cortesi, E. Menegatti, *et al.*, "Effects of phospholipid based formulations on in vitro and in vivo percutaneous absorption of methyl nicotinate," *Journal of controlled release,* vol. 34, pp. 53-63, 1995.
[211] M. B. Delgado-Charro, G. Iglesias-Vilas, J. Blanco-Méndez, M. A. Lopez-Quintela, J.-P. Marty, and R. H. Guy, "Delivery of a hydrophilic solute through the skin from novel microemulsion systems," *European Journal of Pharmaceutics and Biopharmaceutics,* vol. 43, pp. 37-42, 1997.
[212] F. Dreher, P. Walde, P. Walther, and E. Wehrli, "Interaction of a lecithin microemulsion gel with human stratum corneum and its effect on transdermal transport," *Journal of controlled release,* vol. 45, pp. 131-140, 1997.
[213] M. Kreilgaard, E. J. Pedersen, and J. W. Jaroszewski, "NMR characterisation and transdermal drug delivery potential of microemulsion systems," *Journal of controlled release,* vol. 69, pp. 421-433, 2000.
[214] K. Kriwet and C. C. Müller-Goymann, "Diclofenac release from phospholipid drug systems and permeation through excised human stratum corneum," *International journal of pharmaceutics,* vol. 125, pp. 231-242, 1995.
[215] M. Trotta, M. Gasco, O. Caputo, and P. Sancin, "Transcutaneous diffusion of haematoporphyrin in photodynamic therapy in vitro release from microemulsions," *STP pharma sciences,* vol. 4, pp. 150-154, 1994.
[216] M. Trotta, S. Morel, and M. Gasco, "Effect of oil phase composition on the skin permeation of felodipine from o/w microemulsions," *Die Pharmazie,* vol. 52, pp. 50-53, 1997.
[217] S. Peltola, P. Saarinen-Savolainen, J. Kiesvaara, T. Suhonen, and A. Urtti, "Microemulsions for topical delivery of estradiol," *International journal of pharmaceutics,* vol. 254, pp. 99-107, 2003.
[218] Y.-S. Rhee, J.-G. Choi, E.-S. Park, and S.-C. Chi, "Transdermal delivery of ketoprofen using microemulsions," *International journal of pharmaceutics,* vol. 228, pp. 161-170, 2001.
[219] A. C. Sintov, "Transdermal delivery of curcumin via microemulsion," *International journal of pharmaceutics,* vol. 481, pp. 97-103, 2015.
[220] D. J. McClements, "Nanoemulsions versus microemulsions: terminology, differences, and similarities," *Soft matter,* vol. 8, pp. 1719-1729, 2012.

[221] R. Bagwe, J. Kanicky, B. Palla, P. Patanjali, and D. Shah, "Improved drug delivery using microemulsions: rationale, recent progress, and new horizons," *Critical reviews in therapeutic drug carrier systems,* vol. 18, pp. 77-140, 2001.
[222] A. Kogan and N. Garti, "Microemulsions as transdermal drug delivery vehicles," *Advances in colloid and interface science,* vol. 123, pp. 369-385, 2006.
[223] R.J.Babu, L.Chen, and N.Kanikkannan, "Fatty Alcohols, Fatty Acids and Fatty Esters as Penetration Enhancers," in *Percutaneous Penetration Enhancers Chemical Methods in Penetration Enhancement*, N. Dragicevic and H. I. Maibach, Eds., ed Berlin: Springer, 2015, pp. 133-150.
[224] M. Goodman and B. W. Barry, "Lipid-protein-partitioning (LPP) theory of skin enhancer activity: finite dose technique," *International journal of pharmaceutics,* vol. 57, pp. 29-40, 1989.
[225] L. Djordjevic, M. Primorac, M. Stupar, and D. Krajisnik, "Characterization of caprylocaproyl macrogolglycerides based microemulsion drug delivery vehicles for an amphiphilic drug," *International journal of pharmaceutics,* vol. 271, pp. 11-19, 2004.
[226] E. Escribano, A. C. Calpena, J. Queralt, R. Obach, and J. Doménech, "Assessment of diclofenac permeation with different formulations: anti-inflammatory study of a selected formula," *European journal of pharmaceutical sciences,* vol. 19, pp. 203-210, 2003.
[227] P. Špiclin, M. Homar, A. Zupančič-Valant, and M. Gašperlin, "Sodium ascorbyl phosphate in topical microemulsions," *International journal of pharmaceutics,* vol. 256, pp. 65-73, 2003.
[228] J.-Y. Fang, S.-Y. Yu, P.-C. Wu, Y.-B. Huang, and Y.-H. Tsai, "In vitro skin permeation of estradiol from various proniosome formulations," *International journal of pharmaceutics,* vol. 215, pp. 91-99, 2001.
[229] P. p. Sarpotdar and J. L. Zatz, "Percutaneous absorption enhancement by nonionic surfactants," *Drug Development and Industrial Pharmacy,* vol. 12, pp. 1625-1647, 1986.
[230] P. P. Sarpotdar and J. L. Zatz, "Evaluation of penetration enhancement of lidocaine by nonionic surfactants through hairless mouse skin in vitro," *Journal of pharmaceutical sciences,* vol. 75, pp. 176-181, 1986.
[231] P. C. Rigg and B. W. Barry, "Shed snake skin and hairless mouse skin as model membranes for human skin during permeation studies," *Journal of investigative dermatology,* vol. 94, pp. 235-240, 1990.
[232] P. Liu, T. Kurihara-Bergstrom, and W. R. Good, "Co-transport of estradiol and ethanol through human skin in vitro: understanding the permeant/enhancer flux relationship," *Pharmaceutical research,* vol. 8, pp. 938-944, 1991.
[233] D. Friend, P. Catz, J. Heller, J. Reid, and R. Baker, "Transdermal delivery of levonorgestrel I: Alkanols as permeation enhancers in vitro," *Journal of controlled release,* vol. 7, pp. 243-250, 1988.
[234] H. Chen, X. Chang, T. Weng, X. Zhao, Z. Gao, Y. Yang, *et al.*, "A study of microemulsion systems for transdermal delivery of triptolide," *Journal of controlled release,* vol. 98, pp. 427-436, 2004.

[235] K. Moser, K. Kriwet, A. Naik, Y. N. Kalia, and R. H. Guy, "Passive skin penetration enhancement and its quantification in vitro," *European journal of pharmaceutics and Biopharmaceutics,* vol. 52, pp. 103-112, 2001.

[236] S. T. Narishetty, D. Garcia-Tapia, and K. J. Bonnema, "Toxicological Aspects of Chemical Penetration Enhancers," in *Percutaneous Penetration Enhancers Chemical Methods in Penetration Enhancement*, N. Dragicevic and H. I. Maibach, Eds., ed Berlin: Springer, 2015, pp. 387-405.

[237] S. Shafiq-un-Nabi, F. Shakeel, S. Talegaonkar, J. Ali, S. Baboota, A. Ahuja, *et al.*, "Formulation development and optimization using nanoemulsion technique: a technical note," *Aaps Pharmscitech,* vol. 8, pp. E12-E17, 2007.

[238] R. F. Donnelly, M. J. Garland, D. I. Morrow, K. Migalska, T. R. R. Singh, R. Majithiya, *et al.*, "Optical coherence tomography is a valuable tool in the study of the effects of microneedle geometry on skin penetration characteristics and in-skin dissolution," *Journal of controlled release,* vol. 147, pp. 333-341, 2010.

[239] M. R. Prausnitz, "Microneedles for transdermal drug delivery," *Advanced drug delivery reviews,* vol. 56, pp. 581-587, 2004.

[240] O. Olatunji, D. B. Das, M. J. Garland, L. Belaid, and R. F. Donnelly, "Influence of array interspacing on the force required for successful microneedle skin penetration: theoretical and practical approaches," *Journal of pharmaceutical sciences,* vol. 102, pp. 1209-1221, 2013.

[241] S. Kaushik, A. H. Hord, D. D. Denson, D. V. McAllister, S. Smitra, M. G. Allen, *et al.*, "Lack of pain associated with microfabricated microneedles," *Anesthesia & Analgesia,* vol. 92, pp. 502-504, 2001.

[242] M. Haq, E. Smith, D. N. John, M. Kalavala, C. Edwards, A. Anstey, *et al.*, "Clinical administration of microneedles: skin puncture, pain and sensation," *Biomedical microdevices,* vol. 11, pp. 35-47, 2009.

[243] S. M. Bal, J. Caussin, S. Pavel, and J. A. Bouwstra, "In vivo assessment of safety of microneedle arrays in human skin," *european journal of pharmaceutical sciences,* vol. 35, pp. 193-202, 2008.

[244] R. F. Donnelly, T. R. R. Singh, D. I. J. Morrow, and A. D. Woolfson, *Microneedle-mediated Transdermal and Intradrmal Drug Delivery*. West Sussex: Wiley-Blackwell, 2012.

[245] K. Ita, "Transdermal delivery of drugs with microneedles—Potential and challenges," *Pharmaceutics,* vol. 7, pp. 90-105, 2015.

[246] H. L. Quinn, A. J. Courtenay, M. C. Kearney, and R. F. Donnelly, "Microneedle Technology," in *Novel Delivery Systems for Transdermal and Intradermal Drug Delivery*, R. F. Donnelly and T. R. R. Singh, Eds., 1st ed West Sussex: Wiley, 2015, pp. 179-208.

[247] H. Katsumi, S. Liu, Y. Tanaka, K. Hitomi, R. Hayashi, Y. Hirai, *et al.*, "Development of a novel self-dissolving microneedle array of alendronate, a nitrogen-containing bisphosphonate: Evaluation of transdermal absorption, safety, and pharmacological effects after application in rats," *Journal of pharmaceutical sciences,* vol. 101, pp. 3230-3238, 2012.

[248] M. T. McCrudden, A. Z. Alkilani, C. M. McCrudden, E. McAlister, H. O. McCarthy, A. D. Woolfson, *et al.*, "Design and physicochemical characterisation of novel dissolving polymeric microneedle arrays for transdermal delivery of high dose, low molecular weight drugs," *Journal of Controlled Release,* vol. 180, pp. 71-80, 2014.

[249] W. Martanto, S. P. Davis, N. R. Holiday, J. Wang, H. S. Gill, and M. R. Prausnitz, "Transdermal delivery of insulin using microneedles in vivo," *Pharmaceutical research,* vol. 21, pp. 947-952, 2004.

[250] Y. Ito, M. Hirono, K. Fukushima, N. Sugioka, and K. Takada, "Two-layered dissolving microneedles formulated with intermediate-acting insulin," *International journal of pharmaceutics,* vol. 436, pp. 387-393, 2012.

[251] M. Cormier, B. Johnson, M. Ameri, K. Nyam, L. Libiran, D. D. Zhang, *et al.*, "Transdermal delivery of desmopressin using a coated microneedle array patch system," *Journal of controlled release,* vol. 97, pp. 503-511, 2004.

[252] Y. A. Gomaa, M. J. Garland, F. McInnes, L. K. El-Khordagui, C. Wilson, and R. F. Donnelly, "Laser-engineered dissolving microneedles for active transdermal delivery of nadroparin calcium," *European Journal of Pharmaceutics and Biopharmaceutics,* vol. 82, pp. 299-307, 2012.

[253] S. A. Coulman, D. Barrow, A. Anstey, C. Gateley, A. Morrissey, N. Wilke, *et al.*, "Minimally invasive cutaneous delivery of macromolecules and plasmid DNA via microneedles," *Current drug delivery,* vol. 3, pp. 65-75, 2006.

[254] M. Pearton, V. Saller, S. A. Coulman, C. Gateley, A. V. Anstey, V. Zarnitsyn, *et al.*, "Microneedle delivery of plasmid DNA to living human skin: Formulation coating, skin insertion and gene expression," *Journal of controlled release,* vol. 160, pp. 561-569, 2012.

[255] J. A. Mikszta, J. B. Alarcon, J. M. Brittingham, D. E. Sutter, R. J. Pettis, and N. G. Harvey, "Improved genetic immunization via micromechanical disruption of skin-barrier function and targeted epidermal delivery," *Nature medicine,* vol. 8, pp. 415-419, 2002.

[256] R. F. Donnelly, D. I. Morrow, P. A. McCarron, A. D. Woolfson, A. Morrissey, P. Juzenas, *et al.*, "Microneedle-mediated intradermal delivery of 5-aminolevulinic acid: potential for enhanced topical photodynamic therapy," *Journal of Controlled Release,* vol. 129, pp. 154-162, 2008.

[257] A. Alexander, S. Dwivedi, T. K. Giri, S. Saraf, S. Saraf, and D. K. Tripathi, "Approaches for breaking the barriers of drug permeation through transdermal drug delivery," *Journal of Controlled Release,* vol. 164, pp. 26-40, 2012.

[258] R. F. Donnelly, T. R. R. Singh, D. I. Morrow, and A. D. Woolfson, *Microneedle-mediated transdermal and intradermal drug delivery*: John Wiley & Sons, 2012.

[259] P. M. Wang, M. Cornwell, J. Hill, and M. R. Prausnitz, "Precise microinjection into skin using hollow microneedles," *Journal of investigative dermatology,* vol. 126, pp. 1080-1087, 2006.

[260] Y. Ito, E. Hagiwara, A. Saeki, N. Sugioka, and K. Takada, "Feasibility of microneedles for percutaneous absorption of insulin," *European journal of pharmaceutical sciences,* vol. 29, pp. 82-88, 2006.
[261] C. S. Kolli and A. K. Banga, "Characterization of solid maltose microneedles and their use for transdermal delivery," *Pharmaceutical research,* vol. 25, pp. 104-113, 2008.
[262] J.-H. Park, M. G. Allen, and M. R. Prausnitz, "Biodegradable polymer microneedles: fabrication, mechanics and transdermal drug delivery," *Journal of Controlled Release,* vol. 104, pp. 51-66, 2005.
[263] J.-H. Park, M. G. Allen, and M. R. Prausnitz, "Polymer microneedles for controlled-release drug delivery," *Pharmaceutical research,* vol. 23, pp. 1008-1019, 2006.
[264] T.-M. Tuan-Mahmood, M. T. McCrudden, B. M. Torrisi, E. McAlister, M. J. Garland, T. R. R. Singh, *et al.*, "Microneedles for intradermal and transdermal drug delivery," *European Journal of Pharmaceutical Sciences,* vol. 50, pp. 623-637, 2013.
[265] S. Davis, M. Prausnitz, and M. Allen, "Fabrication and characterization of laser micromachined hollow microneedles," in *TRANSDUCERS, Solid-State Sensors, Actuators and Microsystems, 12th International Conference on, 2003,* 2003, pp. 1435-1438.
[266] S. P. Davis, B. J. Landis, Z. H. Adams, M. G. Allen, and M. R. Prausnitz, "Insertion of microneedles into skin: measurement and prediction of insertion force and needle fracture force," *Journal of biomechanics,* vol. 37, pp. 1155-1163, 2004.
[267] A. Römgens, D. Bader, J. A. Bouwstra, F. Baaijens, and C. Oomens, "Monitoring the penetration process of single microneedles with varying tip diameters," *journal of the mechanical behavior of biomedical materials,* vol. 40, pp. 397-405, 2014.
[268] R. E. Lutton, J. Moore, E. Larrañeta, S. Ligett, A. D. Woolfson, and R. F. Donnelly, "Microneedle characterisation: the need for universal acceptance criteria and GMP specifications when moving towards commercialisation," *Drug delivery and translational research,* vol. 5, pp. 313-331, 2015.
[269] H. S. Gill and M. R. Prausnitz, "Coating formulations for microneedles," *Pharmaceutical research,* vol. 24, pp. 1369-1380, 2007.
[270] H. S. Gill and M. R. Prausnitz, "Coated microneedles for transdermal delivery," *Journal of controlled release,* vol. 117, pp. 227-237, 2007.
[271] H. Kalluri, C. S. Kolli, and A. K. Banga, "Characterization of microchannels created by metal microneedles: formation and closure," *The AAPS journal,* vol. 13, pp. 473-481, 2011.
[272] J. S. Kochhar, T. C. Quek, W. J. Soon, J. Choi, S. Zou, and L. Kang, "Effect of microneedle geometry and supporting substrate on microneedle array penetration into skin," *Journal of pharmaceutical sciences,* vol. 102, pp. 4100-4108, 2013.
[273] D. V. McAllister, P. M. Wang, S. P. Davis, J.-H. Park, P. J. Canatella, M. G. Allen, *et al.*, "Microfabricated needles for transdermal delivery of macromolecules and nanoparticles: fabrication methods and transport studies," *Proceedings of the National Academy of Sciences,* vol. 100, pp. 13755-13760, 2003.

[274] J. Gupta, H. S. Gill, S. N. Andrews, and M. R. Prausnitz, "Kinetics of skin resealing after insertion of microneedles in human subjects," *Journal of controlled release,* vol. 154, pp. 148-155, 2011.
[275] Y. A. Gomaa, D. I. Morrow, M. J. Garland, R. F. Donnelly, L. K. El-Khordagui, and V. M. Meidan, "Effects of microneedle length, density, insertion time and multiple applications on human skin barrier function: assessments by transepidermal water loss," *Toxicology in Vitro,* vol. 24, pp. 1971-1978, 2010.
[276] L. Y. Chu and M. R. Prausnitz, "Separable arrowhead microneedles," *Journal of controlled release,* vol. 149, pp. 242-249, 2011.
[277] S. Bal, A. Kruithof, H. Liebl, M. Tomerius, J. Bouwstra, J. Lademann, *et al.*, "In vivo visualization of microneedle conduits in human skin using laser scanning microscopy," *Laser Physics Letters,* vol. 7, p. 242, 2010.
[278] S. A. Coulman, J. C. Birchall, A. Alex, M. Pearton, B. Hofer, C. O'Mahony, *et al.*, "In vivo, in situ imaging of microneedle insertion into the skin of human volunteers using optical coherence tomography," *Pharmaceutical research,* vol. 28, pp. 66-81, 2011.
[279] J. Lee, S. H. Park, I. H. Seo, K. J. Lee, and W. Ryu, "Rapid and repeatable fabrication of high A/R silk fibroin microneedles using thermally-drawn micromolds," *European Journal of Pharmaceutics and Biopharmaceutics,* vol. 94, pp. 11-19, 2015.
[280] C. M. Schoellhammer, D. Blankschtein, and R. Langer, "Skin permeabilization for transdermal drug delivery: recent advances and future prospects," *Expert opinion on drug delivery,* vol. 11, pp. 393-407, 2014.
[281] D. W. Burden, "Guide to the homogenization of biological samples," *Random Primers,* vol. 7, pp. 1-14, 2008.
[282] D. W. Burden, "Guide to the disruption of biological samples," *Random Primers,* vol. 12, pp. 1-25, 2012.
[283] X. Liang, S. Ubhayakar, B. M. Liederer, B. Dean, A. Ran-Ran Qin, S. Shahidi-Latham, *et al.*, "Evaluation of homogenization techniques for the preparation of mouse tissue samples to support drug discovery," *Bioanalysis,* vol. 3, pp. 1923-1933, 2011.
[284] R. Nirogi, N. S. P. Padala, R. K. Boggavarapu, I. Kalaikadhiban, D. R. Ajjala, G. Bhyrapuneni, *et al.*, "Skin sample preparation by collagenase digestion for diclofenac quantification using LC-MS/MS after topical application," *Bioanalysis,* vol. 8, pp. 1251-1263, 2016.
[285] S. Goldberg, "Mechanical/Physical Methods of Cell Disruption and Tissue Homogenization," in *Proteomic Profiling Methods and Protocols*, A. Posch, Ed., ed New York: Humana Press, 2015, pp. 1-20.
[286] M. S. Algahtani, D. J. Scurr, A. L. Hook, D. G. Anderson, R. S. Langer, J. C. Burley, *et al.*, "High throughput screening for biomaterials discovery," *Journal of Controlled Release,* vol. 190, pp. 115-126, 2014.
[287] E. A. Roth, T. Xu, M. Das, C. Gregory, J. J. Hickman, and T. Boland, "Inkjet printing for high-throughput cell patterning," *Biomaterials,* vol. 25, pp. 3707-3715, 2004.
[288] A. Hook, N. Voelcker, and H. Thissen, "Patterned and switchable surfaces for biomolecular manipulation," *Acta Biomaterialia,* vol. 5, pp. 2350-2370, 2009.

[289] A. L. Hook, D. G. Anderson, R. Langer, P. Williams, M. C. Davies, and M. R. Alexander, "High throughput methods applied in biomaterial development and discovery," *Biomaterials,* vol. 31, pp. 187-198, 2010.
[290] M. C. Davies, M. R. Alexander, A. L. Hook, J. Yang, Y. Mei, M. Taylor, *et al.*, "High throughput surface characterization: a review of a new tool for screening prospective biomedical material arrays," *Journal of drug targeting,* vol. 18, pp. 741-751, 2010.
[291] J. Austin and A. H. Holway, "Contact Printing of Protein Microarrays," in *Protein Microarrays*, U. Korf, Ed., ed New York: Humana Press, 2011, pp. 379-394.
[292] M. Schena, D. Shalon, R. W. Davis, and P. O. Brown, "Quantitative monitoring of gene expression patterns with a complementary DNA microarray," *Science,* vol. 270, p. 467, 1995.
[293] G. MacBeath and S. L. Schreiber, "Printing proteins as microarrays for high-throughput function determination," *Science,* vol. 289, pp. 1760-1763, 2000.
[294] A. L. Hook, C.-Y. Chang, J. Yang, J. Luckett, A. Cockayne, S. Atkinson, *et al.*, "Combinatorial discovery of polymers resistant to bacterial attachment," *Nature biotechnology,* vol. 30, pp. 868-875, 2012.
[295] A. L. Hook, H. Thissen, and N. H. Voelcker, "Advanced substrate fabrication for cell microarrays," *Biomacromolecules,* vol. 10, pp. 573-579, 2009.
[296] X. Zárate, D. C. Henderson, K. C. Phillips, A. D. Lake, and D. W. Galbraith, "Development of high-yield autofluorescent protein microarrays using hybrid cell-free expression with combined Escherichia coli S30 and wheat germ extracts," *Proteome science,* vol. 8, p. 32, 2010.
[297] G. Arrabito and B. Pignataro, "Inkjet printing methodologies for drug screening," *Analytical chemistry,* vol. 82, pp. 3104-3107, 2010.
[298] R. Zhang, A. Liberski, F. Khan, J. J. Diaz-Mochon, and M. Bradley, "Inkjet fabrication of hydrogel microarrays using in situ nanolitre-scale polymerisation," *Chemical Communications,* pp. 1317-1319, 2008.
[299] A. Benninghoven, "Chemical analysis of inorganic and organic surfaces and thin films by static time-of-flight secondary ion mass spectrometry (TOF-SIMS)," *Angewandte Chemie International Edition in English,* vol. 33, pp. 1023-1043, 1994.
[300] M. Fartmann, C. Kriegeskotte, S. Dambach, A. Wittig, W. Sauerwein, and H. Arlinghaus, "Quantitative imaging of atomic and molecular species in cancer cell cultures with TOF-SIMS and Laser-SNMS," *Applied surface science,* vol. 231, pp. 428-431, 2004.
[301] H. Arlinghaus, C. Kriegeskotte, M. Fartmann, A. Wittig, W. Sauerwein, and D. Lipinsky, "Mass spectrometric characterization of elements and molecules in cell cultures and tissues," *Applied surface science,* vol. 252, pp. 6941-6948, 2006.
[302] N. Dhanalakshmi and R. Nagarajan, "Ultrasonic intensification of the chemical degradation of methyl violet: an experimental study," *World Academy of Science, Engineering and Technology,* vol. 59, pp. 537-542, 2011.

[303] J. Wu, L. Lin, and F.-t. Chau, "Ultrasound-assisted extraction of ginseng saponins from ginseng roots and cultured ginseng cells," *Ultrasonics sonochemistry,* vol. 8, pp. 347-352, 2001.
[304] D. A. Armbruster and T. Pry, "Limit of blank, limit of detection and limit of quantitation," *Clin Biochem Rev,* vol. 29, pp. S49-52, 2008.
[305] M. Zellner, W. Winkler, H. Hayden, M. Diestinger, M. Eliasen, B. Gesslbauer, *et al.*, "Quantitative validation of different protein precipitation methods in proteome analysis of blood platelets," *Electrophoresis,* vol. 26, pp. 2481-2489, 2005.
[306] D. Howes, R. Guy, J. Hadgraft, J. Heylings, U. Hoeck, F. Kemper, *et al.*, "Methods for assessing percutaneous absorption: the report and recommendations of ECVAM workshop 13," *Alternatives to laboratory animals: ATLA,* 1996.
[307] I. Jakasa and S. Kezic, "Evaluation of in-vivo animal and in-vitro models for prediction of dermal absorption in man," *Human & experimental toxicology,* vol. 27, pp. 281-288, 2008.
[308] A. Boix-Montanes, "Relevance of equivalence assessment of topical products based on the dermatopharmacokinetics approach," *European Journal of Pharmaceutical Sciences,* vol. 42, pp. 173-179, 2011.
[309] R. Bronaugh and T. Franz, "Vehicle effects on percutaneous absorption: in vivo and in vitro comparisons with human skin," *British Journal of Dermatology,* vol. 115, pp. 1-11, 1986.
[310] I. P. Dick, P. G. Blain, and F. M. Williams, "The percutaneous absorption and skin distribution of lindane in man. II. In vitro studies," *Human & Experimental Toxicology,* vol. 16, pp. 652-657, Nov 1997.
[311] T. J. Franz, "Percutaneous absorption. On the relevance of in vitro data," *Journal of Investigative Dermatology,* vol. 64, pp. 190-195, 1975.
[312] J. Hadgraft, D. Beutner, and H. M. Wolff, "In vivo-in vitro comparisons in the transdermal delivery of nitroglycerin," *International journal of pharmaceutics,* vol. 89, pp. R1-R4, 1993.
[313] R. Scott, P. Batten, H. Clowes, B. Jones, and J. Ramsey, "Further validation of an in vitro method to reduce the need for in vivo studies for measuring the absorption of chemicals through rat skin," *Fundamental and Applied Toxicology,* vol. 19, pp. 484-492, 1992.
[314] M. Okamoto, N. Tanji, Y. Katayama, and J. Okada, "TOF-SIMS investigation of the distribution of a cosmetic ingredient in the epidermis of the skin," *Applied surface science,* vol. 252, pp. 6805-6808, 2006.
[315] G. P. Moss, D. R. Gullick, and S. C. Wilkinson, "Methods for the Measurement of Percutaneous Absorption," in *Predictive Methods in Percutaneous Absorption,* ed: Springer, 2015, pp. 25-42.
[316] OECD, "Guidelines for the Testing of Chemicals 428, Skin absorption: in vitro Method," ed. Paris, 2004.
[317] F. P. Schmook, J. G. Meingassner, and A. Billich, "Comparison of human skin or epidermis models with human and animal skin in in-vitro percutaneous absorption," *International journal of pharmaceutics,* vol. 215, pp. 51-56, 2001.

[318] F. Benech-Kieffer, P. Wegrich, R. Schwarzenbach, G. Klecak, T. Weber, J. Leclaire, *et al.*, "Percutaneous absorption of sunscreens in vitro: interspecies comparison, skin models and reproducibility aspects," *Skin Pharmacology and Physiology,* vol. 13, pp. 324-335, 2000.
[319] D. Davies, R. Ward, and J. Heylings, "Multi-species assessment of electrical resistance as a skin integrity marker for in vitro percutaneous absorption studies," *Toxicology in vitro,* vol. 18, pp. 351-358, 2004.
[320] E. Chatelain, B. Gabard, and C. Surber, "Skin penetration and sun protection factor of five UV filters: effect of the vehicle," *Skin Pharmacology and Physiology,* vol. 16, pp. 28-35, 2003.
[321] S. J. Bashir, A. L. Chew, A. Anigbogu, F. Dreher, and H. I. Maibach, "Physical and physiological effects of stratum corneum tape stripping," *Skin Research and Technology,* vol. 7, pp. 40-48, 2001.
[322] S. Chapman, A. Walsh, S. Jackson, and P. Friedmann, "Lipids, proteins and corneocyte adhesion," *Archives of dermatological research,* vol. 283, pp. 167-173, 1991.
[323] U. Jacobi, T. Tassopoulos, C. Surber, and J. Lademann, "Cutaneous distribution and localization of dyes affected by vehicles all with different lipophilicity," *Archives of dermatological research,* vol. 297, pp. 303-310, 2006.
[324] L. J. Gamble, D. J. Graham, B. Bluestein, N. P. Whitehead, D. Hockenbery, F. Morrish, *et al.*, "ToF-SIMS of tissues:“Lessons learned” from mice and women," *Biointerphases,* vol. 10, p. 019008, 2015.
[325] A. L. Mescher, *Junqueira's Basic Histology Text and Atlas*, 14th ed. USA: MCGraw-Hill Education 2016.
[326] J. Malm, D. Giannaras, M. O. Riehle, N. Gadegaard, and P. Sjövall, "Fixation and drying protocols for the preparation of cell samples for time-of-flight secondary ion mass spectrometry analysis," *Analytical chemistry,* vol. 81, pp. 7197-7205, 2009.
[327] M. E. Lane, "Skin penetration enhancers," *International journal of pharmaceutics,* vol. 447, pp. 12-21, 2013.
[328] A. C. Williams and B. W. Barry, "Penetration enhancers," *Advanced drug delivery reviews,* vol. 64, pp. 128-137, 2012.
[329] R. Miller, J. Gerster, M. Owens, H. Slade, and M. Tomai, "Review Article Imiquimod applied topically: a novel immune response modifier and new class of drug," *International journal of immunopharmacology,* vol. 21, pp. 1-14, 1999.
[330] B. W. Barry, "Novel mechanisms and devices to enable successful transdermal drug delivery," *European journal of pharmaceutical sciences,* vol. 14, pp. 101-114, 2001.
[331] USP, "Imiquimod USP pending monograph," vol. version 1, pp. 1-3, 2011.
[332] G. A. Shabir, "Validation of high-performance liquid chromatography methods for pharmaceutical analysis: Understanding the differences and similarities between validation requirements of the US Food and Drug Administration, the US Pharmacopeia and the International Conference on Harmonization," *Journal of chromatography A,* vol. 987, pp. 57-66, 2003.

[333] J. Dolan, "A guide to HPLC and LC-MS buffer selection," *ACE HPLC Columns–ultra inert base-deactivated HPLC columns*, pp. 1-20, 2004.
[334] V. R. Meyer, *Pitfalls and Errors of HPLC in Pictures*: John Wiley & Sons, 2013.
[335] J. W. Dolan, "Ion Pairing-Blessing or Curse? ," *LC GC Magazine-North America-Solutions for Separation Scientists*, vol. 26, pp. 254-261, 2008.
[336] W. J. Long and J. Henderson, "Chromatography of nitrogen-containing compounds without triethylamine; Agilent Technologies," *Inc., Wilmington, DE, USA*, 2007.
[337] L. R. Snyder, J. J. Kirkland, and J. L. Glajch, *Practical HPLC method development*: John Wiley & Sons, 1997.
[338] Y. Yuan, S.-m. Li, F.-k. Mo, and D.-f. Zhong, "Investigation of microemulsion system for transdermal delivery of meloxicam," *International journal of Pharmaceutics*, vol. 321, pp. 117-123, 2006.
[339] P. Karande and S. Mitragotri, "Enhancement of transdermal drug delivery via synergistic action of chemicals," *Biochimica et Biophysica Acta (BBA)-Biomembranes*, vol. 1788, pp. 2362-2373, 2009.
[340] J. Hadgraft, "Passive enhancement strategies in topical and transdermal drug delivery," *International journal of pharmaceutics*, vol. 184, pp. 1-6, 1999.
[341] S. Gao and J. Singh, "Effect of oleic acid/ethanol and oleic acid/propylene glycol on the in vitro percutaneous absorption of 5-fluorouracil and tamoxifen and the macroscopic barrier property of porcine epidermis," *International journal of pharmaceutics*, vol. 165, pp. 45-55, 1998.
[342] L. V. Allen and H. C. Ansel, *Ansel's Pharmaceutical Dosage Forms and Drug Delivery Systems*, 10th ed. Philadelphia: Wolters Kluwer, 2014.
[343] L. Gibson, "Lipid-Based Excipients for Oral Drug Delivery," in *Oral Lipid-Based Formulations*. vol. 170, D. J. Hauss, Ed., ed New Jersey: Informa healthcare, 2007, pp. 33-62.
[344] K. Kawakami, T. Yoshikawa, Y. Moroto, E. Kanaoka, K. Takahashi, Y. Nishihara, *et al.*, "Microemulsion formulation for enhanced absorption of poorly soluble drugs: I. Prescription design," *Journal of Controlled Release*, vol. 81, pp. 65-74, 2002.
[345] H. Nomura, F. Kaiho, Y. Sugimoto, Y. Miyashita, M. Dohi, and Y. Kato, "Percutaneous absorption of indomethacin from mixtures of fatty alcohol and propylene glycol (FAPG bases) through rat skin: effects of oleic acid added to FAPG base," *Chemical and Pharmaceutical Bulletin*, vol. 38, pp. 1421-1424, 1990.
[346] E. Touitou, B. Godin, Y. Karl, S. Bujanover, and Y. Becker, "Oleic acid, a skin penetration enhancer, affects Langerhans cells and corneocytes," *Journal of controlled release*, vol. 80, pp. 1-7, 2002.
[347] K. A. Walters, K. R. Brain, D. M. Green, V. J. James, A. C. Watkinson, and R. H. Sands, "Comparison of the transdermal delivery of estradiol from two gel formulations," *Maturitas*, vol. 29, pp. 189-195, 1998.

[348] N. Ü. Okur, Ş. Apaydın, N. Ü. K. Yavaşoğlu, A. Yavaşoğlu, and H. Y. Karasulu, "Evaluation of skin permeation and anti-inflammatory and analgesic effects of new naproxen microemulsion formulations," *International journal of pharmaceutics,* vol. 416, pp. 136-144, 2011.
[349] B. J. Venton. Calibration Curves, Scince Education Database, Essentials of Analytical Chemistry, JoVE, Cambridge, MA [Online].
[350] U. Food and D. Administration, "FDA guidance for industry: bioanalytical method validation," *US Department of Health and Human Services, Food and Drug Administration, Center for Drug Evaluation and Research: Rockville, MD,* 2001.
[351] V. Jenning, A. Gysler, M. Schäfer-Korting, and S. H. Gohla, "Vitamin A loaded solid lipid nanoparticles for topical use: occlusive properties and drug targeting to the upper skin," *European Journal of Pharmaceutics and Biopharmaceutics,* vol. 49, pp. 211-218, 2000.
[352] S. M. Bal, A. C. Kruithof, R. Zwier, E. Dietz, J. A. Bouwstra, J. Lademann, *et al.*, "Influence of microneedle shape on the transport of a fluorescent dye into human skin in vivo," *Journal of Controlled Release,* vol. 147, pp. 218-224, 2010.
[353] F. Verbaan, S. Bal, D. Van den Berg, J. Dijksman, M. Van Hecke, H. Verpoorten, *et al.*, "Improved piercing of microneedle arrays in dermatomed human skin by an impact insertion method," *Journal of Controlled Release,* vol. 128, pp. 80-88, 2008.
[354] F. J. Verbaan, S. Bal, D. Van den Berg, W. Groenink, H. Verpoorten, R. Lüttge, *et al.*, "Assembled microneedle arrays enhance the transport of compounds varying over a large range of molecular weight across human dermatomed skin," *Journal of Controlled Release,* vol. 117, pp. 238-245, 2007.
[355] K. Takahashi, S. Tamagawa, T. Katagi, H. Yostomi, A. Kamada, J. H. Rytting, *et al.*, "In vitro transport of sodium diclofenac across rat abdominal skin: Effect of selection of oleaginous component and the addition of alcohols to the vehicle," *Chemical and pharmaceutical bulletin,* vol. 39, pp. 154-158, 1991.
[356] D. Paolino, C. A. Ventura, S. Nistico, G. Puglisi, and M. Fresta, "Lecithin microemulsions for the topical administration of ketoprofen: percutaneous adsorption through human skin and in vivo human skin tolerability," *International Journal of pharmaceutics,* vol. 244, pp. 21-31, 2002.
[357] J. Smith and W. Irwin, "Ionisation and the effect of absorption enhancers on transport of salicylic acid through silastic rubber and human skin," *International journal of pharmaceutics,* vol. 210, pp. 69-82, 2000.
[358] E. Farkas, D. Kiss, and R. Zelkó, "Study on the release of chlorhexidine base and salts from different liquid crystalline structures," *International journal of pharmaceutics,* vol. 340, pp. 71-75, 2007.
[359] T. Elliott, M. Faroqui, R. Armstrong, and G. Hanson, "Guidelines for good practice in central venous catheterization," *Journal of hospital infection,* vol. 28, pp. 163-176, 1994.

[360] A. Casey, A. Itrakjy, C. Birkett, A. Clethro, R. Bonser, T. Graham, *et al.*, "A comparison of the efficacy of 70% v/v isopropyl alcohol with

either 0.5% w/v or 2% w/v chlorhexidine gluconate for skin preparation before harvest of the long saphenous vein used in coronary artery bypass grafting," *American journal of infection control*, vol. 43, pp. 816-820, 2015.

[361] A. Judd, D. Scurr, J. Heylings, D. Griffiths, K.-W. Wan, and G. Moss, "Visualisation of the Permeation of Chlorhexidine Within Skin Using Time-of-Flight Secondary Ion Mass Spectrometry (TOF-SIMS)," in *Advances in Dermatological Sciences*, ed, 2013, pp. 340-354.

[362] T. Karpanen, T. Worthington, E. Hendry, B. R. Conway, and P. A. Lambert, "Antimicrobial efficacy of chlorhexidine digluconate alone and in combination with eucalyptus oil, tea tree oil and thymol against planktonic and biofilm cultures of Staphylococcus epidermidis," *Journal of Antimicrobial Chemotherapy*, vol. 62, pp. 1031-1036, 2008.

[363] K. J. Popovich, R. Lyles, R. Hayes, B. Hota, W. Trick, R. A. Weinstein, *et al.*, "Relationship between chlorhexidine gluconate skin concentration and microbial density on the skin of critically ill patients bathed daily with chlorhexidine gluconate," *Infection Control & Hospital Epidemiology*, vol. 33, pp. 889-896, 2012.

[364] T. Koburger, N.-O. Hübner, M. Braun, J. Siebert, and A. Kramer, "Standardized comparison of antiseptic efficacy of triclosan, PVP–iodine, octenidine dihydrochloride, polyhexanide and chlorhexidine digluconate," *Journal of Antimicrobial Chemotherapy*, vol. 65, pp. 1712-1719, 2010.

[365] D. Adams, M. Quayum, T. Worthington, P. Lambert, and T. Elliott, "Evaluation of a 2% chlorhexidine gluconate in 70% isopropyl alcohol skin disinfectant," *Journal of Hospital Infection*, vol. 61, pp. 287-290, 2005.

[366] J. Valles, I. Fernandez, D. Alcaraz, E. Chacon, A. Cazorla, M. Canals, *et al.*, "Prospective randomized trial of 3 antiseptic solutions for prevention of catheter colonization in an intensive care unit for adult patients," *Infection Control & Hospital Epidemiology*, vol. 29, pp. 847-853, 2008.

[367] B. Godin and E. Touitou, "Transdermal skin delivery: predictions for humans from in vivo, ex vivo and animal models," *Advanced drug delivery reviews*, vol. 59, pp. 1152-1161, 2007.

[368] F. Netzlaff, U. F. Schaefer, C.-M. Lehr, P. Meiers, J. Stahl, M. Kietzmann, *et al.*, "Comparison of bovine udder skin with human and porcine skin in percutaneous permeation experiments," *Alternatives to laboratory animals: ATLA*, vol. 34, pp. 499-513, 2006.

[369] C. Herkenne, A. Naik, Y. N. Kalia, J. Hadgraft, and R. H. Guy, "Pig ear skin ex vivo as a model for in vivo dermatopharmacokinetic studies in man," *Pharmaceutical research*, vol. 23, pp. 1850-1856, 2006.

[370] U. Jacobi, M. Kaiser, R. Toll, S. Mangelsdorf, H. Audring, N. Otberg, *et al.*, "Porcine ear skin: an in vitro model for human skin," *Skin Research and Technology*, vol. 13, pp. 19-24, 2007.

[371] R. C. Scott and P. H. Dugard, "The properties of skin as a diffusion barrier and route for absorption " in *Pharmacology of the Skin II*, M. W. Greaves and S. Shuster, Eds., ed Berlin: Springer-Verlag, 1989, pp. 93-114.

Appendix: Ethical Approval Information of *In Vivo* Chlorhexidine Skin Permeation Study

[*In vivo* Assessment of Chlorhexidine Permeation into the Skin]

Aims:

In vivo skin permeation assessment of chlorhexidine (CHG) from commercial (over the counter) products to study the effects of concentration, vehicle type and application time on the skin permeation of CHG in addition to visualise the spatial distribution of CHG within skin following the application of these products.

Methods:

- CHG products (HiBiSCRUB 4% w/ CHG aqueous solution, HiBiSCRUB 2% w/v CHG aqueous solution and ChloraPrep 2% w/v CHG in 70% IPA solution) will be tested.
- Six healthy human volunteers with age between 20-55 years will participate in this study.
- To study the effect of concentration and vehicle type, the products will be applied on the skin of the volar forearm for 2 minutes followed by tape stripping of the application site using adhesive tape strips (D-Squame, USA) for up to 20 strips.
- To investigate the application time effect, the experiment will be repeated but at longer application times such as 5, 10, 15, 30 and 60 minutes.
- The collected tape strips will be analysed within 24 hours using ToF-SIMS analysis and disposed of using the hazardous waste laboratory disposal.

A representation of the procedure to be carried out is shown in Figure 1.

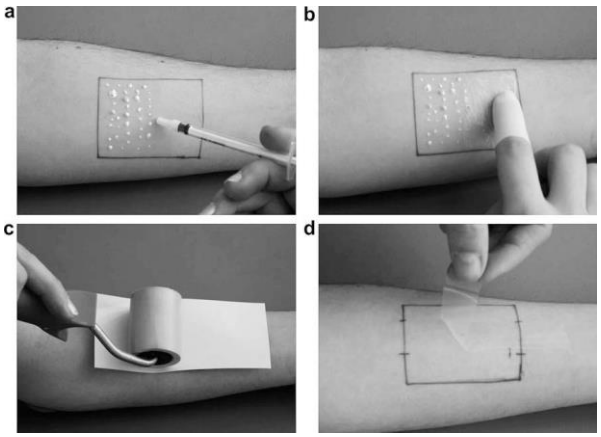

Figure 1. Method of tape stripping (a) application of the formulation on a marked skin area; (b) homogeneous distribution; (c) the adhesive tape is pressed with a roller on the skin, an empty sheet of paper avoids the transfer of the formulation onto the back side of the tape; (d) removal of the tape .

Recruitment of research participants:

For the initial experiment we will use ourselves (myself and my supervisors) and later on we will recruit additional 3 volunteers (PhD students) from the school of pharmacy to get a total number of 6 volunteers. We will try to balance between the gender type recruiting 3 males and 3 females. The age group will be between 20-55 years old.

Participant information leaflet

Thank you for volunteering to help us with our final year project. This information sheet explains the aims of our study and what the study involves. Please take the time to read it.

Aims:

To compare between the skin permeability of chlorhexidine (antiseptic drug) from commercial products regarding the effects of concentration, vehicle type and application time.

Method:

The antiseptic products (HiBiSCRUB and ChloraPrep) will be applied on the marked skin area of the volar forearm for different time intervals such as 2, 5, 10, 15, 30 and 60 minutes followed by sequential application and removal of an adhesive tape at the product application site for up to 20 strips in order to remove the *stratum corneum* layer of the skin.

What is required of participants?

If you decide to participate in this study, we will need you to tell us if you have any systemic allergic diseases such as asthma or hay fever, skin allergy such as contact dermatitis or eczema. Also let us know if you have allergy to medicines especially antiseptics containing chlorhexidine in their formulation or hypersensitivity towards the adhesive tapes. The study should take approximately 90 minutes and will be carried out at Boots Science Building.

We will need your contact details in order to arrange a study time.

Confidentiality and security of information

All information will be confidential and kept in a secure place. Information will only be accessible to the students conducting the study and the project supervisors.

Participation in this study is voluntary and if you do not wish to participate we will not apply the data collected from you in our report. If you wish to withdraw consent of participation at any time during the study, you may do so. A consent form will be provided to participants prior to the scheduled meeting time. If you are willing to take part in the study, a consent form will be given to you for you to sign. Please feel free to ask any questions about our study.

Consent form:

I.....confirm the following:

I have been informed of and understand the purpose of this study.

I have been given the opportunity to ask questions about the study.

I understand that I can withdraw consent of participation at any time during the study without prejudice.

Any information which might potentially identify me will not be used in any published material.

I agree to participate in the study as outlined to me.

Signature:..... Date:.....

Contacts:

Study Leader:

Mohammed AL-Mayahy
PhD Student School of Pharmacy
Room C15 Boots Science Building
University Park
NG7 2RD
United Kingdom

Telephone: 07721646120

E-mail: paxmhal@nottingham.ac.uk

Supervisor: Dr David J. Scurr
Division of Laboratory of Biophysics and Surface Analysis
School of Pharmacy
Room C28 Boots Science Building
University Park
Nottingham
NG7 2RD
UK
Telephone: 0115 846 6276
Email: david.scurr@nottingham.ac.uk

Supervisor: Dr Maria Marlow
Division of Drug Delivery & Tissue Engineering
School of Pharmacy
Room D05 Boots Science Building
University Park
Nottingham
NG7 2RD
UK
Telephone: 0115 846 7045
Email: maria.marlow@nottingham.ac.uk